Annual Report on Nuclear Physics Activities

July 1, 1989 – December 31, 1990

Editors:
H. Beer, J. Wochele
Institut für Kernphysik

Kernforschungszentrum Karlsruhe

KERNFORSCHUNGSZENTRUM KARLSRUHE

Institut für Kernphysik

KfK 4875

ANNUAL REPORT

on

NUCLEAR PHYSICS ACTIVITIES

July 1, 1989 - December 31, 1990

Editors:

H.Beer and J.Wochele

Kernforschungszentrum Karlsruhe GmbH, Karlsruhe

ABSTRACT

This report surveys the research activities from July 1, 1989 to December 31, 1990 at the Institute for Nuclear Physics (IK) of the Kernforschungszentrum Karlsruhe (F.R.G.). The research program of the institute comprises fast neutron physics, neutrino physics, nuclear astrophysics, cosmic ray physics, nuclear reactions with light ions, laser spectroscopy and applied gamma-ray spectroscopy as well as detector technology.

ZUSAMMENFASSUNG

Der vorliegende Bericht gibt einen Überblick über die Arbeiten am Institut für Kernphysik (IK) des Kernforschungszentrums Karlsruhe (Germany) im Zeitraum vom 1. Juli 1989 bis zum 31. Dezember 1990. Das Forschungsprogramm umfaßt die Gebiete Neutronenphysik, Neutrinophysik, nukleare Astrophysik, Höhenstrahlphysik, Kernreaktionen mit leichten Ionen, Laserspektroskopie und angewandte Gammaspektroskopie sowie Detektortechnologie.

PREFACE

This annual report on nuclear physics activities at the Kernforschungs-zentrum Karlsruhe describes experiments carried out in the Institut für Kernphysik (IK). The institute is divided into two sections labelled, for historical reasons, sections IK I and IK III.

- **Astrophysics with Extensive Air Showers** : A new joint project of both sections is the development and construction of a large detector system for studying cosmic rays. It is called KASCADE which stands for KArlsruhe Shower Core and Array DEtector. The main aim of the experiment is to obtain information on the elemental composition of the primary cosmic ray particles. In addition the measurements will help to clarify the question of cosmic ray point sources which have been discovered several years ago and show some enigmatic features.

Construction of the detector system has started after comprehensive prototype work and extensive simulation calculations of the passage of cosmic rays through the atmosphere have been performed.

Additional activities of Section IK I lie in the fields of experimental nuclear and particle physics :

- **Fast Neutron Physics** : The polarized neutron beam of the facility POLKA at the Karlsruhe Cyclotron was used for capture reaction studies on light nuclear systems in the energy range up to 50 MeV. A scintillating liquid Ne sample was employed successfully as an active capture target in these experiments.

The development of cryogenic detectors was continued. Superconducting tunnel junctions have been applied for the detection of X-rays with improved resolution.

- **Neutrino Physics** : The KArlsruhe Rutherford interMediate Energy Neutrino experiment KARMEN makes use of the pulsed 'beam stop' neutrinos v_μ, v_e and $\bar{v}_\mu$ produced at the spallation neutron source ISIS of the Rutherford Appleton Laboratory (England). The program involves experimental studies of fundamental questions in the fields of particle physics (v - oscillations, v - e scattering) and nuclear physics (v - nucleus interactions). Based on experiences from the test measurements in 1988, a number of improvements have been applied concerning triggering and shielding. Since November 1989 the fully assembled KARMEN detector is in its measuring position and is taking data. First results of neutrino-induced reactions are presented.

- **Detector Development** : The work concentrates on liquid ionization chambers using room temperature liquids like TMS and HMDS. The investigations have been done in order to use this type of chambers for the large scale calorimeter of the KASCADE central detector. With a set of chambers first calorimeters with Fe, Pb and U as absorber slabs have been tested in a 6 GeV particle beam of pions, muons and electrons. Preparations for mass production of chambers have been terminated.

Section IK III is mainly working in the following fields :

- **Nuclear Astrophysics** : Capture cross sections of fast neutrons in the keV range are measured in order to understand in detail the synthesis of heavy elements in stars. In this work, a considerable increase in accuracy has been achieved by use of a novel 4π scintillation counter made of BaF_2. First results are reported here and demonstrate a level of accuracy not attained before. Further experiments deal with the measurement of very small neutron capture cross sections by activation and with nuclear spectroscopy to obtain nuclear structure information required for the astrophysical interpretation of the data.

- **Nuclear Reactions** : Experiments in this field have made use of the 26 MeV per nucleon ^6Li beam from the Karlsruhe Isochronous Cyclotron and of the magnetic spectrometer for investigating continuous spectra in break-up reactions. Theoretical studies had shown that Coulomb break-up should allow the determination of radiative capture cross sections between light nuclei at very low relative velocities. Such cross sections are of great importance in astrophysics. These experiments have now been terminated after demonstrating the feasibility of the method, in favour of the cosmic ray studies.

- **Laser spectroscopy** : This technique is applied to sub-ng amounts of radioactive atoms in order to determine hyperfine structure and isotopic shifts of atomic transitions. The results yield information on nuclear moments and on the change of nuclear charge radii due to varying neutron number. Work at present concentrates on elements beyond lead using different experimental techniques such as spectroscopy on collimated atomic beams and on ions stored in an rf trap.

- **Applied Gamma-Ray Spectroscopy** : Here instruments are developed to determine concentration and isotopic composition of fissile materials. The instruments make use either of the intrinsic radioactivity or of X-ray absorption and fluorescence. Their main applications are in the safeguards of nuclear fuel and in process control during fabrication and reprocessing.

- **Section IK III** was also responsible, until the end of 1990, for operating the three accelerators of our institute. The Karlsruhe Isochronous Cyclotron which

was mainly used for fast neutron physics and nuclear reaction experiments in the past but is now increasingly devoted to materials research; the 3.75 MV Van de Graaff accelerator which serves mainly as a source of keV neutrons for the nuclear astrophysics studies; and a compact cyclotron which is basically a commercial installation to produce radioactive isotopes for nuclear medicine and mechanical engineering.

(B. Zeitnitz)   (G. Schatz)

.

CONTENTS   Page

1.   NUCLEAR PHYSICS

1.1.   NUCLEAR ASTROPHYSICS

1.1.1.   THE STELLAR (n,γ) CROSS SECTION OF ^{192}Pt - A NEW CONSTRAINT FOR THE s - PROCESS

M.TEPE, F.KÄPPELER

The stellar (n,γ) cross section of the s-only isotope ^{192}Pt has been measured for the first time via the activation technique. This cross section is important for analyzing the s-process branchings at ^{191}Os and ^{192}Ir, which are expected to yield an independent estimate for the mean neutron density during the s-process. Together with similar information from other branchings, this can be used to constrain the conditions at the stellar s-process site, i.e. during helium shell burning in Red Giant stars.

Isotopically enriched samples of 1.7 and 3.5 mg/cm^2 thickness were prepared by electrodeposition on thin carbon backings. The samples were irradiated in a quasi-stellar neutron spectrum for kT=25 keV that is obtained from the ^{7}Li(p,n)^{7}Be reaction by bombarding a lithium target with protons of 1912 keV [1,2] . The measurements were performed relative to the gold cross section as a standard. Variation of the experimental conditions in different activations and the use of different samples allowed to determine corrections and to evaluate systematic uncertainties.

The ^{193}Pt produced during the activations decays by electron capture with a half-life of 50 yr, which causes two major difficulties :

(i)   The ^{193}Pt activity was rather low despite of the long irradiation periods of several weeks. Therefore, considerable efforts were required for reducing the low energy background in the 4 π Si (Li) spectrometer for X-ray counting.

(ii)   The only accessible radiation emitted in that decay are the iridium LX-rays in the energy range from 8 to 13 keV. Apart from the fact that one has to correct for sizable absorption losses, it turned out that the relative decay intensities as well as the half-life of ^{193} Pt represent the limiting uncertainties of the present measurement. Both quantities are only known to ± 20%.

The X-ray spectrum measured in one of the activations is shown in Fig. 1. The cross section that was eventually obtained is almost a factor of two smaller than

previously calculated [3,4] . In terms of the astrophysical interpretation of the s-process branching, this yields a mean neutron density of

$$n_n = (4.3 + 3.4/-2.5) \cdot 10^8 \text{ cm}^{-3},$$

in good agreement with the respective results obtained for the branchings at A = 147, 148 [5] and at A = 185, 186 [6] .
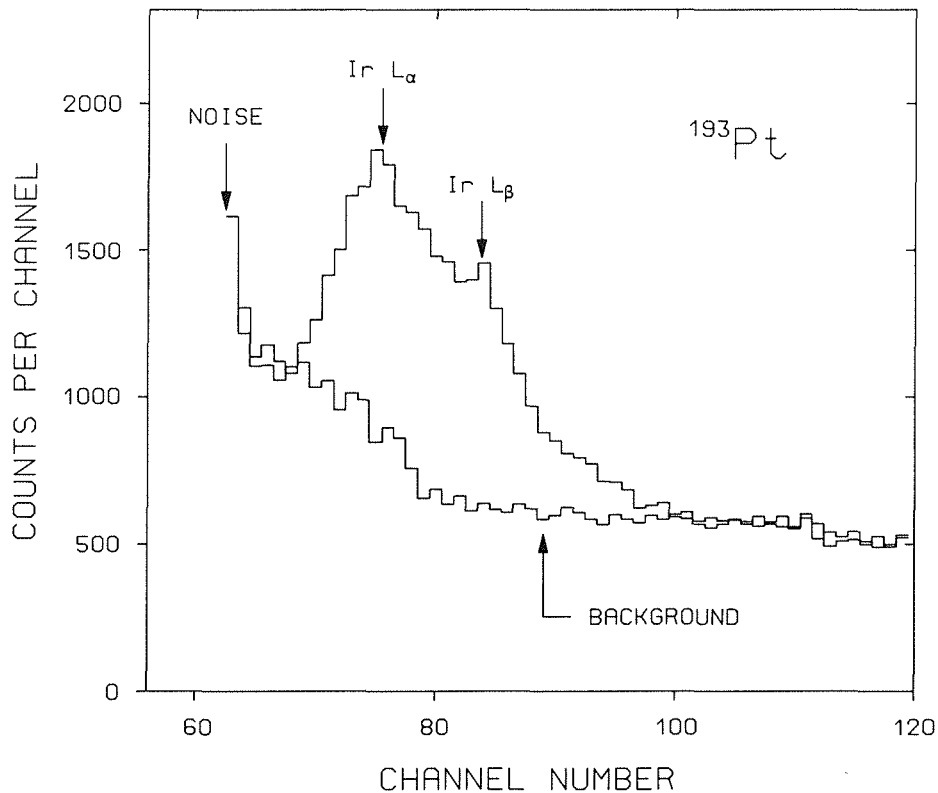
Fig. 1   The X-ray spectrum of an activated [192]Pt sample.

[1]   H.Beer, F.Käppeler, Phys. Rev. C21, 534 (1980) .

[2]   W.Ratynski, F.Käppeler, Phys. Rev. C37, 595 (1988) .

[3]   M.J.Harris, Ap. Space Sci. 77, 357 (1981) .

[4]   J.A.Holmes, S.E.Wooseley, W.A. Fowler, B.A.Zimmerman, Atomic Data and Nuclear Data Tables 18, 305 (1976) .

[5]   F.Käppeler, R. Gallino, M.Busso, G.Picchio, C.M.Raiteri, Ap. J.345, 630 (1990) .

[6]   F.Käppeler, Z.Y.Bao, S.Jaag, G.Reffo, Ap. J. 366,605 (1991) .

1.1.2. ^{87}Rb : s - PROCESS NUCLEOSYNTHESIS AT N = 50

D.NEUBERGER, F.KÄPPELER

^{87}Rb is one of the neutron magic nuclei with N = 50, which are charcterized by particularly small cross sections. Therefore, these isotopes are efficiently produced in the s-process, so that their s-abundances exceed by far the respective contributions from the r-process. The mass range at N = 50 is important because of the fact that two different s-processes - commonly addressed as *weak* and *main s-*process component [1] - contribute about equally to the observed abundances. For a detailed discussion of s-process nucleosynthesis in the mass region 84 < A < 90 it is, therefore, necessary to start with accurate cross sections for these critical nuclei. The present study of the ^{87}Rb cross section continues a program for the investigation of the neutron magic nuclei [2] .

The stellar neutron capture cross section of ^{87}Rb has been measured by the activation technique. Neutrons were produced by the ^{7}Li(p,n)^{7}Be reaction at a proton energy of 1912 keV. The resulting neutron spectrum allows directly to determine the stellar cross section for a thermal energy of kT = 25 keV [3,4] . Natural Rb$_2$SO$_4$ samples with thicknesses between 0.7 and 70 mg/cm^2 were sandwiched between gold foils during the irradiations in order to use the gold cross section as a standard. After irradiation, the induced activity was measured by detecting the beta decay electrons of ^{88}Rb in a 4π Si (Li) spectrometer.

In addition, 1.5 and 2 mm thick self-supporting Rb$_2$SO$_4$ tablets were irradiated as well. In these cases, the induced activity was determined with a HPGe detector via the intense gamma-ray lines at 898 and 1836 keV. With both methods, consistent cross sections were obtained. The present stellar cross section for a thermal energy of kT = 25 keV is compared in Fig. 1 with previous values [5-8]. Note that the uncertainties achieved in the present work are more than two times smaller than those of the existing data. Agreement within the quoted uncertainties is obtained with the recent measurements of Beer and Macklin [7] and Jaag [8]. This holds also for the calculated cross section of Harris [5], but this value carries an uncertainty of least 50%. The astrophysical consequences of the improved ^{87}Rb cross section are presently investigated.
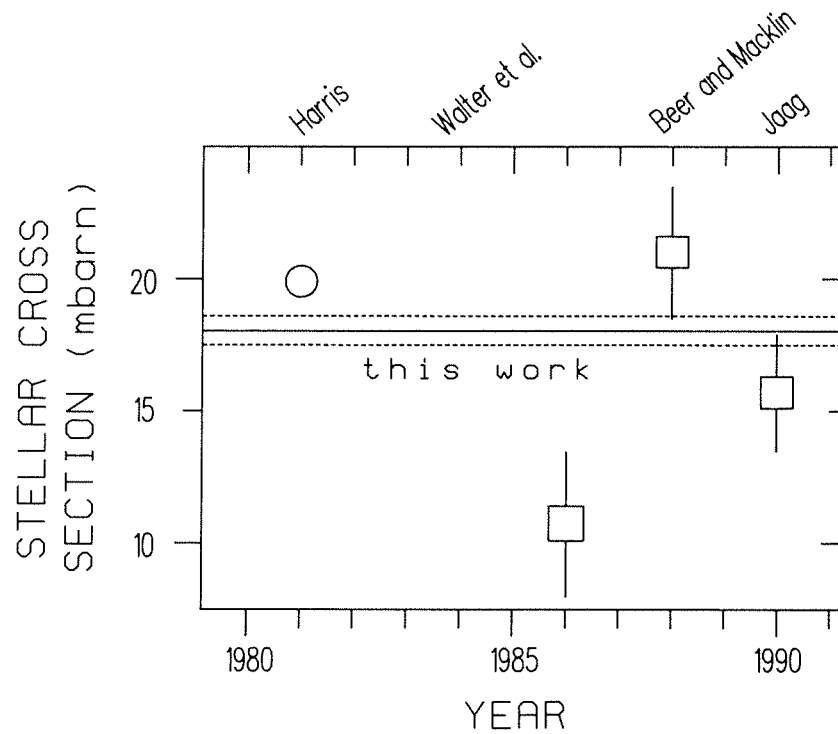
Fig. 1 Comparison of the present stellar [87]Rb cross section with previous results.

[1]   F.Käppeler, H.Beer, K.Wisshak, Rep. Prog. Phys. **52**, 945 (1989).

[2]   F.Käppeler, W.R.Zhao, H.Beer, U.Ratzel, Ap. J. **355**, 348 (1990).

[3]   H.Beer, F.Käppeler, Phys. Rev. **C21**, 534 (1980).

[4]   W.Ratynski, F.Käppeler, Phys. Rev. **C37**, 595 (1988).

[5]   M.J.Harris, Ap. Space Sci. **77**, 357 (1981).

[6]   G.Walter, H.Beer,F.Käppeler,R.-D.Penzhorn, Astron. Astrophys. **155**, 247 (1986).

[7]   H.Beer, R.L.Macklin, Ap. J. **339**, 962 (1989).

[8]   S.Jaag, Dipl. thesis, University of Karlsruhe (1990).

1.1.3. ^{147}Pm - AN EXPERIMENTAL STELLAR CROSS SECTION FOR A SHORT - LIVED s - PROCESS BRANCHING POINT

Th.W.GERSTENHÖFER, F.KÄPPELER, G.REFFO*, K.WISSHAK

Radioactive nuclei with $t_{1/2} < 10$ y hold a key position in the synthesis of the heavy elements. In the s-process, neutron captures occur at rates of ~ 1y and are, therefore, comparable to the beta decay rates of some of the involved isotopes, such as ^{147}Pm ($t_{1/2} = 2.6$ y). The resulting branching of the neutron capture flow yields a characteristic abundance pattern for the neighbouring isotopes that can be analyzed in terms of the physical conditions during the s-process. ^{147}Pm belongs to the three branch points at A = 147, 148, which have been shown to be suited for estimating the mean neutron density during the s-process [1].

For improving the quantitative discussion of this scenario, the neutron capture cross section of ^{147}Pm was measured for the first time in the keV range by means of two independent methods :

(i)   direct detection of the prompt capture gamma-rays by means of Moxon-Rae detectors, using the TOF technique at a flight path of only 2 cm, and

(ii)   activation in a quasi stellar neutron spectrum and detection of the induced ^{148}Pm activity. Both measurements were carried out relative to the standard cross section of ^{197}Au, using the quasi-stellar neutron spectrum produced via the ^{7}Li(p,n)^{7}Be reaction at 1912 keV proton energy [2,3]

On the experimental side, this study was hampered by the high specific activity of the short-lived sample. Because of the excellent sensitivity of the applied techniques, a sample mass of only 5 mg was suffucient in both cases. In this way, the sample-induced background as well as the radiation hazard could be kept at a manageable level, while satisfactory signal-to-background ratios could be achieved at the same time. Presently, the data are under analysis.

[1]   R.R.Winters, F.Käppeler, K.Wisshak,A.Mengoni, G.Reffo, Ap. J. **300**, 41 (1986).

[2]   H.Beer, F.Käppeler, Phys. Rev. **C21**, 534 (1980).

[3]   W.Ratynski, F.Käppeler, Phys. Rev. **C37**, 595 (1988).

*   E.N.E.A. Bologna, I-40138 Bologna, Italy

1.1.4. THE STELLAR CROSS SECTION OF ^{209}Bi : IMPLICATIONS FOR THE s-PROCESS

S.JAAG, F.KÄPPELER

The abundances of the neutron magic nuclei ^{208}Pb and ^{209}Bi at the termination of the s-process path are difficult to reproduce by the classical s-process approach [1,2]. A major part of this problem is to determine the very small (n,γ) cross sections of these isotopes with sufficient accuracy; this has been a challenge for experimentalists since many years. For ^{208}Pb, this problem could be solved by using the activation technique [3], but for ^{209}Bi only the partial cross section to the short-lived ground state could be determined in this way.

Up to now, the only experimental approach avoiding the problem with backscattered neutrons in a direct measurement was to use a setup with very short primary flight path [4]. Capture events were registered by a set of Moxon-Rae detectors located at a larger distance. In this way, prompt capture gamma-rays and scattered neutrons could be discriminated by their different TOF. This setup was modified in order to obtain the required sensitivity for measuring the very small cross sections of neutron magic isotopes. In particular, the energy and the time resolution of the Moxon-Rae detectors were improved by reducing the overall dimensions and by using smaller photomultipliers.

The measurement was carried out at the Karlsruhe Van de Graff accelerator, using the ^{7}Li(p,n)^{7}Be reaction for neutron production [6,7]. The neutrons are collimated due to the reaction kinematics. This keeps neutron induced backgrounds at a minimum, since all massive parts of the setup are located outside of the neutron beam. A primary flight path of only 20 mm between neutron target and sample was sufficient to distinguish true capture events from the intense TOF peak due to gamma-rays created by the interaction of the proton beam pulse with the lithium and the target backing. The comparably high neutron flux at the sample position allows for cross section measurements down to ~1 mbarn.

The stellar cross section for kT = 30 keV, $<\sigma> = 1.70 \pm 0.18$ mbarn, is about six times smaller than the existing differential measurement [8]. Even the partial cross section to the short-lived ground state in ^{210}Bi of 2.54 mbarns, which was determined at kT = 25 keV via activation [3] is larger than the present result. In view of these discrepancies, the reliability of the present technique was checked by including a ^{181}Ta sample in one of the two experimental runs. The resulting cross

section of ^{181}Ta was found to agree within 4% with a recent measurement [9], thus confirming the 10% accuracy claimed for the present ^{209}Bi cross section.

The astrophysical implications of the smaller (n,γ) cross sections of ^{208}Pb [3] and of the present value for ^{209}Bi have been investigated for the classical s-process approach as well as for the successful s-process model for helium shell burning in low mass stars of low metallicity [10,11]. A sketch of the s-process flow at the end of the neutron capture chain is given in Fig. 1 . The respective s-process abundances are superimposed by three types of r-process contributions : r-process yields, decay products from short-lived transbismuth isotopes, and a radiogenic part.
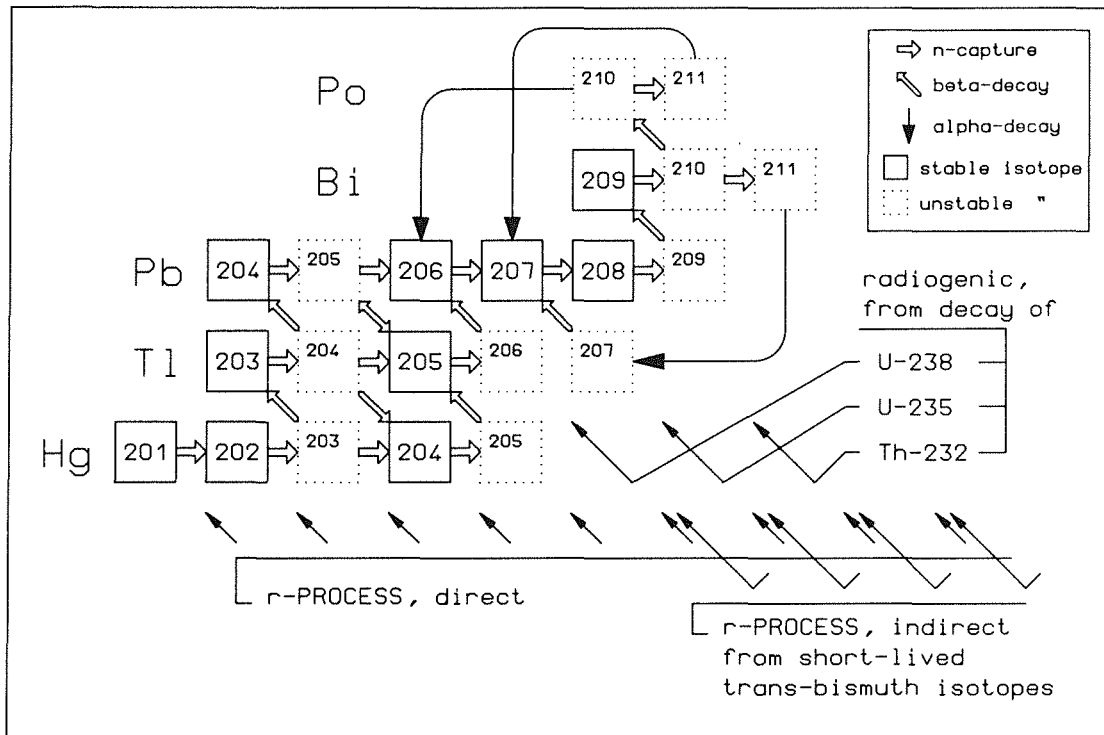
Fig. 1   The neutron capture flow at the end of the s-process path and the various r-process contributions.

The typical problem with the abundances of ^{208}Pb and ^{209}Bi was found to persist: Neither of the two s-process models was capable of reproducing the ^{208}Pb abundance despite of their excellent agreement with the observed values in the entire range $90 < A < 204$ [12]. This result was found practically independent of the assumed time dependence for the neutron pulses. Therefore, an additional *strong* s-process component characterized by a large neutron exposure was postulated in the literature, which eventually produces the correct amount of ^{208}Pb. For the classical approach, the small cross section of ^{209}Bi implies a low

temperature for this strong component ; otherwise, [209]Bi is always overproduced. This problem does not exist in the LMS model, which never produces large amounts of [209]Bi since ~95% of the neutron exposure is due to the [13]C(α,n)[16]O reaction that operates at relatively low temperatures ($T_8 = 1.5$, kT = 12 keV). There, the [208]Pb cross section is so small that only about 5% of the neutron capture chain reaches [209]Bi.

[1]   H.Beer, R.L.Macklin, Phys.Rev. **C32**, 738 (1985).

[2]   F.Käppeler, H.Beer, K.Wisshak, Rep. Prog. Phys. **52**, 945 (1989).

[3]   U.Ratzel, thesis, University of Karlsruhe (1988).

[4]   K.Wisshak, F.Käppeler, Nucl.Sci.Eng. **77**, 58 (1981).

[5]   M.C.Moxon, E.R.Rae, Nucl.Instr. Meth. **24**, 445 (1963).

[6]   H.Beer, F.Käppeler, Phys. Rev. C **21**, 534 (1980).

[7]   W.Ratynski, F.Käppeler, Phys. Rev. C **37**, 595 (1988).

[8]   R.L.Macklin, J.Halperin, Phys. Rev. C **14**, 1389 (1976).

[9]   K.Wisshak, F.Voß, F.Käppeler, G.Reffo, report KfK 4674, Kernforschungszentrum Karlsruhe (1990); Phys. Rev. C **42**, 1731 (1990).

[10]   R.Gallino, M.Busso, G.Picchio, C.M.Raiteri, A.Renzini, Ap. J. (Letters), **334**, L45 (1988).

[11]   R.Gallino, private communications (1990).

[12]   F.Käppeler, R.Gallino, M.Busso, G.Picchio, C.M.Raiteri, Ap. J., **345**, 630 (1990).

1.1.5.   [180m]Ta AT STELLAR TEMPERATURES

Zs.NÉMETH* , F.KÄPPELER

The origin of [180m]Ta , nature's rarest stable isotope, is still an unresolved puzzle of nuclear astrophysics. There were numerous attempts to describe its production by s-, r-, p-, and v-processes. Since an r-process origin is not supported by recent experiments [1], and since significant p-process contributions are excluded by theoretical studies [2,3], the s-process remains the most promising possibility for producing [180m]Ta, which can be investigated experimentally, whereas the v - process [4] represents a more uncertain alternative.

In the s-process, there are two ways for producing [180m]Ta as indicated in Fig. 1 by solid arrows : a weak beta branch in the decay of the isomer [180m]Hf was shown to contribute ~20% to the observed [180m]Ta abundance [5], and an s-process

branching at ^{179}Hf, which causes a small part of the s-process flow to pass through ^{180m}Ta [6] . The terrestrially stable isotope ^{179}Hf becomes unstable under s-process conditions and develops an equilibrium abundance with ^{179}Ta; eventually , neutron captures of the resulting ^{179}Ta nuclei lead to ^{180m}Ta.
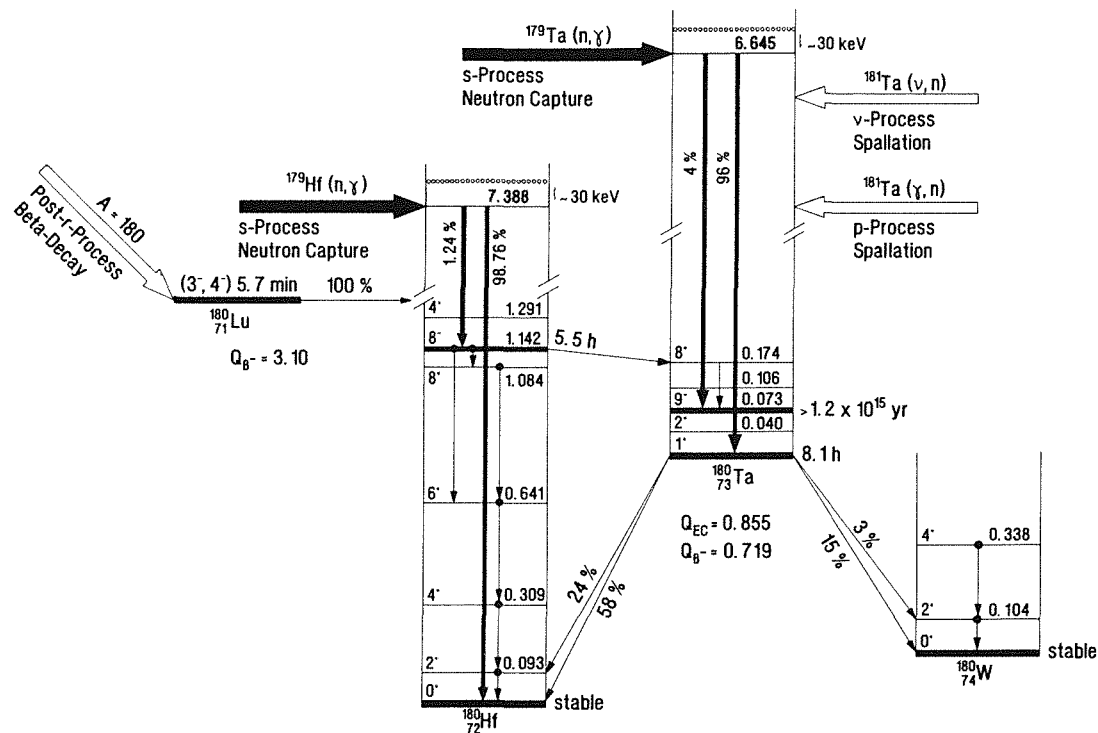
Fig. 1   The level structure at A = 180 and the various production processes of ^{180m}Ta

The so produced ^{180m}Ta, however, could be destroyed again via (γ,γ') reactions if the metastable state is strongly coupled to the ground state by low-lying activation levels. Our knowledge on the decay scheme of ^{180m}Ta is poor and the location of the activation levels is unknown. Therefore, a search for possible activation levels was carried out by irradiating enriched T_2O_5 samples (500 mg, 0.26% ^{180m}Ta) with an intense ^{60}Co source of 1.5 PBq and with 4 MeV bremsstrahlung at the Institute of Isotopes, Budapest. The bremsstrahlung was produced by converting the 4 MeV electron beam of 33 µA by means of a 1 mm thick platinum converter. In total, six irradiations were carried out ; in all cases the cross section of the ^{115}In(γ,γ')^{115m}In reaction was used as a reference standard.

The induced ^{180g}Ta activity was recorded versus time via the hafnium K X-rays, which were easily observable in the spectra. In this way, the background subtraction could be verified by reproducing the 8.1 h half-life of ^{180g}Ta. Since no ^{180g}Ta activity was found after the ^{60}Co irradiatons, an upper limit of 14 nbarns (95% confidence level) could be deduced for the photoexcitation cross section of

^{180m}Ta. In the irradiations with 4 MeV bremsstrahlung, a significant activity was observed; the deduced tantalum/indium cross section ratio of 7.4 ± 1.1 corresponds to an overall ^{180m}Ta photoexcitation cross section of 0.52 ± 0.20 mbarn. Our results are consistent with those of Richter [7], who found finite ^{180m}Ta$(\gamma,\gamma')^{180g}$Ta cross sections only above 2.7 MeV.

The now available results indicate the absence of activation levels in ^{180}Ta below 2.7 MeV; this has the consequence that ^{180m}Ta survives at temperatures below $5 \cdot 10^8$ K, which means, that it is practically stable under all reasonable s-process conditions [5] . The large cross section obtained at 4 MeV implies that 180mTa will be quickly destroyed by photodeexcitation at temperatures above $7 \cdot 10^8$ K. Since these results strongly support the s-process origin of ^{180m}Ta, the neutron capture flow in the mass region around A = 180 will be further investigated, including improved statistical model calculations of the ^{179}Ta and ^{180}Ta cross sections [8] .

[1]   E.Runte,   W.-D.Schmidt-Ott,   W.Eschner,   I.Rosner,   R.Kirchner, O.Klepper, K.Rykaczewski, Z. Phys. **A328**, 119 (1987).

[2]   M.Rayet, N.Prantzos, M.Arnould, Astron. Astrophys. **227**, 271 (1990).

[3]   W.M.Howard, B.S.Meyer, S.E.Woosley, Int. Symp. on *Nuclei in the Cosmos*, Baden, Austria, June 18-22 (1990).

[4]   S.E.Woosley, D.H.Hartmann, R.D. Hoffman, W.C.Haxton, Ap. J., **356**, 272 (1990).

[5]   F.Käppeler, H.Beer, K.Wisshak, Rep. Prog. Phys. **52**, 945 (1989).

[6]   K.Yokoi, K.Takahashi, Nature **305**, 198 (1983).

[7]   A.Richter, personal communication (1990).

[8]   Zs.Németh, F.Käppeler, G.Reffo, *Capture Gamma-Ray Spectroscopy 1990 and Related Topics*, ed. R.W.Hoff (in press).

*   Institute of Isotopes, Budapest, Hungary

1.1.6.   AN ANALYTICAL FORMULATION OF THE DOUBLE PULSE s - PROCESS MODEL

H.BEER

Recently low mass asymptotic giant branch (AGB) stars have been suggested as a site for the s-process nucleosynthesis [1-5] . The associated stellar models imply the successive burning of the $^{13}C(\alpha,n)$ and $^{22}Ne(\alpha,n)$ neutron sources giving rise to a double neutron burst during a thermonuclear instability in the He-shell. So far only numerical computer calculations were carried out to reproduce the solar abundances.

In this work general analytic solutions of this double pulse mechanism are developed. This analytical formulation of the double pulse s-process has the advantage of an understanding of the structure and the properties of the model from its general principles whereas numerical computer calculations can only supply evidence of the special cases considered.

We have developed solutions for a finite series of k double pulses as well as for the asymptotic limit, for an episodic double pulse s-process as well as for a distribution of neutron exposures [6]. Formulae for a finite series of pulses may be of importance in the study of the s-process of individual low mass asymptotic giant branch (AGB) stars with ongoing nucleosynthesis.

The result for a distribution of neutron exposure in the asymptotic limit is especially interesting for the study of solar s-process abundances.The double pulse solution $\sigma N_2^{\,P}$ is constructed from the unpulsed solutions $\sigma N_1^{\,*}$ and σN_2 (with equal total exposure) using the convient matrix notation :

$$\sigma N_2^P = \{ U - r \, exp \, (M_2 \, \Delta \iota_2) \, D_1 \, exp \, (M_1 \, \Delta \iota_1) \, D_2 \}^{-1}$$

$$\{ r_2 \, exp \, (M_2 \, \Delta \iota_2) \, D_1 \, | U - r_1 \, exp \, (M_1 \, \Delta \iota_1) \, | \sigma N_1^* \qquad +$$

$$[U - r_2 \, exp \, (M_2 \Delta \iota_2) \, \sigma N_2 \} \qquad\qquad (1)$$

where the bold symbols are vectors and matrices, respectively. The indices 1 and 2 stand for pulse one and two. U, D, M are unity, decay and coefficient matrices, repectively. The decay matrix accounts for the abundance changes in the interpulse phases by beta deay of the unstable isotopes. The matrix M contains the coefficients of the linear differential equations. σN is the vector of individulal $\sigma N(A)$ values. r is the fraction of overlap of successive double pulses with

$r = \exp[-\Delta\tau / \tau_0] = \exp[-(\Delta\tau_1 + \Delta\tau_2)/\tau_0] = r_1 r_2$ with $\Delta\tau_1$ and $\Delta\tau_2$ the respective exposures per pulse 1 and 2. τ_0 is the total average eposure. The unpulsed solution σN^*_1 stands for σN_1 with the capture cross sections renormalized to the temperature of the second pulse.

The double pulse model leads to consequences for the branched as well as the unbranched s-process and for the population of isomeric states by neutron capture. The consequences for the unbranched s-process and the population of isomers by neutron capture are new aspects of the s-process not included in the single pulse models.

Differences to a continous nucleosynthesis come from the pulsed nature of the neutron exposures and the key for an understanding of the new aspects is the size of the quantity $\beta_i \Delta\tau$. Independence from the pulsed nature of the exposure $\Delta\tau$ is guaranteed if for all nuclei i participating in the branching

$$\beta_i \Delta\tau \gg 1 \tag{2}$$

is obtained, where $\beta_i = \sigma_i/(1 - f)$ if σ_i is the branch point isotope (and f the branching factor) else $\beta_i = \sigma_i$. The condition (2) applied to equation (1) for pulse 1 gives

$$\sigma N^P_2 \approx |U - r_2 \exp(M_2 \Delta\tau_2)| \sigma N_2 + r_2 \exp(M_2 \Delta\tau_2) D_1 \sigma N^*_1 \tag{3}$$

which is approximately

$$\sigma N^P_2 \approx [U - r_2 \exp(M_2 \Delta\tau_2) D_1]^{-1} \{U - r_2 \exp(M_2 \Delta\tau_2)\} \sigma N \tag{4}$$

if we assume $\sigma N_1^* = \sigma N_2 = \sigma N$, i.e. the same neutron density, temperature and electron density for pulse one and two. The double pulse model behaves as a single pulse model if the first pulse is characterized by a sufficiently large exposure so that the pulsed nature of the s-process is visible only from the second pulse. There is, however, one decisive difference to a true single pulse model. The gross structure of the σN curve is due to the first pulse, whereas some necessary additional fine tuning at branchings (e.g. [85]Kr) results from the second pulse. In the single pulse model both these properties have to be fulfilled by the succession of the one pulse.

In contrast to the single pulse model the double pulse model is effective outside branchings as well. For the unbranched s-process nucleosynthesis with $D_{1,2} = U$ we derive from equation (1) for an individual isotope $^A Z$:

$$\sigma N_2^P (A) = F_1 \sigma N_1^* (A) + F_2 \sigma N_2(A) \tag{5}$$

with
$$F_1 = 1 - F_2$$

$$F_2 = \frac{1 - r_2\, exp\, [- \sigma\, (A\, , kT_2)\, \Delta\iota_2]}{1 - r\ exp\, \{ - [\, \sigma\, (A\, , kT_2)\, \Delta\iota_2 + \sigma\, (A\, , kT_1)\, \Delta\iota_1]\, \}}$$

i.e. the influence of pulse one and two on the final abundance of isotope $^A Z$ depends on the respective exposures as well as on the capture cross section at kT_1 and kT_2, respectively.

The surprising consistency in the analysis of most of the s-process branchings using a single pulse model [7] was found to be due to the fact that the exposure per pulse for first and second pulse must be large enough that there is no or only a weak sensitivity to the pulsed nature of the exposures. If the equations (2) are fulfilled for $\Delta\iota_1$ and for $\Delta\iota_2$ as well then equation (1) leads to exp $(M_{1,2}\,\Delta\iota_{1,2}) \approx 0$ and, therefore, to $\sigma N_2^P \approx \sigma N_2$. The exposure $\Delta\iota_1 \approx 0,15$ mbarn^{-1} is necessary to understand the average exposure $\iota_0 = 0.30$ mbarn^{-1} [7] in connection with an overlap factor $r \approx 0.6$. For $\Delta\iota_2$ it was found from the agreement of most of the branchings with the approximations of the single pulse model that its exposure must be larger than 10^{-3} mbarn^{-1}. The synthesis of ^{176}Hf where the ^{176}Lu^m isomer is involved requires an exposure greater than 10^{-3} mbarn^{-1} as well. But if we assume a significant s-process contribution to the rare ^{115}Sn abundance then it cannot be much greater than 10^{-3} mbarn^{-1}, i.e. 2 to 3 $\cdot 10^{-3}$ mbarn^{-1}.

The ^{85}Kr branching turned out to be of great complexity. The branching keeps memory of the first and second pulses, and some cross sections are not propotional $\sim(kT)^{-0.5}$. In the unbranched s-process nucleosynthesis the isotopes with magic neutron numbers can keep memory of the first pulse if the Maxwellian averaged capture cross sections are characterized by a temperature dependence significantly different than $T^{-0.5}$. The double pulse structure of the s-process can show up as well at nuclei with isomeric states which are significantly populated by neutron capture, decay by beta transition and the population of which is not destroyed at the temperature of the first pulse.

[1]   R.Gallino, *The Evolution of Peculiar Red Giant Stars*, IAU Symposium No. 106, eds H.Johnson, B.Zuckerman (Cambridge, Cambridge University Press) p.176 (1989).

[2]   R.Gallino, M.Busso, G.Picchio, C.M.Raiteri, A.Renzini, Ap. J. (Letters),
        334, L45 (1988).
[3]   D.E.Hollowell, I.Iben, jr., Ap. J. **340**, 966 (1989).
[4]   D.E.Hollowell, I.Iben, jr., Ap. J. **349**, 208 (1990).
[5]   F.Käppeler, R.Gallino, M.Busso, G.Picchio, C.M.Raiteri, Ap. J., **345**,
        630 (1990).
[6]   H.Beer, Ap. J. (1991a) in press.
[7]   H.Beer, Ap. J. (1991b) in press.

1.1.7.   THE CALCULATION OF MAXWELLIAN AVERAGED CAPTURE CROSS SECTIONS VS. TEMPERATURE

H.BEER, F.VOSS

The quality of s-process calculaions depends strongly on the reliability of the input data. Three groups of data are needed : (1) stellar reaction rates of the nuclei on the synthesis path, (2) beta half lives of certain unstable species; perhaps vs. temperature kT and electron density n_e [1], and (3) s-process abundances, e.g. from the solar abundance distribution [2]. The most important group of data is the group of stellar reaction rates or Mawellian averaged capture cross sections.

Capture cross sections are determined by activation or time-of-flight (TOF) measurements or statistical model calculations. The final goal of these efforts is a Maxwellian averaged capture cross section $<\sigma>$ as a function of temperatute kT:

$$\langle\sigma\rangle(kT) = (2/\sqrt{\pi})(kT)^{-2}\int_0^\infty \sigma_{n\gamma}(E)\, E \exp(-E/kT)\, dE \tag{1}$$

where $\sigma_{n\gamma}(E)$ is the excitation function vs. neutron energy E. $<\sigma>$ is needed in the interval 5 keV$<$kT$<$100 keV. A characteristic of the (n,γ) reaction is the absence of a reaction threshold. Therefore, the computation according to equation (1) required $\sigma_{n\gamma}$ over the whole neutron energy range especially down to the thermal cross section at 0.025 eV to obtain good accuracies in $<\sigma>$(kT).

Experimental data of $\sigma_{n\gamma}$, if they are complete, consist in a resolved resonance part, where the resonance parameters are specified and in an unresolved resonance part, where the excitation function $\sigma_{n\gamma}$ is given [3,4]. In the unresolved part the integration according to Eq. (1) was directly performed. In the resolved

resonance part the integration over the resonances was carried out using the Breit Wigner formula. Narrow resonances can also be treated as delta functions [5]. Regions, where $\sigma_{n\gamma}$ is unknown have been completed by statistical model calculations which required average level density, radiation width and strength functions. Special treatment required the integral in eq. (1) at the integration limits. The unresolved resonance part of the excitation function was extrapolated, if necessary, to higher neutron energies with an 1/E energy dependence [6]. The lower limit demanded an understanding of the capture cross section at thermal energy (E = 0.025 eV).The thermal cross section is analyzed [4], in general, as the sum of resonance tails from positive and negative resonances (bound states). The two parts were treated separately in the integration. Sometimes, especially for light isotopes, the thermal cross section contains a direct capture contribution insted of a contribution from bound states. This required a different treatment than bound state capture.
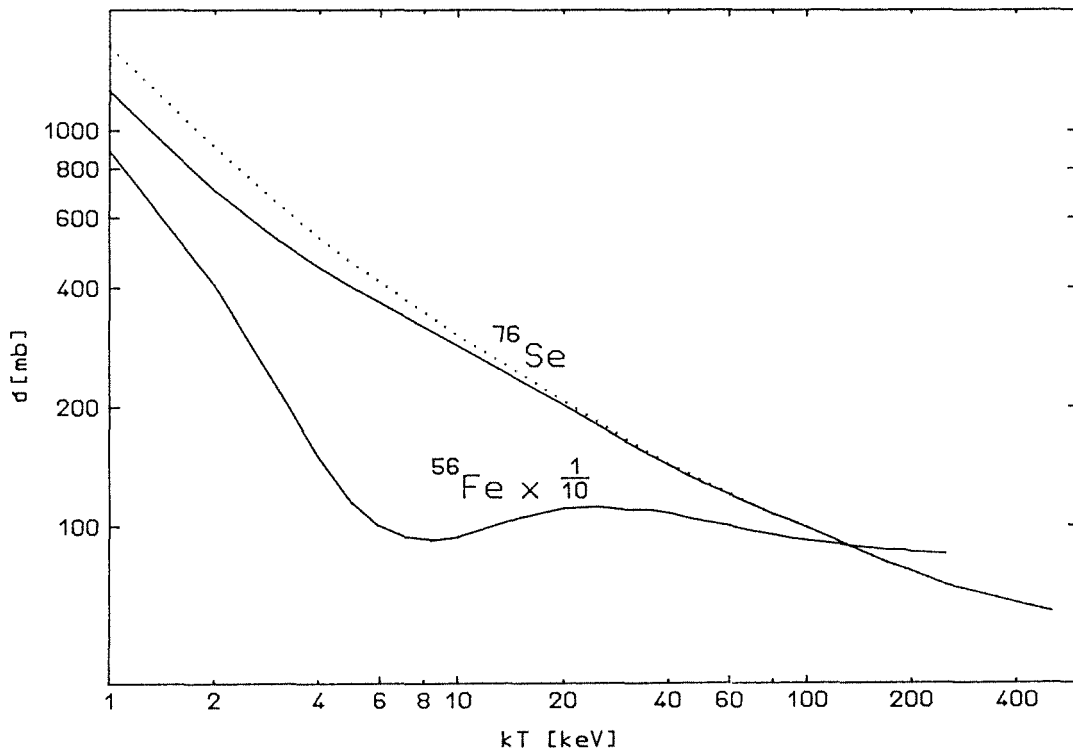
Fig.1   Maxwellian averaged capture cross sections of ^{56}Fe and ^{76}Se vs. temperature

^{76}Se has a typical shape for a Maxwellian averaged capture cross section : $<\sigma> \sim (kT)^{-b}$ where b$\sim$0.4 - 0.8 . In the computation of the dotted curve (Fig. 1) direct capture is assumed instead of bound states capture for the interpretation of the thermal cross section. At kT = 10 keV the solid and dotted curves are different by

6%. The Maxwellian averaged cross sections of a number of isotopes is quite different from a temperature dependence $<\sigma> \sim (kT)^{-b}$. ^{56}Fe is shown as an example (Fig. 1). Each individual isotope required special consideration and calculation from the existing data.

An additional temperature dependence of $<\sigma>$ has been taken into account for nuclei with low lying levels significantly populated at $kT = 5 - 100$ keV so that excited state capture is non neglible. This effect was large, e.g. for ^{187}Os but also important for some even-even s-only nuclei with a 2^+ first excited state, e.g. ^{154}Gd, ^{160}Dy, ^{170}Yb etc..

[1]   K.Takahashi, K.Yokoi, Atomic Data and Nucl. Data Tables **36**, 375 (1987).

[2]   E.Anders, N.Grevesse, Geochim.Cosmochim. Acta **53** ,197 (1989).

[3]   V. McLaine, C.L.Dunfort, P.F.Rose, Neutron Cross Sections, Vol.2, Academy Press New York (1988).

[4]   S.F.Mughabghab, M.Divadeenam, N.E.Holden, Neutron Capture Cross Sections, Vol.1,Part A and B, Academy Press New York (1981).

[5]   R.L.Macklin, J.H.Gibbons, Rev. Mod. Phys. **37**, 166 (1965).

[6]   D.Kompe, Nucl. Phys. A**133**, 513 (1969).

1.1.8.   THE FUNDAMENTAL s-PROCESS PARAMETERS FROM A PHENOMENOLOGICAL MODEL

H.BEER

The new data basis of Maxwellian averaged capture cross sections vs. temperature (see contribution 1.1.7.) is used for an overall s-process analysis to obtain improved fundamental astrophysical parameters . Fig. 1 shows the result of this analysis. We can distinguish two groups of paramaters according to the structures exhibited by the empirical data. There is a gross structure characterized by flat portions and precipices at magic neutron numbers 50, 82, 126 and fine structure at individual isotopes, e.g. ^{152}Gd, ^{164}Er. The gross structures suggest an s-process with an exponential exposure distribution, an irradiation by a series of discrete neutron bursts (main component), and due to the extra steepness for A $<$ 90 a superimposed single exposure component (weak component). The fine structures are interpreted as s-process branchings. With respect to these
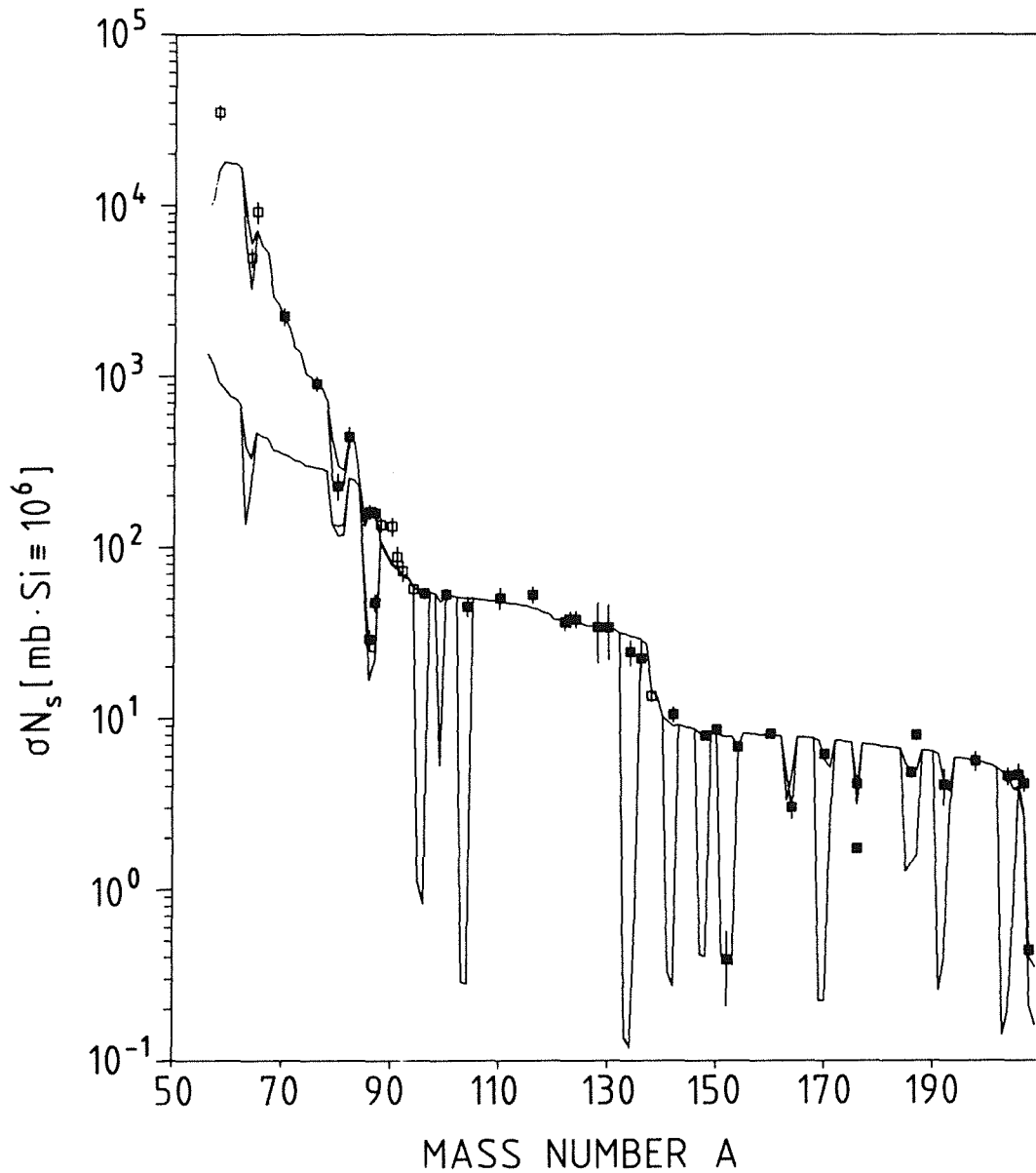
Fig. 1   The σN calculation as a function of mass number. The main component s-process curve is plotted from A=56 to 209. In the region A= 56-90 the composite curve differs from the main component curve due to the superposition of the weak component. Not all empirical data points shown are used to adjust the theoretical curve. Data points at the magic neutron numbers 50 and 82 (^{88}Sr, the Zr isotopes and ^{138}Ba) as well as the data points for ^{58}Fe,^{64}Ni and ^{65}Cu are indicated as open symbols and shown only for comparison. Other empirical data too low (^{176}Lu) or too high (^{187}Os, ^{206,207,208}Pb) are affected by long lived radioactive decay and in the case of ^{206,207,208}Pb contain extra r-process contributions from transbismuth nuclei.

features two groups of data can be distinguished. From the gross structures we obtained average exposure, average number of captured neutrons per iron seed and the fraction of iron seed nuclei, from the fine structures neutron density, temperature, electron density and pulse duration of the s-process. The following astrophysical parameters for the main component were found :

Fraction of iron seed : $F_{Fe} = (0.063 \pm 0.004)\%$,

Average number of captured neutrons per ion seed :

$AVN^H = \Sigma_A (A-56) [N^A_S - N^A(seed)] / N^{56}(seed) = 9.20 \pm 0.53$,

Average time integrated neutron flux :

τ_0 (kT = 25 keV) = (0.276 ± 0.0098) mbarn^{-1} ,

τ_0 as a function of kT in the interval kT = 10 - 30 keV :

$\tau_0(kT) = \tau_0(25) (kT / 25)^{0.518}$,

Temperature : kT = (25 ± 2) keV ,

Neutron density : $n_n = (2.0 + 1.4/-0.8)10^8$ cm^{-3} ,

Pulse width : $\Delta t = (16 + 15.5/-9.2)$ yr .

The technique to determine neutron density n_n ,temperature kT, electron density n_e. and pulse width Δt has been improved. As these parameters are interrelated a four parameter X^2 minimization has been carried out

$$X^2 |n_n, kT, n_e, \Delta t| \sim \sum_i w_i |\sigma N_{obs} - \sigma N_{cal}|^2 / |\Delta(\sigma N_{obs})|^2$$

The sum is over the branchings, w_i is a weight taking into account the different accuracies of the cross sections of the branch point isotopes. σN_{obs} and σN_{cal} are connected with the s-only isotope in the branching.

The branchings were described satisfactorily with constant values of these quantities, but, of course, in reality n_n, kT, and n_e are time dependent. Therefore, the values determined represent actually effective values. A simple time dependence would be $n_n(t) = n_0$ for $0 \leq t < t_0$ and $n_n(t) = n_0 \exp(-t/\tau_p)$ for $t \geq t_0$. The effective neutron density n_n^{eff} can be calculated n_n^{eff} is dependent on the specific parameters of the branching :

$$n_n^{eff} = n_0 \frac{t_0(1 - f_1^m - f_2^m) + \tau_p\{1 - (f_1^m + f_2^m)(1 - f_1^m - f_2^m)^{-1} ln|(f_1^m + f_2^m)^{-2}|\}}{t_0(1 - f_1^m - f_2^m) + \tau_p ln|(f_1^m + f_2^m)^{-1}|} \tag{1}$$

where we have defined $f_{1,2}^m = \lambda_{\beta 1,2}/(\lambda_{\beta 1} + \lambda_{\beta 2} + n_0 \sigma v_T)$ with σ, $\lambda_{\beta 1}$ and $\lambda_{\beta 2}$ the capture cross section, the beta and electron capture decay rate of the branch point isotope, respectively. v_T is the thermal velocity. Equation (1) is for three exit channels.

Branch point isotope	s-only isotope in the branching	$n_n^{eff} 10^8$ (cm^{-3})	t_{tot}^{eff} (yr)
^{85}Kr	$^{86,87}Sr$	2.3	4.6
^{95}Zr	^{96}Mo	3.0	0.25
^{148}Pm	^{148}Sm	3.5	0.019
^{151}Sm	^{152}Gd	1.5	0.22
^{163}Dy	^{164}Er	2.6	0.17
^{170}Tm	^{170}Yb	2.3	0.18
^{185}W	^{186}Os	2.8	0.18
^{192}Ir	^{192}Pt	2.6	0.12

Tab. 1   Effective neutron densities and total effective life times of important branch point isotopes for a neutron density $n_n(t) = n_0 \exp(-t/\tau_p)$ with $n_0 = 6 \cdot 10^8$ cm^{-3} and $\tau_p = 5$ yr, a temperature $kT = 26$ keV, and an electron density $n_e = 1.9 \cdot 10^{27}$ cm^{-3}. It should be pointed out that the final abundance pattern of the s-only isotopes is influenced frequently by additional side branchings and that in some cases a radiogenic contribution (e.g. ^{170}Tm) has to be taken into account. This might explain that in the average n_n in the table is higher than $2 \cdot 10^8$ cm^{-3}.

The following discussion is limited to the special case $t_0 = 0$, $n_n(t) = n_0 \exp(-t/\tau_p)$. In the stellar model of Gallino [1] such a neutron density profile is considered to be responsible for establishing the abundance patterns in the s-process branchings [2], although the model itself is much more complex. The s-process analysis with neutron density $n_n(t) = n_0 \exp(-t/\tau_p)$ means to carry out the calculations with effective values (integration over the time dependent neutron density) and adjust to the maximum neutron density n_0. A best fit of the branchings was obtained for $n_0 = 6 \cdot 10^8$ cm^{-3}, $kT = 26$ keV, and $n_e = 1.9 \cdot 10^{27}$ cm^{-3}. The effective neutron densities of various important branchings are given in Tab. 1. These values are all within the quoted uncertainty of the value $n_n = (2.0 + 1.4/-0.8) \cdot 10^8 cm^{-3}$ from the

calculation with the constant neutron density assumption. The same holds true for the new values of kT and n_e. It should especially be pointed out that the neutron density profile $n_n(t) = n_0 \exp(-t/\tau_p)$ allows for an estimate of the maximum neutron density, n_0, but not for τ_p, the decay constant (n_n^{eff} in the equation (1) is independent of τ_p).

The above considerations on effective neutron density are valid if the time variation of the neutron density, expressed by τ_p, is much slower than the effective time duration of the branch point isotope t_{tot}^{eff}. The branching must have time to adjust quickly to the variations of $n_n(t)$. This condition stated as an inequality is given by:

$$\tau_p \gg t_{tot}^{eff} = [\lambda_n^{eff} + \lambda_\beta]^{-1} = [0.5\, n_0 \sigma v_T + \lambda_\beta]^{-1} \tag{2}$$

If τ_p is chosen greater than about 2 yr the inequality (2) is fulfilled for the studied branchings except for the [85]Kr branching, where an effective time $t_{tot}^{eff} = 4.6$ yr comparable to τ_p is copmuted (Tab. 1). The [85]Kr branching alone is, therefore, dependent on τ_p [3], and was used for its determination. The pulse width $\Delta t = \tau_p$ for the neutron density spike profile was found to be 5 yr. The effect of the pulses on the other branchings is too small to be detected, they have lost memory of the duration of the pulse but not on maximum neutron density. Similar cases like [85]Kr are [63]Ni, and [79]Se, but the effects are masked by the weak s-process component. The most sensitive branchings next to [85]Kr would be the [151]Sm branching [4] and [95]Zr.

[1]   R.Gallino, *The Evolution of Peculiar Red Giant Stars*, IAU Symposium No. 106, eds H.Johnson, B.Zuckerman (Cambridge, Cambridge University Press) p.176 (1989).

[2]   F.Käppeler, R.Gallino, M.Busso, G.Picchio, C.M.Raiteri, Ap. J., **354**, 630 (1990).

[3]   H.Beer, R.L.Macklin, Ap. J. **339**,962 (1989).

[4]   H.Beer, R.L.Macklin, Ap. J. **331**,1047 (1988).

THE s - PROCESS CROSS SECTIONS OF ^{120}Sn, ^{121}Sb, ^{123}Sb, AND ^{128}Te FOR A STUDY OF POSSIBLE BRANCHINGS AT A = 121, 122

W.SCHANZ, G.RUPP, F.KÄPPELER

The s-process neutron capture flow in the mass region $120 < A < 126$ is characterized by possible branchings at $A = 121$, 122 (Fig. 1). Due to the short half-lives of the branch point isotopes ^{121}Sn and ^{121}Sb, these branchings are significant only for the comparably high neutron densities predicted by stellar models. In this case, the s-isotopes ^{122}Te and ^{123}Te would be partly bypassed by the neutron capture flow, and only the third s-isotope, ^{124}Te, would experience the total exposure. The importance of accurate Te cross sections for the definition of these branchings is addressed in contribution 1.1.10. to this report. In addition, improved cross sections of other relevant nuclei were required for a quantitative branching analysis.

In a series of activation measurements, the stellar cross sections of ^{120}Sn, ^{121}Sb, ^{123}Sb, and ^{128}Te were determined. The irradiations were carried out in the neutron field obtained via the ^{7}Li(p,n)^{7}Be reaction at a proton energy of 1912 keV, that is known to yield the proper stellar average cross sections for a thermal energy of
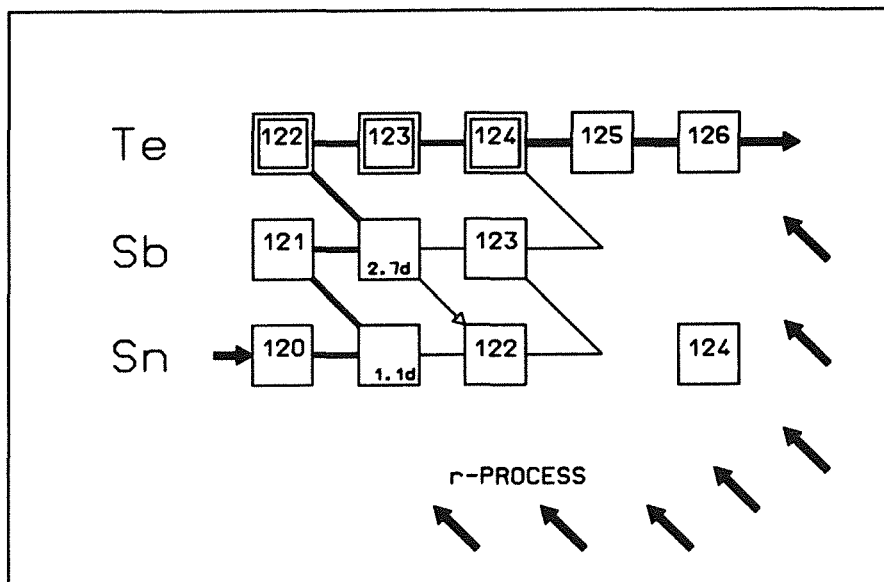
Fig. 1   The s-process flow between ^{120}Sn and ^{126}Te with the possible branchings at A = 121,122 .

kT = 25 keV [1,2]. Repeated activations with different experimental parameters (neutron flux, sample thickness and diameter) allowed for investigation of systematic uncertainties. In the case of the Sb isotopes, the induced activities were determined by gamma counting via the decay lines at 564 keV ([122]Sb) and at 603 keV ([124]Sb) with a calibrated HPGe detector. Since no gamma-rays are emitted in the decay of the other isotopes, the induced activities had to be measured via the beta decay electrons, instead. Accordingly, thin samples of isotopically enriched material were irradiated, which were then counted in a 4π electron spectrometer with an efficiency of 97%. An example of such an electron spectrum is given in Fig. 2 . By the simultaneous irradiation of appropriate gold foils, all cross sections were measured relative to the standard cross section of [197]Au [2] . For the final results, experimental uncertainties between 2.7 and 3.8% could be achieved. The comparison with previous data shows large discrepancies of up to 50%.
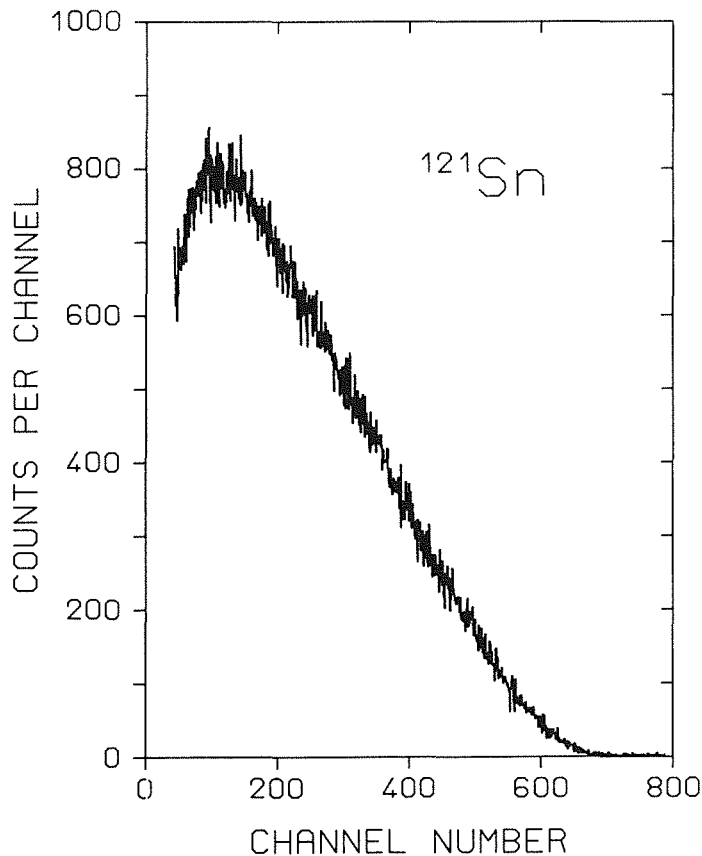
Fig. 2
The electron spectrum from the decay of [121]Sn ($t_{1/2} = 27h$) measured with the 4π electron spectrometer.

The description of the s-process in the mass range $120 < A < 126$ with the classical approach [3] yields practically no branchings at A = 121, 122, thus confirming the σN equality for the s-only isotopes [122]Te, [123]Te, and [124]Te predicted by the 'local approximation'. However, the currently best stellar model for the s-process, i.e. for helium shell burning in low mass AGB stars of low metallicity ([4] and references therein) leads, indeed, to significant branchings, resulting in 5%

lower σN values for ^{122}Te and ^{123}Te than for ^{124}Te. The consequences of this discrepancy between the classical approach and the stellar model are discussed in contribution 1.1.10.

[1]   H.Beer, F.Käppeler, Phys. Rev. C 21, 534 (1980).

[2]   W.Ratynski, F.Käppeler, Phys. Rev. C 37, 595 (1988).

[3]   F.Käppeler, H.Beer, K.Wisshak, Rep. Prog. Phys. 52, 945 (1989).

[4]   R.Gallino, *The Evolution of Peculiar Red Giant Stars*, IAU Symposium No. 106, eds H.Johnson and B.Zuckerman (Cambridge, Cambridge University Press) p.176 (1989).

1.1.10.   MEASUREMENTS OF keV NEUTRON CAPTURE CROSS SECTIONS OF ^{122,123,124,125,126}Te WITH THE KARLSRUHE 4π BARIUM FLUORIDE DETECTOR

K.WISSHAK, F.VOSS, F.KÄPPELER, G.REFFO*

The neutron capture cross sections of ^{122,123,124,125,126}Te have been measured in the neutron energy range from 10 to 200 keV using the Karlsruhe 4π Barium Fluoride Detector for the registration of capture gamma-ray cascades. Neutrons were produced via the ^{7}Li(p,n)^{7}Be reaction by bombarding metallic Li targets with the pulsed proton beam of a 3.75 MV Van de Graaff accelerator. The neutron energy was determined by time of flight. The flight path of the experiment was 78 cm, the time resolution 1 ns. The cross sections were determined relative to the standard cross section of gold.

Three independent runs have been performed with maximum neutron energies of 70, 100 and 200 keV, respectively. While runs with low maximum neutron energies offer optimum signal to background ratio in the most important energy region around 30 keV (see below), the data measured around 200 keV gave optimum accuracy for the absolute normalization of the cross section ratio. The threshold in the sum energy of the 4π detector was varied between 1.8 and 2.5 MeV. In case of the low threshold, the absolute efficiency for capture events was larger than 95% for the even and larger than 98% for the odd tellurium isotopes. Highly enriched metallic samples were used with masses between 0.5 g (^{123}Te) and 4 g (^{126}Te) .
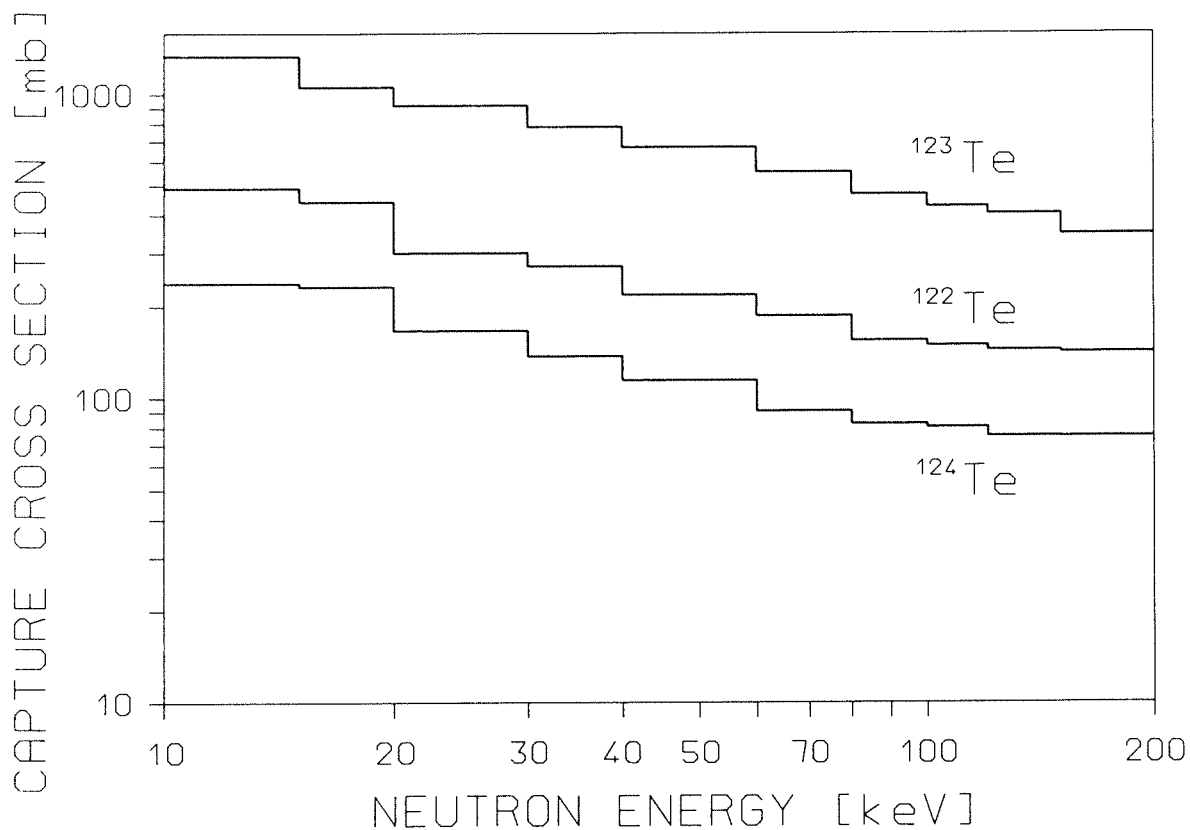
Fig. 1   Preliminary results for the neutron capture cross section of ^{122,123,124}Te in the neutron energy range from 10 to 200 keV.

Preliminary data for the capture cross sections of ^{122,123,124}Te are given in Fig.1 . The experimental cross section ratios have been converted into absolute values using the gold standard cross section from literature as described in [1] .The statistical uncertainty of the cross sections for the energy bins of Fig. 1 is about 1% above 20 keV. The systematic uncertainties are not yet evaluated completely but are expected to be well below 1% for the cross section ratios. The uncertainty of the gold cross section is 1.5% [1] .

The isotopes of tellurium play an important role in s-process studies. It is the only element with three s-isotopes, i.e. ^{122,123,124}Te. Since the isotopic abundances are known with uncertainties of 0.1%, accurate stellar cross sections of these isotopes offer the possibility to check the 'local approximation' predicted by the classical s-process model that the product of s-abundance and stellar cross section is constant for neighbouring isotopes. A preliminary evaluation of the Maxwellian averaged cross sections at kT = 30 keV was made using the data of Fig. 1, the result of our experiments with Moxon-Rae detectors in the energy range from 1 to 10 keV (see contribution 1.1.9.) as well as the data of Macklin and Winters above 200 keV [2]. The ratios $N\sigma(^{122}$Te$)$ / $N\sigma(^{124}$Te$)$ and $N\sigma(^{123}$Te$)$ / $N\sigma(^{124}$Te$)$ found in this way agreed with the prediction of the classical model to better than 1%. Since

the present uncertainties are about five times smaller than those of previous experiments, this result is significant and - if finally confirmed - would question stellar s-process models with comparably high neutron fluxes. These models lead to branchings of the s-process path at ^{121}Sn and ^{122}Sn, which would reduce the No-values of ^{122,123}Te by about 5% compared to ^{124}Te.

[1]   K.Wisshak, F.Voß, F.Käppeler, G.Reffo, Phys. Rev. C42, 1731 (1990).
[2]   R.L.Macklin, R.R.Winters, report ORNL-6561 Oak Ridge National Laboratory (1989).

*   E.N.E.A. Bologna, I-40138 Bologna, Italy

1.1.11.   NEUTRON CAPTURE CROSS SECTIONS OF ^{122}Te , ^{123}Te AND ^{124}Te AT LOW ENERGIES

Y.XIA, T.W.GERSTENHÖFER, S.JAAG, F.KÄPPELER, G.REFFO*, K.WISSHAK

The preceding contribution presents (n,γ) cross section measurements on 5 tellurium isotopes in the energy range from 10 to 200 keV. The experimental uncertainties of $\leq 1\%$ for cross section ratios are essential for the discussion s-process nucleosynthesis in the mass region between A = 120 and 130. Possible branchings in the neutron capture path at A = 121, 122 being excluded by these data would have important consquences for the stellar models of Red Giant stars. The currently favoured s-process model is helium shell burning in low mass stars of low metallicity, which was shown to reproduce the observed s-abundances fairly well [1,2]. Since this model describes a scenario, where most of the neutron exposure takes place at rather low temperatures of $\sim 1.5 \cdot 10^8$ K, corresponding to a thermal energy of kT = 12 keV, the range covered by the 4π BaF$_2$ detector in contribution 1.1.10. needs to be extended to lower neutron energies.

For this purpose, we have used a setup of Moxon-Rae detectors (see contributions 1.1.3. and 1.1.4.), which yields sufficient sensitivity down to energies of 1 keV. The measurements were carried out with a flight path of 20 mm under identical conditions as described in the above contributions. In this way, we were able to determine the differential (n,γ) cross sections in the energy range from 1 to 100 keV with statistical uncertainties smaller than 2%. Normalization

to the results obtained with the 4π BaF_2 detector in the region of overlap yields then a reliable cross section extrapolation to 1 keV neutron energy.

In addition to the Moxon-Rae detectors, the setup includes a [6]Li glass detector under zero degree with respect to the proton beam, which is normally used as a neutron monitor. With that detector it was possible to determine the total neutron cross sections for these isotopes in the present experiment as well. These data are important for the analysis of the results obtained with the 4π BaF_2 detector, since they are required for evaluating the respective neutron scattering corrections [3]. Up to now, sufficiently complete total cross sections for the tellurium isotopes were not available in literature. The present results, which exhibit uncertainties of typically 5% are given in Tab. 1 .

Neutron energy interval	Total cross section (mbarns)		
(keV)	[122]Te	[123]Te	[124]Te
1 - 3	8044	14628	10214
3 - 5	7488	11783	7392
5 - 10	7664	8800	5946
10 - 15	6327	8853	5665
15 - 20	6511	9102	6042
20 - 30	6263	8400	6277
30 - 40	6051	8114	6198
40 - 60	5862	7812	6131
60 - 80	5821	7355	6000
80 - 100	5555	6936	6058

Tab.1   The total neutron cross sections of [122]Te, [123]Te, and [124]Te.

[1]   R.Gallino, The Evolution of Peculiar Red Giant Stars, IAU Symposium No. 106, eds H.Johnson, B.Zuckerman (Cambridge, Cambridge University Press) p.176 (1989).

[2]   F.Käppeler, R.Gallino, M.Busso, G.Picchio, C.M.Raiteri, Ap. J., 345, 630 (1990).

[3]   K.Wisshak, F.Voss, F.Käppeler, G.Reffo, report KfK 4674, Kern-
           forschungszentrum Karlsruhe (1990); Phys. Rev. C42, 1731 (1990).

*   E.A.N.A Bologna, I-40138 Bologna, Italy

1.1.12.   RELAXATION IN NUCLEI AND EOS

P.DOLL

We are investigating the dependence of the relaxation of a deeply bound nucleon hole in a nucleus like ^{208}Pb on the parameters like effective mass m* and spreading width Γ. While the energy dependence of m* is assumed to follow the dispersion relation approch from Mahaux and Ngo [1], the spreading width we assume as an experimental observable. In exclusive electron knockout experiments [2], the spreading width of deeply bound hole states in ^{208}Pb follows an empirical description for Γ as deduced by Brown and Rho [3] and seems to approach a limiting value with increasing binding energy for the nucleon. A large spreading width corresponds to a fast relaxation in nuclear matter, however, a large sound velocity is related to a large incompressibility K. Our preliminary
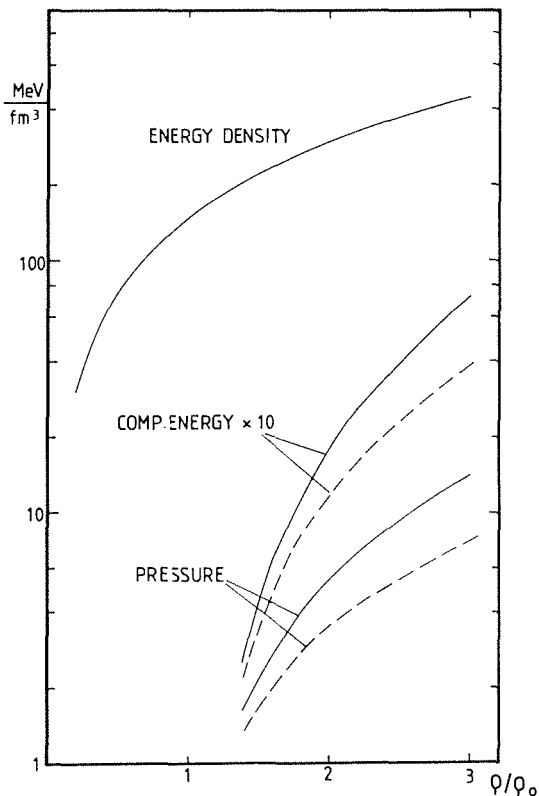
Fig. 1   Total energy density, compression energy and pressure as a function of particle density (solid curves). A modified density dependence accounts for non-central effects (dashed curves).

value comes out to be around 200 MeV/fm^{-3}. In the parametrization of the compressional energy for $\rho > \rho_0$ as provided by the form used by Baron et al [4], we have calculated in Fig. 1 the total energy density and pressure as a function of ρ/ρ_0 and for an adiabatic index $\gamma = 2$. The compression energy is separately shown. Since the effective mass is known to cover a good fraction of the mean field dependence, and therefore, exhibiting a strong variation with momentum, we have parameterized a dependence of the spreading width on the density, which reduces like non-central interactions the compression energy and pressure as shown in the Fig. 1 by the dashed curves. This behaviour is interesting in the context, that a softening of the equation-of-state (EOS) of neutron-rich nuclear matter at high density and the effects of general relativity play a crucial role in generating successful and prompt supernovae explosions [4].

[1]   C.Mahaux, H.Ngô, Nucl. Phys. A431, 486 (1984).

[2]   L.Lapikás, NIKHEF Preprint EMIN 89-01 .

[3]   G.E.Brown,M.Rho, Nucl. Phys. A372,397 (1981).

[4]   E.Baron, J.Cooperstein, S.Kahana, Phys. Rev. Lett. 55, 126 (1985).

1.1.13.A s-PROCESS NUCLEOSYNTHESIS: CLASSICAL APPROACH AND ASYMPTOTIC GIANT BRANCH MODELS FOR LOW-MASS STARS [1]

F.KÄPPELER, R.GALLINO, M.BUSSO, G.PICCHIO, C.M.RAITERI

A critical comparison is made between the results of s-process nucleosynthesis obtained with the phenomenological classical approach and a stellar model for helium shell burning in low-mass stars. For the first time, close agreement is found between the abundances determined by the classical analysis and the results of a stellar model. The calculated abundances are found in good agreement with the s-process yields observed in solar material, and the corresponding quantities characterizing the neutron exposure are outlined in detail. Emphasis is laid on the information deduced from the abundance patterns in s-process branchings, i.e., neutron density and temperature. Despite the conceptual differences between the steady flow approximation of the classical approach and the dynamical environment of thermal pulses in low-mass stars, the results of both models are quite similar, but still obscured by the present uncertainties of the nuclear input data; further improvements are required to quantify the trends of the true physical conditions during the s-process which start to emerge from the above studies.

1.1.14.A THE STELLAR NEUTRON CAPTURE CROSS SECTIONS OF ^{94}Zr AND ^{96}Zr [1]

K.A.TOUKAN, F.KÄPPELER

The neutron capture cross sections of ^{94}Zr and ^{96}Zr have been determined relative to that of gold by means of the activation method. The samples were irradiated in a quasi-stellar neutron spectrum for kT = 25 keV using the ^{7}Li(p,n)^{7}Be reaction near threshold. Variation of the experimental conditions in different activations and the use of different samples allowed for the reliable determination of corrections and the evaluation of systematic uncertainties. The

resulting stellar cross sections can be given with uncertainties around 4%, considerably lower than previous data. The new data made it possible for the first time to deduce the s-process neutron density from the branching at ^{95}Zr.

1)   published in : Ap. J., **348**, 357 (1990)

1.1.15.A ^{88}Sr AND ^{89}Y: THE s-PROCESS AT MAGIC NEUTRON NUMBER N = 50 [1]

F.KÄPPELER, W.R.ZHAO, H.BEER, U.RATZEL

The neutron capture cross sections of ^{88}Sr and ^{89}Y were measured in a quasi-stellar neutron spectrum for kT = 25 keV via the activation method. Relevant systematic uncertainties were determined experimentally by repeated activations under different conditions and with different samples. Gold was used as a cross section standard. The resulting stellar cross sections for kT = 30 keV are 6.13 ± 0.18 mbarn for ^{88}Sr and 19.0 ± 0.6 mbarn for ^{89}Y. The partial cross section ^{86}Sr(n,γ)^{87m}Sr was measured to 48.1 ± 1.2 mbarn. Compared to previous data, the associated uncertainties are reduced by factors of 3 and 5, respectively. The implications for s-process nucleosynthesis around magic neutron number N = 50 are discussed in the light of new information on neutron density and temperature.

1)   published in : Ap. J., **355**, 348 (1990)

1.1.16.A THE s-PROCESS BRANCHINGS AT ^{185}W AND ^{186}Re [1]

F.KÄPPELER, S.JAAG, Z.Y.BAO, G.REFFO

The stellar neutron capture cross sections of ^{185}Re and ^{187}Re have been measured for kT = 25 keV via the activation technique. The resulting cross sections are $<\sigma v>/v_T = 1677 \pm 65$ mbarns and 1269 ± 62 mbarns for ^{185}Re and ^{187}Re, respectively. These data have been complemented by calculated cross sections for the unstable isotopes ^{185}W and ^{186}Re, using statistical model

parameters that were derived from a consistent systematics for the neighbouring nuclei. This information represents a considerably improved basis for s-process analyses in the mass range $184 < A < 188$. With the classical approach, a mean neutron density for the s-process of $n_n = (4.1 + 1.2/-1.1) \cdot 10^8$ cm $^{-3}$ could be derived from the branchings at ^{185}W and ^{186}Re. The corresponding s-process abundances are in good agreement with those obtained in model calculations for low-mass asymptotic giant branch stars. The latter calculations also provide evidence that the chronometric pair ^{187}Os / ^{187}Re may still be a useful cosmic clock.

1)   published in : Ap. J., **366**, 000 (1991)

1.1.17.A   THE KARLSRUHE 4 π BARIUM FLUORIDE DETECTOR [1]

K.WISSHAK, K.GUBER, F.KÄPPELER, J.KRISCH, H.MÜLLER, G.RUPP, F.VOSS

A new experimental approach has been implemented for accurate measurements of neutron capture cross sections in the energy range from 5 to 200 keV. The Karlsruhe 4π barium fluoride detector consists of 42 crystals shaped as hexagonal and pentagonal truncated pyramids forming a spherical shell with 10 cm inner radius and 15 cm thickness. All crystals are supplied with reflector and photomultiplier, thus representing independent gamma-ray detectors. The energy resolution of the 4π detector is 14% at 662 keV and 7% at 2.5 MeV gamma-ray energy, the overall time resolution is 500 ps and the peak efficiency 90% at 1 MeV. The detector allows to register capture cascades with 95% probability above a threshold energy of 2.5 MeV.

Neutrons are produced via the ^{7}Li(p,n)^{7}Be reaction using the pulsed proton beam of a Van de Graaff accelerator. A collimated neutron beam is passing through the detector and hits the sample in the centre. The energy of captured neutrons is determined via time of flight, the primary flight path being 77 cm. The combination of short primary flight path, a 10 cm inner radius of the spherical BaF$_2$ shell, and the low capture cross section of barium allows to discriminate background due to capture of sample-scattered neutrons in the scintillator by time of flight, leaving part of the neutron energy range completely undisturbed. This feature, together with the high efficiency and good energy resolution for capture gamma-rays, allows to separate the various background components reliably

enough, that the capture cross section ratio of two isotopes can be determined with an accuracy of $\leq$ 1.0 %. The detector will be used for nuclear astrophysics to investigate the origin of the heavy elements in the slow neutron capture process.

1) published in : Nucl. Instr. and Meth. in Phys. Res., **A292**, 595 (1990)

1.1.18.A MEASUREMENTS OF keV NEUTRON CAPTURE CROSS SECTIONS WITH A 4 π BARIUM FLUORIDE DETECTOR : EXAMPLES OF ^{93}Nb, ^{103}Rh, AND ^{181}Ta [1]

K.WISSHAK, F.VOSS, F.KÄPPELER, G.REFFO

A new experimental method has been implemented for precise measurements of neutron capture cross sections in the energy range from 3 to 200 keV. Neutrons are produced via ^{7}Li(p,n)^{7}Be reaction using a pulsed 3 MV Van de Graaff accelerator. The neutron energy is determined by the time-of-flight (TOF) technique using flight paths of less than 1m. Capture events are detected with a 4π barium fluoride detector. This detector is characterized by a resolution in gamma-ray energy of 14% at 662 keV and 7% at 2.5 MeV, a time resolution of 500 ps, and a peak efficiency of 90% at 1 MeV. Capture events are registered with ~95% probability above a gamma-ray threshold of 2.5 MeV. The combined effect of the relatively short primary flight path, the 10 cm inner radius of the detector sphere, and of the low capture cross section of BaF_2 shifts the background due to capture of sample scattered neutrons in the scintillator to later TOF and therefore leaves the high-energy portion of the TOF spectrum undisturbed. The high efficiency and good energy resolution for capture gamma-rays yields a further reduction of this background by using only the relevant energy channels for data evaluation. In the first measurements with the new detector, the neutron capture cross sections of ^{93}Nb, ^{103}Rh, and ^{181}Ta were determined in the energy range from 3 to 200 keV relative to gold as a standard. The cross-section ratios could be determined with overall systematic uncertainties of 0.7 to 0.8 %; statistical uncertainties were less than 1% in the energy range from 20 to 100 keV, if the data are combined in 20 keV wide bins. This represents an improvement of factors 5-10 compared to existing experimental methods. The necessary sample masses were of the order of one gram. Maxwellian averaged capture cross sections were calculated in the

temperature range relevant for s-process studies. Severe discrepancies were found compared to the data reported in literature.

1)   published in : Phys. Rev., C42(4), 1731 (1990)

1.2. NEUTRON INDUCED REACTIONS

1.2.1. RADIATIVE CAPTURE OF POLARIZED NEUTRONS BY ^{12}C IN THE ENERGY RANGE FROM 20 TO 35 MEV

G.D.WICKE*, F.SMEND*, G.FINK, P.DOLL, S.HAUBER, M.HAUPENTHAL, H.O.KLAGES, H.SCHIELER

In continuation of the work reported in the previous annual report [1], the polarized neutron capture experiment on ^{12}C was finally analyzed. The motivation of the experiment was the investigation of the Isovector Giant Quadrupole Resonance (IVGQR) strength in light and medium heavy nuclei [2,3]. The contribution of the IVGQR to the dominating Giant Dipol Resonance (GDR) can be identified in the excitation function of the forward - backward asymmetry of the angular distribution of the capture gamma rays and in the analyzing power.
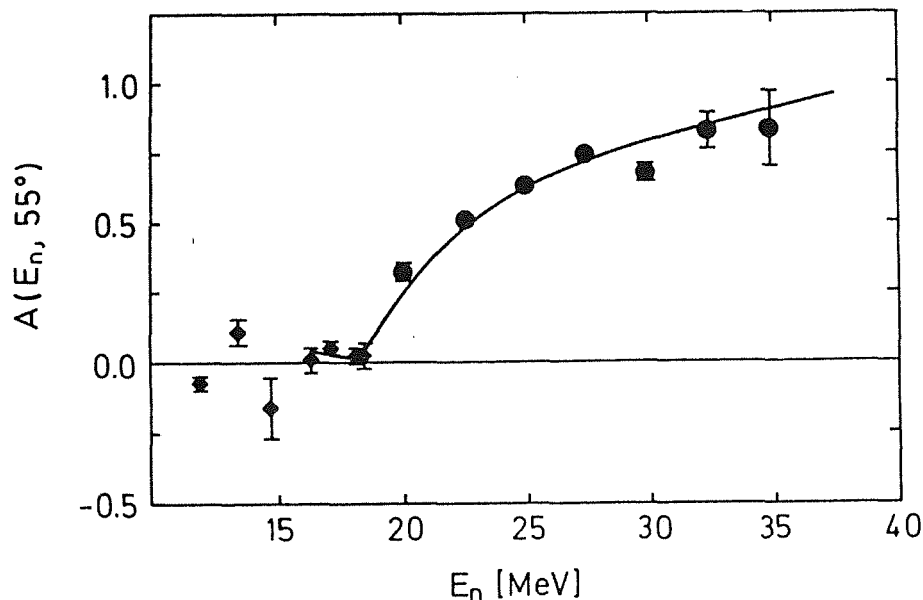
Fig. 1   Forward-backward asymmetry of the angular distribution of the ^{12}C(n,γ)^{13}C reaction

The analysis of the experiment was completed and angular distributions of the capture gamma photons and analyzing powers were extracted at laboratory angles of 55°, 90° and 125° and neutron energies E_n = 20 to 35 MeV. Capture photons and recoiling ^{13}C nuclei were detected in coincidence, the photons being identified by measuring the time of flight between the scintillating NE213 target and the NaI

detectors and analyzing the pulse shape in the NaI crystals. As Fig.1 shows, in the energy range above the centre of the GDR in ^{13}C, a pronounced rise of the forward - backward asymmetry for the ^{12}C(n,γ_0)^{13}C reaction was observed, indicating the presence of E2 capture interfering with direct and collective E1 capture. Experimental data at $E_n < 20$ MeV are taken from [4]. The Direct - Semidirect (DSD) Model of radiative capture does not give a satisfactory description of the experimental results.

[1]   G.D.Wicke, F.Smend, P.Doll, G.Fink, S.Hauber, M.Haupenthal, H.O.Klages, H.Schieler, Report KfK 4660, Kernforschungszentrum Karlsruhe, p.32 (1990)

[2]   L.Nilsson, AIP Conf. Proc. No 125 458 (1985)

[3]   H.Ejiri, M.J.A. de Voigt, Gamma-Ray and Electron Spectroscopy in Nuclear Physics, ch. 4.5, Oxford, Clarendon 1989

[4]   R.A.August, PhD Thesis, Durham N.C., 1984 (unpublished)

*   II.Physikalisches Institut, Universität Göttingen, Germany

1.2.2.   RADIATIVE CAPTURE OF POLARIZED NEUTRONS BY NEON IN THE ENERGY RANGE FROM 18 TO 30 MEV

G.MONDRY*, F.SMEND*, P.DOLL, G.FINK, H.O.KLAGES, H.SKACEL

The capture reaction Ne(n,γ) was started to be analyzed after taking data with a similar experimental set-up as described in the previous capture experiment on ^{12}C (see 1.2.1). However, in this experiment a steel vessel containing liquid neon at a temperature of T = 25.5 K and a pressure of 900 Torr was employed as a target. The interesting features of this target in providing pulse height information from various neutron induced reactions are described in a technical contribution to this report (see 5.1.5). The primary motivation is, like in the ^{12}C experiment, to investigate the excitation energy range and strength of the Isovector Giant Quadrupole Resonance (IVGQR) by means of the forward - backward asymmetry of the angular distribution of the capture gamma rays. Fast neutron capture is especially suited for investigation of the IVGQR because the

effective charge of the neutron is so small that almost any E2 amplitude observed in neutron capture may be taken to be of collective character.
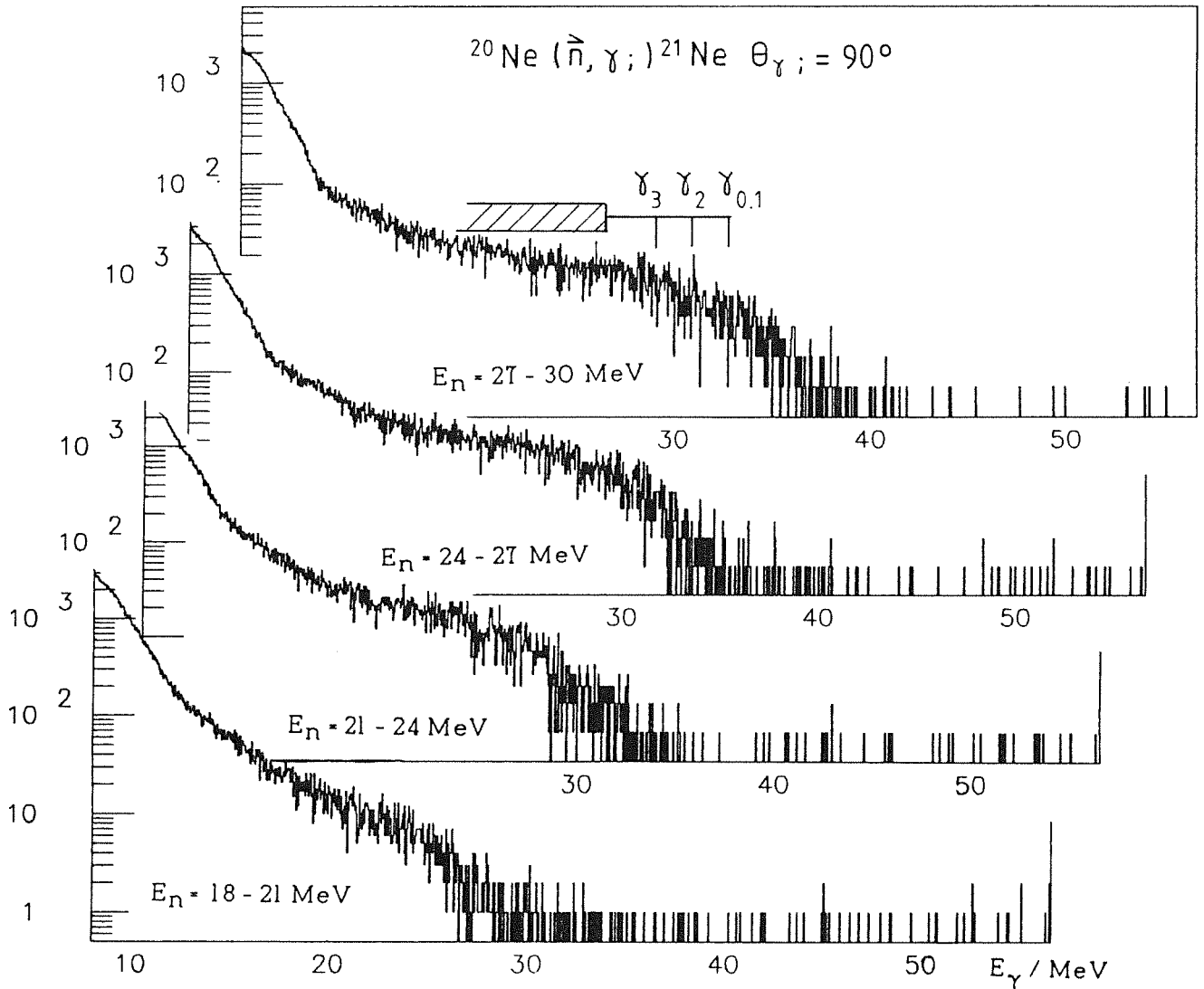
Fig.1   Photon spectra of the 90°-detector obtained for various incident neutron energies E_n. In one spectrum the position of capture γ's of the $^{20}Ne(n,\gamma)^{21}Ne$ reactions are marked.

A very elaborated analysis has been started indicating already a much reduced capture rate to the ground state and low-lying excitation states in ^{21}Ne compared to the ^{12}C experiment, probably because of the comparatively large deformation of the target nucleus. Photons were identified by measuring the time of flight between the scintillating neon target and the NaI detectors and analyzing the pulse shape in the NaI crystals. Fig.1 shows photon spectra obtained for various incident neutron energies. Because of the limited statistics broad energy intervalls were chosen in the primary neutron flux distribution masking the

separation between various final states in ^{21}Ne. It is hoped that with the inclusion of the data from a second beam time, smaller neutron flux intervalls can be selected supporting a decent decomposition of the gamma yields based on the known response function [1] of each NaI detector. A tentative assignement to various photon groups is given by a previous capture experiment leading to ^{21}Ne [2].

[1]   G.Fink, P.Doll, S.Hauber, H.O.Klages, K.T.Knöpfle, Report KfK 4508, Kernforschungszentrum Karlsruhe, p.127 (1989)

[2]   H. Putsch, T.M. Krischak, E. Kuhlmann, Nucl. Phys. **A480**, 387 (1988)

*   II. Physikalisches Institut, Universität Göttingen, Germany

1.3. NUCLEAR REACTIONS BY CHARGED PARTICLES

1.3.1. INTERMEDIATE - MASS FRAGMENT EMISSION INDUCED BY 104 MeV α - PARTICLES

M.PÂRLOG*,   D.POPESCU*,   J.WENTZ,   S.ZAGROMSKI,
I.M.BRÂNCUŞ, V.CORCALCIUC, M.DUMA*, H.J.GILS, H.REBEL

The mechanism of intermediate mass fragment (IMF) emission from various colliding systems studied over a large range of projectile energies, has attracted considerable interest. At incident energies corresponding to the Fermi velocities, binary emission with forward peaked angular distributions and energy spectra reaching beyond the projectile energy coexist with statistical decay of an equilibrated compound nucleus which is considered to be the prevailing process at lower energies. The new component, analoguous to precompound light particle emission, develops to a dominant contribution of IMF emission at higher energies. Recently the extended sum rule [1] describing sucessfully the angle and energy integrated IMF production cross section, relates the observed phenomena to dissipative fragmentation of the system, i.e. a process like asymmetric fast fission and deep inelastic reactions. In order to extent the basis of systematic comparisons and the theoretical considerations, we continued previous [2] ^{6}Li induced IMF emission experiments by using 104 MeV α-particles as projectiles. Unlike heavy ion induced reactions, light ion projectile data allow a clear source definition and identification of the forward angle yield, with minimal kinematic distortions. In addition light ions minimize the effect of high angular momenta and compression of the system.

Our investigations are based on inclusive measurements of energy spectra and angular distributions of light and intermediate-mass fragments up to Si after bombarding ^{12}C, ^{46}Ti, ^{58}Ni and ^{nat}Ag in normal kinematics. The reaction products were detected by a dE-E1-E2 telescope consisting of a gas ionization chamber (with transverse field) and two Si-solid state detectors. The telescopes were able to measure small and large Z products simultaneously. The data of two large experimental runs have been taken by list-mode on tape and are not completely analysed up to now. The laboratory angular distributions are strongly forward-peaked, similar in shape for consecutive elements, but significantly decreasing with Z and with the mass number of the target. Fig. 1 displays preliminary results of integrated cross sections (Z= 5 to 8) together with an independent prediction of the extented sum-rule model [1] without any adjustment of the temperature T

(estimated by the excitation energy) and of the change of Coulomb energy (represented by the distance $R_C = r (A_1^{1/3} + A_2^{1/3})$). The agreement appears promising.
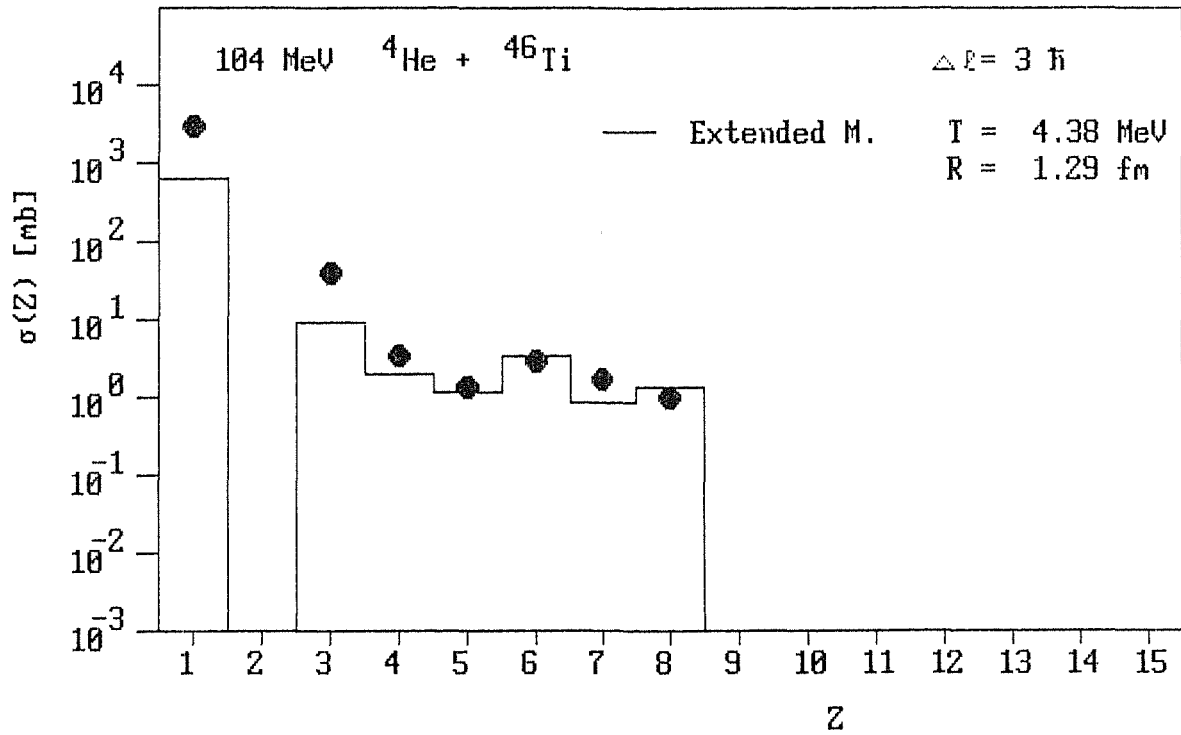
Fig. 1   Extended sum-rule prediction of IMF emission from the reaction $\alpha + {}^{46}\text{Ti}$ at $E_\alpha = 104$ MeV as compared to preliminary experimental results.

[1]   I.M.Brâncus, H.Rebel, J.Wentz, V.Corcalciuc Phys. Rev. C42, 2157 (1980).

[2]   K.Grotowski et al , Phys. Lett. B223, 287 (1989).

*   Institute of Atomic Physics, Buckarest, Romania

1.3.2. INVESTIGATION OF THE SEQUENTIAL BREAK - UP MODE ^{6}Li → ^{6}Li* $(3_1{}^+)$ → α + d , OF 156 MeV ^{6}Li PROJECTILES ON ^{208}Pb IN THE VERY FORWARD ANGULAR HEMISPHERE

J.KIENER*,   G.GSOTTSCHNEIDER,   H.J.GILS,   H.REBEL,
V.CORCALIUC**, S.N.BASU***, G.BAUR****, J.RAYNAL*****

There is a cosiderable interest on the interplay of Coulomb and nuclear interactions, inducing break-up processes of loosly bound light ions in the field of atomic nuclei. Low energy radiative capture reaction cross sections of astrophysical interest can be inferred via Coulomb break-up [1] by using detailed balance relation. The present investigation considers, the sequential break-up of 156 MeV ^{6}Li ions scattered on ^{208}Pb which proceeds through $3_1{}^+$ state in ^{6}Li ($E_x = 2.18$ MeV) followed (lifetime $\tau = 10^{-19}$ s) by the disintegration ^{6}Li*$(3_1{}^+)$ → α + d far away from the nucleus.
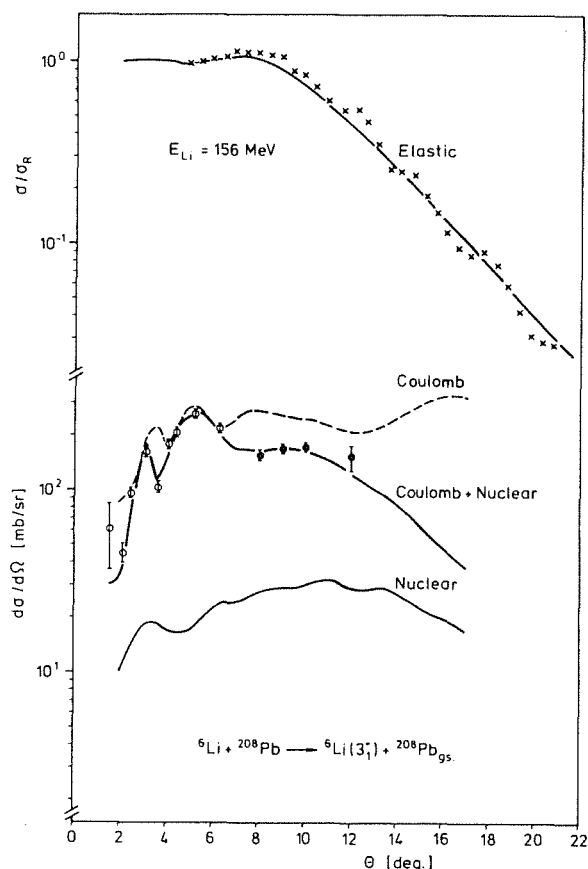
Fig. 1
Differential cross section for elastic scattering and for the sequential break-up reaction
^{208}Pb(^{6}Li,^{6}Li*→α + d)^{208}Pb$_{g.s.}$
as compared with various theoretical predictions.

The experimental data were taken at the Karlsruhe Cyclotron, using a dedicated experimental arrangement [2,3] of the magnetic spectrograph "Little John". Coincidently emitted fragments have been observed at small relative

emission angles ($<2°$) in the very forward angular hemisphere, with target nucleus left in the ground state (elastic break-up). Proper transformations of the measured triple differential cross sections and careful integration result in the differential cross section $d\sigma/d\Omega$ (Fig. 1). Also shown in Fig. 1 is the elastic scattering cross section in the same angular range.

The calculated curves in Fig. 1 are results of coupled channel analyses in the frame of the vibrational model by coupling the ground ($I=1^+$) and the first excited states ($I=3^+$) in ^6Li . Simultaneously fitting the elastic and inelastic cross sections determines the optical model parameters (Saxon-Woods shape) and transition probabilities ($B(I2) = 19.2$ e^2fm^4, $B(E2) = 18.1$ e^2fm^4 to the compared to $B(E2) = 21.8 \pm 4.8$ e^2fm^4 from electron scattering [4]).

It is obvious from Fig. 1 that the nuclear part brings a very small contribution to the break-up cross section in the measured angular range while at very forward angles the Coulomb contribution alone gives a good description of the experimental data.

[1]   G.Baur, C.A.Bertulani, H.Rebel, Nucl. Phys. **A458** 188 (1986)
[2]   J.Kiener, KfK-report 469 (Feb. 1990)
[3]   G.Gsottschneider, KfK-report 4803 (Dez. 1990)
[4]   F.Ajzenber Selove, Nucl. Phys. **A490,** 98 (1988)

*   Present adress : C.S.N.S.M., F-91403 Orsay, France
**   On leave from Institute of Atomic Physics, Bucharest, Romania
***   On leave from Bhaha Atomic Research Center, VECC Calcutta, India
****   Forschungsanlage Jülich, Institut für Kernphysik
*****   Service Physique Théoretique CE-Saclay, France.

1.3.3.   REFINED FORMULATION OF THE EXTENDED SUM - RULE MODEL BY EXPLICIT INCLUSION OF DISSIPATIVE FRAGMENTATION OF PARTIALLY FUSING SYSTEMS

J.M.BRÂNCUȘ*, H.REBEL, J.WENTZ, V.CORCALCIUC**

Recently the original sum-rule model [1] for complete and incomplete fusion processes has been generalized [2] by adopting the view, that the emission of

intermediate mass fragments (IMF) preferentially originates from cluster emission during the dissipative evolution of the dinuclear system before complete equilibration. The formation of fully equilibrated compound nuclei (production of evaporation residues σ_c) and dissipative fragmentation (σ') are considered as two competing dissipative processes of the total dinuclear target-projectile system. This is represented by the partial cross sections

$$\sigma_l^c(1) + \sum_{i=2}^{n} \sigma_l'(1 \to i)$$

The incomplete fusion channels arising from massive transfers where only part of the total system undergoes dissipative interactions, lead to additional contributions $\sigma_l(i)$ by the noninteracting clusters. The extended sum-rule model (ESM) may be refined by an explicit account of IMF emission (into the channel i) from dissipative fragmentation of the *partially* fusing system (k), too, competing with full equilibration ($\sigma_l^c(k)$) by

$$\sigma_l^c(k) + \sum_{k=2}^{n} \sigma_l'(k \to 1)$$

Thus, we explicitly discriminate two different kinds of entry states : *"complete" fusion* and *"incomplete" fusion* which both lead to dissipative fragmentation, the latter correlated with emission of remainders of massive transfers. Generalizing the arguments, basing the extended sum-rule model and adopting its notation [2], the contribution of the channel k to IMF emission into the exit channels (i > 1) is given by

$$\sigma_l'(k \to i) = \pi \lambda^2 (2l + 1) N_l^{(k)} T_e'(k) P_{ki}$$

The probability factor P_{ki} explicitly depends on the subsystem k, in particular through the Q-value dependence when seperating a particular fragment from the total or partial system, respectively. Similarly, the transmission coefficients are differently limited by different values of the critical angular momenta of the different subsystems. The refined formulation [3] of the ESM includes the extreme limit of the formation of excited systems with subsequent decay into various final channels. Some exploratory studies (ignoring emission from partially fusing systems) have been performed applying the two-step procedure to the case of 156 MeV ^{6}Li collisions with ^{nat}Ag, with the extreme assumption that in the first step a compound nucleus is formed which subsequently decays by IMF emission. The results lead to an unreasonably low value of the temperature. This indicates that compound nucleus formation and IMF emission (attributed to a larger angular momentum window) are competing rather then subsequent processes.

[1]   J.Wilczyński, K.Siwek-Wilczyńska, J. van Driel, S.Gonggrijp, D.C.J.M.Hageman, R.V.F.Janssens, J.Lukasiak, R.H.Siemssen, S.Y. van der Werf, Phys. Rev. Lett. 45 606 (1980).

[2]   J.M.Brâncuş, H.Rebel, J.Wentz, V. Corcalciuc, Phys. Rev. C42 2157 (1990).

[3]   J.M.Brâncuş, H.Rebel, J.Wentz, V. Corcalciuc, KfK-report 4646 (Nov. 1989).

1.3.4. EXCITATION AND DECAY OF SPIN - ISOSPIN - MODES IN THE REACTION ^{12}C(^{6}Li,^{6}He p) AND ^{90}Zr(^{6}Li,^{6}He p)

M.MOOSBURGER*, N.SCHOLZ*, H.DENNERT*, W.EYRICH*, A.LEHMANN*, H.WIRTH*, H.J.GILS, H.REBEL, S.ZAGROMSKI

During the last years the excitation of spin-isospin-modes via the (^{6}Li, ^{6}He) - reaction was studied at several nuclei ranging from ^{12}C to ^{90}Zr [1,2] . The experiments were performed at the 156 MeV-^{6}Li^{3+} - beam of the Karlsruhe Isochron Cyclotron and the magnetic spectrograph "Little John". To gain further information about the excitation mechanisms and decay properties coincidece measurements of emitted particles were started. The investigation of the charged
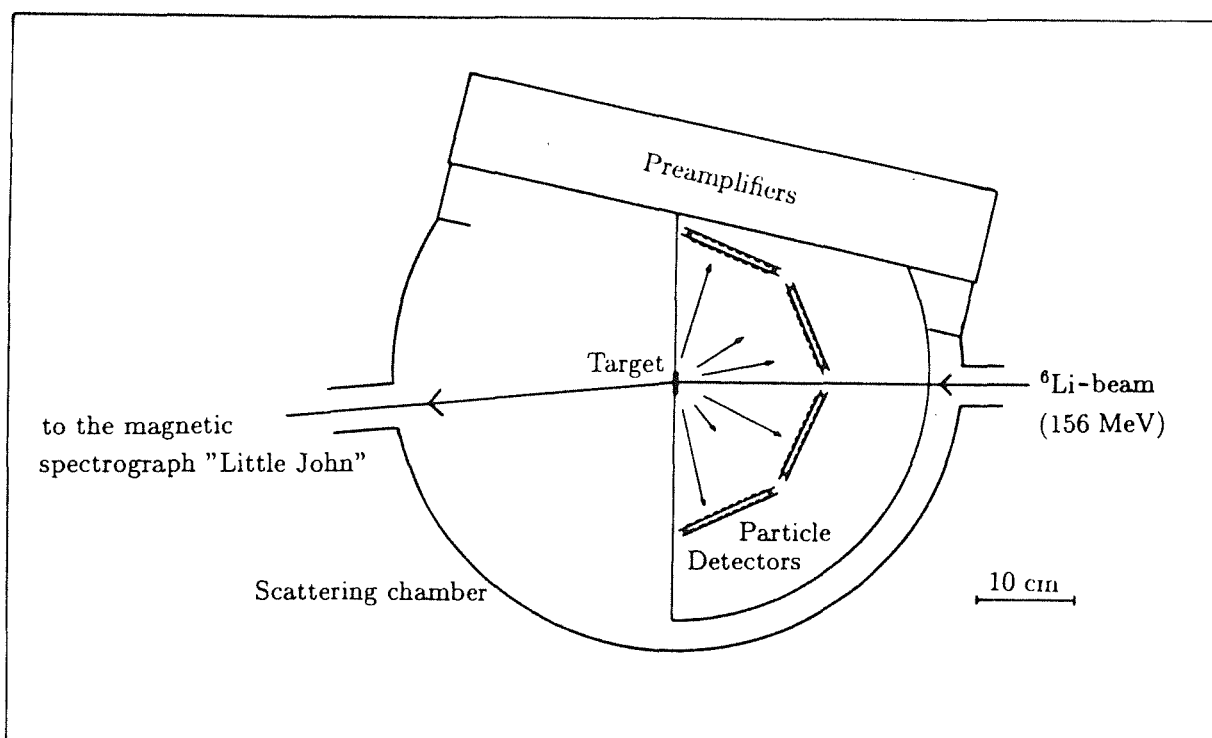
Fig. 1   Scattering chamber with the four pairs of strip detector.

decay channel (^{6}Li, ^{6}He p) was chosen for the systems ^{12}C(^{6}Li, ^{6}He p) and ^{90}Zr(^{6}Li, ^{6}He p). To detect the decay proton an arrangement of large area ion implanted silicon strip detectors, located in the scattering chamber at backward angles (between 100° and 170° symmetrically on both sides) was developped (Fig. 1). Each detector with a thickness of 500 µm and an active area of 24 ×60 mm^2 = 1440 mm^2 is devided into 10 strips with seperate readout. In total, 8 detectors were combined to four pairs of telescopes to reach a total thickness of 1000 µm. In the used setup a total solid angle of 330 msr could be covered, with an angular resolution better than ±3° for each strip.

^{12}C(^{6}Li, ^{6}He)^{12}N*(p)^{11}C

$E_{6Li} = 156$ MeV

singles

a

total coinc

b

E_x(MeV)
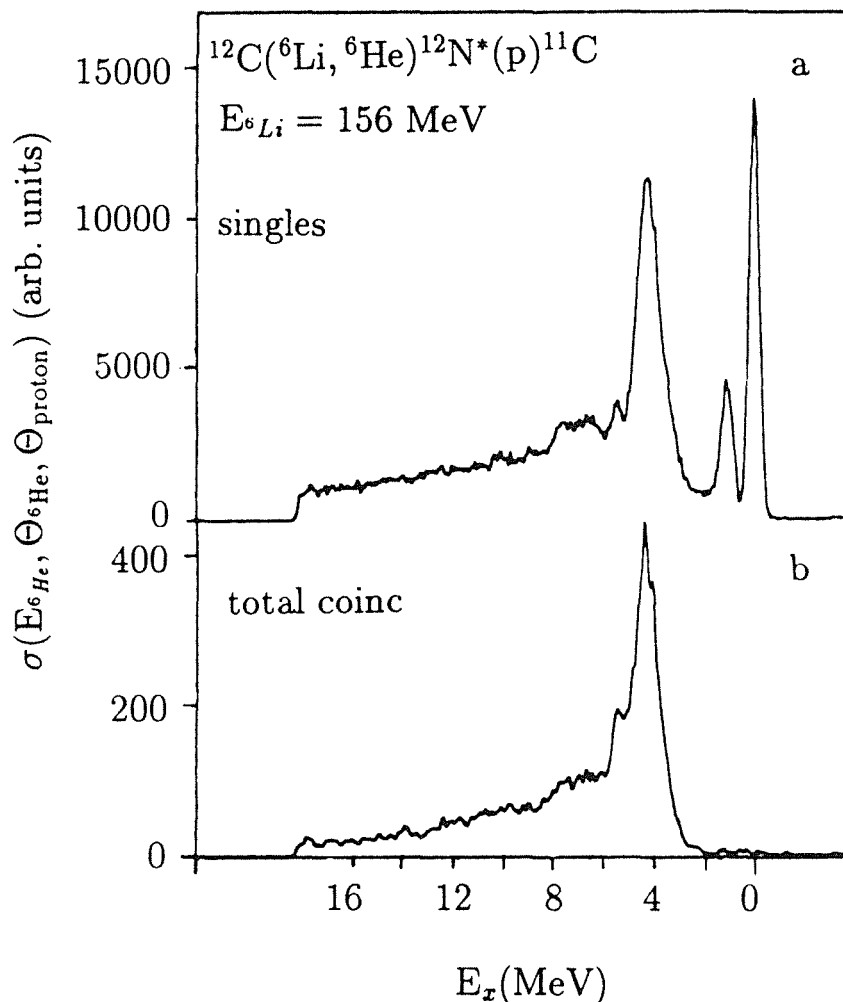
Fig.2   Singles (a) and total coincidence spectra (b) for the reaction ^{12}C(^{6}Li, ^{6}He p) at $\Theta_{6He} = 0°$.

For first investigations the system ^{12}C(^{6}Li, ^{6}He)^{12}N*(p)^{11}C was chosen for several reasons :

● the final nucleus ^{11}C is characterized by well seperated states at lower excitation energies.

- comparable measurements via the (^{3}He, t p) - reaction were already performed [3].

- a broad resonance like-structure in ^{12}N at 4.14 MeV excitation energy is not yet fully understood. Thus the observation of coincident angular-correlated decay protons will possibly give information about the structure and multipolarity of this mode.

The measurements were performed at 0° for the ^{6}He - ejectiles. Fig. 2 presents the single and coincident spectra of ^{12}N. The smooth opening of the proton emission threshold at 2.1 MeV and a reduction of backround for higher energies can be observed. In Fig. 3 a two - dimensional plot of the E $_{6_{He}}$ - E $_{proton}$ plane is shown. The different loci belonging to the decay to the states at 0.00 MeV and 2.00 MeV and the two unresolved levels at 4.32 and 4.81 MeV of the final nucleus ^{11}C can be seen. The broadening of the states is mainly caused by energy loss in the target and the uncorrected angular dependence of the kinematics.
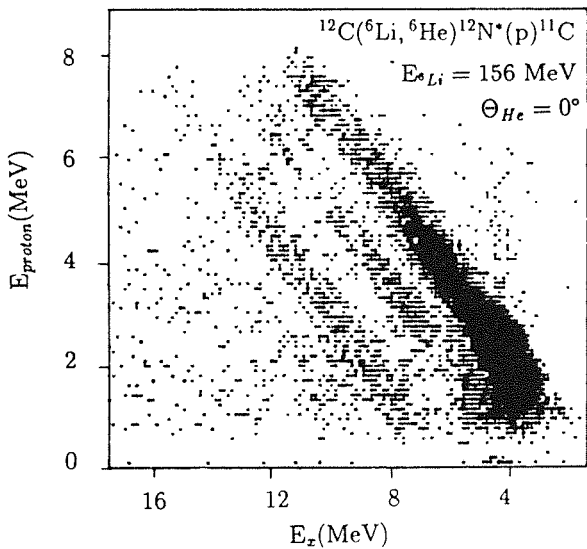
Fig. 3   Dot- plot of E $_{proton}$ vs. E$_x$ (^{12}N) visualizing the different energy levels of the final nucleus ^{11}C
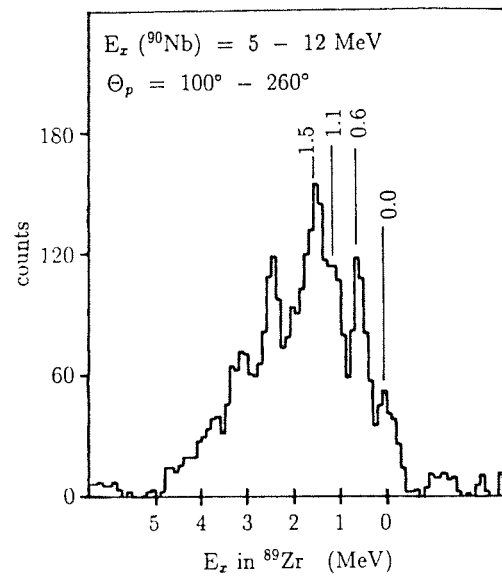
Fig. 4   Decay spectrum of the final nucleus ^{89}Zr for the reaction ^{90}Zr(^{6}Li,^{6}He p)

Furthermore the proton decay of the Gamow-Teller-resonance in the system ^{90}Zr is another subject of our investigations with this coincidence apparatus. A first preliminary decay spectrum of protons originating from the giant resonance region of ^{90}Nb can be presented in Fig. 4, for which an integration over the complete solid angle of the decay detectors was done. Well known states of the residual nucleus ^{89}Zr appear. More precise evaluations in the two systems ^{12}C and ^{90}Zr leading to quantitative results as well as angular correlation functions in dependence of the exciting energy are still in progress.

[1]   M.Moosburger, E.Aschenauer, H.Dennert, W.Eyrich, A.Lehmann, R.Rudeloff, H.Schlösser, H.J.Gils, H.Rebel, S.Zagromski, Phys. Rev. C41, 2925 (1990) .

[2]   H.Wirth, E.Aschenauer, W.Eyrich, A.Lehmann, M.Moosburger, H.Schlösser, H.J.Gils, H.Rebel, S.Zagromski, Phys. Rev. C41, 2698 (1990).

[3]   W.A.Sterrenburg, M.N.Harakeh, S.Y. van der Werf, A. van der Woude, Nucl. Phys. A405, 109 (1983).

*   Physikalisches Institut der Universität Erlangen-Nürnberg, D-8520 Erlangen, F.R.G.

1.3.5.   GAMOW - TELLER STRENGTH IN THE SYSTEMS $^{37}Cl \rightarrow ^{37}Ar$ AND $^{71}Ga \rightarrow ^{71}Ge$

E.ASCHENAUER*,   H.DENNERT*,   W.EYRICH*,   H.J.GILS, A.LEHMANN*,   M.MOOSBURGER*,   H.REBEL,   H.WIRTH*, S.ZAGROMSKI

A serious problem in astrophysics is the discrepancy that the capture rate of solar neutrinos observed in the ^{37}Cl-experiment, which uses the ^{37}Cl(v,e$^-$)^{37}Ar inverse β-decay, is only about one third of that predicted by the standard solar model (SSM). In order to remove the sensitivity to parameters of the solar model two experiments use ^{71}Ga as a target material. The solar neutrinos are detected especially via the transition ^{71}Ga(g.s.,$3/2^-$) $\rightarrow$ ^{71}Ge(g.s.,$1/2^-$) with a threshold of only 0.236 MeV, which gives response to pp-neutrinos. Excited state transitions with higher thresholds in comparison to the ground state transitions may also contribute and considerably affect the sensitivity of the ^{71}Ga-detector to neutrinos from the decay of ^{8}B and ^{7}Be [1].

We measured the distributon of Gamow-Teller (GT) strenght in ^{37}Ar and ^{71}Ge using the charge transfer reaction (^{6}Li,^{6}He). The selection rules of $\Delta S = 1$ and $\Delta T = 1$ together with successful measuring at a reaction angle of zero degree are responsible for a high sensitivity to Gamow-Teller transitions. The measurements were performed at the Karlsruhe Isochronous Cyclotron with the 156 MeV ^{6}Li^{3+}- beam, using the magnetic spectrograph "Little John".

Fig. 1 shows a ^{37}Cl(^{6}Li,^{6}He)^{37}Ar spectrum at zero degree. The GT transition to the ground state of ^{37}Ar is well seperated from the next excited states.
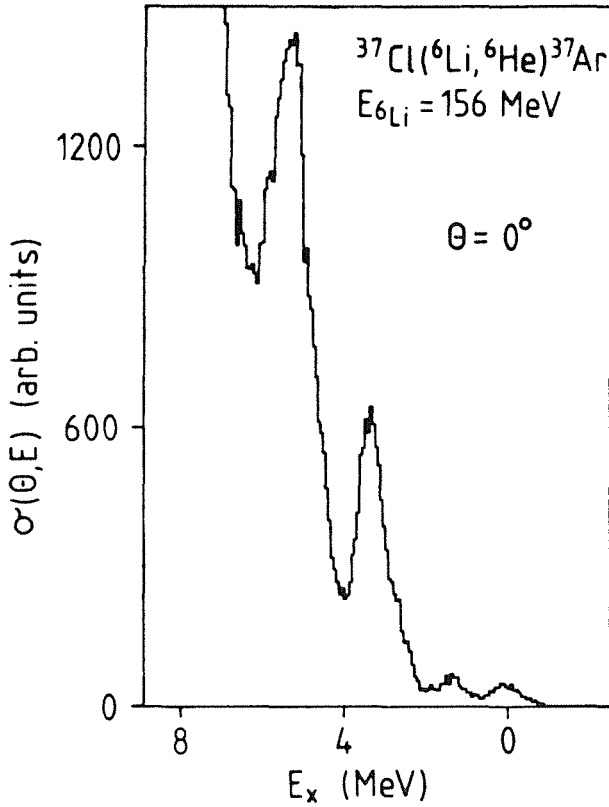
Fig. 1   A zero degree spectrum of the reaction $^{37}Cl(^6Li,^6He)^{37}Ar$.

In Fig. 2a we present a 0° spectrum of the reaction $^{71}Ga(^6Li,^6He)^{71}Ge$, where the GT monopole strength is in its maximum, and a 1° spectrum, where it has strongly decreased. To extract the GT-strength we used the "Maximum-Minimum Method" subtracting the one degree from the zero degree spectrum. Because the cross section of higher multipolarities are nearly constant in the region of lower angles, in the subtraction spectrum only GT-states will contribute significantly [2] . By this way we got the spectrum of Fig. 2b, representing the GT-strength distribution of the observed ^{71}Ga system. The low Gamow-Teller states are reproduced by gaussian curves. These Gamow-Teller states together with the strength up to 8 MeV are also important for the interaction of the neutrinos with higher energy.

The B(GT)-values related to measured cross sections in the interesting energy region of solar neutrinos were calculated with the help of the following formula :

$$\frac{\dfrac{\sigma_{DWBA}(Q=0)}{\sigma_{DWBA}(Q)} * \sigma_{exp}(0°)}{F(A)} = B(GT)$$

The factor

$$\frac{\sigma_{DWBA}(Q=0)}{\sigma_{DWBA}(Q)} = k$$

is necessary to correct the momentum transfer at 0°, caused by the Q-values of the $^6Li,^6He$)-reaction [3]. For the g.s. region of ^{37}Cl and ^{71}Ga it is equal 1.0 and can be

neglected, but at higher excitation energies it increases to about 1.5 and must be taken into consideration. It is also necessary to correct the $\sigma_{exp}(0°)$-value with a mass factor F(A), because the relation between $k \cdot \sigma_{exp}(0°)$ and B(GT) is mass dependent, like at (p,n) measurements [3,4].
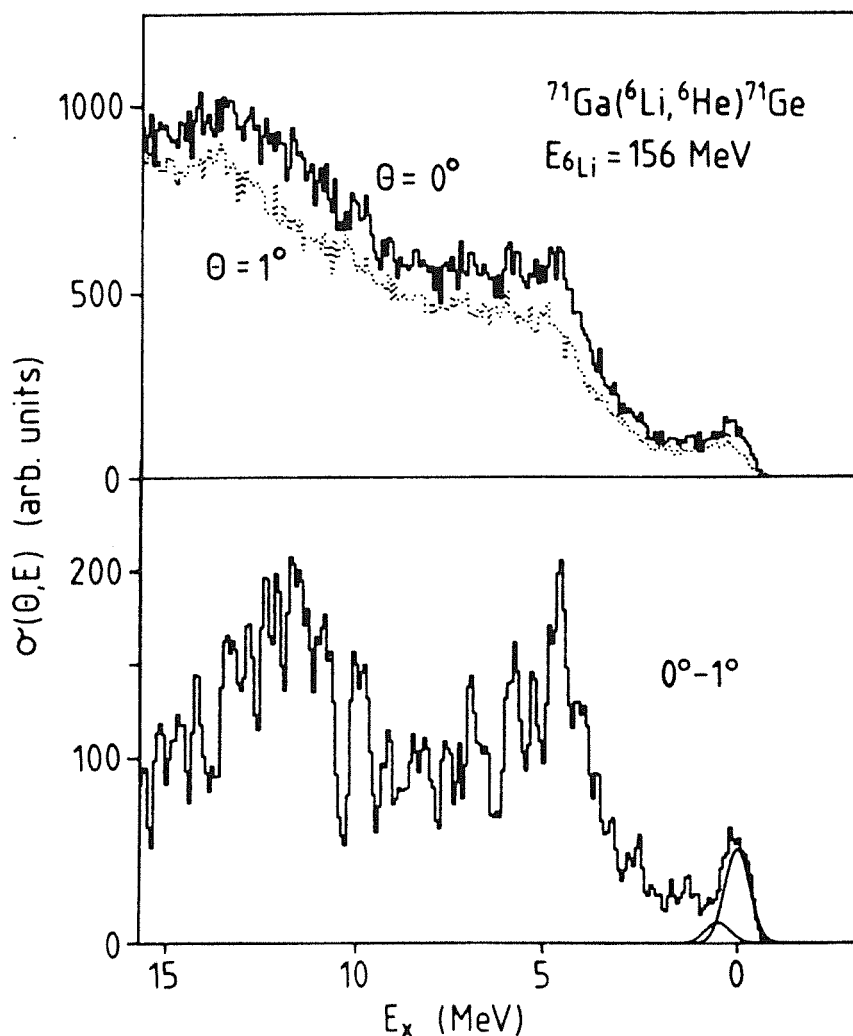
Fig. 2   a: A zero degree and an one degree spectrum of the reaction $^{71}Ga(^6Li,^6He)^{71}Ge$ before subtraction.

b: The subtraction spectrum with fits for the Gamow-Teller states at low energies.

This yields a B(GT)-value of 0.032±0.007 and of 12±0.03 for the g.s. transitions of ^{37}Cl and ^{71}Ga, respectively. Our results for the ground state are compared with (p,n)-and β-decay data in Tab. 1. The values of all methods show a rather good agreement within the error bars. In Tab.2 a quantitative summary of .the extracted B(GT)-values in the system $^{71}Ga\rightarrow^{71}Ge$ is given in 1 MeV steps to an excitation energy of 8 MeV. The summed strength up to 8MeV of 2.9±0.7 has to be compared with the higher value of 4.3±0.7 from the (p,n) work [6]

	g.s.	^{37}Ar	^{71}Ge
B(GT) (^{6}Li,^{6}He)	0.032±0.007	0.12±0.03
B(GT) (p,n)	0.034±0.007	0.085±0.015
B(GT) (E.C)	0.0316±0.0008	0.091±0.0002

Tab. 1   A comparison of the B(GT)-values deduced of (^{6}Li,^{6}He), (p,n)-measurements [5,6] and E.C. [7,8].

E_x [MeV]	0 - 1	1 - 2	2 - 3	3 - 4	4 - 5	5 - 6	6 - 7	7 - 8	Σ
B(GT)	0.19	0.08	0.13	0.36	0.60	0.57	0.47	0.48	2.88
	±0.04	±0.02	±0.03	±0.07	±0.14	±0.14	±0.12	±0.12	±0.68

Tab. 2   B(GT)-values for the whole energy range of solar neutrino interaction in the system ^{71}Ga → ^{71}Ge .

In summary we may conclude that the (^{6}Li,^{6}He)-reaction is a useful alternative to calibrate SND's.

[1]   J.N.Bahcall, R.K.Ulrich, Rev. of Mod. Phys. **60**, 297 (1988) .

[2]   H.Wirth,   E.Aschenauer,   W.Eyrich,   A.Lehmann,   M.Moosburger, H.Schlösser, H.J.Gils, H.Rebel, S.Zagromski, Phys. Rev. C41, 2698 (1990) .

[3]   M.Moosburger,   E.Aschenauer,   H.Dennert,   W.Eyrich,   A.Lehmann, R.Rudeloff, H.Schlösser, H.J.Gils, H.Rebel, S.Zagromski, Phys. Rev. C41, 2925 (1990) .

[4]   T.N.Taddeucci,   C.A.Goulding,   T.A.Carey,   R.C.Byrd,   C.D.Goodman, C.Gaarde, J.Larsen, D.Horen, J.Rapaport, E.Sugarbaker, Nucl. Phys. **A469**, 125 (1987).

[5]   J.Rapaport at al, Phys. Rev. Lett. **47**, 1518 (1981).

[6]   D.Krofchek at al., Phys. Rev. Lett. **55**, 1051 (1985).

[7]   P.M.Endt, C van der Leun, Nucl. Phys. **A310**, 471 (1978).

[8]   W.Hampel and L.P.Remsberg, Phys. Rev. C31, 666 (1985).

*   Physikalisches Institut der Universität Erlangen-Nürnberg, D-8520 Erlangen, FRG

1.3.6.   EXCITATION OF ISOSCALAR GIANT MONOPOLE RESONANCE IN ^{90}Zr AND ^{208}Pb USING ^{6}Li - SCATTERING

H.DENNERT*,   E.ASCHENAUER*,   W.EYRICH*,   H.J.GILS,
A.LEHMANN*,   M.MOOSBURGER*,   N.SCHOLZ*,   H.REBEL,
H.WIRTH*, S.ZAGROMSKI

One of the fundamental quantities to describe nuclei and nuclear matter is the compression modulus, which is also interesting in connection with astrophysical
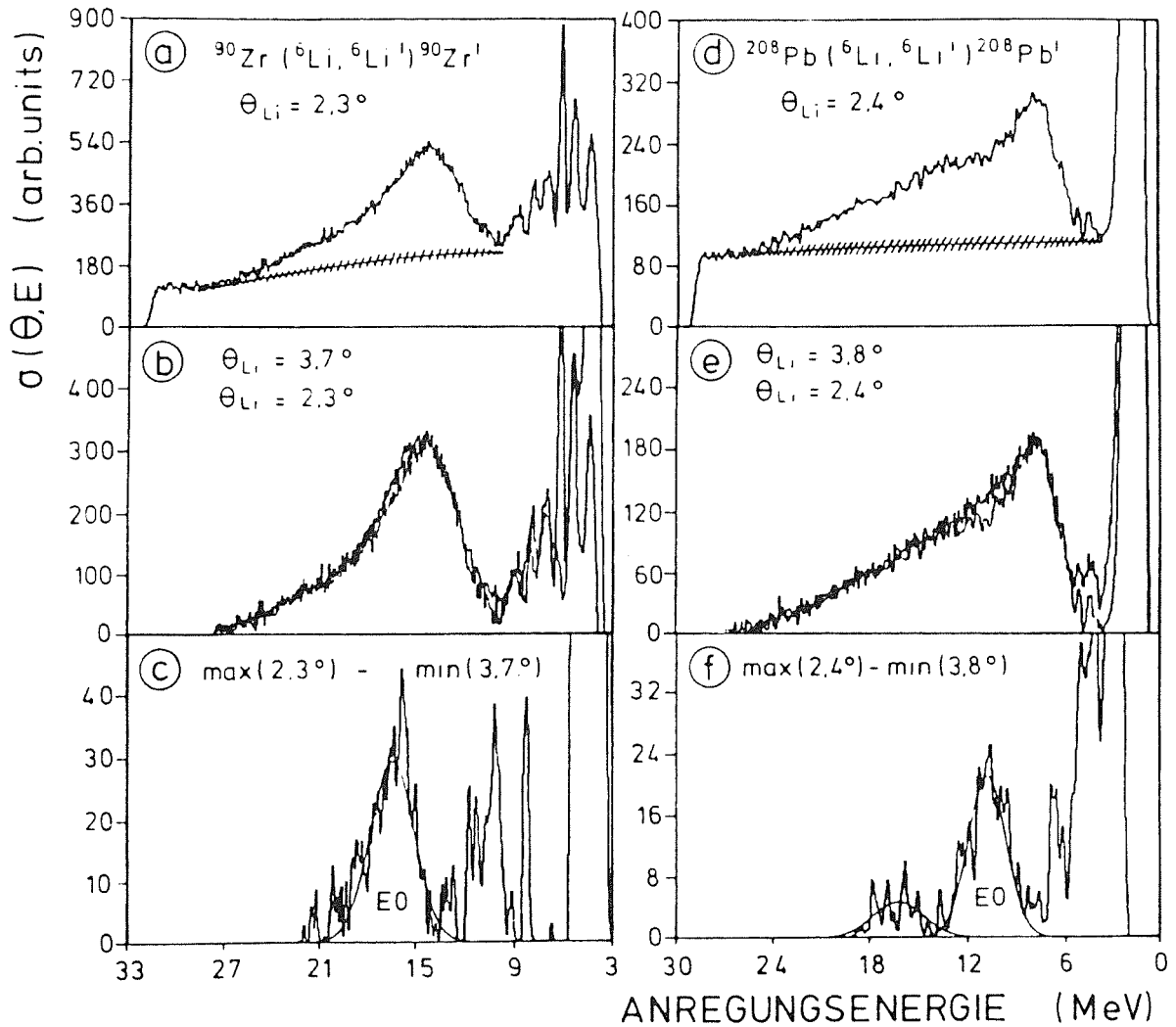
Fig.1   a/d : Single spectra measured at the minimum of the GMR cross section for ^{90}Zr (a, 2.3°) and ^{208}Pb (d, 2.4°).

b/e : Minimum and maximum subtracted from background : ^{90}Zr (b) and ^{208}Pb (e).

c/f : The difference of minimum and maximum shows a clear GMR bump (E_0) for both nuclei : ^{90}Zr (c) and ^{208}Pb (f).

problems like the dynamics of supernova explosions and neutron stars. A direct source of information on the nuclear incompressibility are the parameters of the isoscalar giant monopole resonance (GMR).

In continuation of our earlier scattering experiments on a sample of Sn-isotopes we performed experiments with the 156 MeV ^{6}Li beam of the Karlsruhe Isochronous Cyclotron for the nuclei ^{90}Zr and ^{208}Pb. Due to the diffraction pattern the determination of the GMR from underlying multipolarities and the overlapping giant quadropole resonance (GQR) requires measurements under extreme forward angles, which were performed using the magnetic spectrograph "Little John". In order to reduce the high experimental background, additional devices such as active slits and frames in the dipol of the spectrograph were developed. In addition the advantage of a small physical background of the (^{6}Li,^{6}Li') reaction in comparison to the usually used alpha scattering from earlier experiments enables us to determine the excitation energy more exactly.

Fig.1b shows the GR bump of ^{90}Zr in a minimum of the GMR cross section. Subtraction from underlying background (Fig. 1b) shows a minimum (2.3°) and a maximum (3.7°), respectively. The difference of both spectra identifies clearly the GMR bump in Fig. 1c due to the fact that the GQR and strengths with higher multipolarities are nearly constant in the region of forward angles. Results of the corresponding analysis for the nucleus ^{208}Pb are displayed in Fig. 1d-f.

In theoretical models one obtains with a three parameter fit the compression modulus K_∞ using the experimental excitation energies of the giant monopole resonance over a wide range of nuclei. In contrast to the currently "accepted" value $K_\infty = 210 \pm 30$ MeV [1] a more recent analysis extracted a significant higher value around 300 MeV [2] taking into account a refined theoretical model and including light nuclei. Our analysis with the experimental excitation energies of ^{90}Zr, ^{208}Pb, the earlier work on Sn-isotopes and preliminary results on ^{24}Mg and ^{64}Zn listed in Tab. 1 favours a higher value too, $K_\infty = 284 \pm 30$ MeV.

Nucleus	^{24}Mg	^{64}Zn	^{90}Zr	^{112}Sn	^{116}Sn	^{120}Sn	^{124}Sn	^{208}Pb
E_x (MeV)	18.3	18.0	16.50	15.8	15.6	15.4	15.3	13.86

Tab.1   GMR excitation energies E_x of various nuclei.

[1]   J.P.Blaizot, Phys. Rev. 64, 171 (1980

[2]   M.M.Sharma, Phys. Rev. C38, No.6 (1989) 2562

*   Physikalisches Institut der Universität Erlangen-Nürnberg, D-8520 Erlangen, F.R.G.

1.3.7.A   EXTENDED SUM - RULE MODEL VIEW OF LIGHT AND INTERMEDIATE MASS FRAGMENT EMISSION IN NUCLEAR REACTIONS AT INTERMEDIATE ENERGIES [1]

I.M.BRÂNCUŞ, H.REBEL, J.WENTZ, V.CORCALCIUC

The original sum-rule model worked out by Wilczyński et al. and successfully used for a global description of complete an incomplete fusion reactions has been extended by a term accounting for dissipative processes of the dinuclear system on its way to fusion. When applying to light- and heavy- ion collisions with various targets at energies in the transitional region, the new term proves to be rather essential for reproducing the element distributions of the fragments emitted from rather asymmetric systems.

1.3.8.A   ELASTIC BREAK - UP OF 156 MeV ^{6}Li PROJECTILES WITH LARGE ASYMPTOTIC RELATIVE MOMENTA OF THE FRAGMENTS : EXPERIMENTAL OBSERVATIONS AND THE DIFFRACTIVE DISINTEGRATION APPROACH [1]

N.HEIDE, H.REBEL, V.CORCALCIUC, H.J.GILS, H.JELITTO, J.KIENER, J.WENTZ, S.ZAGROMSKI, D.K.SRIVASTAVA

The triple-differential cross sections for elastic break-up of 156 MeV ^{6}Li projectiles by the reactions ^{208}Pb(^{6}Li,ad)^{208}Pb$_{g.s.}$ and ^{12}C(^{6}Li,ad)^{12}C$_{g.s.}$ have been measured with large asymptotic relative momenta of the outgoing fragments. The data exhibit rather unfamiliar shapes of the energy spectra, often replacing the

usual bell-shape distributions by double-peaked structures and varying rapidly with the relative emission angles. The origin of these features has been explored and the cross sections have been analysed on the basis of a diffractive disintegration approach.

1)   published in : Nucl.Phys. **A504**, 374 (1989)

.

1.3.9.A   A PRIOR - FORM DISTORTED - WAVE BORN APPROXI-MATION ANALYSIS OF THE ELASTIC BREAKUP OF 156 MeV ^{6}Li PROJECTILES [1]

D.K.SRIVASTAVA, H.REBEL, N.HEIDE

Features of the prior-form distorted-wave Born approximation theory of elastic breakup of 156 MeV ^{6}Li ions scattered off ^{208}Pb are investigated. Nuclear breakup for large relative energies of the outgoing α-particle and deuteron fragments studied here ($E_{\alpha d} > 5$ MeV) is found to proceed dominantly via the quadrupole scattering state of the $\alpha + d$ system when transition potentials from elastic fragment-target scattering are used for the calculations. The coherent contributions of different multipole components to the triple-differential cross sections appear to be very sensitive to the potentials generating the distorted waves representing the cluster fragment-target interactions. The results of the analysis of the experimental data require transition potentials rather different from the on-the-mass shell optical potentials deduced from elastic α-particle and deuteron scattering.

1)   published in : Nucl.Phys. **A506**, 346 (1990)

1.3.10.A ORBITAL DISPERSION AND WAVEFUNCTION MAPPING IN INCLUSIVE BREAK - UP EXPERIMENTS [1]

D.K.SRIVASTAVA, D.N.BASU, H.REBEL, H.J.GILS

Inclusive break-up cross sections of the reactions $^{12}C(^6Li,\alpha)X$ and $^{208}Pb(^6Li,\alpha)X$ at 26 MeV/amu, observed for the emission of break-up fragment into the forward hemisphere, are analysed in view of the information about the internal momentum distribution of the projectile. The longitudinal momentum distribution of the fragments in the projectile rest-frame is found to reflect the internal momentum distribution of the clusters whereas the transverse distribution is affected by the projectile-target interaction.

1.3.11.A BREAK - UP OF LIGHT PROJECTILES : A SOURCE OF ASTROPHYSICAL INFORMATION [1]

H.REBEL

Experimental studies of the binary break-up of light nuclear projectiles in the Coulomb field of heavy target nuclei have been proposed as an alternative access to astrophysically interesting information about radiative fusion cross sections at low relative energies of the fragments.

As a pilot experiment we have started to study the break-up of $^6Li \rightarrow \alpha + d$ at $E_{Li} = 156$ MeV. Both fragments have been detected in coincidence in the focal plane of the Karlsruhe spectrograph "Little John". Triple differential cross sections have been measured at mean reaction angles $\Theta_R = 2\text{-}6°$.

The cross section for the resonant break-up via the 3^+- state at $E_x = 2.18$ MeV shows up to agree at angles $\Theta_R < 4°$ with the Coulomb excitation probability deduced from other sources confirming that dominantly Coulomb break-up is observed at these angles. The non-resonant component of E2-Coulomb break-up has been definitively observed in this experiment. The promising results will be analysed and discussed in detail.

1.3.12.A INTERFERENCE AND OFF - SHELL EFFECTS OF FRAGMENT SCATTERING IN ELASTIC BREAKUP OF LIGHT IONS [1]

N.HEIDE, D.K.SRIVASTAVA, H.REBEL

The triple-differential cross sections for elastic breakup of 156 MeV ^{6}Li measured at larger relative momenta of the outgoing α-particle and deuteron fragments exhibit conspicuous double-peaked structures in their momentum-transfer dependence. The origin of these features is explored, sensitively revealing interference and off-shell scattering effects in the fragment-target interaction. Elastic breakup data of 56 MeV deuterons and 90 MeV ^{3}He are reanalyzed in view of these effects on the basis of the prior-form distorted-wave Born-approximation theory

1.3.13.A LIMES : A COMPUTER PROGRAM FOR ANALYSES OF LIGHT AND INTERMEDIATE - MASS FRAGMENT EMISSION IN HEAVY ION REACTIONS BY AN EXTENDED SUM - RULE MODEL [1]

I.M.BRÂNCUŞ, J.WENTZ, H.U.HOHN

The computer program LIMES is based on a improved version of extended sum-rule model for light and intermediate-mass fragment emission in heavy ion reactions. It includes a code for dynamical calculations of the critical angular momentum for fusion following the suggestion of C.Ngô (Prog. Part. Physics 16 (1986) 139). The report briefly describes the use of this program, the necessary input for the calculations of the element distribution and partial cross sections and gives a Fortran listing. Using the fitting routine FITEX the program provides an option for fast parameter adjustments. The use is demonstrated by an application to a specific example.

1.3.14.A INVESTIGATION OF SPIN - ISOSPIN STRENGTH IN ^{48}Ca → ^{48}Sc AND ^{90}Zr → ^{90}Nb USING THE (^{6}Li,^{6}He) REACTION [1]

H.WIRTH, E.ASCHENAUER, W.EYRICH, A.LEHMANN, J.GILS, H.REBEL, S.ZAGROMSKI, M.MOOSBURGER, H.SCHLÖSSER

The (^{6}Li,^{6}He) reaction was studied on the target nuclei ^{48}Ca and ^{90}Zr at $E_{Li} = 156$ MeV at extreme forward reaction angles. From the zero degree spectra Gamow-Teller strength was extracted for excitation energies $0 \leq E_x \leq 20$ MeV. The results are compared with distorted-wave Born approximation calculations and (p,n) data.

1)   published in : Phys. Rev. C41(6), 2698 (1990)

1.3.15.A (^{6}Li,^{6}He) REACTION AND GAMOW - TELLER β DECAY [1]

M.MOOSBURGER, E.ASCHENAUER, H.DENNERT, W.EYRICH, A.LEHMANN, R.RUDELOFF, H.SCHLÖSSER, H.WIRTH, H.J.GILS, H.REBEL, S.ZAGROMSKI

The (^{6}Li,^{6}He) reaction was studied on targets of ^{12}C, ^{18}O, ^{26}Mg and ^{42}Ca, at a beam energy of 156 MeV. Zero degree measurements of all systems are presented. The evaluated cross sections for Gamow-Teller transitions at $\Theta = 0°$ and the corresponding strengths of analogous beta decays are compared.

1)   published in : Phys. Rev. C41(6), 2925 (1990)

2. ASTROPHYSICS WITH EXTENSIVE AIR SHOWERS

2.1. THE KASCADE PROJECT

2.1.1. STATUS OF THE KASCADE PROJECT

J.ENGLER, H.J.GILS, H.O.KLAGES, H.REBEL, G.SCHATZ, B.ZEITNITZ

Forthcoming astrophysical studies with extensive air showers will be based on measurements with KASCADE, the KArlsruhe Shower Core and Array DEtector, which is currently being under construction at the KfK site. The main aim of the experimental set-up is to obtain information on the elemental composition of the primary cosmic rays in the energy range 10^{14}-10^{17}eV which is of great astrophysical interest [1] . For that purpose the electromagnetic, muonic and hadronic components of extensive air showers induced in the atmosphere by ultra high energy cosmic primaries will be measured by KASCADE.

The main components of KASCADE are an array of 316 detector stations positioned on a rectangular grid of 13 m grid size and a central detector of 16×20 m^2 size. The detector stations in the array are electronically coupled to groups of 16 called a 'cluster' and controlled by a cluster station placed in the centre of it. The full arrangement is shown in a photomontage (Fig. 1) in the north east corner of the KfK site. During the period of this report, in which the efforts for KASCADE could be considerably increased, some improvements as compared to the first design [2] have been made. For detection of the soft (electron/gamma) component of showers a special type of liquid scintillator detector was developed [3] replacing the formerly suggested plastic scintillator. In the central detector, which should analyze the shower core, the absorber of the calorimeter will be made from iron instead of concrete [4] thus leading to a higher average density. More details of the current design are given in the following contributions of this chapter.

The KASCADE site was partly and provisionally prepared (ballasted road, power supply) so far for the position of the central detector and a few array clusters close to it. The basements for the first prototype cluster of detector stations were built by the KfK departement for underground engeneering and finally supplied by a prefabricated concrete plate. The underground pipes for interconnecting
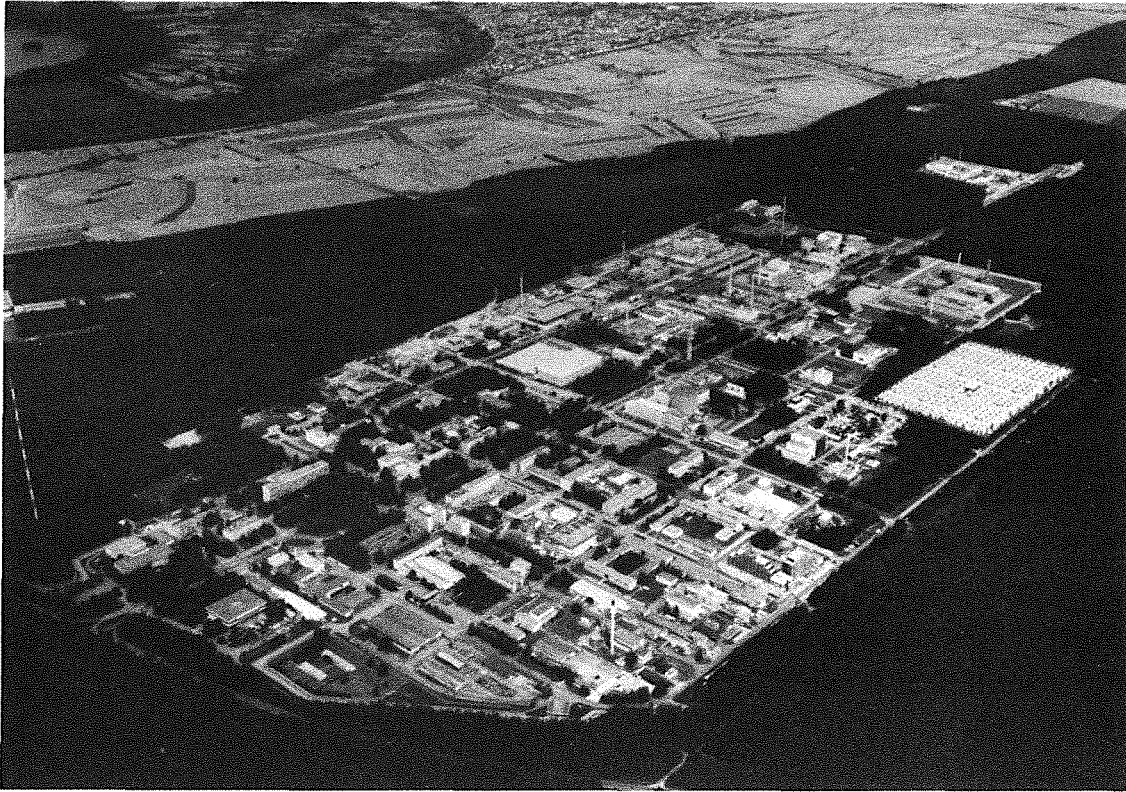
Fig. 1   Photomontage of the planned arrangement of KASCADE on site

cables were included in this phase of construction as well. It turned out that the chosen design and procedures are cheap, fast and practical for further installations. After delivery and positioning of the absorber plates [3] the weather protecting wooden huts were mounted. Whether this particular solution will be also chosen furtheron is a still open question. Some aspects of cable guiding and confectioning has also to be studied. The cluster is now ready for detector mounting which will be finished within the next month.

The design of the concrete basement for the central detector has been finished and its construction can be started as soon as the building licence from the responsible civil administration is given which is expected for early springtime 1991. Design and engeneering of the iron absorber for the calorimeter has also been accomplished and the iron plates are being weekly delivered from the foundry (140 out of 1400 were available at the end of 1990). Hence, mounting of the absorber can be started immediately after finishing the basement.

The specifications for a calorimeter loading machine [1] have been fixed and the order for its design and construction has been given to an external manufacturer. Specifications for mounting and installations of the muon detectors are currently being studied.

[1]   P.Doll et al., Report KfK 4686, Kernforschungszentrum Karlsruhe (1990)

[2]   P.Doll et al., in report KfK 4660, (eds. G.Drexlin, H.J.Gils) Kernforschungszentrum Karlsruhe (1990), contr. 2.1.

K.Daumiller et. al., ibid, contr. 2.2.

J.Engler et. al., ibid, contr. 2.3.

[3]   P.Doll et al., this report, contr. 2.1.3.

[4]   J.Engler et. al., this report, contr. 2.1.2.

2.1.2.   THE CENTRAL DETECTOR OF KASCADE

J.ENGLER,   P.GABRIEL,   H.J.GILS,   H.KEIM,   J.KNAPP, H.J.MATHES, H.H.MIELKE, H.REBEL, S.ZAGROMSKI, P.ZIEGLER

The principal lay-out of the central detector is shown in Fig. 1. All the absorber slabs of the calorimeter are made of iron, which is cast from steel of dismantled nuclear facilities. The first charge of 200 slabs, as delivered by the time of writing, has a mean activity of 2 Bq / g, which is low enough to ensure a background-free trigger for muon bundles of about 8 muons on the 320 m surface of the central detector.
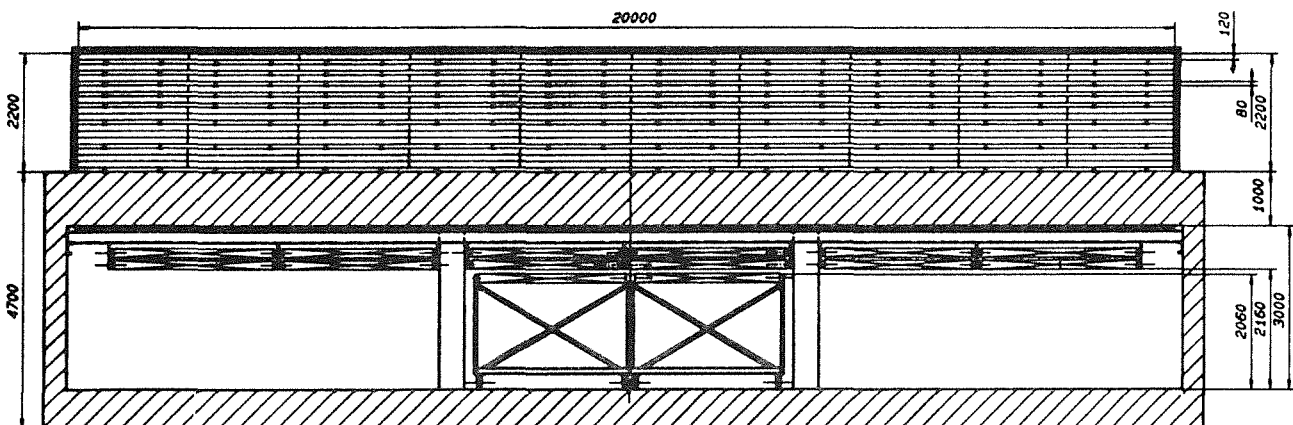
Fig. 1   Principal lay-out of the central detector.

The absorber block is sliced into 8 layers starting with iron slabs of 12 cm thickness at the top and ending in the concrete ceiling of the foundations. The energy resolution to be expected for all gaps filled with active elements is shown in Fig. 2. The signals have been weighted according to the absorber slab thickness in front of it. Also the resolution for a partly equipped calorimeter is shown, when

only 5 slots are filled with chambers and the second layer left unequipped for fast trigger counters.

Active Layers. Ionization chambers using the liquid TMS (tetramethyl-silane) have been developed at the institute which are particularly suited as active elements in calorimeters. 50 prototype chambers have been built and have been tested at the Karlsruhe cyclotron with 96 MeV tritons and at the ITEP synchrotron with 6 GeV electrons, pions and muons. For the chambers, which all use PTFE as spacer material, a small signal loss of 6.5 % per year was found.
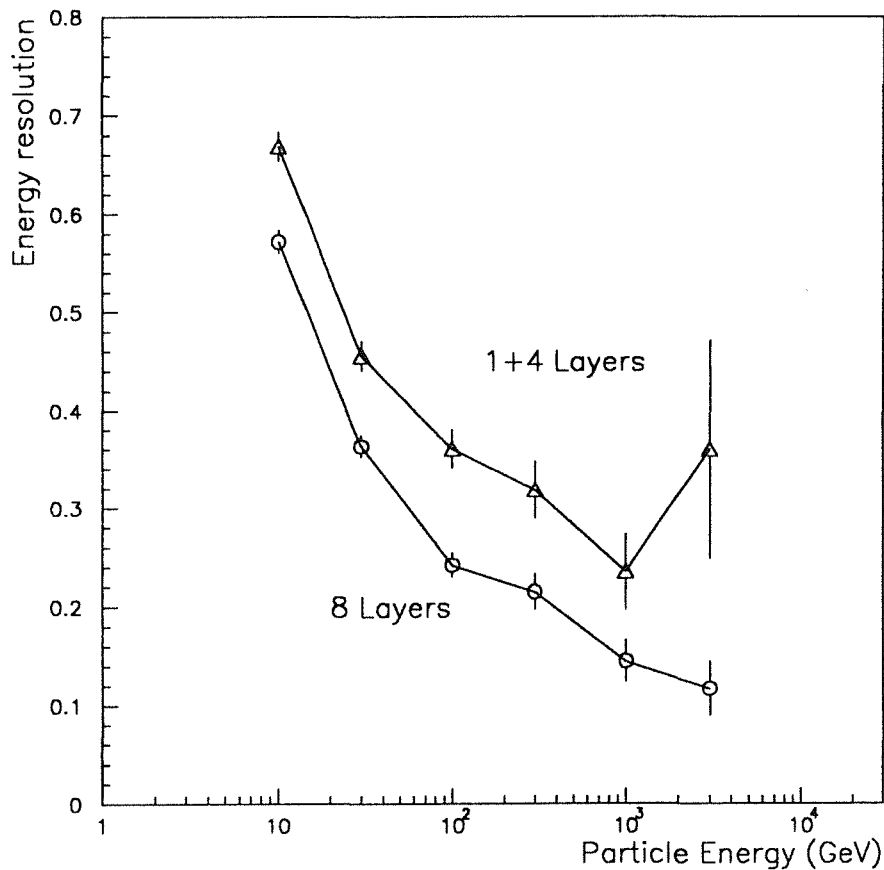
Fig. 2   Expected energy resolution σ(E)/E for hadrons in the calorimeter (Monte Carlo results). The signals have been weighted according to the absorber slab thickness. 8 layers represent a fully equipped calorimeter. 1+4 layers indicate the completion of the first 5 layers, the second layer left free for installation of fast trigger counters

The series production of chambers is starting. In the final version only ceramic is used as material for spacers and high voltage feed-throughs. This will reduce the signal loss to an even lower level. Also an efficient method of dry plasma cleaning by glow discharge has been developed allowing to clean and to fill a chamber within one day. This is an important aspect for mass production of chambers.

Muon detection. At the bottom of the calorimeter all throughgoing muons are detected by multi-wire proportional chambers. The position of a muon hit is determined by a crossing-point of three coordinates as is illustrated in Fig. 3. It shows an event with two simultaneous muons as obtained in a test set-up.

PATT.: 000 100 8 000 10 6:2
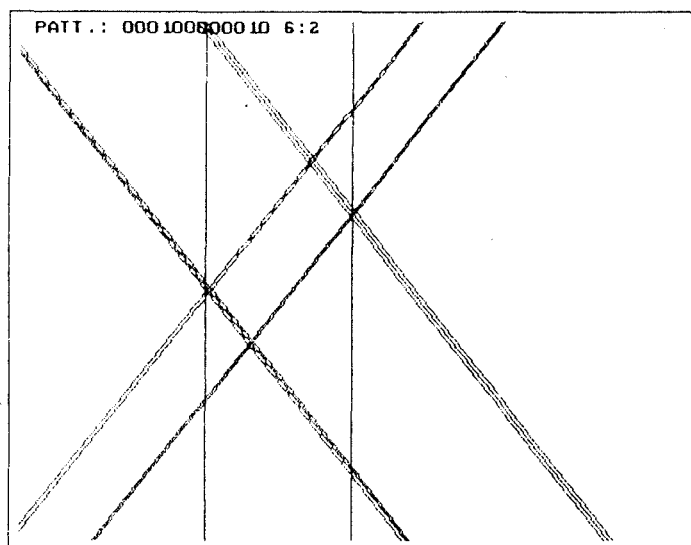
Fig. 3   Example of an event in a muon chamber. Pattern of two traversing muons.
Vertical lines represent anode wires set and inclined lines represent cathode wires set.

The knowledge of the exact position of a muon is important for a rough estimation of its energy. In the off-line analysis the shower direction is known and all the muon trajectories can be followed back through the iron absorber. Muons with energy above 1 TeV can be recognized by their high energy loss due to ionization and radiation. The spatial segmentation of the ionization chambers is fine enough to avoid particle overlapping at least in the lower layers of the calorimeter.

Test calorimeter. In order to study in detail the performance of the central detector, a test calorimeter has been set up using the first charge of ion slabs. It uses the prototype chambers and first chambers out of the series production. Two muon chambers are installed below the calorimeter to study the muon recognition in conjunction with hadron showers.

2.1.3. THE PROTOTYPE CLUSTER OF THE KASCADE ARRAY

F.BAUER, P.DOLL, R.GLASSTETTER, D.HAUNSCHILD, H.KERN,
H.O.KLAGES, W.KRIEGLEDER, F.KRÖNER, G.MONDRY,
C.RÄMER, A.SCHALLER, G.SCHMALZ, H.J.SIMONIS, H.SKACEL,
G.VÖLKER, Y.WETZEL

The first cluster of 16 detector stations has been set up on the experiment area at the KfK laboratory site. Detectors are completed and installed presently at a rate of 2 to 4 per day. The HV supply lines and the signal cables to the central electronics container are connected accordingly. The picture shows the status around December 1., 1990. Detector installation and set-up of the data acquisition system should be completed by mid-February, 1991.

Fig.1   Prototype cluster of the KASCADE array

Details of the present detector designs and the selection procedures for PM tubes and scintillator sheets can be found in the following contributions to this report. The data acquisition system in the prototype cluster will be based on commercially available NIM- and CAMAC-electronics, supplemented by a few custom made modules. CAMAC readout will be organized by a LSI 11/73 system.

The first series of measurements will make use of uncorrelated single muons for detector adjustement, calibrations and checks for stability with time and temperature changes. The aim of this procedures is to reach a uniform response for all e/γ-detectors and for all μ-detectors in the cluster, respectively, by variation of the HV-supplies. Secondly, the individual signal delay times of the e/γ-detectors will be determined by use of a pulsed laser and a fiber optics system.

After the calibration procedures the cluster will become operational for the first measurements of the e/γ-and the μ-component of extensive air showers. Depending on the detector multiplicity required as a trigger condition for the data acquisition we will start measuring at a rate of about 10.000 events/day.

By use of this data set the reconstruction schemes for shower events which have been developed using Monte Carlo simulation results can be tested and further improved. Extensive tests of detector properties and long term stability will continue.

The results of these measurements should enable sound decisions on possible changes of detector design, e.g., the influence of a thin lead converter on top of the e/γ-detectors will be studied carefully.

In early summer, 1991, the second cluster of detector stations will be installed adjacent to the prototype cluster. The provisional NIM/CAMAC electronics will then be moved to the 2. cluster to start detector operation and testing.

We hope to have 4 clusters installed at the time of the next annual report.

2.1.4. SIMULATION OF THE KASCADE ARRAY

H.J.MAYER

For design studies of the KASCADE array and investigations concerning the reconstruction accuracy of shower parameters a general purpose Monte Carlo program has been developed. The whole array with all detector stations is described in the program. Complete air showers, generated with a seperate program and expressed in terms of the kinematic variables of the individual shower particles, are input to the simiulation. For the simulation of the detector setup and its response to the electromagnetic cascade af an air shower, the program package Geant3 [1] is used. Geant3 is a highly developed system of detector description and simulation tools and widely distributed in the domain of high energy physics.

Particles, incident to a detector station, will explicitly be followed through the whole setup, taking into account all relevant physical interaction mechanisms with the detector materials. Secondaries, which might be created in these interactions will be generated and followed too. Fig. 1 displays as an example the tracks of a simulated event, which was initiated by a single 1 GeV gamma ray particle, together with the geometry of one detector station as it is realized in the program. During the tracking phase, all information necessary for the computation of the detector response will be recorded and stored. After all particles of a particular event have been tracked, this information is converted into a corresponding photomultiplier signal, from which the detector response, i. e. signal time and pulse height, are extracted. A list of digitised times and pulse heights, written in a data format similar to the future real raw data, forms the final output of the simulation. This allows to analyze the Monte Carlo data with the same software that will be used for the real data.
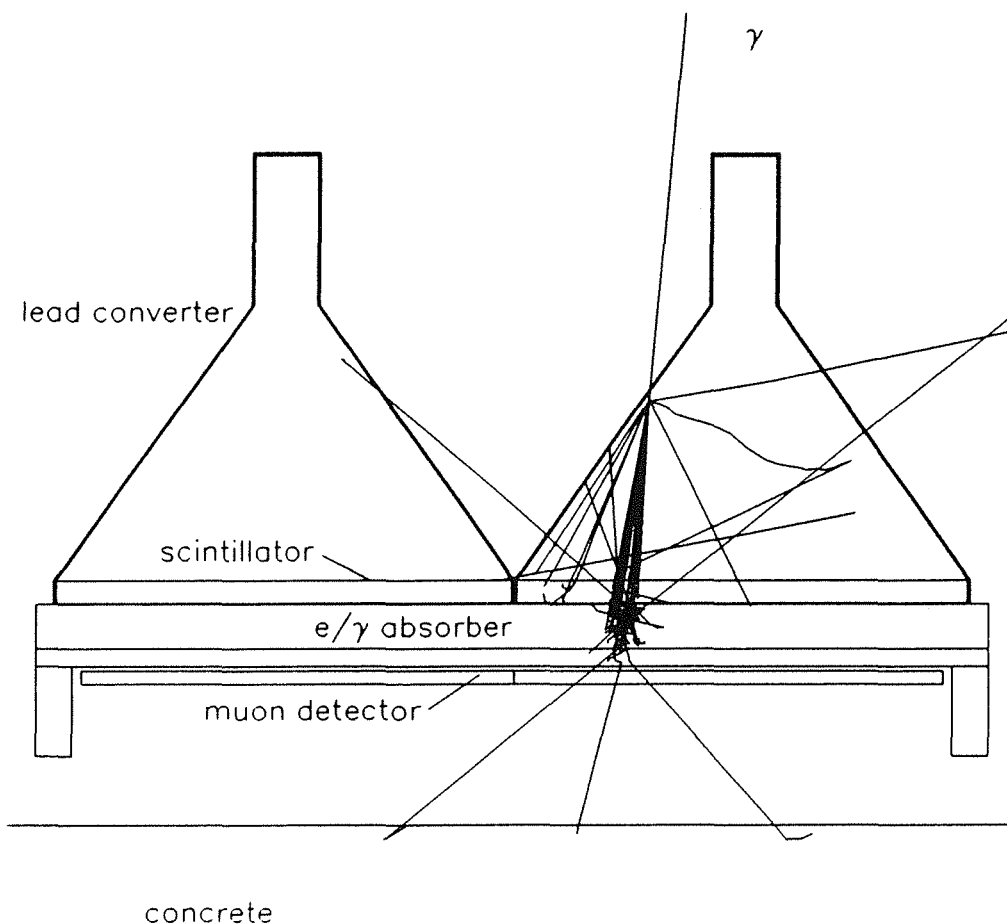
Fig. 1   A simulated detector event initiated by a single incoming γ ray of 1 GeV

Results:

The detectors of the KASCADE array will be equipped with a thin lead converter, which has been shown to improve the angular reconstruction accuracy of an extended air shower array significantly [2]. This effect has been studied in detail by simulation and subsequent reconstruction of more than 2500 air shower events [3]. The investigation has confirmed the predicted improvement in the angular resolution. For the KASCADE array structure and for showers near the energy threshold of the array ($N_e \sim 300$) a total increase of about 60% in the angular accuray was found. For larger showers with $N_e \sim 10^5$ one still observes a 30% effect (Fig. 2). The optimum thickness concerning the angular accuracy has been found
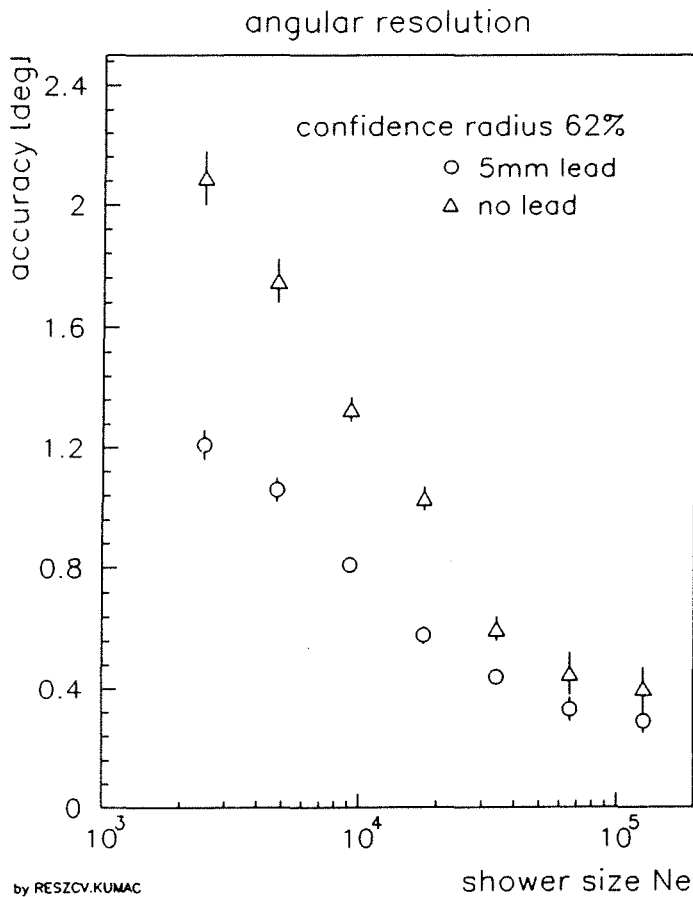
Fig.2 Angular resolution as a function of shower size for an array without converter and for 5 mm lead converter above the e/γ detectors.

to be in the range of 5 to 10 mm. The measurement of the lateral electron distribution however favours a thin converter with only a few mm thickness, a 10 mm converter e. g. would diminish the resolution in the shower size by about 30%. As the best compromise a value of 4-5 mm turned out for the thickness of the lead converter. One then nearly exhausts the potential gain in the angular resolution, optimises the lower energy threshold and maintains the accuracy in the determination of the age parameter by loosing less than 20% in the shower size resolution.

[1]   Geant3, Cern Data Division.

[2]   J.Linsley, Proc. 20th Int Cosmic ray Conf. Moscow 2, 442(1987)

[3]   H.J.Mayer, Nucl. Instr. and Meth. A294 , 651(1990)

2.1.5.   RECONSTRUCTION SCHEMES FOR EVENTS IN THE KASCADE ARRAY (EAS)

H.J.MAYER

The development of the software needed for the offline-reconstruction of the KASCADE array events has been started. For the design and testing of the program a large set of shower event data has been created using the above KASCADE array simulation program and, in addition, shower events generated with CORSIKA. In its current form, the program already allows a full event

detectors hit   955
maximal energy 930 MeV
at det. ID 11 169 676

analysis results IL = 2
Xc,Zc   0.8   0.0 m
Th,Ph   0.1 −113.7 deg
Ne,S   256.E3 1.18

E‹TASE   event   4   run 11101   deposited energy ED RAW
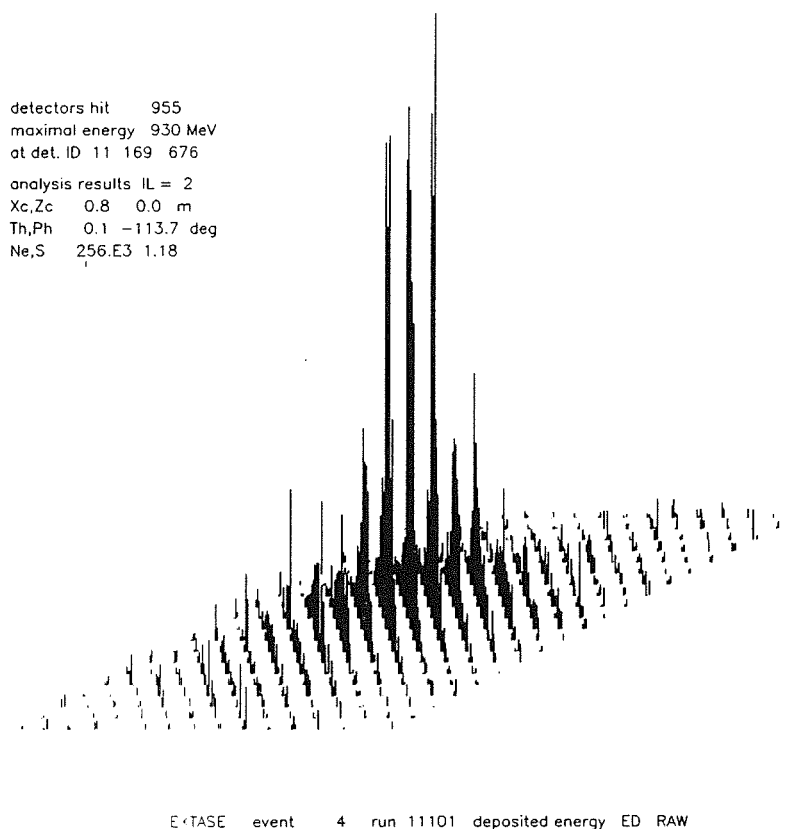
Fig.1   Map of e/γ detector hits initiated by a $2 \cdot 10^{15}$ eV proton induced EAS. The length of the vertical bars indicate the energy deposit in an individual detector.

analysis in terms of shower direction, shower size, lateral distribution and muon content. An interactive version of this program permits a graphical display of the individual shower events, its analysis under various aspects (e.g. lateral distribution of the e/γ and muon component, energy and time spectra, fit curves etc.) and an interactive step-by-step analysis.

As an example Fig. 1 shows an event display of the measured energy deposits in the e/γ-detector caused by an individual vertical (proton induced) air shower of energy $2 \cdot 10^{15}$ eV (Fig. 2) and its NKG analysis of the lateral distribution of the e/γ component giving core position, shower size and shower age.

EγTASE   event   4   run 11101   lateral distribution ED ENP
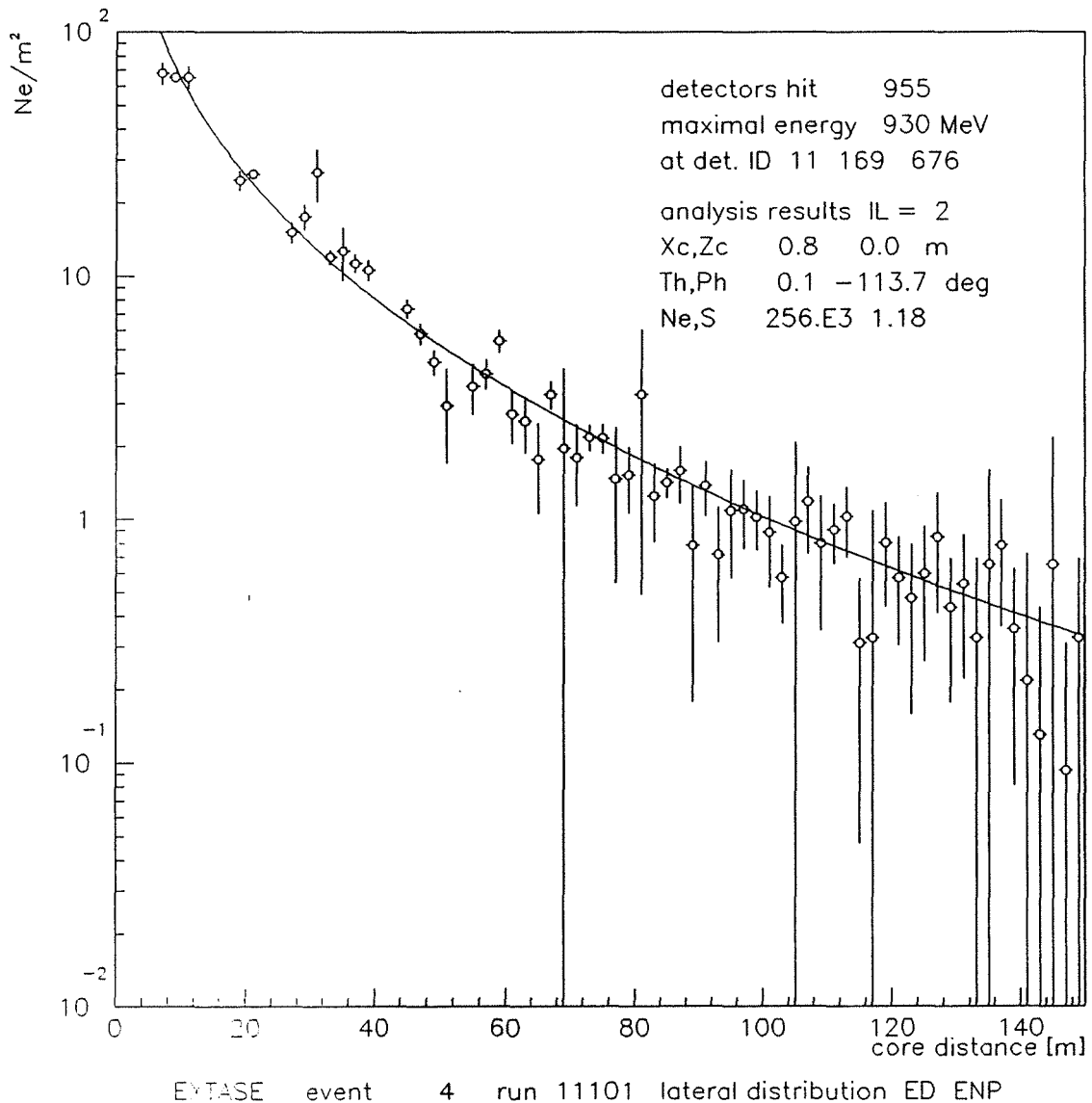
Fig.2   NKG fit to the measured e/γ lateral distribution for a proton induced air shower of $2 \cdot 10^{15}$ eV. $N_e = 2.56 \cdot 10^5$, age s$=1.18$

2.1.6.   MEASUREMENTS ON AIR SHOWERS

G.VÖLKER, H.O.KLAGES

The development of the KASCADE array detector for the e/γ-component of EAS (Extensive Air Showers) has been finished. In comparison to ref. [1] the detector geometry and the light reflecting scheme inside the detector have been changed (Fig. 1).
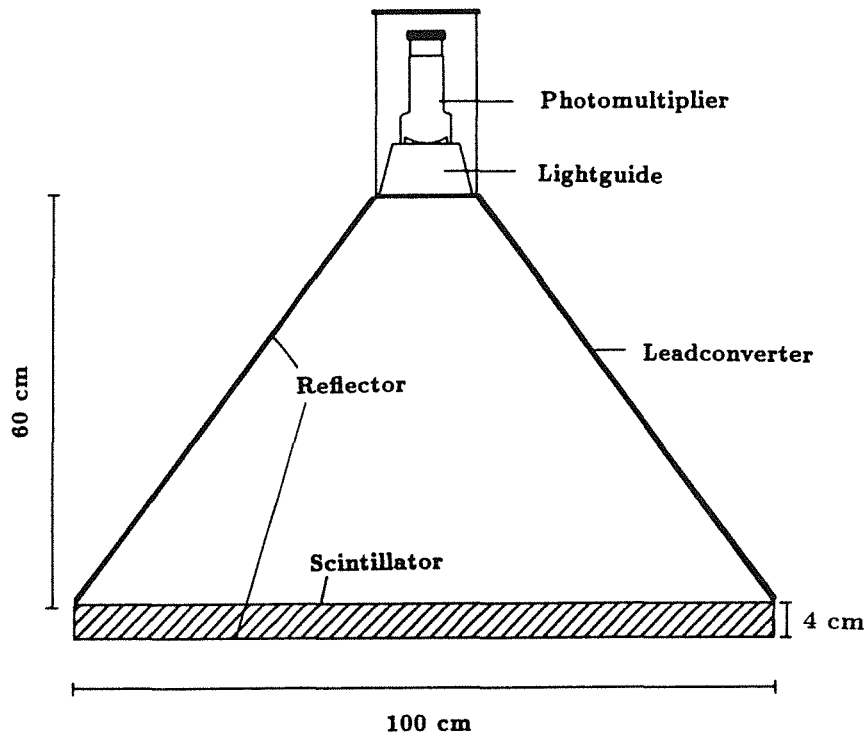
Fig.1   Schematic drawing of the e/γ-detector for the KASCADE array.

The energy resolution for penetrating muons improved to about 10% and the time resolution remains about 0.8 nsec. Fig.2 shows an experimental pulse height and time spectrum taken with a muon telescope of two identical array detectors with a vertical distance of about 160cm.

Using four prototype detectors a small air shower array had been set up in front of the neutron hall near the cyclotron (Fig. 3).

In a little experiment the detector stability in time (all four detectors were running since August'90 in a temperature range of 30 to -10 degrees without any problem), and the response to real air showers has been studied. An EAS in this setup was defined by a four-fold coincidence of all detectors. Eight parameters were measured and stored as event list on tape:

● Time differences between all four detectors and det. 3

● Four detector pulse heights
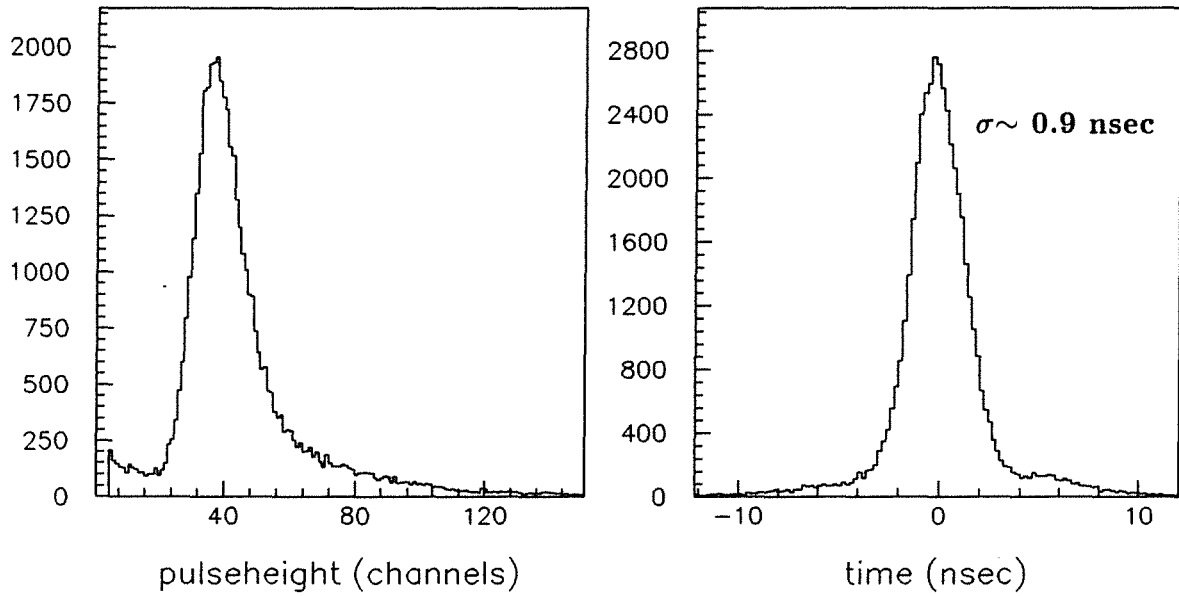
Fig. 2   Experimental pulse height (a) and timing distribution (b) for single muons traversing the counter in the whole detector area; (b) has not been corrected for the timing effect in the muon telescope.
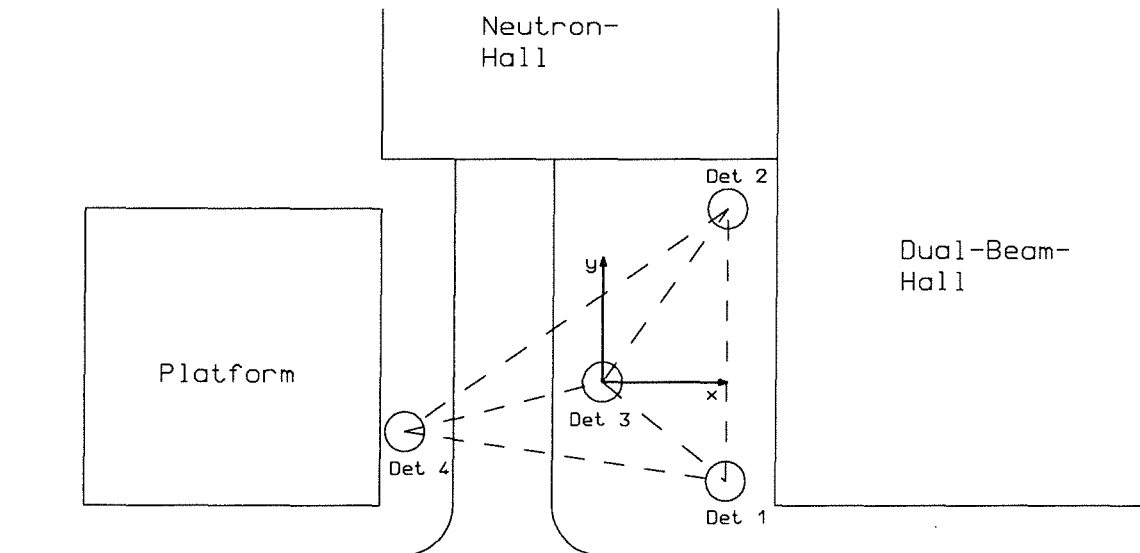
Fig. 3   Schematic setup of the air shower experiment near the cyclotron building.

First, the angles of the shower axis have been calculated by using the four time differences and a very simple calculation method. In a first step the normal vectors of three planes, defined by the distance and time differences of detectors 1-3 and 2-3, respectively, 2-3 and 2-4, respectively, 4-3 and 1-3 respectively, have been calculated. In a second step an averaged vector was calculated by a simple addition of the three normal vectors. Then the zenit and azimuth angle of the showers were given by the direction of this final vector. The result of these evaluations are shown in Fig. 4.
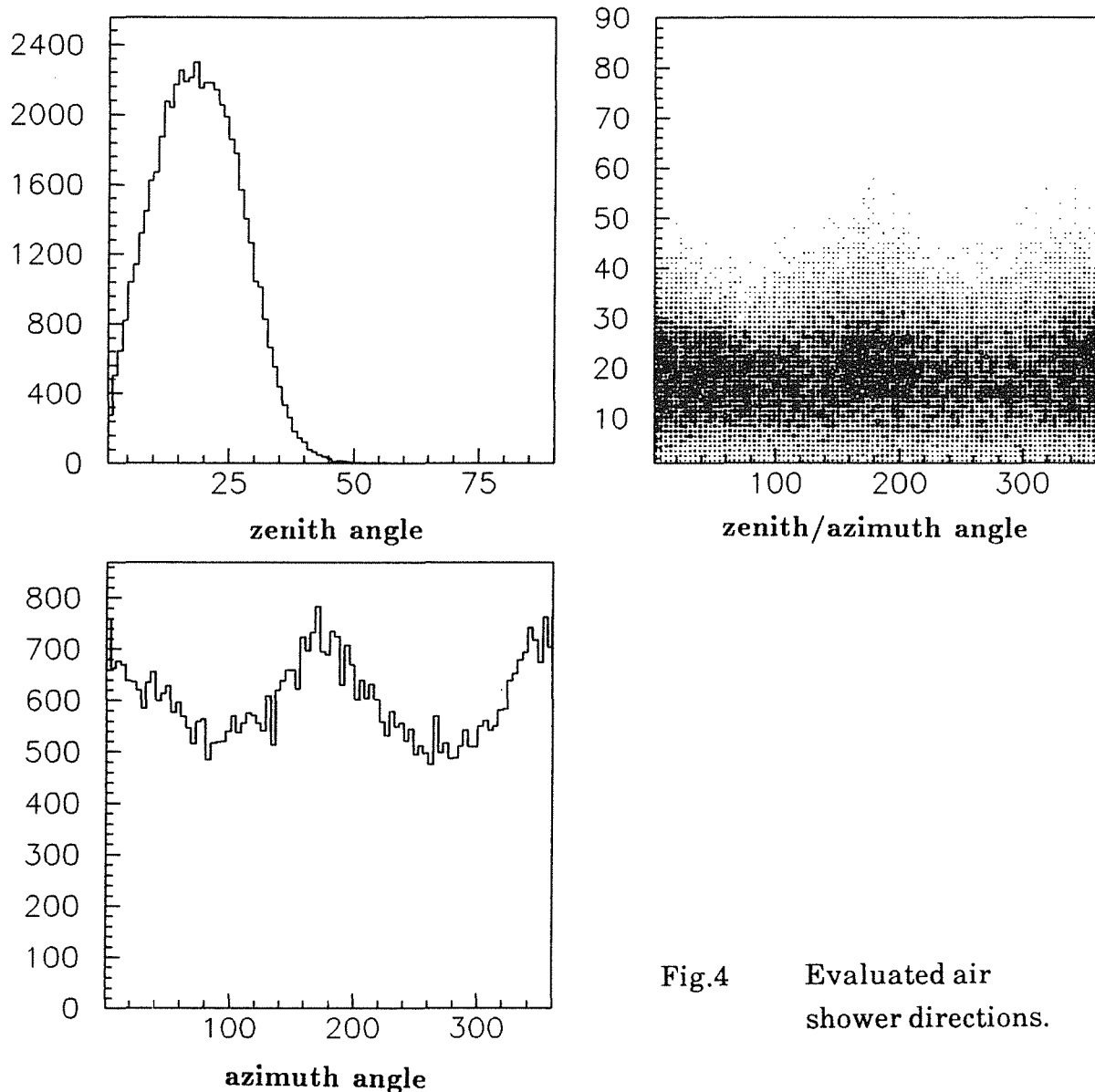
Fig.4   Evaluated air shower directions.

In the angular distribution of events the shadow of the massive iron platform and the dual beam hall can be seen in comparison to northern directions where no buildings disturbed the measurement. There was also no big effect by the thin walls of the neutron hall.

With this simple air shower experiment shower directions could roughly be determined, and the behaviour of the array detectors could be controlled in realistic working conditions over an extended period of time.

[1]   G.Völker, H.O.Klages, KfK report 4660, Kernforschungszentrum Karlsruhe p.113 (1990)

2.1.7.   MUON DETECTION IN THE KASCADE ARRAY

W.KRIEGLEDER, H.O.KLAGES

For the EAS experiment KASCADE, a scintillator based muon detector with a partitioned structure was developed to measure the number and lateral distribution of muons outside the shower core.

Fig. 1 gives a schematic view of the detector layout which is determined for the first prototype cluster of the array. The muon counter consists of 4 squares of NE 114 ($90 \times 90 \times 3$ cm^3), read out by wave length shifter bars ("Y7") at all edges.
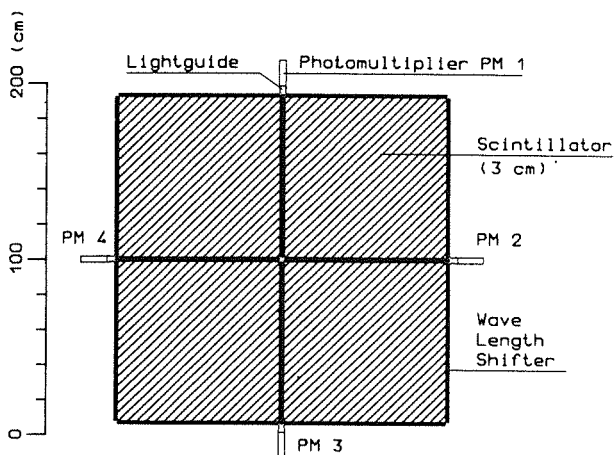
Fig.1   Schematic view of the muon detector.
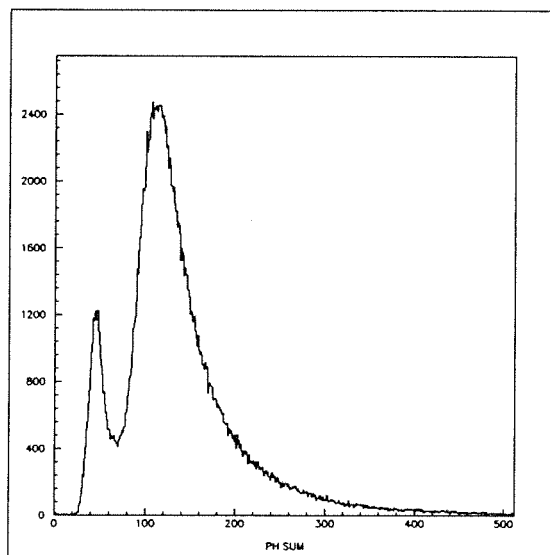
Fig.2   Experimental pulse height distribution for one quadrant of the muon detector.

Fig. 2 shows a typical pulse height spectrum of one square counter for cosmic muons and a background of electrons and photons. This measurement was triggered by a coincidence of PM1 and PM4 with low thresholds. The signals of these two photomultipliers are summerized to compensate light attenuation effects in the scintillator. The peak/valley ratio as shown in Fig. 2 is about 6/1. This is sufficient to seperate the muons from electrons and photons by an energy cut.

In the first cluster of the array 16 detectors of this type are used, consisting of 64 scintillator sheets and 192 WLS bars in total. To achieve a uniform detector quality in this mass production, the components and materials have been studied carefully.

Fig. 3 shows several light transport curves of a WLS bar ($88 \times 3 \times 1$ cm^3), doped with 20 ppm "Y7". The influence of different handling of the far side of the bar is demonstrated. The measurements were done using a ^{137}Cs source, fixed on a NaI-crystal as a light source.
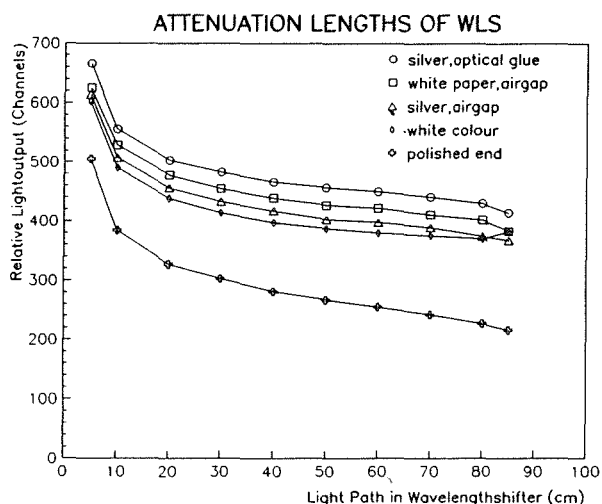
Fig. 3   Light transport curves of a Kyowa WLS bar with different preparation of the bar end.
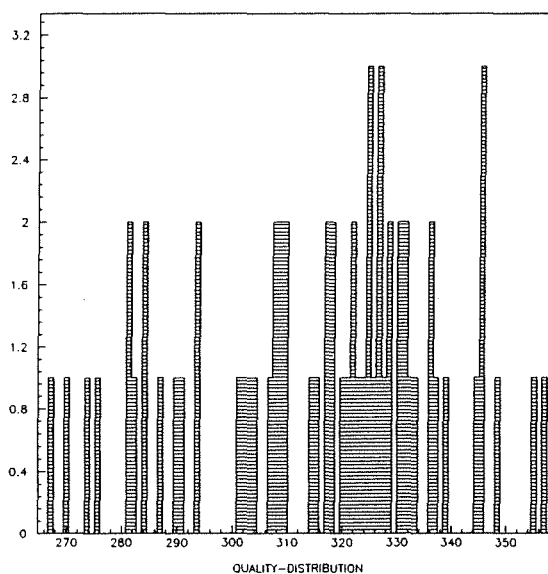
Fig. 4   Relative light output distribution of 64 sheets of NE 114 scintillator.

For each detector we need 4 squares of scintillator with matched light output. To get comperable quality information, we measured the relative light output of 64 sheets of NE 114 for traversing single muons. Fig. 4 shows that there is a broad distribution of the effective light output. We believe that the reason must be a

variation in the production process, because the distribution is not correlated with mechanical parameters like sheet thickness or surface quality.

The material tests were finished in December 1990. All components are delivered. The building of the detectors for the prototype cluster has started in January 1991 and was finished in February 1991.

2.2.   AIR SHOWER SIMULATION

2.2.1.   FRAGMENTATION OF NUCLEI INTO KASCADE

F.P.BRADY, H.O.KLAGES, J.KNAPP, G.SCHATZ, H.J.SIMONIS, T.THOUW et. al.

The interpretation of data from KASCADE requires comparison of the measurements with air shower simulations, now beeing carried out via the program CORSIKA [1]. Each simulation is based on successive generations of collisions over a wide energy range. Thus, cross sections and their energy dependence from array detector threshold up to the highest incident energies are important quantities.

Some of the primary cosmic particles are nuclei such as O, Si and Fe (and a smaller fraction of heavier nuclei). Relative to protons, nuclei (A,Z) of the same energy per nucleon have a larger magnetic field rigidity ($= \beta \gamma A / Z$) However, at the same total energy (per particle), protons are much (by a factor of Z) more rigid, and so can escape confining magnetic fields. Thus it is clear, that a determination, as a function of energy, of the nuclear composition of the cosmic particle flux is important in understanding the origin and transport of these particles.

Presently, the CORSIKA simulation code has only limited treatment of these cases (or distinct from the case of incoming protons). In the collision of a projectile nucleus with an air nucleus (nitrogen, oxygen or argon) it is assumed that a calculated fraction of the projectile nucleons participate in collisions with the nucleons of the air nucleus. The rest of the projectile nucleus is assumed to fragment into free nucleons moving with the original velocity (or energy per nucleon) of the projectile. However, fragmentation data mainly at lower energies (from $\simeq 1$ to 350 GeV / nucleon) show that the above treatment of nucleus-nucleus interactions is incomplete : In most collisions at least one relatively large projectile fragment survives and subsequently de-excites to a particle-stable nucleus which can collide again, and so on. It has been shown [2] that the effective interaction lengths are different for the case of complete fragmentation (as assumed in CORSIKA) and no fragmentation of a nucleus in air.

The fact that a large fraction of the collisions are peripheral and give rise to 'heavy' fragments can be seen from the model of colliding 'black' spheres, where the interaction cross section is $d\sigma_I = 2\pi b \cdot db$. b is the impact parameter and ranges from $b = 0$ for perfectly central collisions to $b = R_p + R_T$ for grazing

collisions. At the mean impact parameter $\langle b \rangle = 2/3 (R_p + R_T)$ large fragments are produced.

As measured at GeV per nucleon energies, the projectile fragments have a very small downshift in mean longitudinal (or z) momentum and receive a relatively small (500 MeV/c) transverse (T) momentum impulse. Following the collision the x, y and z momentum distributions are well approximated by gaussians with width parameters

$$\sigma_x^2 = \sigma_y^2 = \sigma_z^2 = \sigma_0^2 \cdot A_F (A_P - A_F) / (A_P - 1) ; \qquad \sigma_T = \sqrt{2} \, \sigma_x$$

In the projectile frame, $\langle p_x \rangle = \langle p_y \rangle = 0$ and $\langle p_z \rangle \simeq -30$ MeV/c. In the theory of Goldhaber [3], which, it should be noted, is energy independent, σ_0 is a parameter which depends on the momentum of nucleons inside the nucleus. In the simple Fermi gas model of uncorrelated nucleons where

$$\langle p^2 \rangle = 3P_F^2 / 5 \, , \, \sigma_0^2 = P_F^2 / 5$$

or $\sigma_0 \simeq 100$ MeV/c. Fragmentation data at GeV per nucleon energies for ^{12}C and ^{16}O [4] and for ^{40}Ar [5] and ^{139}La [6] projectiles support the theory. However it appears that σ_0 is increasing with fragment mass (probably due to collective effects from Coulomb and nuclear forces).

We are developing an appropriate model of nuclear fragmentation at KASCADE energies, where no data exist. Then fragmentation cross sections, transverse momenta, etc. can be provided for the CORSIKA simulation. We have compiled a rather complete summary of existing fragmentation data as available from the experiments at the Bevalac (0.2 to 2.1·A GeV), BNL (= 10·A GeV), and CERN (60 and 200·A GeV), and have also surveyed available collision models. Very complicated Monte Carlo interaction models, such as the Lund color string fragmentation model, FRITIOF, exist. However, these do not treat the spectator nuclear fragments except as independent nucleons. The model which appears to provide the best description of available nuclear fragmentation data and to be most applicable to KASCADE energies, is the Abrasion-Ablation (AA) model [7]. This model, which is sometimes called the participant-spectator model, describes the features of "limiting fragmentation" (energy scaling) and "factorization" which are displayed by the data at energies above about 1 GeV per nucleon. The main assumptions of this model have been justified using Glauber theory [8]. It is assumed, that the collision happens very rapidly, and that the projectile and target nuclei carve (or abrade) pieces out of each other in the region

where they overlap. The nucleons in this overlap region undergo collisions and are thus called participants, while the remaining pieces are called the (projectile- and target -) spectators. See Fig.1 . It is also assumed that there is little energy and momentum transfer between the spectators and the participant regions. Thus, in the lab frame the target spectator essentially remains in place following the abrasion stage while the projectile spectator continues on with essentially the incident velocity.

Due to surface energy changes and some 'frictional' interactions, the spectators are in excited states and lose energy by emitting particles (mainly nucleons). This is the ablation or evaporation stage, and calculating or estimating the excitation energy of the spectators is one of the most difficult things. The cross section data for Fe and Ar fragmentation at GeV per nucleon energies indicate spectator excitation energies of $\simeq 100$ MeV, and a good part has to be put in by hand, because the surface energy plus the 'frictional' energy of cutting all the nucleus wave functions is not enough [9]. Thus it is conjectured that additional energy [8,9] and transverse momentum [6] are transferred to the spectators via nucleon-nucleon scattering from the participant region.

Fig. 2 shows the computational procedure which can be used to obtain the fragmentation cross sections, $\sigma(Z_f, A_f)$. We are investigating obtaining the appropriate abrasion and ablation (evaporation) codes and linking them. And as well we are investigating further the validity of the model at KASCADE energies.

For example, the nucleon-nucleon collisions of the participants will be at much higher energies, and many more hadrons (mainly pions) will be produced. However, the available data show that the transverse momenta of the hadrons are small and increase very slowly with energy. In addition, as viewed from the participant 'fireball' (Fig. 1) the spectator fragments will be Lorentz-contracted discs receding from the fireball at $v \simeq c$. Also finite pion formation times (~1 fm/c), from eg, Δ decay, further reduce the probability of pion-spectator interactions. Thus it seems improbable that enough scattered hadrons or secondary pions will be absorbed by the spectators so as to cause their disintegration. This point is under further investigation.

We expect quite soon to be able to introduce nuclear fragmentation into the CORSIKA shower simulation code. (Some parameterization of the fragmentation cross sections, as given by Silverberg and Tsao for low energies, may be possible.) Then we can investigate if there are differences in the space-time or energy structure of the shower particles which will allow better isotope determination of the incident Cosmic particles.
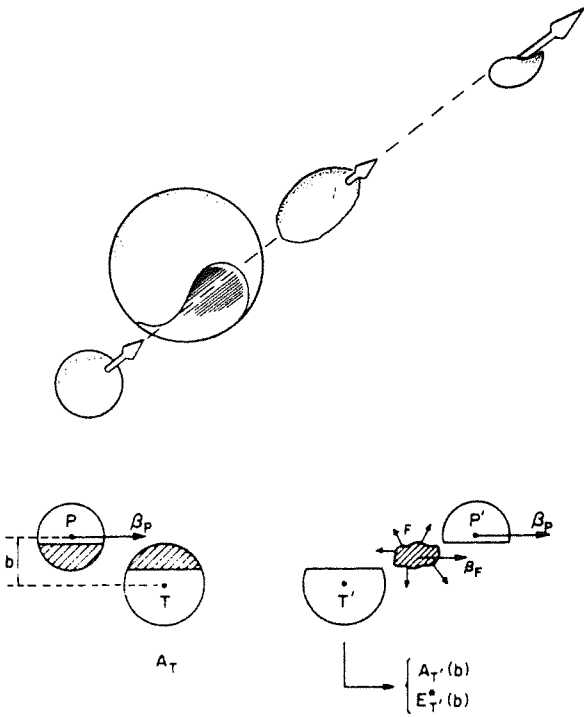
Fig. 1   Models of fireball abrasion in 3D and 2D (see [9,10]. The participant region is shaded.
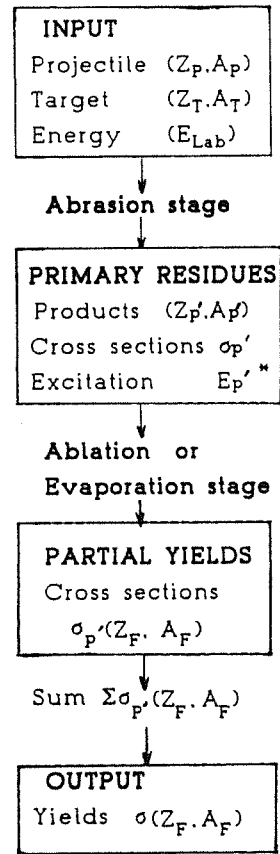
Fig. 2   Computational procedure for Abration-Ablation model calculation of projectile fragment cross sections

[1]   CORSIKA (COsmic Ray SImulations for KASCADE) see J.N.Capdevielle et al., KFK 4660 (1990). J.N.Capdevielle, J.Phys. G15, 909 and J.Knapp, CORSIKA Mini-Workshop, ibid ref.2 (1989) .

[2]   G.Schatz, CORSIKA Mini-Workshop, Dec. 6-7 Institut für Kernphysik, Kernforschungszentrum, Karlsruhe (1990) .

[3]   A.S.Goldhaber, Phys. Lett. 53B, 306 (1974) .

[4]   D.E.Greiner et al. Phys. Rev.Lett. 35, 152 (1975).

[5]   Y.P.Viyogi et al., Phys. Rev.Lett. 42, 33 (1979).

[6]   F.P.Brady et al., Phys. Rev.Lett. 60, 1699 (1988) .

[7]   W.J.Swiatecki, LBL report, 1976 (unpublished), and J.D.Bowman, W.J.Swiatecki and C.F.Tang, LBL-2908, 1973 (unpublished) are usually given credit for AA model. However Y.Eisenberg, in analysing cosmic ray data, [Phys. Rev. 90, 1378 (1954).] first introduced the salient features of this model.

[8]   J.Hüfner, K.Schäfer and B.Schürman, Phys. Rev. C12, 1888 (1975) .

[9]   L.F. Oliveira, R.Donangelo, J.A.O.Rasmussen, Phys. Rev. C19, 896 (1979).

[10]   J.Gosset et al., Phys Rev. C16, 629 (1977).

2.2.2.   AIR SHOWER SIMULATION AND ANALYSIS

J.N.CAPDEVIELLE*, P.GABRIEL, H.J.GILS, P.K.F. GRIEDER**, D.HECK, N.HEIDE, J.KNAPP, H.J.MAYER, J.OEHLSCHLÄGER, H.REBEL, G.SCHATZ, T.THOUW, T.WIBIG***

Simulations of extensive air showers are an important task accompanying the design and construction of the KASCADE experiment and, in future, the interpretation of data taken. Therefore, a detailed Monte Carlo simulation program CORSIKA (COsmic Ray SImulations for KASCADE) was developed [1,2] which has continuously been extended and improved.

In the high energy interaction part (above 10 GeV center of mass energy) of the code following items were added or changed as compared to the previous versions [2] .

The parametrization of the average number of secondary particles per interaction was updated to fit data from the Tevatron collider at $E_{cms} = 1.8$ TeV.

A proper correction of the number of secondary baryonic particles due to hyperon production was included. These particles make a significant contribution to the inelasticity and have the same rapidity distribution as the light meson but considerably higher masses.

In diffractive interactions diffractive masses as low as the sum of projectile and π^0 mass are now allowed in reactions with a low number of secondaries.

Moreover, some flag controlled optional features have been introduced enabling an easy study and comparison of different models. These options concern charge exchange reactions of pions and kaons, a narrower rapidity width for neutral pions as compared to charged ones and additional fluctuations of π^0 production numbers.

For nucleus-nucleus collisions the number of interacting projectile nucleons is now allowed to be larger than one and to fluctuate according to Glauber calculations based on experimentally determined nucleon distributions in nuclei.

Finally, the decay of pions and kaons was treated properly by calculating the 2- and 3-body decays using Dalitz amplitudes.

With these modifications a large number of air showers induced by gammas, protons, oxygen, and iron primaries in the energy range $2 \cdot 10^{14}$ - $4 \cdot 10^{15}$ eV, have been simulated. For the electromagnetic component the full Monte Carlo option based on the EGS4 code was used. This leads to very long computation time which can nevertheless be dealt with using our special parallel computer [3]. The energy spectra and lateral distributions of shower particles obtained from these simulations are important for the design of detectors and a reliable simulation of the detector response [4].

A Principle Components Analyis was applied to a number of shower particle observables including the hadrons. This determines the expected element
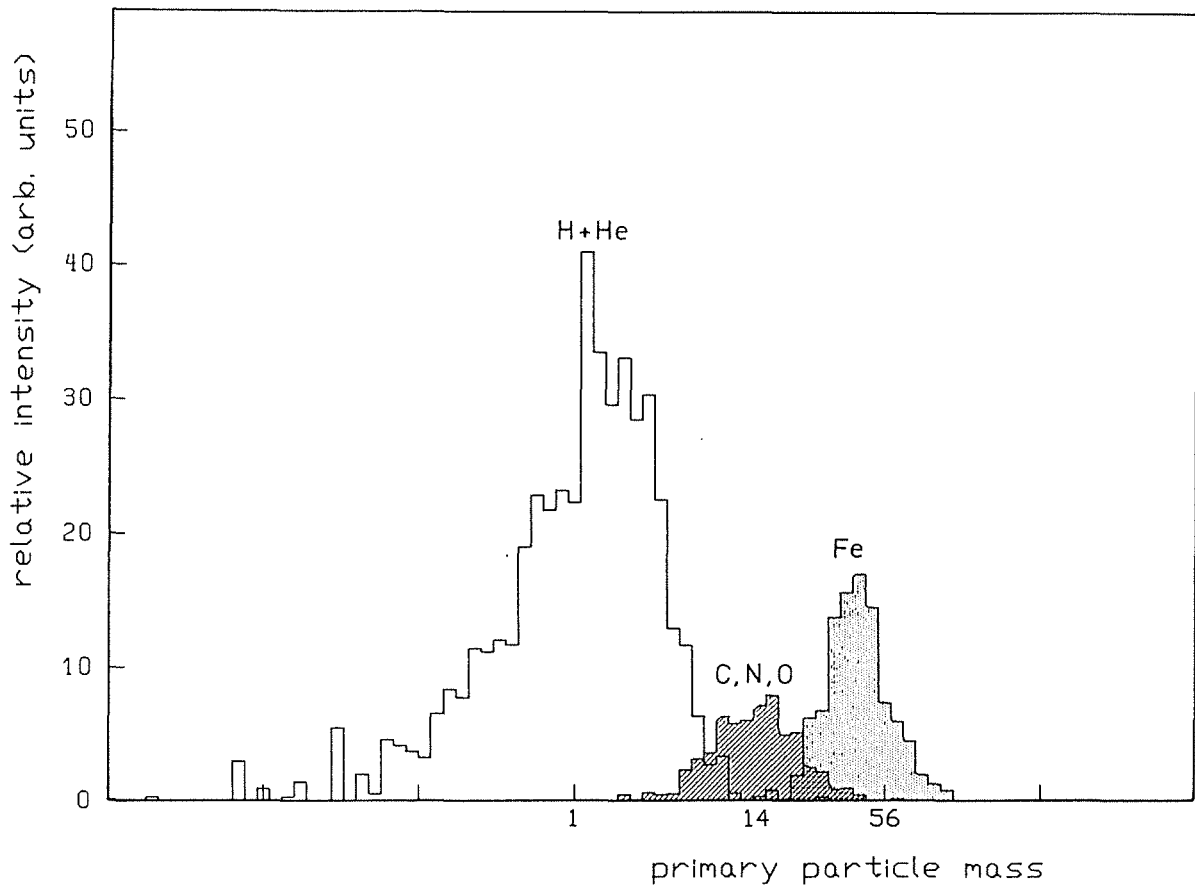
Fig. 1   Element resolution of the KASCADE experiment obtained from a Principle Component Analysis of various observables from simulated air showers induced by H,O and Fe-primaries in the energy range $2 \cdot 10^{14}$ - $4 \cdot 10^{15}$ eV. A relative abundance of 6:1:1.7 was assumed. The abscissa is a linear combination of three components being most sensitive to the primary element.

resolution of the KASCADE arrangement [5]. The result of this analysis is shown in Fig. 1, where a relative abundance of 6:1:1.7 between H:O:Fe was assumed. The H-Peak includes the contribution of α-particles and the O-peak the whole CNO group.

The simulation results have also been compared with existing data from experiments. It appears that the simulated proton induced showers develop too deep in the atmosphere whereas iron showers seem to reproduce the longitudinal development quite well. This is in agreement with results of the other simulations which show, however, that iron primaries cannot account for the large fluctuations of the depth of maximum [6].

[1]   J.N.Capdevielle et al., in Report KfK 4660, (eds. G.Drexlin,H.J.Gils) Kernforschungszentrum Karlsruhe (1990), contr. 2.4.

[2]   P.Doll et al., in Report KfK 4686, Kernforschungszentrum Karlsruhe (1990).

[3]   H.J.Gils et al.,Comp. Phys. Comm. **56**, 105 (1989).

[4]   H.J.Mayer, this report, contr. 2.1.4.

[5]   P.Gabriel, KASCADE-note MCS 90-1. Kernforschungszentrum Karlsruhe (1990), unpublished.

[6]   G.L.Cassiday et al., Proceed. 21st Internat. Cosmic Ray Conf., Adelaide, **3**, 154 (1990).

*   Laboratoire de Physique Théoretique, Université de Bordeaux, Gradignan, France.

**   Physikalisches Institut, Universität Bern, Bern, Switzerland.

***   On leave from Institute of Nuclear Studies (Cosmic Ray Laboratory) and University of Lodz (Poland).

2.3. DETECTOR DEVELOPMENTS

2.3.1. CALORIMETRIC MEASUREMENTS WITH TMS IONIZATION CHAMBERS

J.ENGLER, M.GETTERT, H.KEIM, J.KNAPP

Liquid ionization chambers using room temperature liquids are of interest for future particle physics detectors. Especially tetramethylsilane (TMS) is very well suited for calorimetry at high energies, high radiation doses and event rates. The KASCADE experiment will use such ionization chambers to measure energy and location of hadrons in the core of extensive air showers. Fig 1 shows the principle structure of a TMS chamber.
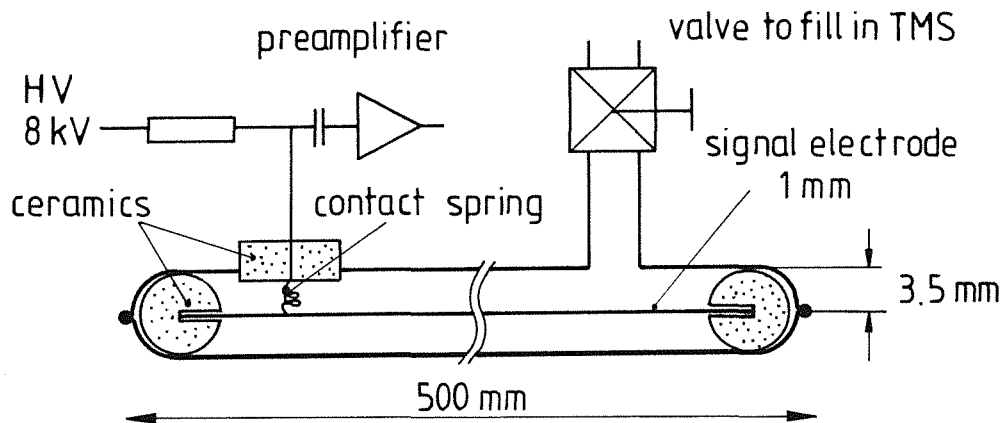
Fig. 1   Structure of the TMS chamber

12 prototype chambers have been assembled for calorimetric measurements of electrons and pions, and had been tested at the 10 GeV synchrotron of the ITEP in Moscow. Each chamber contains 6 readout strips. Electrons, pions and muons of momenta up to 6 GeV/c were simultaneously present in the test beam and classified by an appropriate trigger system. Several adsorber materials and thicknesses were available. Because of the small number of chambers it was not possible to construct a set-up for optimal measurement of electrons and hadrons at the same time. In Tab. 1 the parameters of the different set-ups are summarized.

In Fig. 2 The mean energy deposits for each channel is shown. Channel 1-6 belong to the first chamber, channel 7-12 to the second one and so on. The chambers were positioned in a way that the test beam penetrated the chambers in their 4th channels. The upper picture pesents 6 GeV electrons on iron. The shower is contained in the calorimeter and the lateral shower width is of the order of 1 X_0

	adsorber	tot. thickness	$\sigma(E)/\sqrt{(E)}$
e-measurement	25 mm Fe	17.0 X_0	0.36
	5 mm U	18.8 X_0	0.40
π-measurement	50 mm Fe	3.6 λ_0	1.29
	42 mm Pb	2.9 λ_0	1.39
	25 mm U	2.9 λ_0	1.47

Tab.1   calorimeter set-ups and energy resolutions

of the absorber material. The lower picture shows 6 GeV pions in the lead calorimeter. The hadrons are broader and leakage to the side and at the end of the set-up becomes important. The energy sum over all channels depending on the particle momenta are given in Fig. 3. The energy deposit is linearly rising with the primary energy. The fluctuations of hadron showers are bigger than of
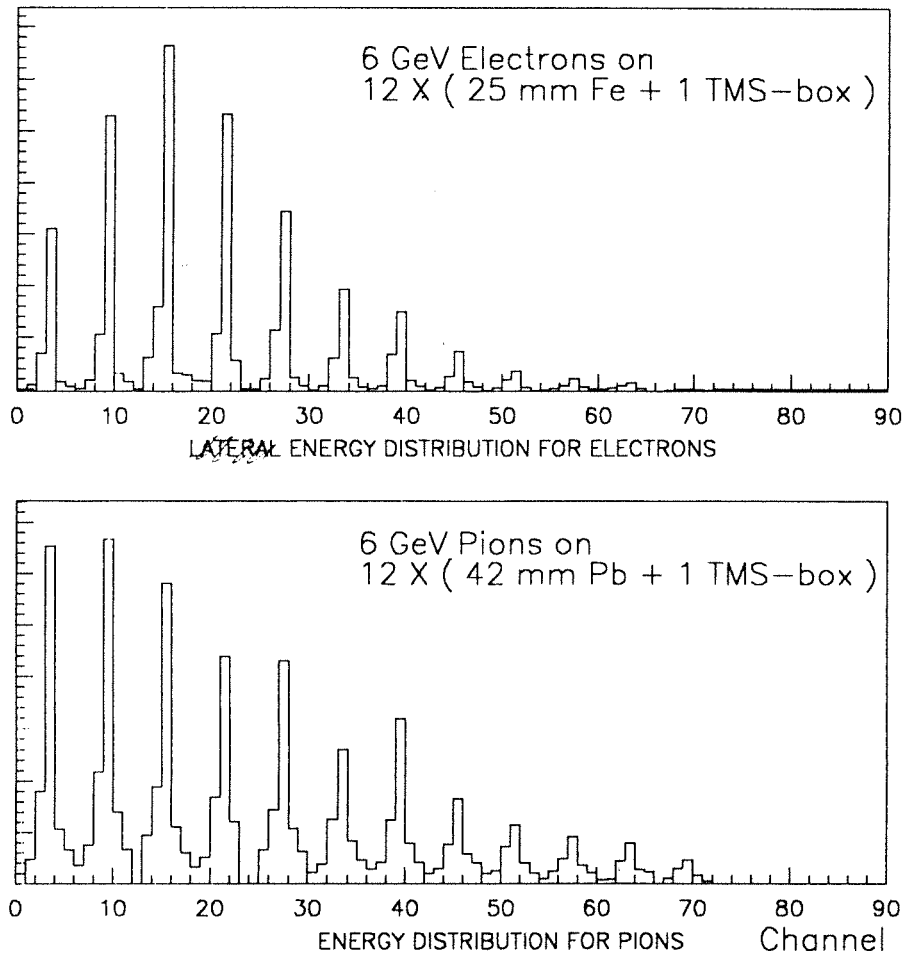
Fig. 2   Mean energy deposits for each channel

electron showers, as one expects. The energy resolutions are obtained by fits of the form $\sigma(E)/\sqrt{(E)} = \text{const.}$ to the measured points. The results are listed in Tab. 1.
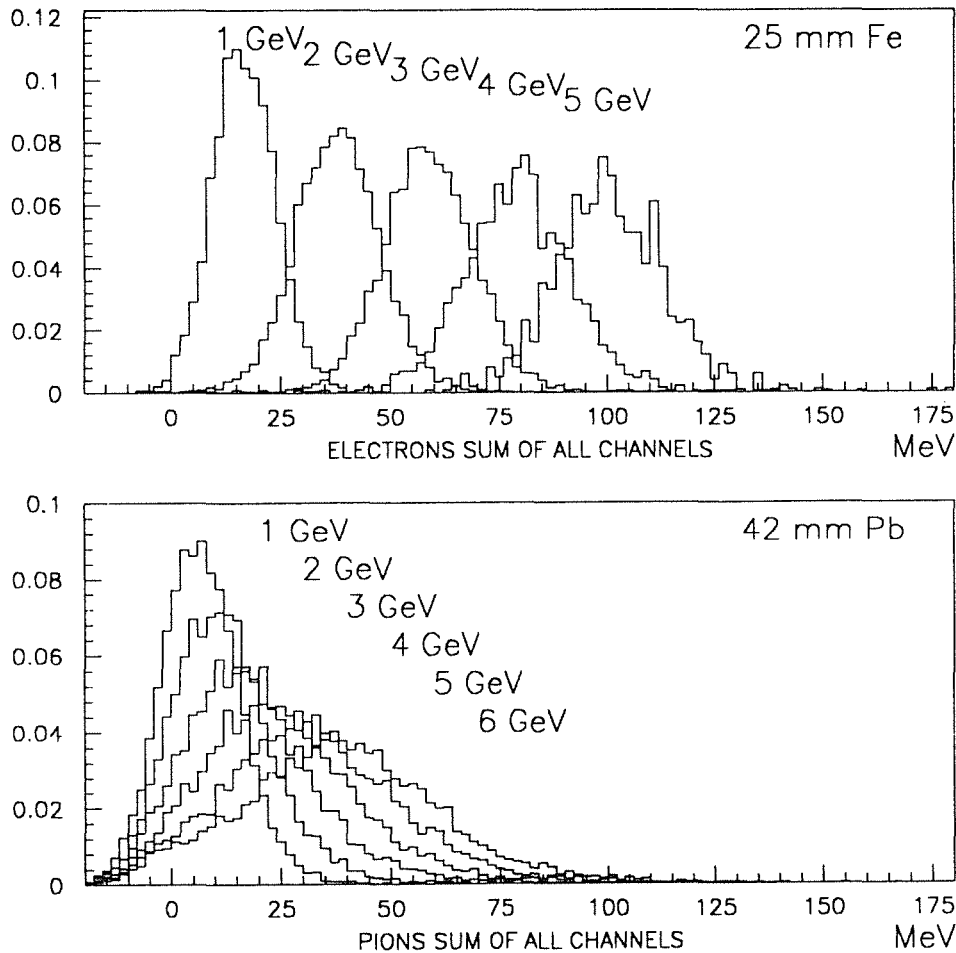
Fig. 3   Energy Sum

Detailed MC-calculations reproduce the measured results reasonably well for iron and lead adsorbers. This gives confidence to predict pulse heights and resolutions for calorimeters made of these materials with finer segmentation and full containment. An iron calorimeter with 25 mm absorbers would lead to an energy resolution for pions of $\sigma(E)/E = 0.88/\sqrt{E}$ and to a signal ratio of pions and electrons at the same energy of $n/e = 0.52$. In the the same way one can predict an energy resolution for electrons of $\sigma(E)/E = 0.18/\sqrt{E}$ and for pions of $\sigma(E)/E = 0.72/\sqrt{E}$ for a calorimeter consisting of 6 mm Pb-sheets. The ratio of pion to electron signals turns out to be $n/e = 0.71$.

In order to understand the uranium measurements, where discrepancies between simulation and data appeared, further studies and improvements of the simulation of low energy hadron interactions are necessary.

In october 1990 a second beam time in Moscow could be used. 40 chambers were available and have been assembled to fine segmented calorimeters, again using

Fe, Pb and U absorbers. Electronics an data taking have been improved and electrons and hadrons could be measured with the same calorimeter. The analysis of the new data is performed presently.

2.3.2.   AN EXPERIMENTAL SETUP FOR RELIABILITY AND PERFORMANCE TESTS OF LARGE AREA MUON - DETECTORS FOR KASCADE

H.J.MATHES, J.HORZEL, S.ZAGROMSKI, N.HEIDE, M.RIEGEL, H.J.GILS, H.REBEL, T.THOUW

For muon detection underneath the central detector of the KASCADE experiment [1], large area multi-wire proportional chambers (MWPC) will be installed. These chambers (available in different sizes) originate from the CELLO-detector at DESY [2], but they have been out of operation for some time.

The chambers consist of two cathode strip planes and an anode wire plane with alternately anode and potential wires. The wires have a distance of 6 mm to one another and of 8 mm to the cathode planes. The signals coming from a hit can be read out from all three planes. The rotation angle of $+34.16°$ and $-34.16°$, respectively, of the stripes of each cathode plane with respect to the anode wires, allows the determination of the hit's coordinates.

The chambers are operated with a mixture of 2/3 argon and 1/3 isobutane. It has been necessary to design an improved gas system. The chambers are supplied with different high voltages of $+2.1$ kV for the anode and -500 V for the potential wires respectively. More details about the chambers are reported elsewhere. [3,4]

A stack of four chambers of the smallest size type (2.2×2.4 m^2 sensitive area) was mounted into a test frame. Above and below the stack, segmented scintillator counters of smaller size (0.9×2.0 m^2) were placed. Their coincidence signal was used to trigger the chambers. A large fraction of the coincident events registered with this test setup, are expected to be muons from cosmic rays.

Presently, a CAMAC based readout system is used, taken over from the DESY experiment. This system was especially developed for readout and data compression for chambers of that type. Data acquisition is controlled by a PDP-11 based computer system. For reasons of compatibility to the data readout system of KASCADE, a VME based acquisition system is being developed. The chambers frontend electronic will be replaced by new modules, too, because the existing ones

have insufficient delay lines and a very high power consumption. In addition this allows a transputer aided adjustment of trigger levels and delays for all readout channels.

The offline software determines the hits in the chambers. Scatter plots of these hits and their projection onto the coordinate axes provide a tool to check the
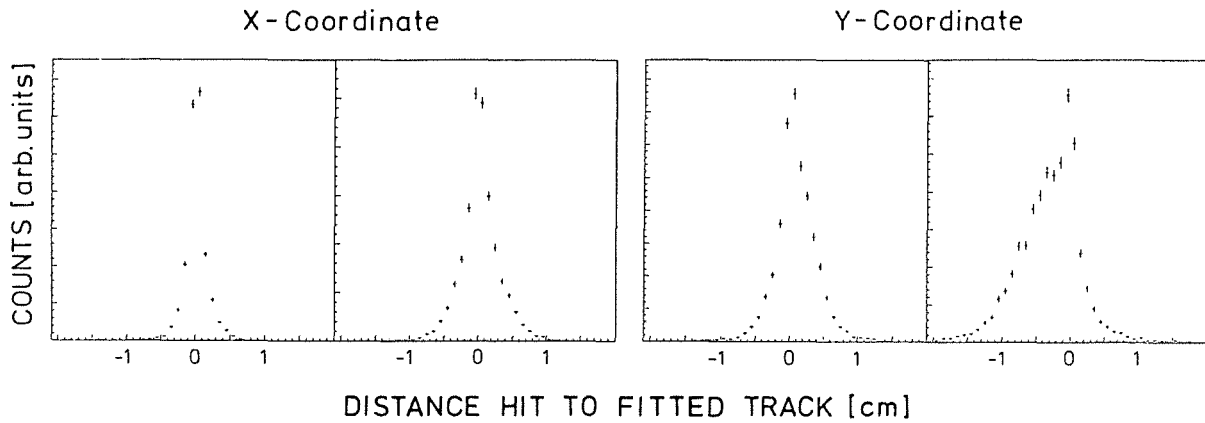
Fig. 1   Distance from calculated hit positions to the fitted track. The differences in x- and y-coordinates are separately presented for two different chambers. A shift of the almost gaussian shaped peaks indicates a misalignment of the chamber.
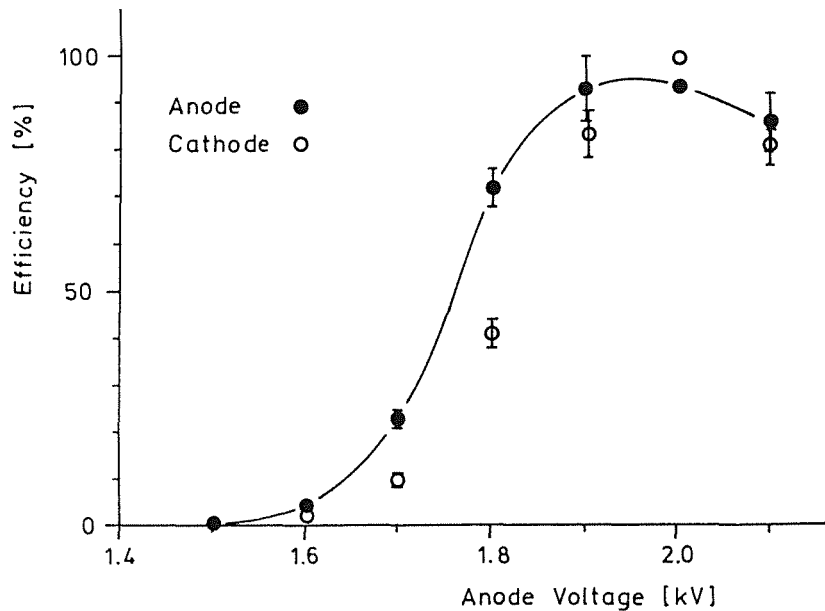
Fig. 2   Efficiency versus anode voltage for cathode and anode planes. The gas mixture and the high voltage on the potential wires were kept constant. The influence of the trigger upon the efficiency measurements and the probably by dead time caused drop of the efficiency at higher voltages, require some further investigations.

detector's operation. Using the hits in each chamber tracks are reconstructed by software. The criterion used requires a minimum number of three hits identified near a straight line. With this condition we find a spatial resolution of $\sigma_x = \pm 5$ mm, $\sigma_y = \pm 7$ mm, in the worst case, and $\sigma_x = \pm 2$ mm, $\sigma_y = \pm 3$ mm in the best case as shown in Fig. 1.

The measured efficiency is better than 90% at 2 kV anode voltage. For the anode plane it is slightly higher than for the cathode planes as shown in Fig. 2.

Measurements were performed with the trigger counters at different positions in order to obtain the angular distribution of the incident particles. Comparing the results of these measurements to simulations and additional measurements in a self-triggering mode gives a reasonably good agreement with a $\cos^2\Theta$-distribution [5].

[1]   P.Doll et al., KfK report 4686 (1990)

[2]   R.Aleksan et al., Nucl. Instr. Meth. 185, 91 (1981)

[3]   H.J.Mathes, J.Horzel, S.Zagromski, H.Rebel, unpublished report 1990

[4]   J.Horzel, KfK report 4815 (1991)

[5]   O.C.Allkofer, P.K.F.Grieder, Cosmic Rays on earth, Physics Data Series 1984

2.3.3.   SUITABILITY OF LIQUID SCINTILLATORS FOR KASCADE

Y.WETZEL

For the e/γ-detectors that are under construction for KASCADE a suitable liquid scintillator has to be found. The liquid scintillator should not show any temperature dependence in order to guarantee uniform year-round performance. Therefore eight different types of liquid scintillator have been examined for their temperatur dependence in the range from $-30°C$ to $+50°C$. The compton spectrum of a ^{22}Na-source has been measured and through differentiation the endpoint was determined.

Except for two liquid scintillators whose performance deteriored seriously at low temperatures there was nearly no temperature dependence found for the position of the endpoint. The position of the endpoints corresponde to the light output of the liquid scintillator.

As a high light output is desireable only the two brightest, temperature independent liquid scintillators were in the final selection. These are Quickszint 801A from Zinsser Co. and NE217B from NE Technology.

There have been further measurements of the light output and the time resolution using a muon telescope set-up with a fixed NE102A slab. At first NE217B showed a monotonic decrease in muon peak position and only stabilized after several days, whereas Quickszint 801A showed a rather constant muon peak position from the beginning. In addition, NE217B has about 10% lower light output than Quickszint 801A.

The time differences between the liquids and the plastic scintillator were measured for incident muons. Unfolding the measurements the effective time resolution of the liquid scintillators has been determined. The results are a time resolution of 0.80 ns for NE217B and 0.78 ns for Quickszint 801A, compared with 0.63 ns for NE102A.
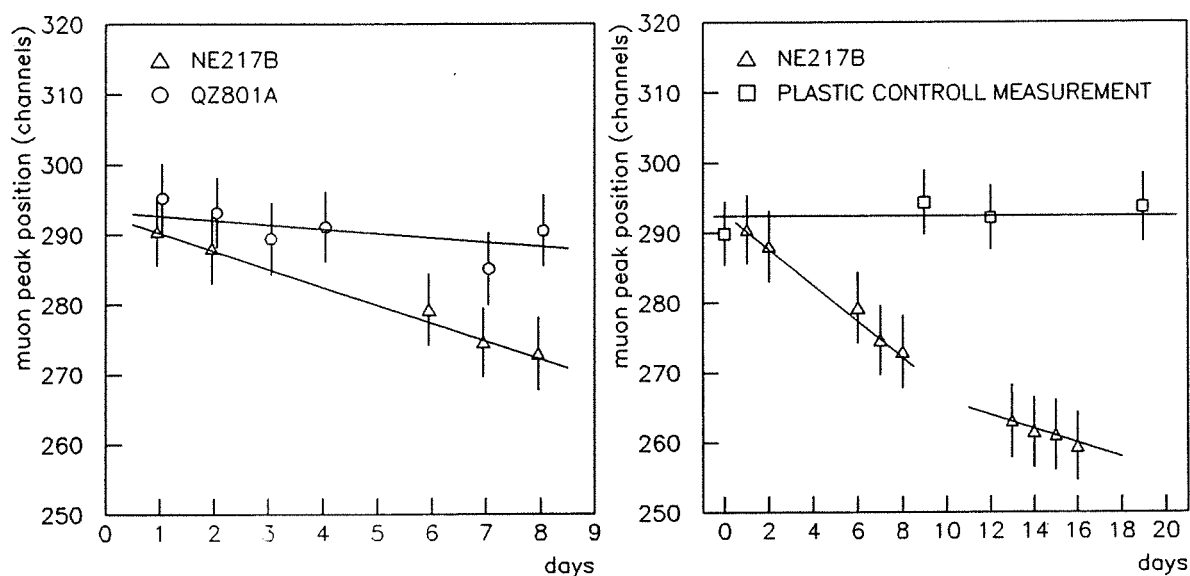
Fig. 1   Muon peak position for NE217B and Quickszint 801A

2.3.4. STUDIES TOWARDS A TRIGGERING AND TIMING FACILITY FOR THE CENTRAL DETECTOR OF KASCADE

B. SCHULZE, A. HANSER

The operation of the central detector of KASCADE needs a trigger. In addition, a timing facility measuring the relative arrival time of individual hadrons with an accuracy of a few nanoseconds would extend the experimental possibilities of the planned set-up. In the present layout of the hadron calorimeter for the second active layer level (behind 24 cm Fe + 5 cm Pb) plastic scintillators can be placed providing a trigger signal as required for a single impinging high energy hadron or few simultaneous muons. Since the iron of the absorbers originates from a dismantled nuclear plant and contains a weak ^{60}Co activity, the detectors must discriminate against ^{60}Co radiation. With respect to moderate cost and restricted vertical spacing the following concept is considered : Two thirds of the whole area are layed out with plastic scintillation detectors of dimensions 50 cm x 50 cm x 2 or 3 cm. Fig. 1 shows possible geometrical arrangements. Simple and cheap light
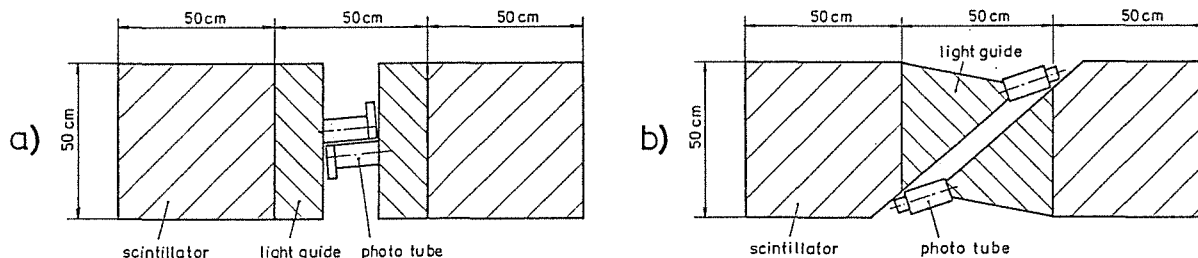
Fig. 1   Possible geometrical arrangements for the 2/3-lay-out of the trigger level of the central detector.

guides are machined from plexiglas slab material of the same thickness as the scintillator plates. One prototype detector for each geometry has been set up using Bicron BC 408 scintillation material of 2 cm thickness and a Philips XP 2262 phototube (2" end window). The detectors have been tested with electrons of about 1.6 MeV, which were magnetically filtered out of a Sr^{90}-Y^{90}-β-spectrum, and with cosmic muons. In order to get uniform and short detector output pulses, the light reflexion at the rear edge is suppressed by blackening this edge. Fig. 2 shows the output pulses averaged over the jitter. The pulse heights vary over the detector area within a factor of ∼ 2.5 as can be seen by local energy deposition using the test

electron source. The variation of rise time and pulse length is small. This is valid for both detector geometries.
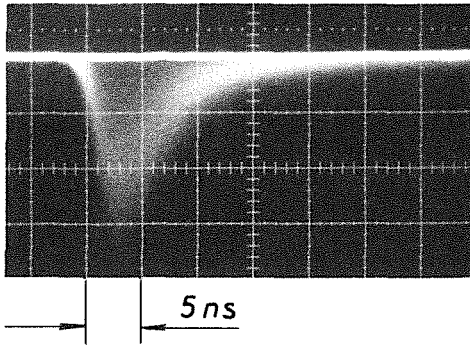
Fig.2   Typical waveform of the detectors under investigation.
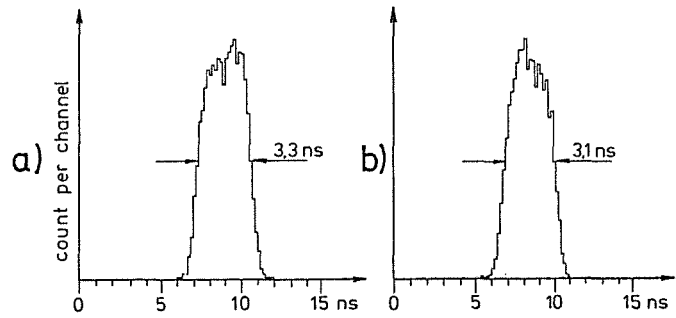
Fig. 3   Time spread spectra for the scintillation detectors with 50x50 cm^2 active area. The identifications a) and b) in Fig. 1 and 3 are corresponding.

The time resolution of the detectors in connection with constant fraction timing has been measured with cosmic muons in the following way : According to the fact that the time resolution is primarily governed by the different light transmission times within the detector, the active detector area is subdivided into 25 sections of 10 cm x 10 cm. Within one section the light transmission time differences are negligible. Then time spread spectra relative to the same "start" detector are measured for each section using a time-to-amplitude-converter and a multichannel analyzer. The "start" detector is a small plastic scintillation detector with dimensions 10 cm x 10 cm x 2 cm positioned directly above the large detector and defining the section of choice. A third plastic scintillation detector of 30 x 30 cm^2 area arranged 20 cm above the two other detectors and in slow coincidence, limits the variation of the direction of the muons used for the measurement. The sum of the 25 time spread spectra each one showing a peak of individual time position amounts to the time spread spectrum of the whole 50 x 50 cm^2 detector. Fig. 3 shows these time spread spectra for both detector geometries (Fig. 1).

2.4. INSTRUMENTATION

2.4.1. SOFTWARE BASED HIGH VOLTAGE CONTROL

D.HAUNSCHILD, H.O.KLAGES, H. SCHIELER, P.WEGNER

For the KASCADE-Experiment it is necessary to control a large number of high voltage supplies for photomultipliers in different detectors.

For this purpose high voltage crates [SY127,CAEN] with 40 independent channels are used. The crate can be controlled in various ways :

Local control is performed manually through a key-pad and a LED display located on the front panel. Optionally one can control the crate in a more sophisticated way by means of a video terminal (ANSI VT52 or compatible) plugged into an RS232C connector, also located on the front panel. This method makes use of interal software implemented by the manufacturer.

Access to the high voltage supplies from VME bus is possible via a 48 kilobaud high speed serial link [CAENET] connected to a HV-controller [A200, CAEN] in a VME-crate. One can daisy-chain up to 100 crates, each consisting of 40 channels. This connection is realized with RG174 coaxial cable for total distances up to 300 m. One can use RG58 cable for longer distances (max. 1200 m). It is not possible to manipulate the implemented software for own purposes. For this reason we developed a software package to control the HV-crates via the HV-controller. This software consists of two parts, the main menu and the program library, both written in C. The menue driven program performs several functions adapted to the experiment:

- select different crates
- display status of HV-channels or groups of channels
- modify parameters for single channels or channel groups
- set protections against unauthorized use of the keypad

The programm was developed and tested with a Motorola 68020 processor of a VME-UNIX-System, where a special device driver was added to allow access to the HV-controller's hardware registers. (see Fig. A).

As a next step a modified version of the program was downloaded from the UNIX-Host to a T800 transputer board. This board is a VME-master and -controller in an external VME-crate (see Fig. B). A further version will be used in the outfield experiment to control the voltage supplies for the detectors of the KASCADE array and the central detector system.
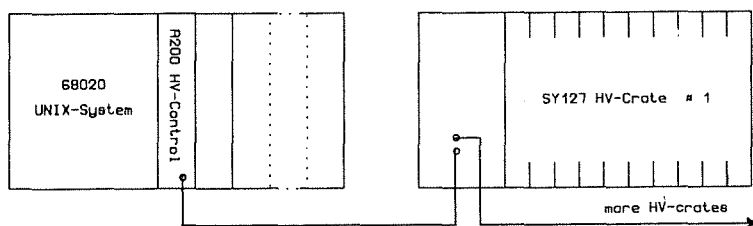
Fig. A
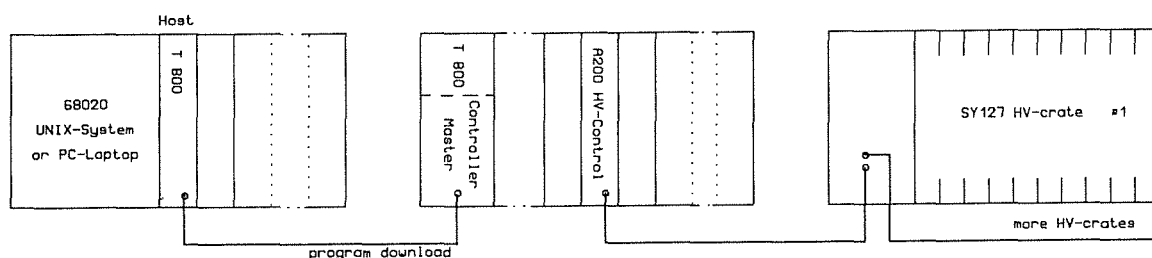
Fig. B

2.4.2. THE DATA ACQUISITION SYSTEM FOR THE KASCADE CLUSTER

D.HAUNSCHILD, H.O.KLAGES, H.LEICH*, U.MEYER*, H.MÜL -
LER, H.SCHIELER, G.SCHMALZ, P.WEGNER*, J.ZABIEROWSKI**

A cluster is composed of 16 detector stations on a rectangular grid and a central electronics station, where power supplies and the data acquisition system are located. Each detector station contains 8 photomultipliers, which process the signals of 8 scintillation detectors. Four detect the e/γ - and four the μ - part of an air shower [1].

The components of the data acquisition system are located in two VME - Crates.The required 16 modules of the front-end electronics [2] in a cluster are located in VME-Crate 2 together with the clock module.

A central synchronized clock, which is a rubidium oscillator (10 MHz, 1 Hz) in connection with a DCF 77 radio clock, is used for absolute time measurement (UTC). From these oscillator pulses the clock module produces a precise 5 MHz timing pulse. The 5 MHz and 1 Hz timing pulses are distributed simultaneously via RG174 coaxial cables to each of the 16 front-end electronic modules (FE-modules) and to the Trigger Unit, where the 5 MHz pulses are counted in a register and which is reset by the 1 Hz pulse.
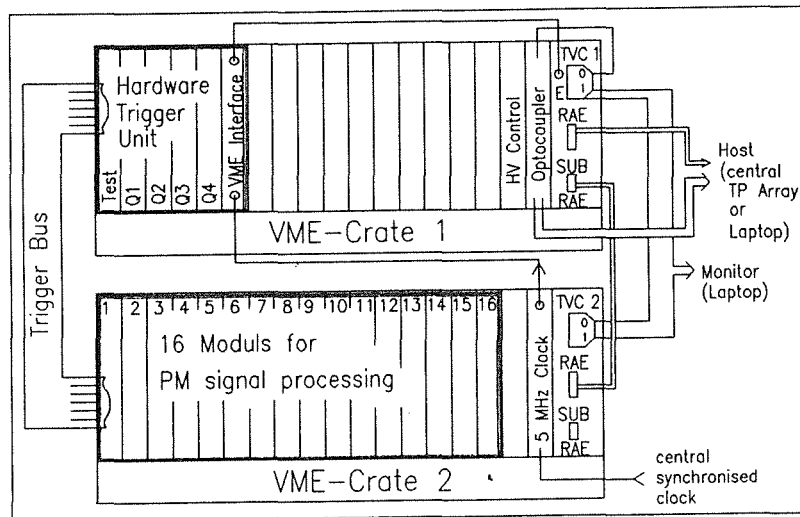
Fig. 1   Data Acquisition System

Together with the high voltage control module [3] the modules of the Trigger Unit are located in VME-Crate 1. The Trigger Unit and the FE-modules are connected via flat ribbon cables, the so called "Trigger Bus".

In each of the two crates the VME-bus is controlled by a module called "Transputer based VME-Controller" (TVC). A short description of that module is given in the last paragraph.

TVC 1, located in Crate 1, gets interrupts from the Trigger Unit via a RG174 coaxial cable on the "Event-Input" (E) or via the VME-bus. The local microprocessors are connected via a very fast transputer-specific serial interface ("Link") and control cables (RAE), whereas TVC 2 is a subsystem of TVC 1. In the case of an interrupt - or an external demand from a superior host - TVC 2, which is continuously reading-out the FIFO-registers of the FE-electronics, is requested via this Link to look for data with valid 5 MHz time labels and to send them to TVC 1. These data are either stored in calibration spectra or sent via optocouplers and fiber optics cables to a superior host, which could be a central Transputer (TP) Array or a Laptop. The TVC 1 in each cluster is a subsystem of this superior host and is also connected with it via control cables (RAE).

Each of the two TVCs is connectable to a monitor (Laptop) via another Link but without RAE cables. In this way it is possible to monitor but not control the TVC independent of a host; e.g. to look at calibration spectra or high voltage parameters.

The Trigger Unit consists of 6 single VME-modules. There are 4 "Quadrant Modules" (Q1, Q2, Q3, Q4) with the proper trigger logic, a "Test Module" and a VME-Interface module. These modules are connected via a private bus on the P2-Connector of the VME-Crate. FE-electronics modules are connected to the Trigger Unit via flat ribbon cables ("Trigger Bus"). Each Quadrant Module receives

signals from 4 FE-modules. There are two coaxial connections to the TVC ("Event-In" and "Event-Acknowledge") and two others, also coaxial, from the clock module (5 MHz and 1 Hz pulses). In the VME-Interface module a number of registers are located. Before every experimental run some of these registers must be preset with two different trigger conditions, the single muon suppression factor and the Julian Date. The Time Label (TL) register counts the pulses of the clock module. With the information from these registers and the input from the FE-electronics, the Trigger Unit produces two kinds of interrupts. The "EXTEVENT"-Interrupt for a shower trigger is sent with high priority to the TVC via a coaxial cable. The other one, a VME-Interrupt for a single muon trigger is sent to the TVC VME-bus with lower priority. The interrupt service routines of the TVC have to read some output-registers where the Trigger Unit has written some additional information like Time Label, which detector was hit and the total number of detector-hits.

The TVC (Transputer based VME-Controller) is a VME-Master and -Controller module with a 32-Bit Transputer (T800; 20 MHz) and 4 MByte external memory. In addition a TRAM (TRAnsputer Module) can be mounted on the board.

The TVC is able to control 3 subsystems. In this case the signals Reset (R) and Analyse (A) go to and Error (E) comes from one of the subsystems. Beside these subsystem ports the TVC has also a system port, so that the TVC itself can be controlled by a superior Transputer-module, with (RA) coming from and (E) going to the superior module. For this reason, any number of VME-Crates can be cascaded.

[1]   K.Daumiller, P.Doll, H.J.Gils, D.Heck, H.O.Klages, W.Kriegleder, H.J.Mayer, H.Müller, H.Schieler, G.Schmalz, G.Voelker, Report KfK 4660, Kernforschungszentrum Karlsruhe p. 73 (1990)

[2]   H.Müller, this report, contr. 2.4.6.

[3]   D. Haunschild, H.O. Klages, H. Schieler, P. Wegner, this report, contr. 2.4.1.

*   Institut für Hochenergiephysik, Zeuthen, Germany
**   INS, Lodz, Poland

2.4.3. CONSTRUCTION OF A LASER SUPPORTED CALIBRATION SYSTEM FOR THE e / γ - DETECTORS OF THE KASCADE ARRAY

F.C.BAUER, H.O.KLAGES, H.J.SIMONIS, G.VÖLKER

Since in the KASCADE - Project the method of relative arrival times is employed for the determination of the direction of a high energetic air shower, an accurate measurement of the time-offset values of the PMT's is required. Therefore the system shown in Fig. 1 has been designed.
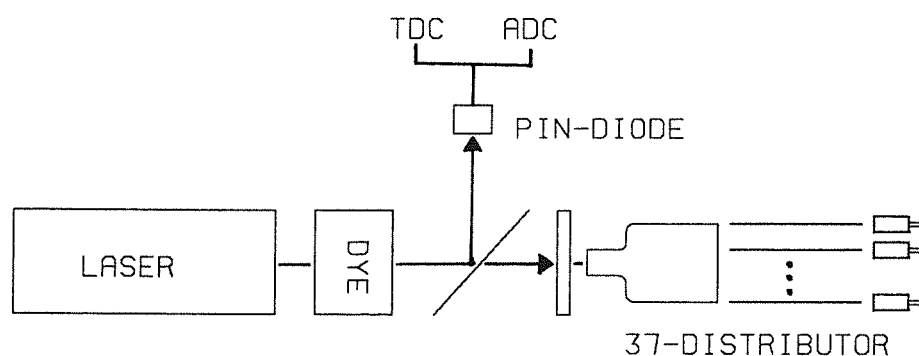
Fig. 1   Schematic view of the test light pulse system

A nitrogen-gas laser (Laser Science VSL-337) serves as a calibration light source. It can be externally triggered at a rate of 1-20 Hz and gives UV laser pulses of wavelength 337.1 nm with a time-width of 3 ns each to a dye laser module (Laser Science DLM-120) with adjustable wavelength from 360-720 nm, beam cross section of 2 mm $\times$ 3 mm and a peak output power of 7 kW at 500 nm. For best performance of the PMT's, laser pulses of wavelength 420 nm are used with Stilbene 3 (LC 4200) as dye.

The pulse laser light is divided by a semitransparent mirror into two parts. The reflected part, about 40% of the total intensity, is detected by a fast PIN-diode (Hamamatsu S2216-01) with a rise time < 1 ns. The signal from the PIN-diode is used to trigger the time measurement, the data acquisition, and, in addition, to monitor the intensity of the laser light.

The transmitted part, about 60% in intensity, passes through a milky glass disk and is guided into a light distributor which consists of 37 bundled optical quartz fibers of lenght 50 cm and of core diameter 100 µm (Suhner 01-1G100/J-W(ZN)T). The transmitted light intensities from the 37 fibers have a Gaussian-type spatial distribution. This system is placed in a light thight box. The test

pulses generated by this system are fed to each e/γ-detector through the optical arrangement as shown in Fig.2.
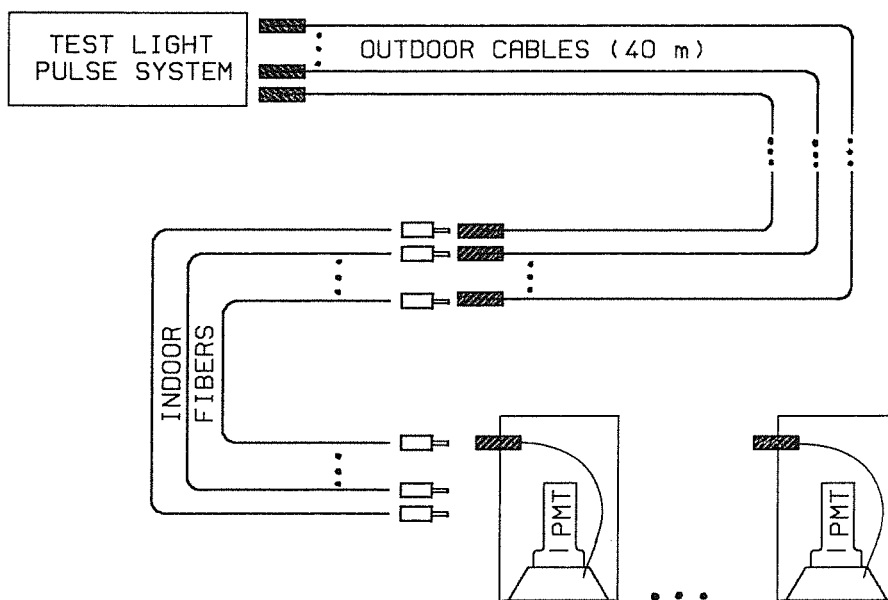
Fig.2   Optical transmission lines between the laser system and the e/γ-detectors.

For the transmission to the detector stations 16 optical quartz fibers of lenght 40 m and core diameter 100 μm with special protection for outdoor-use (Suhner 01-1G1000/A-W(ZN)NY) are connected to the 37-channel distributor. For better indoor handling, a further optical fiber (Suhner 01-1G100/J-W(ZN)T) of lenght 2 m is connected to each of these cables. This quartz fiber of core diameter 100 μm feeds the light pulses to the individual e/γ-detectors. By a special custom made coupling it is connected to a PMMA-fiber of core diameter 1 mm and lenght 40 cm (Cunz CWK-1001) inside the PM housing. Its output end is glued with optical cement (NE 581) into the top of a lucite light-collector at an angle of 105°. The fraction index of the PMMA-fiber has a value similar to the indices of the optical cement and the light-collector. Finally the PMT's are indirectly illuminated by total reflection at the bottom of the light-collector cone.

The optical length of all the transmission lines can be measured with high accuracy.

2.4.4. A PM CALIBRATION SYSTEM WITH PULSED N_2-LASER

F.C.BAUER,   F.P.BRADY,   D.HAUNSCHILD,   H.O.KLAGES,
H.J.SIMONIS

The construction of the KASCADE detector array [1] requires more than 2000 photomultipliers. Since 4 tubes will be sharing one high voltage power supply channel, a detailed study of the dependence of the gain on the applied voltage is required, so that tubes with similar characteristics can be selected.

Therefore, a test device has been constructed which uses a pulsed N_2-laser (Laser Science VSL-337) pumping a subsequent dye-laser as lightsource. Hence the wavelength can easily be changed between 420 nm and 510 nm which are the wavelengths of the fluorescence light of the two different scintillator systems utilized in the KASCADE-array. The laser beam is devided into partial beams using a bunch of 7 lightguides with a diameter of 1 mm each, in order to test several tubes at the same time (see Fig. 1). Milky glass plates are used at the entrance of the lightguides as well as in the front of each multiplier tube to minimize inhomogenities of light intensity over the beam area.

One fixed PM-tube is used as a reference for all other tubes, and the ratio G of the gains with respect to this reference tube is taken as a quantity which is independent of the laser fluctuations. An additional monitor of the laser intensity is obtained using a PIN-diode intercepting a part of the laser beam reflected by a semitransparent mirror at 45° with respect to the primary beam axis as shown in Fig. 1.
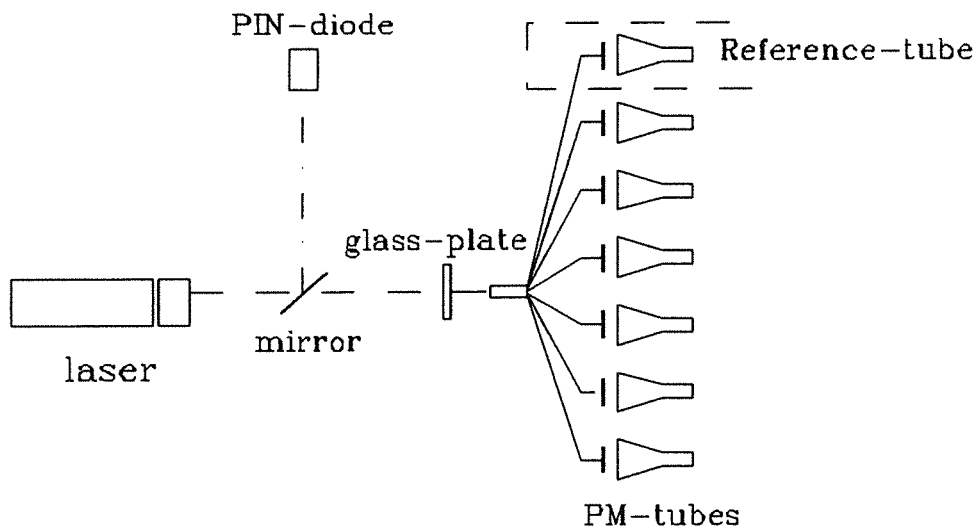
Fig. 1   Schematic view of the experimental setup

The high voltages U on the test-tubes are varied over the range of interest and the relative gain G is measured. From the straight linear behaviour of log(G) versus log(U) the slope S is obtained by a fit to these data and the voltage U_0 which corresponds to a fixed gain G_0 can be calculated. Hence, a multiplier tube is mainly characterized by the two quantities:

1. the slope S resulting from a straight line fit to log(G) versus log(U)
2. the voltage U_0 required to achieve the fixed gain G_0

These two quantities are plotted in Fig. 2 in a two dimensional representation for the first eighty 1.5" PM-tubes, tested at a wavelength of 510 nm. Although the tubes show a wide spread in both the above quantities, sufficient quartets of tubes which match within a 5% uncertainty ellipse in the two parameter plane can be found, whereas only a few ones have to be disregarded.
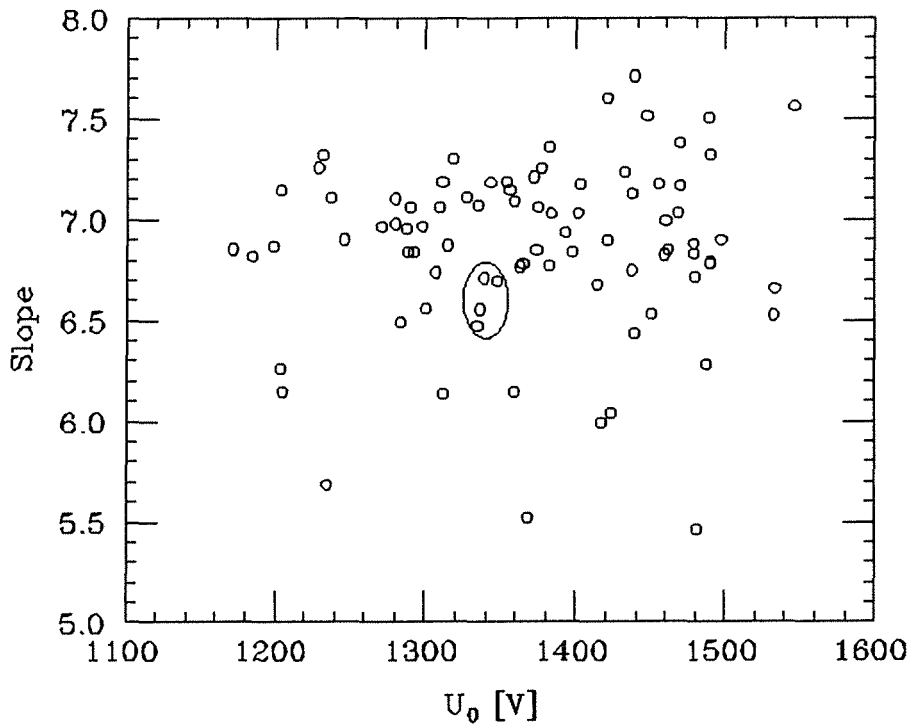
Fig. 2   Two-parameter plot characterizing the phototubes. The voltage given at the X-axis is required to obtain the same gain for all tubes, whereas the slope at the Y-axis indicates the behaviour at voltage changes. The ellipsis shoes an example for four matched tubes

Since the risetime of the laser pulses is extremely short ($\tau < 1$ ns) a third quantity, the change of electron drift time with applied voltage can easily be measured and is found to be within the interval 0.95 ns$\leq \Delta t \leq$ 1.05 ns for a voltage change of 100 V for all measured tubes.

[1]   The KASCADE-Collaboration, KfK report 4686 (1990)

2.4.5.   A TRANSPORTABLE FILLING AND PURIFICATION UNIT FOR LIQUID SCINTILLATION DETECTORS

R.GUMBSHEIMER

To fill 1200 detectors with liquid scintillator it was necessary to build a special device. It has to fulfill the following tasks :

● During a filling procedure no oxygen is supposed to be in contact with the scintillator. This is done by a gas link between storage tank and detector. During the filling of the detector from the storage tank the gas is being pushed into the storage tank by the liquid.
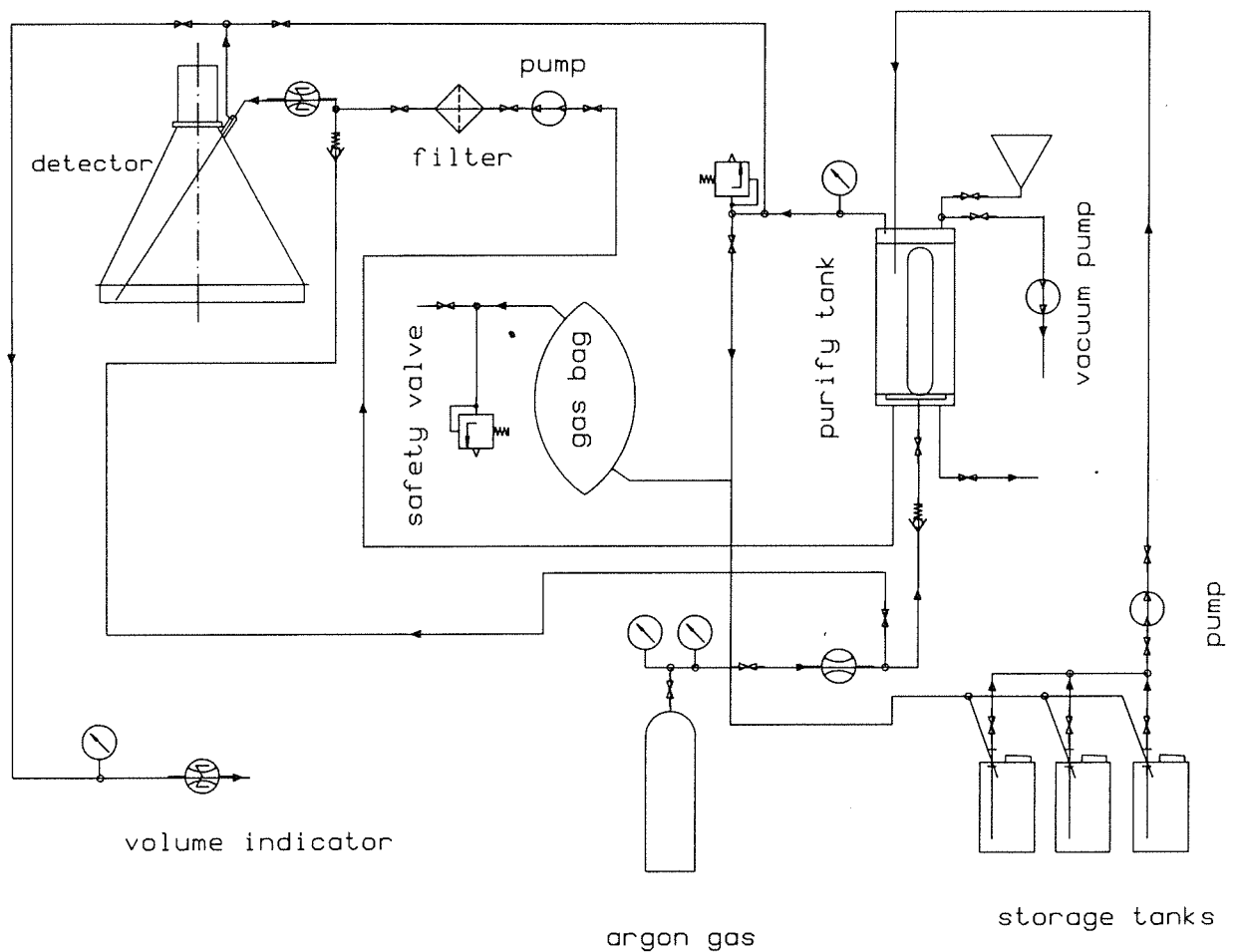
Fig.1   Process cycle of the filling and purification unit

● To make sure that the quality of the scintillator always stays the same, the scintillator will be gased with argon and pumped through a 3 μm filter.

● The pressure inside the detector should not be more than ± 200 Pa. This is guaranteed by a siphon filled with 20 mm silicon oil.

- If necessary the filling device can also be used to drain the detector. The change of the flow direction in the pipe is done by switching valves.

Since the filling device should also operate outdoors, it is equipped with a special weather protection.

2.4.6. FRONT END ELECTRONIC DEVELOPMENT FOR THE KASCADE ARRAY

H.MÜLLER

Each of the 20 clusters from the array contains 128 signal-sources (photomultiplier) which transmit signals via coaxial cables to their central electronic station. These signals can be connected in single or tieded form (analog sum) to the 16 moduls in the VME-Crate 2.

The precise time-measurement is accomplished with a 200 ns voltage ramp and counts of 5 MHz clockpulses above a cycle of 1 second. These digitized time values are stored in two time-registers (Nano-Time,Time-Label) and, after transfer via the VME bus, assigned to the central time (Julian Date).

After conversion and digitization, the signal-amplitude is stored in the energy-register. If all registers are loaded, the data are written as a block, beginning with the channel-address, in the FIFO-memory. Per module (board) are 6 to 8 channels projected. These write data with a suitable flow control to the FIFO-memory.

A status-register contains the present flag-information (empty or full) of the FIFO. It must be addressed first and read-out by the Crate Controller. Depending on "FIFO not empty" the Crate Controller addresses the FIFO and reads out a datablock of four 16-bit-words. If the FIFO is empty (EF set) the Crate Controller addresses the status-register of the next module. This address-polling gives the modules a fair distribution to the VME bus. The addresses between status word and FIFO of each module differ only in the lowest byte, so that a fast access to the FIFO in the nibble-mode is possible. The great number of modules with boards and electronic components require a careful design with use of SMT and PAL's to reduce volume and price.

The picture shows the circuit of a test unit to optimize and test transfer software. Addresses and data for three 16-bit-words are set by code-switches. The datawords are shifted in serial order in the FIFO-memory with adjustable clock-

frequencies from 1 Hz to 20 kHz. If the FIFO-full flag is set, the shift is inhibited for 10 ms.
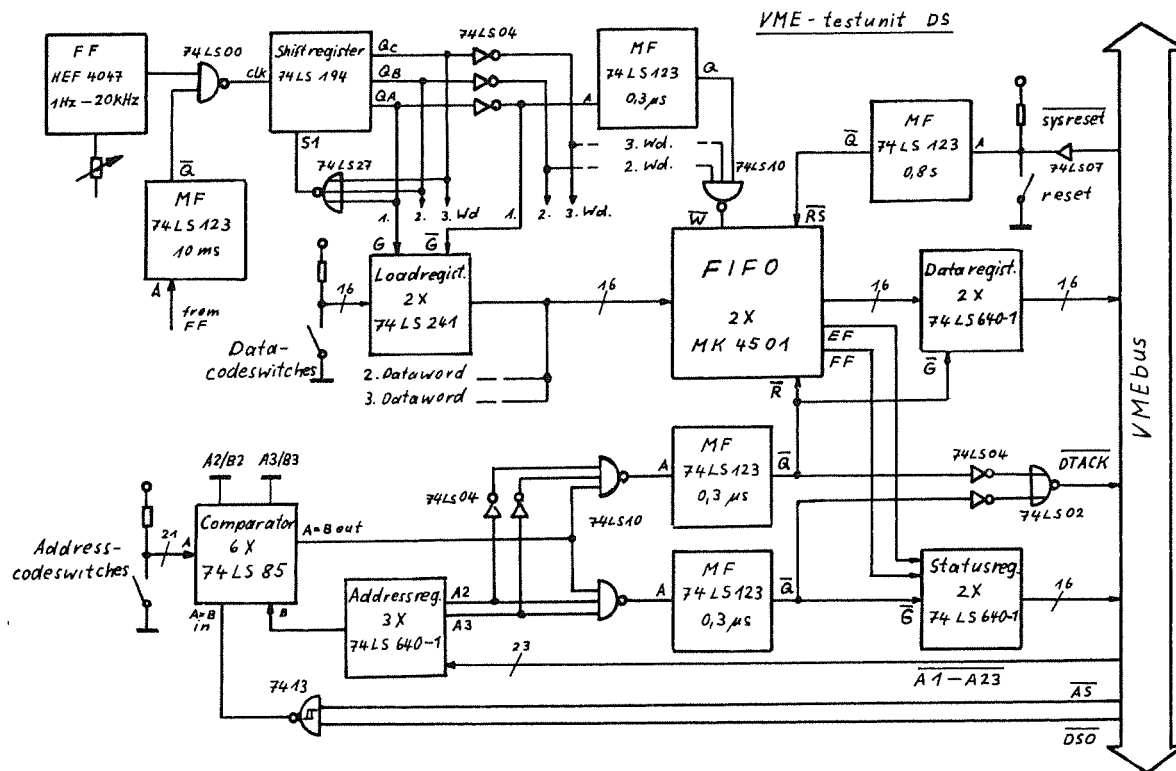
Fig.1   Circuit diagram of the test unit

2.4.7.   CENTRAL DATA ACQUISIATION AND PROCESSING IN THE KASCADE EXPERIMENT

K.BEKK,   H.J.GILS,   H.LEICH*,   D.MANGER,   U.MEYER*, U.SCHWENDICKE*

The detector plant KASCADE consists of two major components : the detector array with 20 cluster stations and the central detector containing about 40,000 ionization chambers and about 20,000 muon detector channels. More details of the detector set up are described in other contributions of this report. Fig. 1 shows the scheme for the data processing.

For the primary front-end data acquisition and experiment control via the standard industrial data bus system VME a dedicated "Transputer based VME Controller" (TVC) was developed. In the detector array 40 of these TVC's [1] (two
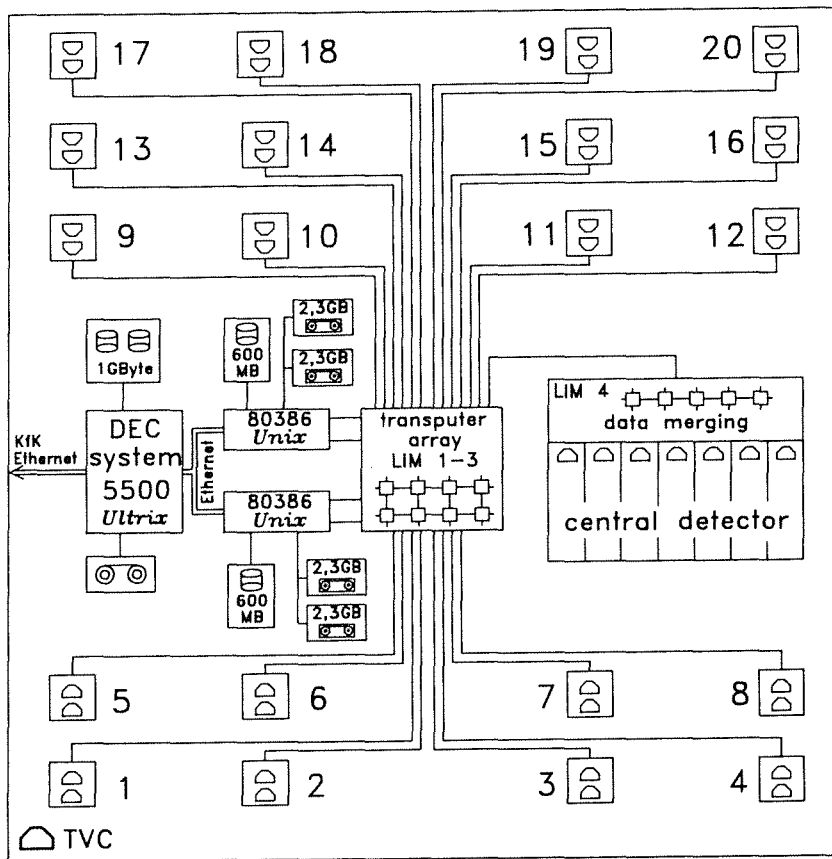
Fig. 1   Schematics of the data acquisition system

for every cluster station) will be installed and 7 in the central detector. Data exchange between all these TVC's and the central transputer array will be done via the fast transputer links using fiber optic cables to the 20 cluster stations.

For merging and processing of the data a special VME module called "LInk-controller/Multiplexer" (LIM) was developed performing a variable transputer array. On one LIM module up to 8 TRAM's (Transputer Module) can be plugged in . Dependent on the tasks TRAM's with a T425 of T800 processor with adequate memory will be used. Each of these TRAM's can be seperately loaded. With two link swiches (C004) any desired transputer configuration will be possible which can be changed even during data acquisition. One LIM module will be used to merge the data coming from the 7 TVC's of the central detector and send them to the central transputer array. This array consists of at least 3 LIM modules with at least 10 transputers where all the data of the detector array and the central detector will be collected and sent to the host computer. Also a first evaluation of the data can be done in the central transputer array.

The central host computer has two main tasks. First the data from the central transputer array have to be recorded on tapes for the archive and distributed to other computers. The second task is the online evaluation of the data and graphical presentation. Also, the status of the experiment has to be visualized for

experiment control concerning the hardware (e.g. high voltage) and the software of any transputer of the experiment. To fulfill the very different requirements of these two functions dedicated systems will be used for each.

For secure data recording, redundance is highly necessary. For the system a standard transputer interface should be available. For this purpose we chose two PC's with a 33 MHz 80386 CPU. Each PC is equipped with two gigatape devices storing 2.3 GByte on one tape cassette, and a hard disk with at least 600 MByte storage capacity. UNIX will be used as operating system including the distributed file system NFS (Network File System) . The standard transputer PC interface reaches a data transfer rate of 220 kByte/sec. With a simple add on module the transfer rate scales to 800/1200 kByte/sec dependent of the transfer direction.

A high performance system is necessary for the (number crunching) evaluation and visualization of the experiment data as well as the experiment control carried out interactively by the user. A RISC based system (DEC station 5500, cycle time 33 ns/28.2 MIPS) with a UNIX operating system (ULTRIX) will be used for these tasks. For efficent interactive information including graphics the X-Window system should be introduced. Connected to the data storing system (80386 PC's) via a private Ethernet interface, the data access is realized by the NFS. Via a second Ethernet interface connected to the KfK wide LAN, other systems, e.g. a VAX Cluster or the IBM mainframe, can access the data using NFS or file transfer. With SCI, DSSI, SDI and Q-Bus as I/O channels and Ethernet, FDDI and X.25 as communication channels, the DEC 5500 is well equipped for future extensions.

[1]   Contribution 2.4.2. this report

*   Institut für Hochenergiephysik, Zeuthen

2.4.8. DEVELOPMENT OF THE TRIGGER ELECTRONICS FOR THE CENTRAL HADRON CALORIMETER OF KASCADE

M.BRENDLE*

The central detector consists of alternating layers of absorbers and radiation detectors. Most of these are "liquid" ionization chambers; the bottom layer is made up from gas-filled multi-wire proportional chambers. Since digitizing the output

signals of those detectors takes about 1ms, it must be started in the case of true events only. The signals from the ionization and proportional chambers are too slow for identifying such events sufficiently fast. Moreover, they are too slow for defining the event micro-time precisely enough. Therefore, one of the detector layers will be made from up to 840 scintillation counters. These are to produce a suitable trigger [1].

The tasks of the trigger electronics are the following :

a) Preprocessing the photomultiplier anode pulses. For each scintillation counter, two amplitude discriminators are provided, a"muon" and a "hadron"discriminator. In order to compensate for gain differences between individual scintillation counters, the thresholds can be varied under computer control. Similarly, to compensate for delay time differences, computer controlled delay lines are provided.

b) The muon and hadron discriminator output pulses are stretched by monostable multivibrators until the final trigger decision has been made. Then, the muon and hadron patterns are stored in the computer-readable pattern registers.

c) The muon and hadron pulses are processed by programmable majority logic circuits (m-out-of-n coincidence circuits). They can produce a "few-muons", a "many-muons", a "few-hadrons", and a "many-hadrons" trigger.

d) These triggers are combined with triggers from the sorrounding clusters to produce a valid-event trigger.

e) The valid-event trigger is used to generate the event micro time word.

f) Due to the large dimensions of the central detector, at an angle of incidence of 45° the distribution of the arrival times of shower particles is 60 ns wide. This is close to the limit of acceptable timing jitter for the ionization and proportional chambers. Therefore, the timing of those triggers may be derived from smaller subgroups of the scintillation counter array.

g) For detecting photomultiplier gain drifts, the background counting rates are to be measured. For monitoring the muon and hadron pulse rates of one or a few scintillation counters, a computer controlled multiplexer is provided. Gain drifts can be compensated by readjusting the discriminator thresholds. A malfunctioning scintillation counter can be inhibited to contribute to the generation of muon and hadron triggers.

h)   A pulse generator system is to provide test light pulses for the scintillation counters. These can be used for monitoring drifts of time delays.

The costs for implementing the trigger electronics by commercially available instruments completely would be prohibitive. Therefore, design of three modules has been started :

a)   A module for reprocessing the anode pulses of eight photomultipliers. This module contains muon and hadron discriminators, digital-to-analog converters (DACs) for generating the disciminator thresholds, programmable delay units, monostables, a monitoring multiplexer, and a VME-bus interface.

b)   A first-level majority-logic module. This module accepts the muon and hadron discriminator pulses from 32 scintillation counters and produces analog partial muon-count and hadron-count signals.

c)   A second-level majority-logic module. This module is used to generate the final analog muon-count and hadron-count signals. By means of pulse-height discriminators, few-muons, many-muons, few-hadrons, and many-hadrons triggers are generated. The thresholds are defined by DACs, which can be loaded via a VME-bus interface. Modules of the same type generate subgroup triggers from the partial muon- and hadron-count signals.

Yet, the designs have not been completed. Which tasks have to be tackled then ? Drivers for distributing the trigger signals to the ionization and proportional chambers are needed. These drivers should include AND gates for combinig the subgroup triggers with the true-event trigger. The test-pulser system must be designed. But instead of designing a micro-time capture module, the solution of the array-electronics group should be utilized. For generating the valid-event trigger from the output signals of the main second-level majority-logic module, commercially available coincidence circuits and gate generators could be used.

[1]   P.Doll et al., Report KfK 4686, Kernforschungszentrum Karlsruhe,(1990)

*   Physikalisches Institut der Universität Tübingen

2.4.9.A A MULTI-TRANSPUTER SYSTEM FOR PARALLEL MONTE CARLO SIMULATIONS OF EXTENSIVE AIR SHOWERS [1]

H.J.GILS, D.HECK, J.OEHLSCHLÄGER, G.SCHATZ, T.THOUW, A.MERKEL

A multiprocessor computer system has been brought into operation at the Kernforschungszentrum Karlsruhe. It is dedicated to Monte Carlo simulations of extensive air showers induced by ultra-high energy cosmic rays. The architecture consists of two independently working VMEbus systems each with a 68020 microprocessor as host computer and twelve T800 transputers for parallel processing. The two systems are linked via Ethernet for data exchange. The T800 transputers are equipped with 4 Mbyte RAM each, sufficient to run rather large codes. The host computers are operated under UNIX 5.3. On the transputers compilers for PARALLEL FORTRAN, C and PASCAL are available. The simple modular architecture of this parallel computer reflects the single purpose for which it is intended.

The hardware of the multiprocessor computer is described as well as the way how the user software is handled and distributed to the 24 working processors. The performance of the parallel computer is demonstrated by well-konwn benchmarks and by realistic Monte Carlo simulations of air showers. Comparisons with other types of microprocessors and with large universal computers are made. It is demonstrated that a cost reduction by more than a factor of 20 is achieved by this system as compared to a universal computer.

3. LASER SPECTROSCOPY

3.1. ISOTOPE SHIFTS AND HYPERFINE STRUCTURE IN POLONIUM ISOTOPES BY ATOMIC BEAM LASER SPECTROSCOPY

D.KOWALEWSKA, K.BEKK, S.GÖRING, A.HANSER, W.KÄLBER, G.MEISEL, H.REBEL

Isotope shift in heavy elements map rather directly variations of the mean-square radius $<r^2>$ of the nuclear charge distribution since influences of mass-dependent effects are minimized there. Thus, systematic studies of relative isotope shifts in neighbouring heavy elements provide a basis of interesting isotopic and isotonic comparisons. With this aspect and following the discovery of rather
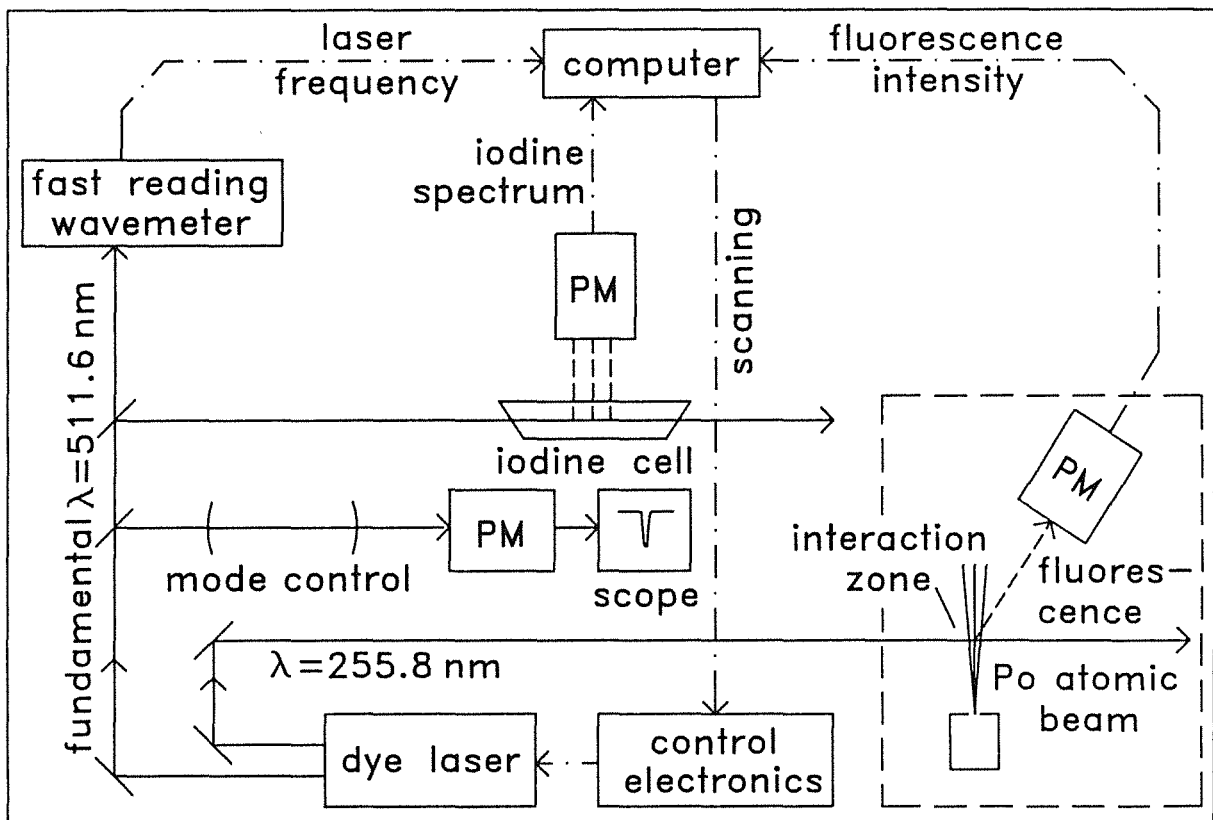
Fig. 1   Experimental setup for laser induced resonance fluorescence in a thermal atomic beam of polonium. For safety reasons the atomic beam apparatus is mounted inside a glove box. PM: = photomultiplier.

peculiar nuclear structure effects in light Hg isotopes [1], the region in the vicinity of the double magic nucleus ^{208}Pb has attracted considerable attention. Nevertheless, there is a conspicuous lack of experimental data for elements heavier than Pb like Bi, Po and At. This situation has prompted the present laserspectroscopic studies of polonium isotopes for which the experimental information on ground state properties is rather scarce and data on IS or nuclear radii, respectively are completely missing.

Mass number	A [MHz]	B [MHz]	μ_I [nm]	Q [b]
209	2127(4)	-	0.606(45)	-
207	564(4)	368(34)	0.793(55)[a]	0.28[b]
205	542(5)	241(53)	0.760(55)[a]	0.17[b]

a : P.Herzog et al (1983)   b: C.M.Olsmat et al (1961)

Tab. 1   HFs constants of the $6p^3\,7s\,{}^5S_2$ level in PoI and nuclear moments of the odd-mass Po isotopes.

mass number	nuclear spin	isotope shift v^A-v^{208} [MHz]	$\delta < r^2 >^{A,208}$ [fm^2]
210	0	3464(5)	0.118(3)
209	1/2	1295(12)	0.044(4)
208	0	0	0
207	5/2	-2307(24)	-0.078(5)
206	0	-3064(7)	-0.104(1)
205	5/2	-5457(43)	-0.185(6)
204	0	-6077(12)	-0.206(2)
202	0	-8852(12)	-0.300(3)
200	0	-11154(22)	-0.379(7)

Tab. 2   Isotope shifts of $6p^4\,{}^3P_2 \rightarrow 6p^3\,7s\,{}^5S_2$ ($\lambda = 255.8$ nm) transition on PoI and changes $\delta < r^2 >$ of the mean-square charge radii relative to ^{208}Po. Experimental errors include statistical errors and systematic uncertainties in the evaluation of $\delta < r^2 >$.

The measurements are based on the observation of resonance fluorescence after excitation of the atomic transition $6p^4 \, ^3P_2 \to 6p^3 \, 7s \, ^5S_2$ of PoI in a collimated thermal atomic beam (Fig. 1). The required UV light ($\lambda = 255.8$ nm) was generated in a cw ring dye laser with intracavity frequency doubling using a beta barium borate crystal (see contr. 3.4.) The Po isotopes with shorter lifetime studied, have been prepared by (α,xn) and (p,xn) reactions at the cyclotron, while the longliving nuclides (^{208,209,210}Po) were commercially available. Using the literature information about the hyperfinestructure splitting of the atomic ground state and the electromagnetic moments of ^{205}Po and ^{207}Po, the observed hyperfine splitting of the odd Po isotopes has been evaluated. Results are given in Tab. 1

Tab. 2 compiles the results for the measured isotope shifts and changes in the mean square charge radius. The conversion of IS into $\delta < r^2 >$ is hampered by lack of knowledge of calibration from other experimetal sources, and of the electronic factor from theoretical consideration. Therefore a calibration by the nuclear droplet model predicting $<r^2>^{206} - <r^2>^{208}$ (Po) $= - 0.104$ fm^2 has been used.
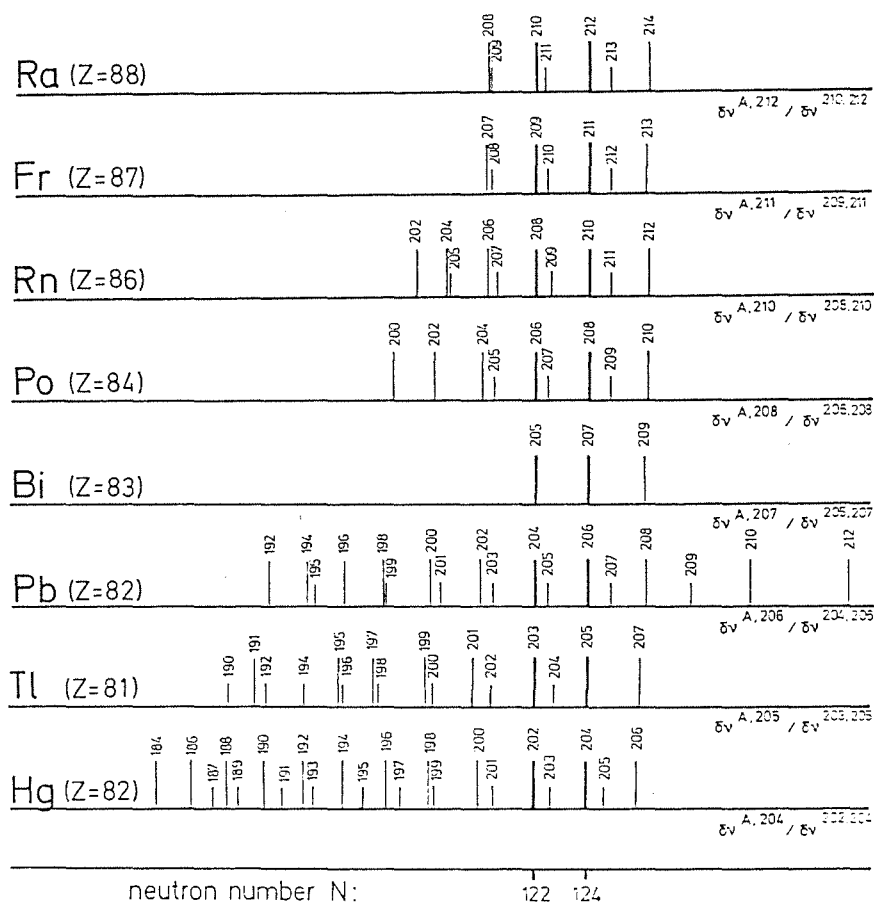
Fig. 2   Relative isotope shifts for elements in the vicinity of Po. The shifts are normalized to the isotope shifts between the neutron numbers N = 122 and 124.

Fig. 2 presents the relative isotope shifts $((v^N\text{-}v^{124}) / (v^{122}\text{-}v^{124}))$ versus the neutron number N together with the data for neighbouring elements. This systematics reveals striking similarities, even in detail (like odd-even staggering), of the radius variation of heavy elements. It establishes a nontrival *scaling behaviour* of radii of near-stable heavy nuclei as long as instabilities of the (N + Z) nucleon system far off the stability line do not include specific polarization deformation effects.

[1]   G.Ulm et al, Z. Phys. **A325**, 247 (1986) and references therein

[2]   P.Herzog et al. Z. Phys. **A311**, 351 (1983)

[3]   C.M.Olsmat et al, Ark. f. Fys. **19**, 469 (1961)

3.2.   LASER SPECTROSCOPY ON HAFNIUM IONS IN A PAUL TRAP

J. RINK, B. GORSKI*, A. HANSER, W. KÄLBER, G. MEISEL, H. MIELKE, Y. OGANESSIAN*, H. REBEL

There is an intriguing Yrast trap in the ^{178}Hf nucleus by a 16^+ isomeric state (E_x = 2.45 MeV; $T_{1/2}$ = 31 y) formed as a four-quasi particle state through the alignment of two protons and two neutrons in a high-spin orbital. Its K value is the highest known of all K-isomers in doubly even nuclei. Since the high spin is most likely generated by few-particle degrees of freedom rather than by collective motion, the structure of the isomeric state is quite different from the ground state. The difference may be reflected by a change of the charge radii which can be determined, in principle, with extreme precision by optical spectroscopy. This has prompted us to prepare laser spectroscopic measurements of the isomeric shift of an optical transition of Hf ions stored in an rf Paul trap. The experimental set-up presently used for our preparatory studies with stable Hf is shown in Fig. 1.

The hafnium sample is transferred to a $HfCl_4$ solution of a few µl and dried on the tip of a tantalum wire filament. After evacuation and baking of the UHV-chamber the tantalum wire is heated and thus the sample is evaporated. A part of the evaporation products is ionized by the electrons from the filament so that hafnium ions are stored in the trap. Nevertheless, every 10^7th atom is captured in the trap.
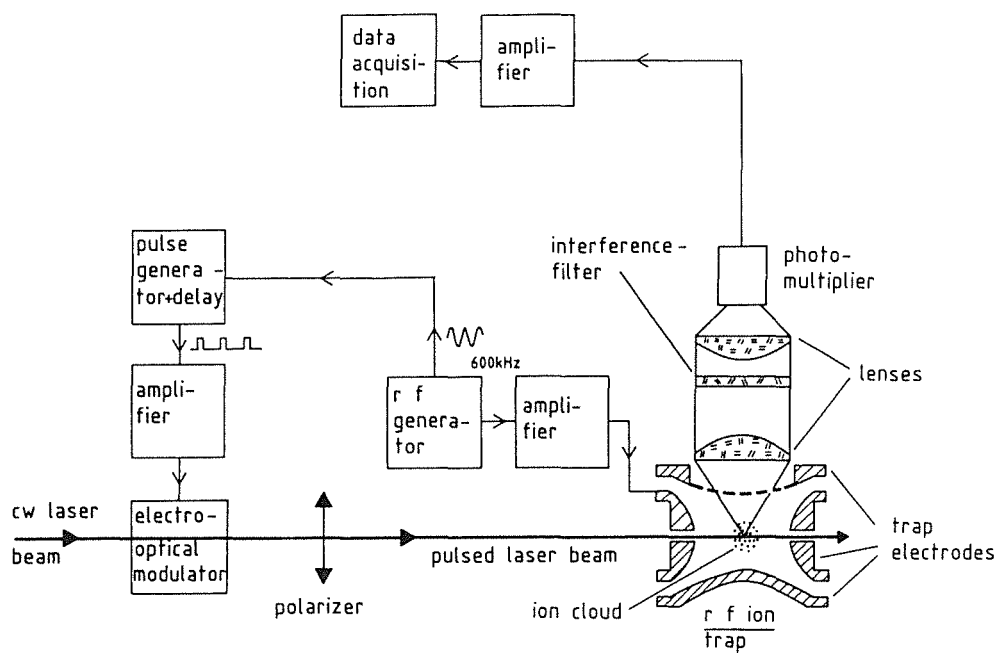
Fig. 1   Experimental set-up

The ion storage time depends among others on the gas filled into the UHV-chamber. The longest storage time was achieved with hydrogen gas at a pressure of $5 \cdot 10^{-5}$ mbar. The half-life of the stored ions measured via the fluorescence strength was 23 minutes. After optical excitation the ions decay into metastable states and subsequently reach the ground state by collisions with buffer gas molecules. Chemical reactions of the stored ions with some unidentified gas molecules limit the storage time.

The excitation of adequate transitions in Hf II requires UV light. For the transition $5d6s^2$ ($a^2D_{3/2}$) $\rightarrow$ $5d6s6p$ ($z^2D°_{5/2}$) at 301,3 nm we use a ring dye laser with Rhodamine 6G dye . The pump power of an argon ion laser at 514 nm is 8.9 W, resulting in a single mode output power of the dye laser of 1400 mW at 602.6 nm. This light is frequency doubled in an external $LiJO_3$ crystal. About 0.5 mW of the frequency doubled light is available in the ion trap. With this power the optical transition is already saturated and the fluorescence signal is about 200 kHz with H_2 as quenching gas; it was possible to perform measurements with samples containing 10pg hafnium.

Fig. 2 shows a spectrum with natural hafnium (35 % ^{180}Hf, 15 % ^{179}Hf, 30 % ^{178}Hf, 20 % ^{177}Hf). The low resolution is due to the Doppler broadening caused by the alternating electric field in the trap. The linewidth (FWHM) is 3000 MHz in comparison to the natural linewidth of presumably 50 MHz. The lines can be narrowed by a factor of 4 by time selective excitation [1]; the setup for this particular method is shown in Fig. 1. The result is shown in Fig. 3; this spectrum
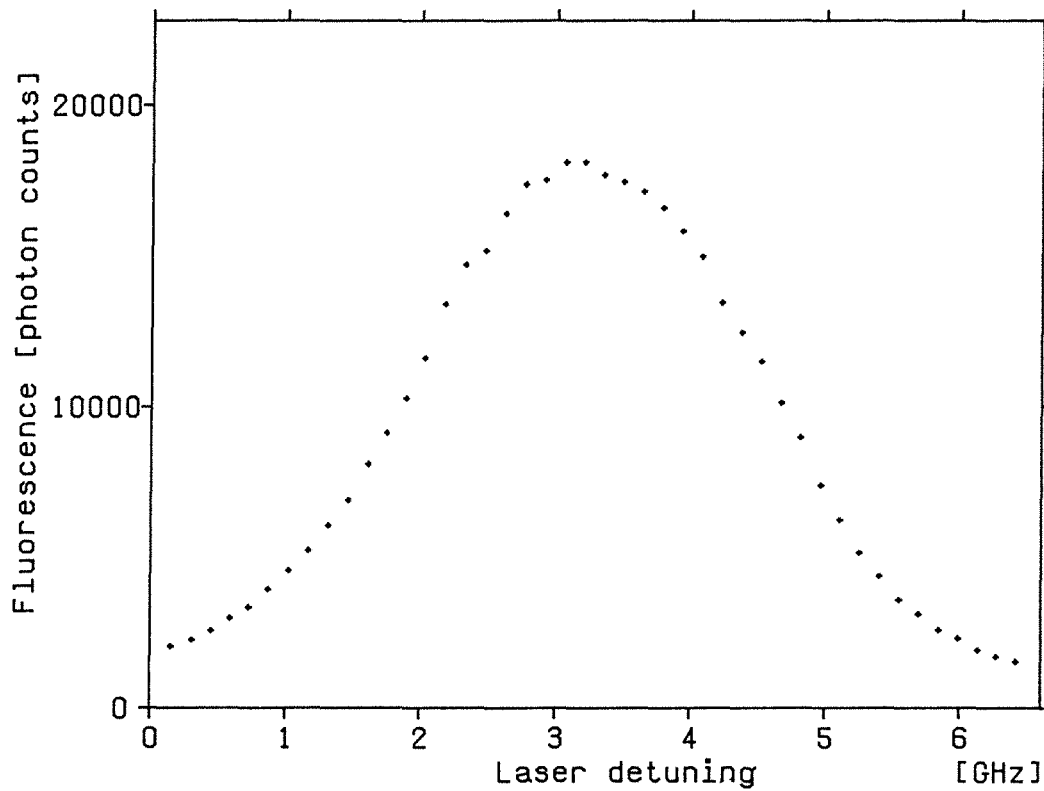
Fig. 2   Spectrum of natural hafnium with full Doppler Broadening.
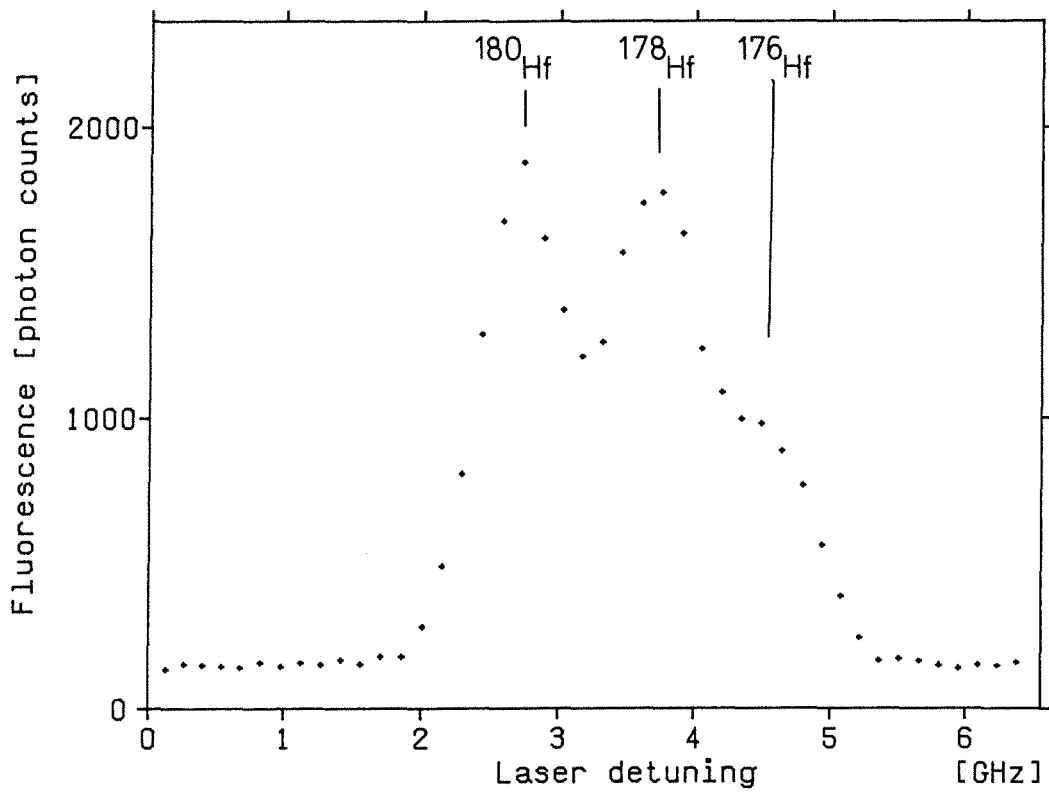
Fig. 3   Time selective excitation with an interrupted laser beam resulting in a
          reduced Doppler broadening

was taken from the same sample as that one in Fig. 2. The two isotopes ^{178}Hf and ^{180}Hf are separated but the hyperfine splitting of the isotopes ^{179}Hf and ^{177}Hf is still unresolved since the linewidth still is 600 MHz. As the Hf isomer is expected to have hyperfine splitting, an improved resolution is necessary. As was shown in our laser spectroscopic studies on thorium isotopes [2, 3], a resolution of the order of the natural linewidth can be achieved with two step excitation combined with time selective excitation [1]. This technique will require frequency doubled light from two dye lasers, one for each step, in the present case of Hf.

The hafnium isomer ^{178m}Hf is currently being produced by ^{176}Yb (α, 2n) ^{178m}Hf reactions in the cyclotron at the JINR in Dubna, USSR. A target with ^{176}YbO$_3$ is irradiated by 40 MeV α-particles. Thus mainly ^{178}Hf in the nuclear ground state and other Hf isotopes are produced; the ^{178m}Hf to ^{178}Hf ratio is only a few percent [4]. Therefore mass separation to remove the other hafnium isotopes is required. The hafnium amount required to fill the trap completely is about 1 ng or $3 \cdot 10^{12}$ atoms on the filament. We estimate that a 1:100 isomer to ground state ratio is tolerable to perform the spectroscopic measurements. In total we expect that a few 10^{12} atoms of the isomer are needed to measure all hyperfine structure components.

[1]   W. Kälber, J. Rink, G. Meisel, R. C. Thompson, KfK-Report 4660, Kernforschungszentrum Karlsruhe 87 (1990)

[2]   W. Kälber, KfK-Report 4513, Kernforschungszentrum Karlsruhe ,87 (1989)

[3]   W. Kälber J. Rink, K. Bekk, W. Faubel, S. Göring, G. Meisel, H. Rebel, R. C. Thompson, Z. Phys. A334, 103 (1989)

[4]   S. A. Karanijan, private communication, 1990

*   JINR Dubna, Heavy Ion Laboratory, USSR

3.3.   PERFORMANCE TESTS FOR A FAST READING WAVE-METER

R.SCHRUFT, W.KÄLBER, D.KOWALEWSKA, G.MEISEL

A wavemeter designed for the determination of laser frequencies [1, 2] had been supplemented by a preprocessing electronics to speed up the data evaluation

[3]. Thus one reading every 50 msec had been obtained whereby the evaluation requires 5 msec on a DEC MICRO/J-11 based on-line processor in the multi-tasking mode of operation. It is important to find out which loss of accuracy and precision is caused by the loss of information due to the data reduction in the preprocessor.
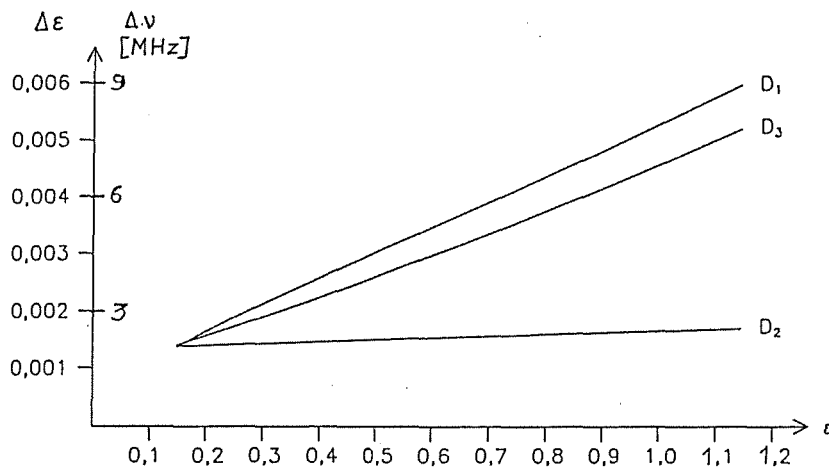
Fig. 1   Laser frequency change Δv (or change in etalon excess $\Delta \varepsilon$) reqired to shift the peak position from one diode to the next neighboring one, as function of the etalon excess for an etalon with FSR = 1.5 GHz. D1, D2 and D3 refer to the inner, mid and outer interference ring, respectively.

Calculations were performed concerning the resolution. For the evaluation the innermost three interferometer rings are taken, i.e. 6 diode positions are used in the calculation. If the laser frequency is tuned continuously, each peak changes continuously, too; in more datail, the intensity on one side of the peak diode increases while it decreases on the opposite side. The intensity for the peaking diode may rise or fall. The peaking diode remains the same until its next neighbour with increasing intensity has passed it. Thus the reading of the wavemeter is unchanged until the frequency has changed enough to replace one of the six peak positions by its neighbour. The readings therefore are not smooth but a staircase function with steps that depend on the actual etalon excess and the particular diode which is replaced next.

Fig. 1 shows the results of the calculation for the longest of the three interferometers which is responsible for the final resolution. It shows that the step height can be as large as 9 MHz; the average step is about 4 MHz. This resolution is sufficient in view of the design goal for the instrument which is 1 % of the FSR or 15 MHz. The result is, that due to the limited resolution a single reading for an arbitrary frequency can have a worst case error of ± 9 MHz whereby the average error is ± 4 MHz.
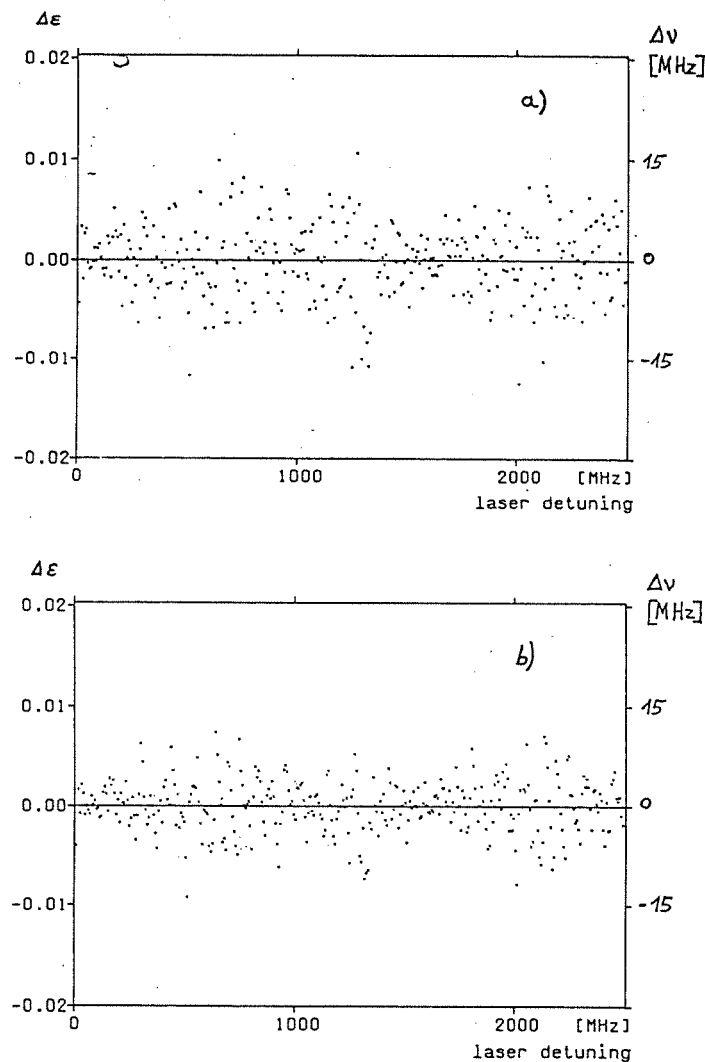
Fig. 2   Scattering of readings if (a) only the peaking diode or (b) also the two next neighbouring diodes are used to determine the interferogram ring diameters.

For a comparison of the peak detection based on a single diode or on several diodes, a cw dye laser was tuned in 7.5 MHz steps over 2500 MHz. The laser frequency was controlled to within 0.1 MHz by counting beat frequencies. The etalon excess was determined from the peaking diodes as well as by fitting a quadratic parabola to the intensities for the peaking diode and its two next neighbours. A straight line was fitted to the results of the full scan; the differences between the fit line and the single readings are given for both methods in Fig. 2. The single reading standard deviation increases from 4 MHz to 5.6 MHz if the single diode peak detection is applied. No systematic effect was observed, i.e. the slope and the intercept of both fitting lines coincide very well to within their statistical errors. It is seen from the data that there are further sources of fluctuations than those discussed before since single readings can be displaced as much as ± 15 MHz.

Another typical application for the wavemeter is the determination of frequency differences, e.g. hyperfine spacings, in some spectra. For this purpose

e.g. a dye laser is scanned continuously or stepwise over the spectral region of interest while successive readings from the wavemeter are taken to determine the actual laser frequencies. If the frequency difference between successive readings is below 15 MHz, their scattering may lead to non-monotonous confused data. We therefore tried to smooth the data to generate improved wavemeter results. The method is to determine the regression line over some wider frequency range around the point of interest and to take its frequency from the regression line. If 100 to 15 points over a 500 MHz wide range are used for smoothing, the improved frequencies nominally have a standard deviation from 0.7 to 1.5 MHz.

In order to test the usefulness of this concept and to determine the actual errors of the improved data, we have investigated dye laser induced resonance fluorescence on a collimated atomic beam of cobalt in a series of experiments. The lower state hyperfine splittings of Co are well known [4] and therefore were remeasured using the wavemeter for determinations of frequency differences. In a preliminary evaluation the purely statistical errors were found to be below 1 MHz if 3 to 5 repetitive Co resonance records were fitted to a Lorentzian profile using smoothed frequencies. A comparison of the results for 13 different hyperfine spacings shows that the correct values [4] are only reproduced to within ±6 MHz or better, the discrepancy typically is ±3 MHz or below. Further studies are required to identify the source of this additional error.

[1]   A. Fischer, R. Kullmer, W. Demtröder, Opt. Comm. 39, 277 (1981)
[2]   A. Steiger, KfK-Report 3820 (1984)
[3]   R. Schruft, G. Meisel, K. Bekk, KfK-Report 4660, 95 (Mai 1990)
[4]   W. J. Childs, L. S. Goodman, Phys. Rev. 170, 50 (1968)

3.4. FREQUENCY DOUBLING AROUND 510 nm BY BBO IN A CW DYE RING LASER

D. KOWALEWSKA, G. MEISEL

Efficient UV generation in the special range ~ 255 nm - as required for spectroscopic investigations of polonium atoms [1] - can be performed by laser intracavity frequency doubling of green light at $\lambda \approx 510$ nm by means of a BBO (barium beta borate) crystal [2].

A ring dye laser model 699-21 by Coherent is operated with Coumarin 498 and pumped by the $\lambda = 457.9$ nm emission of an Ar^+ laser; the available pump power, depending on the age of the discharge tube, is 1.5 - 2.2 W. The obtainable internal dye laser power is very sensitive to intracavity losses, especially if the pump power is low. The available Brewster cut BBO crystals usually have considerable insertion losses, seldom below 1 %. It is therefore necessary that all the other internal losses, in particular those of the frequency selective elements used to achieve single mode operation, be minimized, so that sufficient intracavity power for frequency doubling is obtained. For type I phase-matching (oo → e) in BBO in the spectral region $\lambda \approx 510$ mn the phase-matching angle amounts to $\Theta_m \approx 50°$. BBO is a highly birefringent crystal (walk-off angle $\rho \sim 5°$) and the generated UV beam on the exit surface of the crystal is considerably spread in the phase-matching plane and thus astigmatic.

A BBO crystal is placed into the auxiliary waist of the ring resonator, which has a size $w_0 = 27$ μm. For the crystal lengths available, typically 5 - 7 mm, the present focussing is considerable weaker than the optimum one and the doubling efficiency is ~ 40 % of the maximum value obtainable; for a crystal with length $\ell = 5$ mm, as used in our system, this efficiency amounts to $C \approx 35$ μW/W². It is nevertheless sufficient for many experiments if the available internal power is high. Routinely we had 15 - 20 W internally, depending on the pump power, age of the dye solution and the loss of the crystal at the spot being used. The generated UV power suffers a 30 % loss inside the laser resonator : ~ 20 % reflection loss on the crystal's exit surface (s-polarized light) and 15 - 20 % loss upon transmission through the UV dichroic output coupling mirror. Thus the UV power, routinely available outside the laser resonator, ranged from 5 to 10 mW. The maximum obtained power at $\lambda = 255.8$ nm (the transition in Po atoms) amounted to ~ 20 mW, corresponding to a pump power of 2.2 W and a path through the crystal where the insertion loss was particularly low : 0.5 %.

[1]   D. Kowalewska, G. Meisel, KfK-Report 4660, 93 (1990)
[2]   Chen Chuangtian, Wu Bochang, Jiang Aidong, You Guiming, Sci. Sinica B28, 235 (1985)

3.5 TESTS OF THE ACCURACY AND PRECISION OF STABILIZED CW DYE RING LASERS FOR OPTICAL FREQUENCY METROLOGY

W. KÄLBER, A. DORN, G. MEISEL

Two cw dye ring lasers designed for precision measurements of optical frequency differences [1-3] have been modified for online computer control of the required multistep procedure. The following elements are used to set the laser frequency : A Lyot filter that is rotated for tuning by a step motor, an uncoated 80 GHz etalon that is tilted by a galvo scanner, a piezo driven mirror for small changes of the laser resonator circumference, and a beam shutter to interrupt the laser oscillation to induce mode hops. A fast reading wavemeter [4, 5] is used to supervise the laser frequency stepping. Thus it is possible to set any laser frequency within the tuning range of the dye, in particular to tune the lasers to any resonance frequency of the reference interferometer to which the laser is locked for stabilization [2, 3]. The time needed for changing the laser frequency from one interferometer resonance to another one is about 3 to 5 sec. In order to determine a frequency difference of 16 THz by the multistep heterodyne technique [1] about 200 steps are necessary which are expected to require a total of 25 minutes including the data acquisition time.

In order to study the precision of the multistep heterodyne technique, we have investigated the frequency fluctuations of the stabilized dye lasers applying the beat technique. An iodine stabilized HeNe laser at λ = 633 nm was used as reference [6]. The photodiodes used were the Hewlett Packard type 5082-4220 for DC to 1.2 GHz, and the Hewlett Packard model QSCH 5965 as well as the Telefunken BPW 28A for beat frequencies from 0.8 to 4.5 GHz. For an integration time of 1 sec the observed short term stability is 0.5 to 2.0 kHz, even without the fast feedback facility, i. e. for a unity gain frequency of about 6 kHz. This is sufficient for our purpose.

As to the long term stability, we have measured beat frequencies over 3 hours (Fig. 1). The transfer cavity used was a 25 cm long confocal resonator with an FSR = c/2L $\approx$ 600 MHz. The cavity was stabilized by locking one of its resonances to the HeNe laser; therefore the cavity was only protected against external perturbations by mounting it inside an airtight housing. The dye laser was locked to the two neighboring resonances above and below the HeNe resonance; the lock was changed every 10 seconds. Thus the two traces of Fig. 1 were obtained in one run.

It is found that the frequencies are reproduced to within 1 to 2 kHz after the laser was locked to the other resonance, see the flat portions in Fig. 1. We also observe almost periodic beat frequency drifts. The repetition time is about 15 to 20 minutes, the peak-to-peak amplitude of this fluctuation is limited to about 20 kHz.
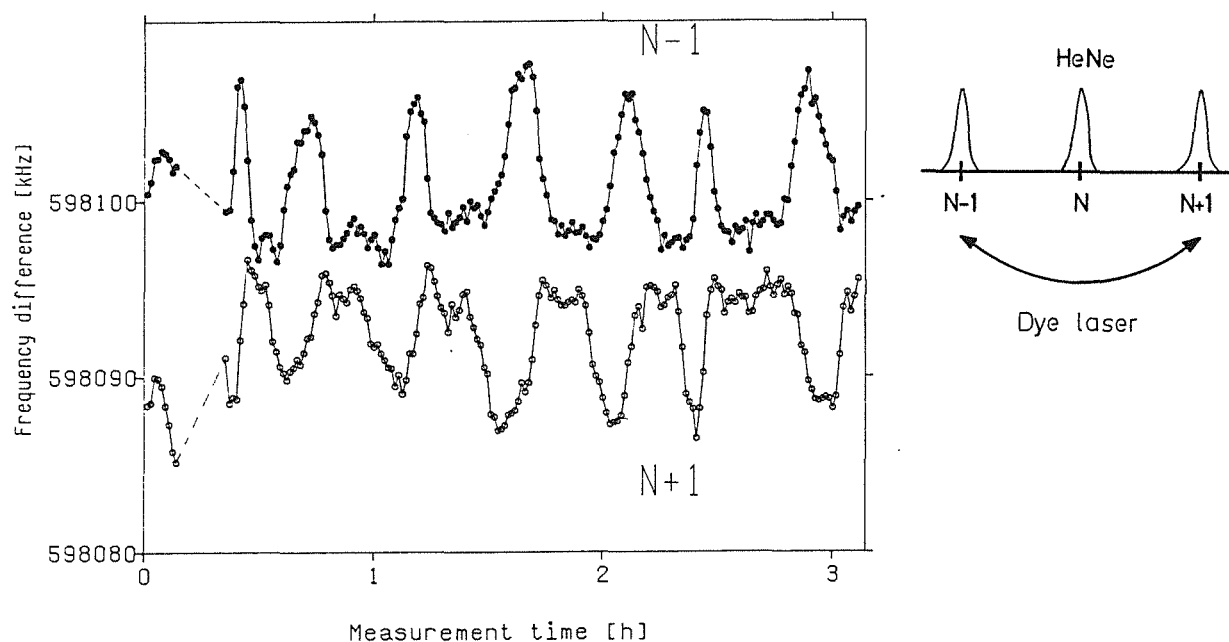
Fig. 1   Fluctuations of laser beat frequencies.

These fluctuations most likely arise from small changes of the etalon lock point of the HeNe and/or of the dye laser. Obviously the lock points are not perfect since the HeNe frequency is not centered with respect to the two dye laser frequencies; the sum for both traces, however, is quite constant and close to 2·FSR. Similar effects were also observed if the transfer cavity was made slightly non-confocal, i.e. if the degeneracy was removed. Sometimes the quasi-oscillations on the two traces were 90 degrees out of phase rather than in opposite phase. If the cavity's housing was slightly warmed up, the speed of the 20 kHz fluctuations was increased while the amplitude remained almost unchanged.

If lock points are used that are ± 1 to ± 4 FSR away from the HeNe frequency, roughly the same phenomena are observed, i. e. the peak-to-peak drift amplitude is still limited to about 20 kHz.

Further investigations are required to identify the cause of these fluctuations. It is to be noted that the dye laser is locked to the peak of a reference interferometer with a FWHM of 2 MHz; the observed 20 kHz drift amplitude is less than 1 % of the reference resonator width which might overcharge its frequency discriminating power [7]. Therefore it is planned to study this effect with a transfer cavity of higher finesse, i. e. with narrower resonances.
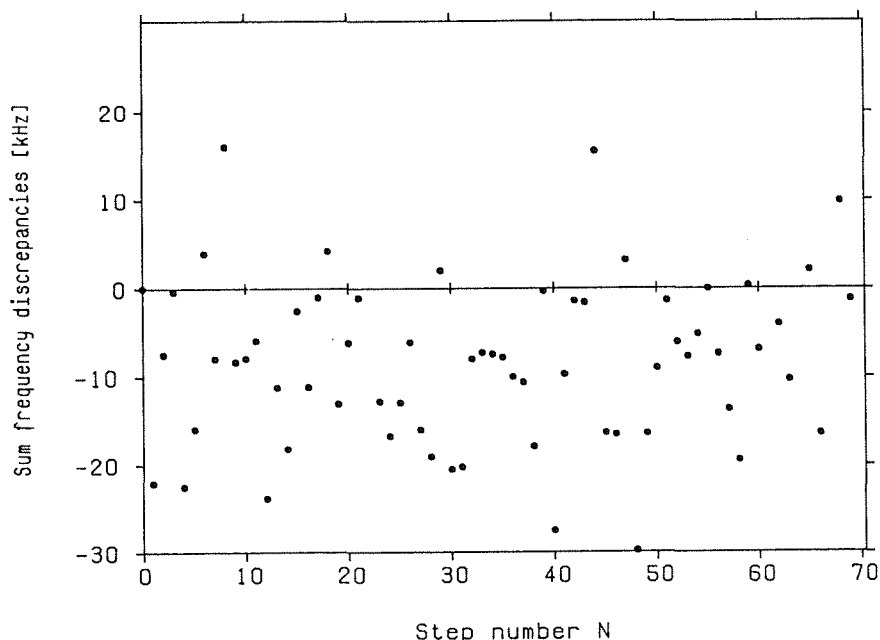
Fig. 2   Differences of the frequency sums for two 69 step runs. The average step width was 3.9 GHz. Each run spanning 269 GHz required 6 minutes with a counting time of 1 sec for each step.

To test the multistep heterodyne method, we have measured and summed up the frequency differences of 69 successive steps with an average stepwidth of about 3.9 GHz. Two such runs were performed; the results are given in Fig. 2: The frequency sums for both runs were subtracted after the same number of steps and the differences are plotted against the step number. It is obvious from Fig. 2 that the second run reproduces the first one to within $\pm$ 30 kHz; the discrepancies do not increase as the number of steps increases. There is a small permanent difference of 10 kHz in the results.

[1]   B. Burghardt, H. Hoeffgen, G. Meisel, W. Reinert, B. Vowinkel, Precision Measurement and Fundamental Constants II, B. N. Taylor, W. D. Phillips, Eds., Natl. Bur. Stand. (U.S.), Spec. Publ. 617, 49 (1984)

[2]   A. Dorn, G. Meisel, KfK-Report 4508, 77 (1989)

[3]   A. Dorn, W. Kälber, G. Meisel, KfK-Report 4709B (1990)

[4]   A Steiger, KfK-Report 3820 (1984)

[5]   R. Schruft, W. Kälber, D. Kowalewska, G. Meisel, this report contribution 3.3

[6]   F. Bayer-Helms, Ed., PTB-Bericht ME-17 (Physikalisch-Technische Bundesanstalt, 1977)

[7]   M. Anselment, S. Göring, G. Meisel, Z. Phys. D7, 113 (1987)

3.6.A A cw DYE LASER WITH HIGHLY STABILIZED FREQUENCY [1]

A.DORN, W.KÄLBER, G.MEISEL

Two ring dye lasers were modified. By changes of the ring geometry the efficiency of both lasers was doubled. For DCM dye the peak efficiency is about 20% in single mode operation at 640 nm. At this wavelength the output power is 600 mW for a pump power of 3 W. The lasers can be tuned from 620 nm to 678 nm.

The dye lasers are frequency stabilized by locking them to the peak of a resonance of a confocal reference interferometer. For this purpose part of the laser beam is phase modulated and fed to the reference interferometer; the error signal is deduced from the transmitted intensity

An electro-optic crystal and a piezo mirror mount are used as transducers to correct the laser frequency. The reference interferometers in turn are locked to an iodine stabilized HeNe laser.

The short term stability of a stabilized dye laser was determined to be 300 Hz for an integration time of 1 sec.

4.   *NEUTRINOPHYSICS*

T.CSABO, G.DREXLIN, V.EBERHARD, K.EITEL, H.GEMMEKE,
W.GRANDEGGER, R.GUMBSHEIMER, H.HUCKER, L.HUSSON,
J.KLEINFELLER, M.KLEIFGES, R.MASCHUW, P.PLISCHKE,
J.RAPP, F.K.SCHMIDT, G.SPOHRER, J.WOCHELE, S.WÖLFLE,
J.WOLF, B.ZEITNITZ, B.BODMANN[+], F.BURTAK[+], E.FINCKH[+],
T.HANIKA[+], J.HÖßL[+], W.KRETSCHMER[+], R.MEYER[+], F.SCHIL-
LING[+], J.A.EDGINGTON[++], A.MALIK[++], B.SELIGMANN[++],
A.DODD[+++], A.G.D.PAYNE[+++], N.E.BOOTH[++++]

INTRODUCTION

KARMEN denotes an experimental program of neutrino physics being
performed at the spallation facility ISIS of the Rutherford Appleton Laboratory.
From the decay of stopped π^+ produced in the UD_2O-beam stop of the 800 MeV 200
μA proton beam one gets monoenergetic v_μ with $E_{v_\mu} = 29.8 MeV$ whereas the
subsequent μ^+-decay provides v_e and $\bar{v}_\mu$ with energies up to 52.8 MeV. The
neutrino beam has a distinct pulse structure correlated to the proton beam from
the 50 Hz rapid cycling synchrotron. Due to the short lifetime of the π^+ there are
two prompt v_μ bursts within the first 500 nsec (duty cycle 10^{-5}) whereas after
0.5 μsec one is left with $\bar{v}_\mu$ and v_e (duty cycle $2.5 \cdot 10^{-4}$) from the slower μ^+-decay.
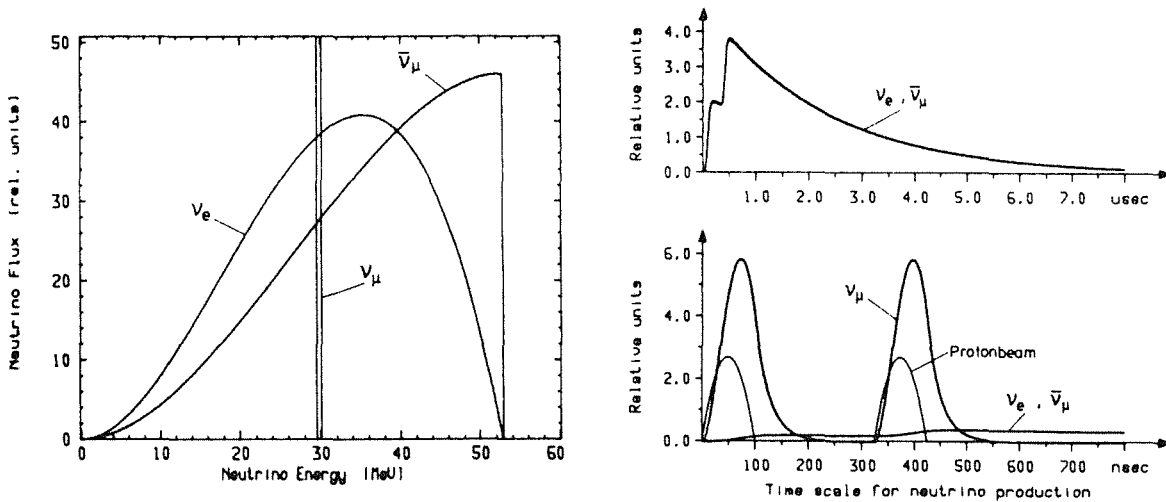
Fig. 1   Energy spectrum (a) and 50 Hz time structure (b) of the ISIS beam stop
neutrino source

This time structure with its low duty factor provides effective suppression of background as well as stringent signatures on events induced by the different neutrinos.

A 56 t all active scintillation calorimeter is housed in a 6000 t shielding blockhouse with the detector center located 17.7 m from the v-source. Major physics aims of this experiment are the search for neutrino appearance oscillations $v_\mu \rightarrow v_e$ and $\bar{v}_\mu \rightarrow \bar{v}_e$ simultaneously, an investigation of neutrino nuclear reactions $^{12}C(v_e,e^-)^{12}N$ (CC) and ^{12}C $(v,v')^{12}C^*$ (NC) [1,2,3] to study properties of the electroweak interaction and the measurement of neutrino electron scattering with respect to the NC and CC interference in weak interactions.

THE KARMEN DETECTOR

The scintillation calorimeter [4] consists of a large rectangular steel vessel filled with 65,000 l mineral oil based liquid scintillator PPP (paraffin, pseudocumene, PMP-fluor). An optical segmentation providing total internal reflection divides the detector volume into 512 optically separated modules of 17.7×18.1 cm^2 cross section and 350 cm length, each module viewed by two 3" phototubes (XP 3462) from either end. This central detector with an active mass of more than 98% is surrounded on four sides by a layer of modules of 9 cm width serving as inner anticounter to define a 'contained' event. In total 2240 photomultipliers are looking into the scintillator volume. 20 cm thick steel slabs providing the mechanical strength of the detector are used as passive inner shield followed by a 3 cm plastic scintillator cover (NE110) as active outer shield detector [5].

After completion KARMEN has been commissioned for data taking in November 1989. Calibration runs with cosmic muons confirmed the excellent calorimetric properties of the detector (see below). First data runs with ISIS 'beam on' allowed easy identification of neutrino events. Event analysis with respect to their time, energy and spatial distributions also provided detailed information about different sources of remaining background and indicated how background conditions could be further improved. With a 5 cm layer of borated polyethylene surrounding the detector, background identified to stem from slow (thermal) neutrons was significantly reduced. Fig. 2 shows the effect of one side wall of the KARMEN calorimeter covered with borated polyethylene reducing the background intensity on that side by factor of 6. The KARMEN data also pointed out

some hot spots of fast neutrons in the ISIS experimental hall which are now removed by improved shielding.
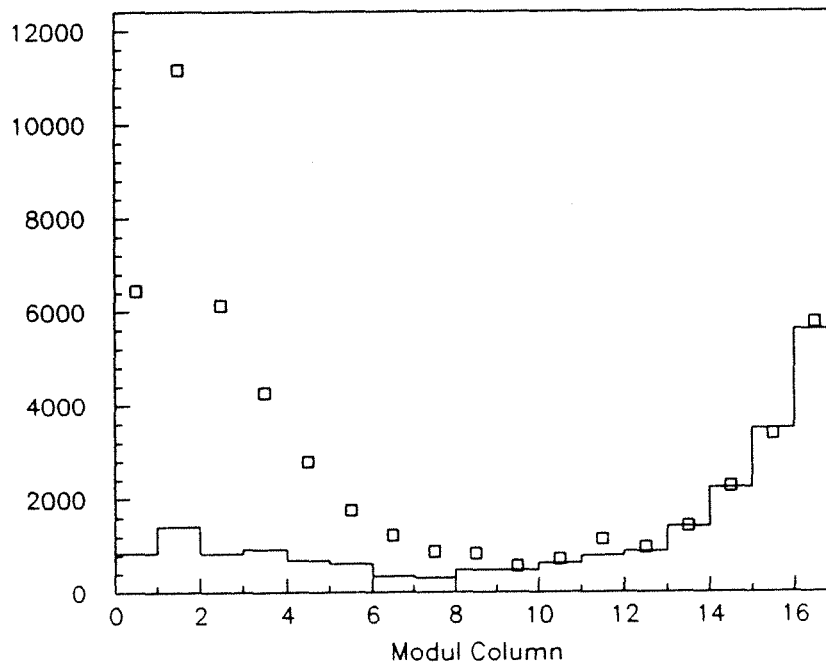
Fig.2   Reduction of single prong contained events in the KARMEN detector by borated polyethylene shielding on one side of the detector.

The event trigger has been steadily improved to minimize deadtime as well as to identify and mark any neutrino faking background i.e. bremsstrahlung and other neutrals, unidentified stopped muons etc.

In 1990 data have been taken with KARMEN at ISIS for about 1000 C protons on target which is only one third of the design specifications of ISIS. Therefore, to ensure the scientific aims of the KARMEN experiment an agreement between the Bundesminister für Forschung und Technologie and the Science and Engineering Research Council has been signed to improve operation of ISIS to run at its design values of 800 MeV energy with 200 μA beam intensity with 90% reliability.

ANALYSIS OF MUON-INDUCED REACTIONS

Careful analysis of muon induced reactions in the KARMEN detector is of vital importance to the experiment as various interactions of cosmic muons particularly when the muon track remains unidentified could lead to serious neutrino faking background. On the other hand these reactions provide an ideal tool to investigate detector and electronics performance.

From the decay of stopped muons $\mu \to e\nu\bar{\nu}$ the decay spectrum with its Michel shape as well as the muon lifetime have been measured with high precision. From the muon capture reaction $\mu^- + {}^{12}C \to n + {}^{11}B + \nu_\mu$ where the neutron is subsequently detected via the Gd $(n,3\gamma)$ reaction the neutron detection efficiency could be deduced, needed to measure $\bar{\nu}_e + p \to n + e^+$ reactions with respect to the search for neutrino oscillations $\bar{\nu}_\mu \to \bar{\nu}_e$. Capture processes of stopped μ^- on ${}^{12}C$ leading to bound states of ${}^{12}B$ i.e. ${}^{12}C(\mu^-,\nu_\mu){}^{12}B$ are unique 'monitor' reactions for the neutrino induced reaction ${}^{12}C(\nu_e,e^-){}^{12}N_{g.s.}$ as the subsequent β-decay of ${}^{12}B_{g.s.} \to {}^{12}C + e^- + \bar{\nu}_e$ is very similar to the ${}^{12}N$-decay ${}^{12}N$ -- (16 msec) $\to {}^{12}C + e^+ + \nu_e$ used to identify the exclusive channel of the charged current reaction. Fig. 3 shows the experimental signature of the ${}^{12}B$-decay electrons with respect to their visible energy and their decay time. The Kurie plot shows the expected linear behaviour of the allowed transition and yields an end point energy of $E_0 = 13$ MeV which is close to the theoretical value of 13.36 MeV. The linear shape of the Kurie plot further demonstrates the excellent energy resolution of the 56 t detector as well as the calorimetric properties of KARMEN for low energy electrons.
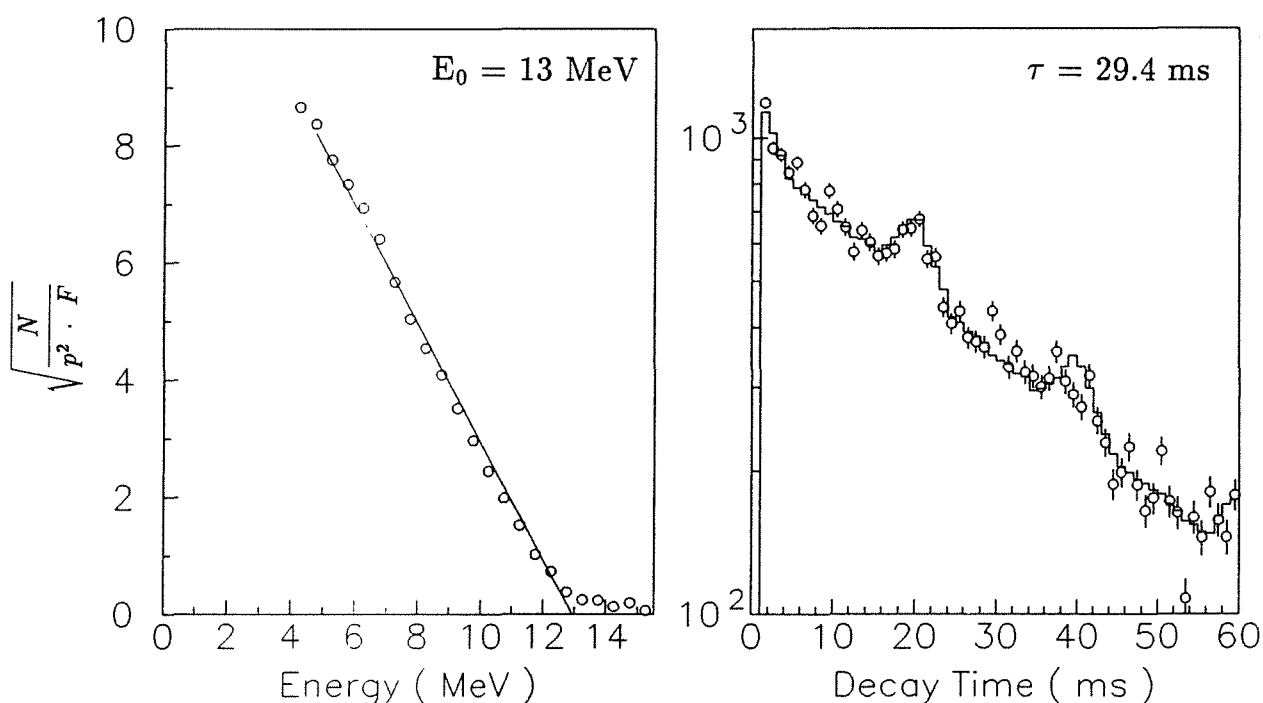
Fig. 3   Energy- (Kurie plot) and time distribution of ${}^{12}B$-decay electrons from the μ^- capture reaction ${}^{12}C(\mu^-,\nu_\mu){}^{12}B \to {}^{12}C + e^- + \bar{\nu}_e$

The calculated end point energy finally confirmed the validity of the energy calibration of the detector using the Landau energy loss distribution of cosmic muons. The measured lifetime spectrum of ^{12}B-decays yields a lifetime $\tau = 29.4$ msec and is in very good agreement with the Monte Carlo (MC) simulation taking into account the fixed KARMEN read out cycle of 50 Hz.

The ratio of identified ^{12}B-decays to primary stopped muons can be used to calculate the branching ratio of muon capture reactions to all bound states of ^{12}B. Using the MC calculated detection efficiency for ^{12}B-decays and the measured μ^+/μ^- charge ratio in the detector from a high statistics muon lifetime plot one calculates a capture rate $\Lambda_c = 6.7 \cdot 10^3$ sec^{-1} which is close to the best theoretical estimate of $(7.01 \pm 0.27) \cdot 10^3$ sec^{-1}. This good agreement demonstrates the high reliability of the GEANT 3 MC-code which is also used to calculate the detection efficiencies for the various neutrino induced reactions.

ANALYSIS OF NEUTRINO INDUCED REACTIONS

The search for neutrino induced reactions was first concentrated on the charged current (CC) reaction ^{12}C (v_e,e^-) ^{12}N$_{g.s.}$. Neutrino identification was straightforward looking for the delayed coincidence between the prompt electron from the inverse β-decay on ^{12}C and the delayed positron from the subsequent decay ^{12}N $--(16\,\text{ms}) \rightarrow {}^{12}$C $+ e^+ + v_e$ at the same position of the calorimeter. Cuts on energy and time of the prompt and delayed signal respectively as well on its spatial correlation yield an overall detection efficiency of $\varepsilon(v_e) = 0.45$. From about 10^8 primary events for 1027 C protons on the ISIS target 52 events survived these cuts denoted as neutrino candidates. Fig. 4 shows such a neutrino event in its detector projections top-side-front for the prompt and delayed signal which within the ^{12}N lifetime are located exactly at the same position of the detector. The energy and time distributions of these events are shown in Fig. 5 together with the corresponding MC-simulations. 5a) reflects the energy spectrum of v_e's, with their time structure 5b) being determined by the μ^+-lifetime. Similarly 5c) represents the ^{12}N decay spectrum with its lifetime distribution given in 5d).

Applying the same cuts to 'beam off' periods a corresponding background rate of only 4.1 events has been found which means a signal background ratio of better than 10:1. With 47.9 $\pm$7.2 events the flux averaged cross section for the CC reaction ^{12}C$(v_e,e^-)^{12}$N$_{g.s}$ was deduced to be

$$\bar{\sigma}_{exp}(^{12}\text{C}(v_e,e^-)^{12}\text{N}_{g.s.}) = (0.855 \pm 0.129 \text{ (stat.)} \pm 0.10 \text{ (syst.)}) \cdot 10^{-41} \text{ cm}^2$$

in good agreement with the theoretical prediction of $\bar\sigma_{th} = (0.9 \pm 0.1) \cdot 10^{-41}$ cm^2 [1,2,3]. The estimated systematic error is due to uncertainties in the ν-beam intensity related to a pion to proton ratio in the spallation target of $n^+/p = 0.0345$.

Neutrino Event

Prompt event   Delayed event

E = 29.5 MeV
t = 4.88 μs

E = 6.7 MeV
t = 15.2 ms
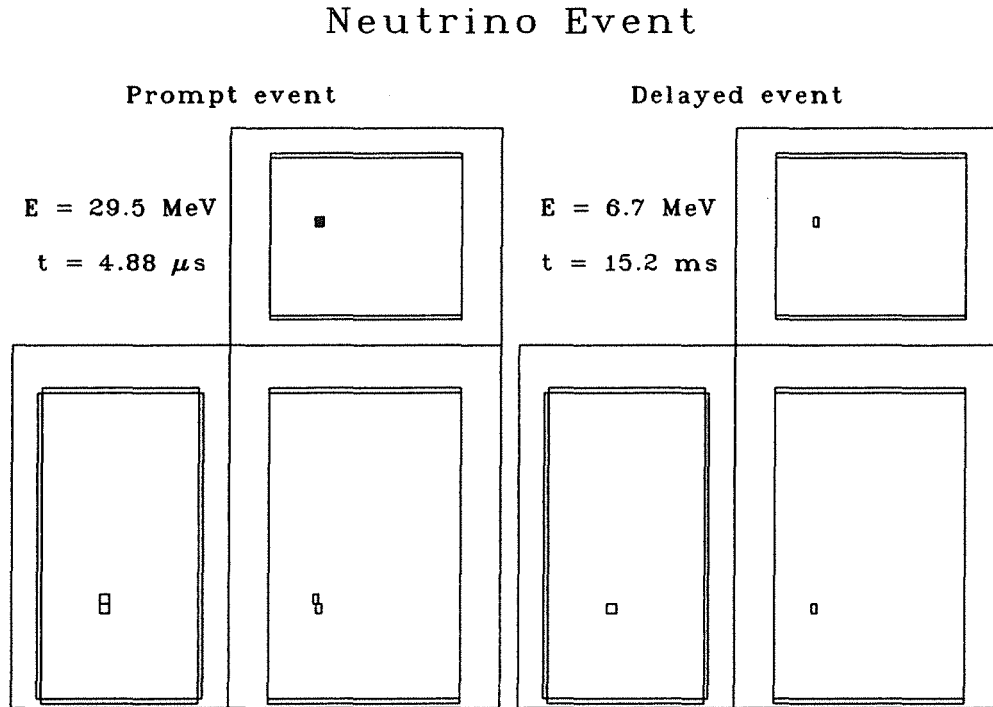
Fig. 4   Neutrino event of type $^{12}C(\nu_e,e^-)^{12}N_{g.s.} \to {}^{12}C + e^+ + \nu_e$. Prompt and delayed signal in its detector projections top-side-front.

From the KARMEN data there is also an indication that for the first time neutral current (NC) nuclear excitation has been observed in the inelastic neutrino scattering process $^{12}C\{(\nu_e\bar\nu_\mu),(\nu_e{'}\bar\nu_\mu{'})\}^{12}C^*$ (1$^+$,1; 15.1 MeV). The signal for this reaction is the detection of a 15 MeV γ-quantum within the time window of electron- and muonantineutrinos ν_e and $\bar\nu_\mu$. In Fig. 6 the visible energy of single prong events in this time window shows a clear peak around 15 MeV associated to the inelastic scattering process as well as a bump at somewhat higher energies to be related to inclusive neutrino reactions i.e. $^{12}C(\nu_e,e^-)^{12}N_{ex.st.}$, $^{13}C(\nu_e,e^-)^{13}N$, ν-e scattering etc. . This interpretation is backed by the good agreement of the data with a corresponding MC-simulation (dashed line).
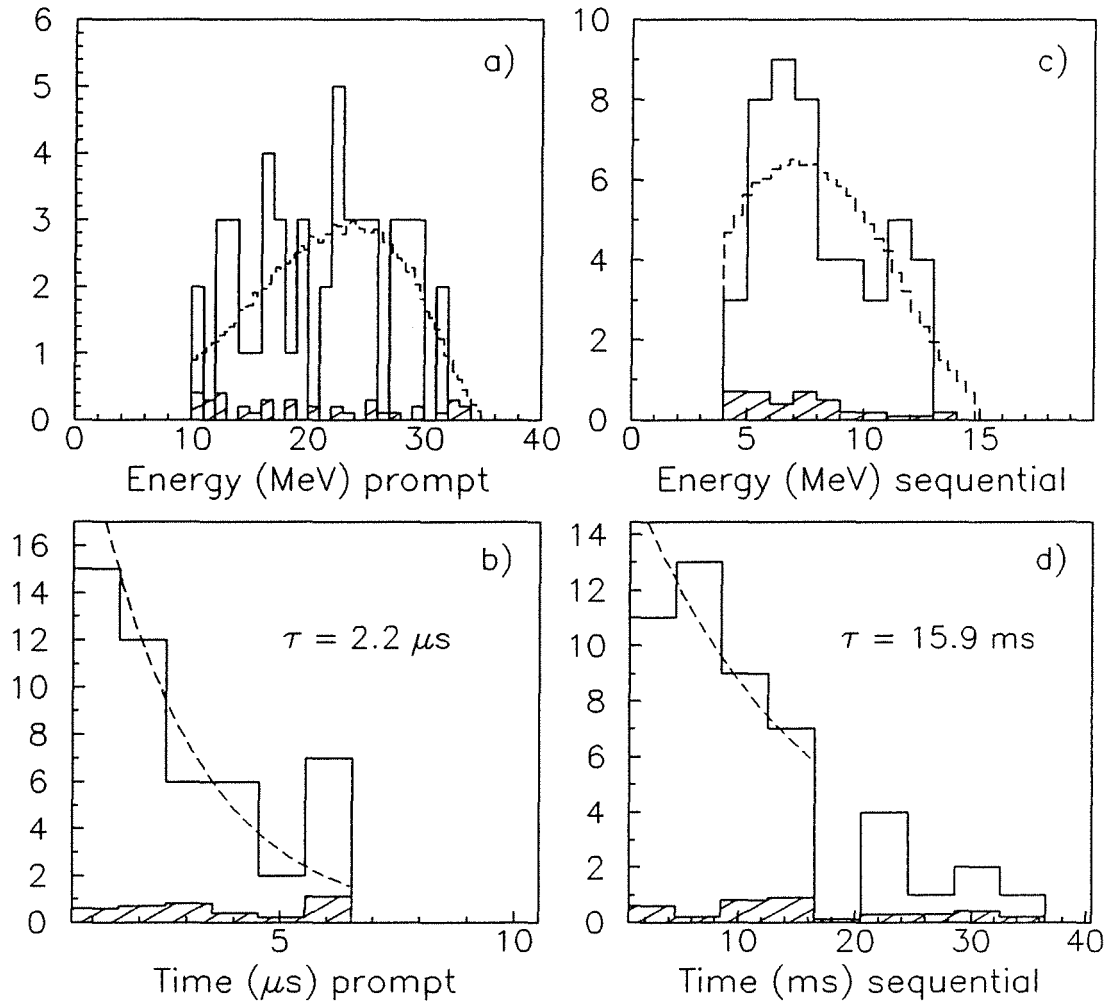
Fig.5   Energy and time distribution of the prompt {a),b)} and delayed {c),d)} signal for neutrino events of the type $^{12}C(v_e,e^-)^{12}N_{g.s}$ with subsequent decay ^{12}N -- (16 msec) $\rightarrow^{12}C+v_e+e^+$. Experimental distributions (histogram) are compared to the MC results (dotted) and normalized background (hatched).

These first encouraging results demonstrate the quality of the KARMEN experiment. Data taking is planned to continue for the next five years. With steady improvements of the ISIS beam quality, improved shielding and an even more sophisticated trigger one can expect that the experiment will significantly contribute to the questions of neutrino oscillations and neutrino nucleus interactions.
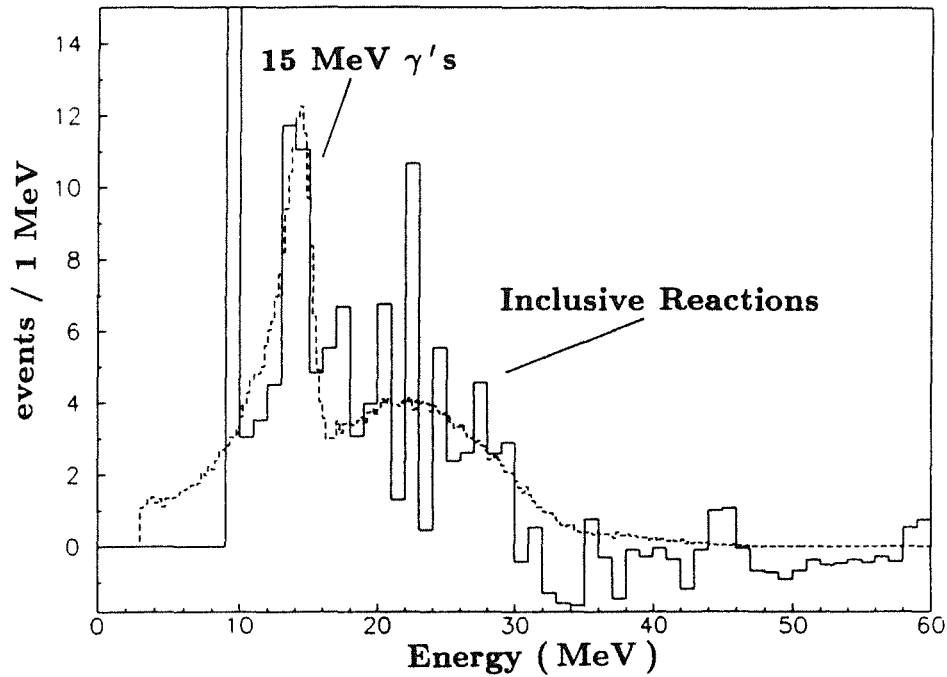
Fig.6   First indication of neutral current nuclear excitation in the reaction
$^{12}C \{(v_e \bar{v}_\mu),(v_e' \bar{v}_\mu')\}$ $^{12}C^*$ $(1^+,1; 15.1$ MeV$)$

[1]   T.W.Donnelly, Phys. Lett. 43B, 93 (1973) and preprint (1988).

[2]   S.L.Mintz, Phys Rev. C25, 1671 (1982) and S.L.Mintz, M.Pourkaviani,
       Phys. Rev. C40, 2458 (1989).

[3]   M.Fukugita, Y.Kohyama, K.Kubodera, Phys. Lett. 212B, 139 (1988).

[4]   G.Drexlin et al. (KARMEN collaboration), Nucl. Instr. & Meth. A289,
       490 (1990)

[5]   B.Bodman et al., Nucl. Instr. & Meth. A286, 214 (1990).

+   Physikalisches Institut, Universität Erlangen-Nürnberg

+ +   Queen Mary and Westfield College, London, UK

+ + +   Rutherford Appleton Laboratory, Chilton, Didcot, UK

+ + + + Oxford University, Oxford, UK

5. ASTROPHYSICS WITH EXTENSIVE AIR SHOWERS

5.1. DETECTOR DEVELOPMENT

5.1.1. SIGNAL DAMPING OF STRONG IONIZING PARTICLES IN LIQUID IONIZATION CHAMBERS

J.BOLZ, J.ENGLER

Ionization chambers using the liquid tetramethylsilane (TMS) will be used as active elements in a calorimeter for high energy cosmic ray hadrons. The cascade initiated in the absorber of the calorimeter is composed of a variety of particles ranging from low energy nuclear fragments to high energy pions of several TeV. In order to be able to interprete the signal response of such a cascade and to deduce from the primary energy of the converted hadrons, the signal response in the chamber has to be known for minimum ionizing particles as well as for strong ionizing particles. As strong ionizing particles tritons of 45 to 75 MeV had been used with an energy loss in the liquid of 21 to 30 MeV / g / cm². These tritons could traverse the container walls of the chamber which consisted of 1 mm stainless steel each.

The room of 8 mm between the two chamber walls was filled with liquid. In the centre an electrode of 0.5 mm thickness collected the electrons. The electrode was on a high voltage potential of typical 5 kV and via a coupling capacitor the induced signal was taken off and fed to a preamplifier. By a small calibration capacitor a definite amount of charge could be injected into the input circuit, giving a calibrated signal within 1% rms uncertainty.

The signal is compared with the signal for minimun ionizing particles. The corresponding reference is the signal of 1 MeV conversion electrons of a [207]Bi source. Usually the signal S is parametrized according to Birks' law :

$$S = A \frac{\frac{dE}{dx}}{1 + kB \frac{dE}{dx}}$$

where dE/dx is the energy loss and A a constant.

The factors kB obtained are plotted in Fig.1. They depend on the angle between the ionizing particle track and the electric field. One observes a large value of kB, i.e. strong signal reduction for parallel incidence, which flattens off at larger

angles. Only up to 40° could be measured due to the thickness of the chamber walls. However, with a chamber with special windows it is planed to extend the measurements further.

How well Birks' ansatz parametrizes the signal damping was tested by varying the triton energy and consequently the specific ionization loss. The corresponding kB factors are plotted in Fig. 2. Also values obtained with pions at $dE/dx = 7$ MeV/gcm^{-2} and with protons at $dE/dx = 55$ MeV/gcm^{-2} [2] are indicated. The figure shows that in the accessible range Birks' law is not fulfilled, and that a two parameter ansatz has to be chosen.
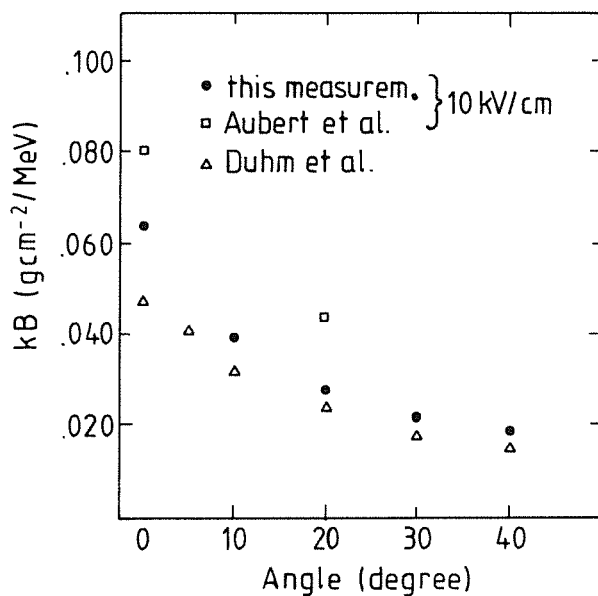
Fig. 1   kB in TMS as a function of incident angle at an electric field of 10 kV/cm
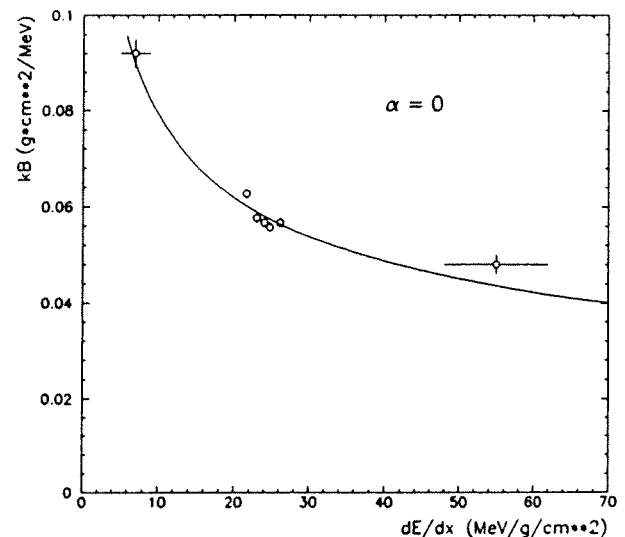
Fig. 2   kB as a function of the specific energy loss at 0° and 10 kV/cm.

[1]   B.Aubert et al., Nucl. Instr. and Meth. **A286**, 147 (1990)

[2]   H.H.Duhm et al., Nucl. Instr. and Meth. **A277**, 565 (1989)

5.1.2. PROPERTIES OF LIQUIDS SUITABLE FOR FAST IONIZATION CHAMBERS

G.VATER, J.ENGLER

Twenty years ago for the first time electron conduction was observed in a room temperature liquid, namely in neopentane [1]. Since then several other liquids are known to exhibit this property, among which tetramethylsilane (TMS) has a high electron mobility μ and high charge yield G. However, TMS has a relative high vapour pressure of 0.8 bar at room temperature, which is impractical for use in particle detectors because of security considerations.

Therefore, mixtures of TMS with a liquid of low vapour pressure have been investigated, especially to be used as an operating liquid for ionization chambers in the KASCADE central calorimeter. Hexamethyldisilane (HMDS) has a vapour pressure of 10 mb and is well available at reasonable prices due to its application in the varnish industry.

The measurements were carried out with an ionization chamber using the conversion electrons of a ^{207}Bi source. Its anode and cathode are separated by 8.4 mm. The source is attached to the cathode, to which a voltage of maximal 25 kV can be applied. The signal is read out on ground level at the anode. The monoenergetic electrons of about 1 MeV are observed with a reasonable good energy resolution of 25%, despite of the fact that no Frisch grid is used to shield the anode against the charge influenced by the positive ions.
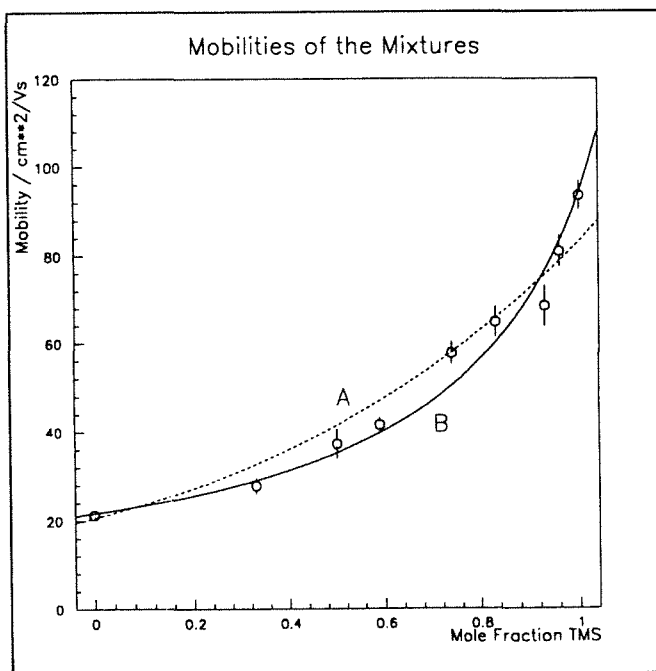
Fig. 1   Mobility of a mixture of HMDS and TMS. Curve A represents a fit due to a "trapping" model with $\chi^2 = 36$, curve B for a "scattering" model with $\chi^2 = 17$.

The drift time of the ionization electrons and the corresponding mobility were measured by using different integration times in the charge sensitive amplifier.

The mobilities as measured for mixtures of TMS and HMDS are presented in Fig. 1 . One observes that the mobility is not a linear function with respect to the mole fraction. The high mobilities in the pure liquids suggest, that the electrons occupy extended states in a manner similar to electrons in a band in solid state crystals. This can be presumed from the fact that the de Broglie wave length is smaller than the mean free path ℓ between two scattering events for these liquids. The scattering length can be inferred from the mobility μ and the thermal velocity v according to $\ell = v \cdot \mu \cdot m/e$ to be $\ell = 54$ Å for TMS and $\ell = 12$ Å for HMDS.

In the case of different scattering centres in a mixture, ℓ should be composed of the reciprocal mean-free path of the pure liquids. As can be seen in Fig. 2, a corresponding fit explains the data rather well.

Also a fit is shown using a "trapping" model, which has been proposed to explain the mobilities in liquids exhibiting a low moblility.

In Fig.2 the charge yield G_0 at zero electrical field is shown. Again one observes no linear dependence. Surprisingly even a shallow minimum is seen to exhibit around a mole fraction of 0.4 with a smaller G_0 value as in the pure states. This result indicates that in a mixture the electrons are thermalized more efficiently than in pure liquids.
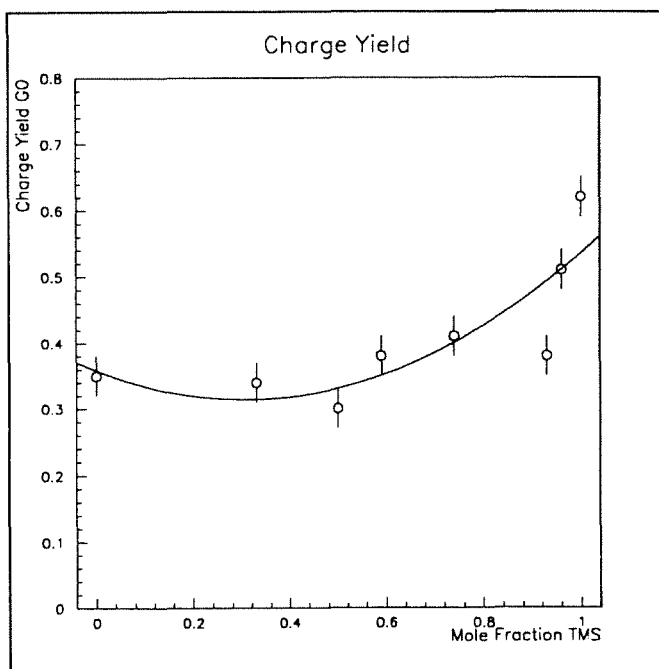
Fig. 2   Charge yield at zero electrical field in a mixture of HMDS and TMS. The line represents a fit with a second order polynominal.

The ionization electrons, ejected from their parent ions, seem to come into thermal equilibrium with the surrounding liquid at a shorter distance to their

parent ion. Therefore, recombination of the geminate electron is easier and less electrons can be collected in an external electric field.

However, no quantitative calculations exist yet on this effect, which has also been observed by S.Geer at al.[2]

For practical applications the non-linear dependence, both in μ and G_0, is rather disappointing. In a mixture we have to face relative small drift velocities and a small charge yield. The latter is even smaller than for the pure liquids. Another possible drawback in applying mixtures might be a high-voltage stability which is less than for the pure states. In experimenting with mixtures we had the impression that mixtures show more easily additional noise at voltages beyond 10 kV. But definite conclusions cannot be drawn, because thorough investigations concerning this question have not been done yet. They will be performed in the future.

[1]   W.F.Schmidt and A.O.Allen, J. Chem. Phys. 52 (1970) 5788
[2]   S.Geer at al., Nucl. Instr. and Meth., A287 (1990) 447

5.1.3.   GLOW DISCHARGE CLEANING OF STAINLESS STEEL SURFACES FOR IONIZATION CHAMBERS

J.BOLZ, J.ENGLER, D.MOUCKA

Liquid ionization chambers need very clean operation conditions. Therefore, the ionization chambers, which have been developed for the KASCADE central calorimeter, have been treated chemically in a wet process followed by a conditioning of the chamber in a dc-glow discharge (dry cleaning). The ions accelerated in the cathode fall desorb all strongly bound molecules from the surface, which are then pumped away. To clean electrodes and container equally well, the polarity is switched in regular terms. Our investigations lead to a current density of 60 μA / cm^2 and a pessure of 100 Pa. Argon gas. The gas with desorbed impurities is pumped away periodically every 15 s.

The plasma exhaust is monitored after each cleaning step in a mass spectrometer [1]. Typical mass spectra of the Ar gas before and after a discharge step are presented in Fig. 1. The desorption of CO is well noticeable. How the detachment of O_2, CO and H_2O evolves is shown in Fig. 2. Other contaminants

show a similar behaviour. One observes that the bulk of material desorbs fast, i.e. within an accumulated dosage of 1×10^{16} ions / cm^2. Most of the chambers have been treated with a total dosage of 1×10^{17} ions / cm^2 before being flushed and filled with TMS. Quantitatively, the amount of desorbed CO is equivalent to about 1.5 monolayers, H_2O to about 1 monolayer and all other molecules like CO_2 and O_2 much less. The chambers seem to be already very clean after the wet cleaning.
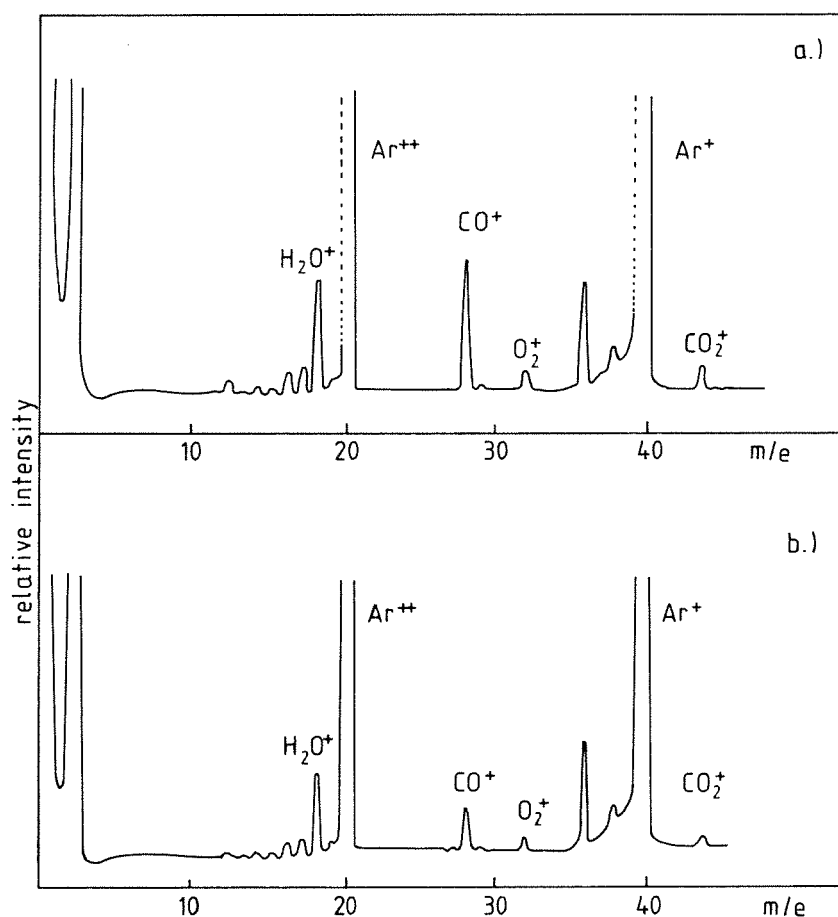
Fig. 1:   Mass spectra of Ar gas before and after the cleaning process at a dosage of 5×10^{15} ions / cm.

Following the glow discharge cleaning the chambers are filled with clean TMS. From the life time of free electrons in the filled ionization chamber the concentration of impurities are calculated to be 0.2 ppm Mol / l in the case of O_2 or 7.7 ppm Mol / l in the case of CO_2. The corresponding thickness of dissolved monolayers would be 0.015 for O_2 and 0.70 for CO_2, respectively. In the literature [2], the majority of systems is concerned with reactant gases like H_2 or Ar / O_2 mixtures. Both gases have been tried, too. However, in both cases no benefits were found of removal of a larger amount of surface contamination. Therefore, both gases, H_2 and O_2, were abandoned and the effort concentrated on pure Ar cleaning.

With the conditioning by Ar glow discharge the chambers can be sealed off hermetically after a flush when the liquid stayed in the chamber for about 16 h. In contrast, without this dry cleaning process the chambers have to be flushed several times and the liquid has to be kept in contact with the surface for about a week before the chamber can be pinched off.
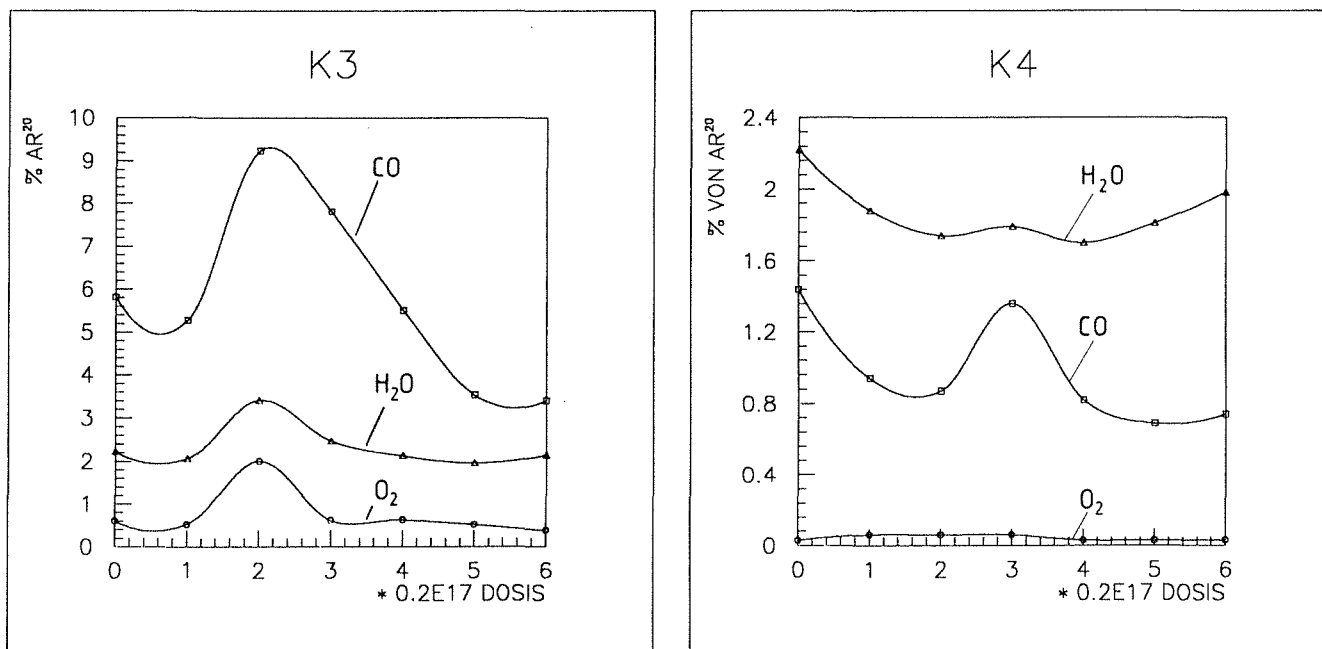
Fig. 2:   Desorption yield of O_2, CO and H_2O molecules with respect to accumulated dosage of the two chambers K3 and K4, for cleaning with Ar.

[1]   Leybold-Heraeus Quadruvac Q 200

[2]   H.F.Dylla, J. Vac. Sci. Technol.,A6, 1276 (1988)

5.1.4. TIME - RESOLVED SPECTROSCOPY OF LIGHT EMITTED FROM THE SELF - QUENCHING STREAMER (SQS) MODE

P.DOLL, K.DAUMILLER, H.O.KLAGES

While already extensive and systematic studies of the light producing mechanism have been carried out for gas ionization or proportional scintillation counters [1], the usefullness of rare gas scintillation [2], for X-ray detection in X-ray astronomy and as a position detector in high energy physics is undisputed. The investigation of light production in the SQS mode is still at the beginning and far away from the systematic studies, e.g. of the emission spectra from rare gas, liquid or solid scintillators [3] and their corresponding light decay curves. Preparational studies (see 5.1.8.) with commercial streamer tubes and custom made tubes for the air-shower experiment KASCADE, motivated the studies of various SQS features and a time-resolved spectroscopy of the light emitted in the SQS mode, combined with a study of charge multiplication near the anode wire and a corresponding pulse shape analysis.
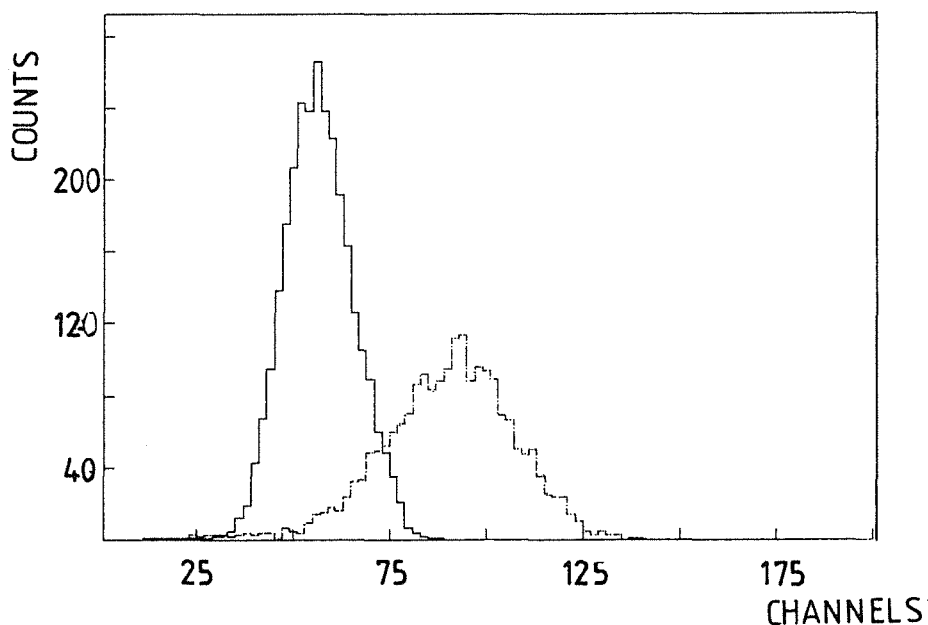
Fig. 1   Photon pulse height distributions for streamer discharges of about 200 pC (solid curve) and of 450 pC (dashed curve).

A commercially available steamer tube of Iarocci type and with a cross section of 30×30 mm^2 was modified by cutting an opening to allow a XP2062B phototube to view the discharge through an interference filter. Fig. 1 shows two pulse height distributions taken with the phototube for light of 430 ± 20 nm.The two

distributions correspond to a SQS streamer charge of around 200 pC and 450 pC, respectively, for which the streamer tube was operated in the plateau region at 6200 Volt and with a gas mixture of 35.7% Ar and 64.3% C_4H_{10}.There is sofar no spatial constraint on the SQS charge centroid. The average number of 430 nm photons derived on the basis of Poisson statistics indicates to about 6 orders of magnitude less photons than electrons recorded on the anode wire. This drastic quenching of photons, increasing further with the amount of charge recorded at the anode wire, is the natural feature of the SQS mode and is systematically investigated.
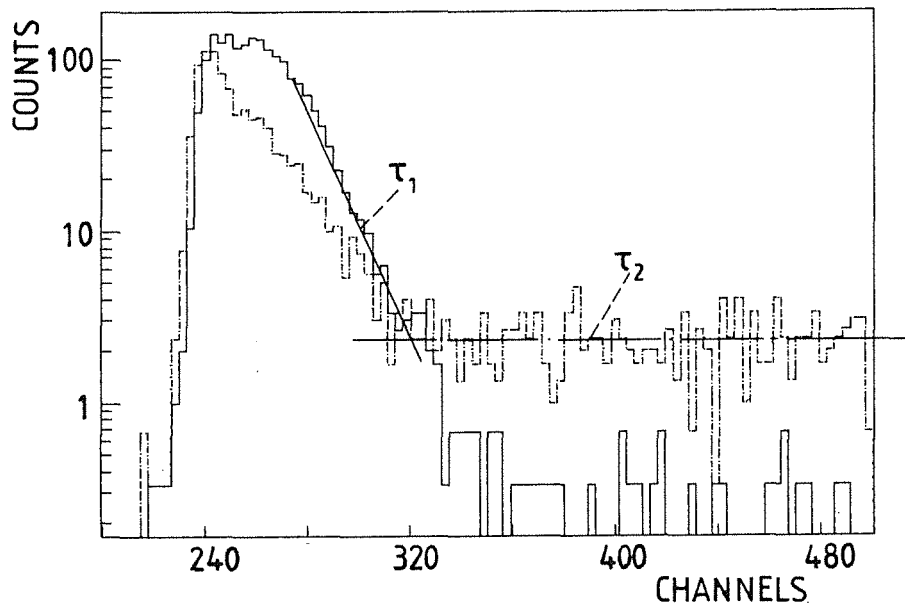
Fig. 2   Light decay curves for streamer discharges of 200 pC (solid curve) and of 450 pC (dashed cuve).

Fig. 2 shows for the same anode charge values the time decay spectra measured with respect to the anode time signal. The spectra show a superposition of various light components. The very early component, especially visible for the large charge, and even earlier than the τ_1 component, is not yet understood, but may be attributed to the C_4H_{10} gas component. The τ_1 decay time of around 4 ns is known from argon dimers [4] and also the slow τ_2 component. The latter is increasingly more produced for increasing SQS charges. However, the τ_2 component seems to be strongly quenched in the presence of the C_4H_{10} gas component. The observed dependence for the various decay rates as function of operation voltage and gas mixture suggests an analysis very common in the investigation of the production and destruction rates of excited molecular states [4].

[1]   A.J.P.L.Policarpo, Space Science Instrumentation 3, 77 (1977)

[2]   M.Suzuki, S.Kubota, Nucl. Instr. and Meth. 164 197 (1979)

[3]   S.Kubota, M.Hishida, M.Suzuki and J. Ruan , Nucl. Instr. and Meth. 196, 101 (1982)

[4]   J.W.Keto, R.E.Gleason, G.K.Walters, Phys. Rev. Lett. 33, 1365 (1974)

5.1.5.   SCINTILLATING LIQUID - NEON TARGET AND PULSE HEIGHTS FROM NEUTRON INDUCED REACTIONS

G.MONDRY*, F.SMEND*, P.DOLL, H.O.KLAGES, H.SKACEL

In the previous annual report [1] we described the construction of a scintillating neon target operated in the continuous energy neutron beam [2] for a neutron capture experiment (see also contribution 1.2.2, this report). From gaseous Ne at low pressure [3] it is known that the main light emission stems from dimers emitting in the wave length range between 70 and 100 nm. Therefore, the target walls were coated inside with a wave length shifter (DPS). Since neon is in the liquid state over a very narrow temperature range only (24.6 K to 27.7 K), the temperature has to be regulated precisely by balancing the net cooling power of the refrigerator by a controlled electrical heating of the neon cell. The scintillating mechanism of rare gases is due to the production and decay of the dimers; the latter are molecules, which are bound only in excited states. This process is described by Forstbauer [4] in the case of argon. The operation of the liquid neon target provided pulse height information from various neutron induced reactions like $^{20}Ne(n,n')^{20}Ne^*$, $^{20}Ne(n,n'\alpha)^{16}O^*$ (Q = -4.73 MeV), $^{20}Ne(n,p)^{20}F^*$ (Q = - 7.03 MeV), and even $^{20}Ne(n,n'\alpha\alpha)^{12}C^*$ (Q = -11.9 MeV). These reactions were identified for various neutron energy intervalls by their time of flight between the neon target and the neutron source and by their gamma ray lines of the residual nuclei, observed in the NaI crystals. The target exhibits only a moderate pulse height resolution but peaks or edges from various reactions can be identified riding on a background due to multiple scattering.

Fig. 1 shows the variation of pulse heights with the neutron energy for recoiling $^{20}F + p$ and $^{16}O + \alpha$. Inspite of the more negative Q-value the light yield from $^{20}F + p$ is larger than from $^{16}O + \alpha$. The $^{12}C + 2\alpha$ exit channel becomes important for high incident neutron energies. The hatched region shows the pulse height region for elastic and inelastic neon scattering which appears however
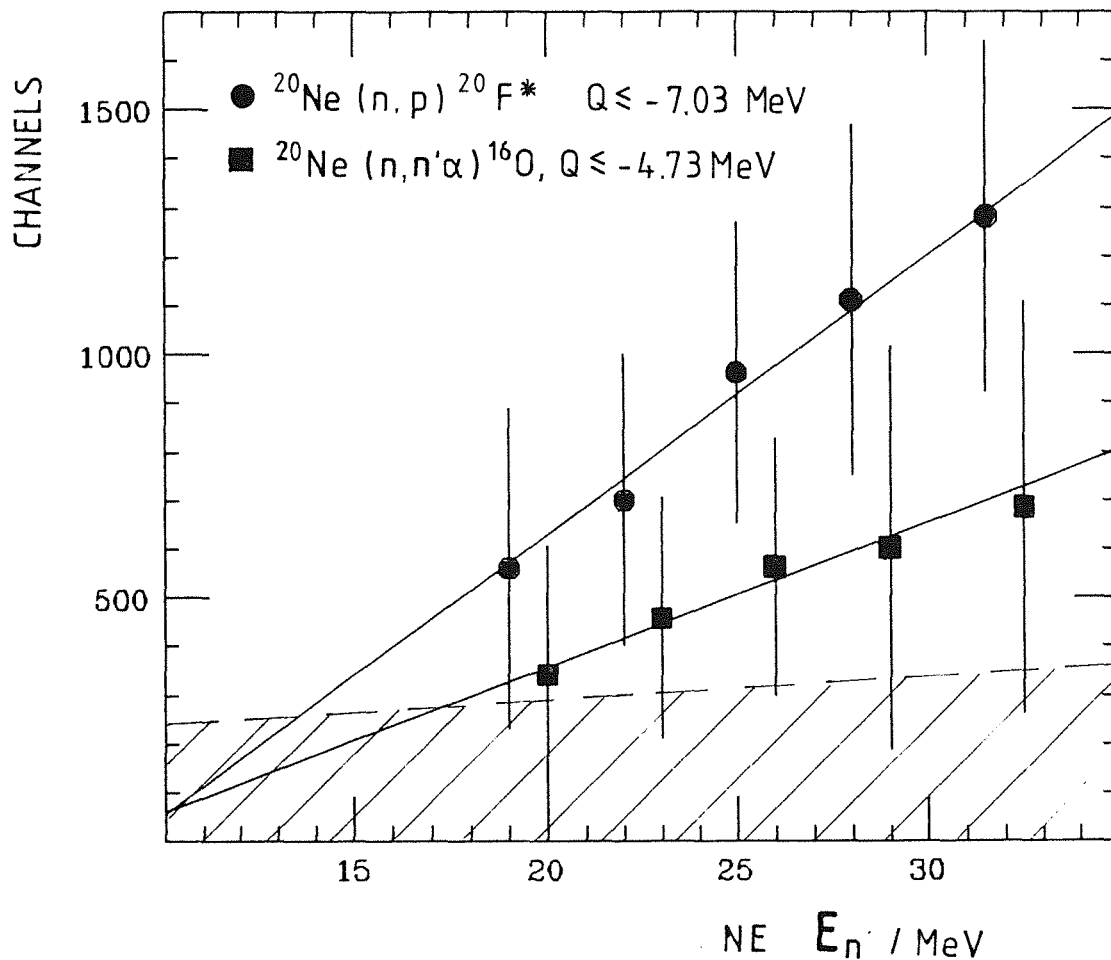
Fig. 1   Pulse height variation of the LNe-Target with the incident neutron energy for recoiling $^{20}F + p$ and $^{16}O + \alpha + n$

masked through multiple scattering effects. Enlarging the data base in the future analysis will help to sharpen the target pulse height information and put tighter constraints on the n-^{20}Ne capture data.

[1]   G.Mondry, F.Smend, P.Doll, H.O.Klages, H.Skacel, Report KfK 4660, Kernforschungszentrum Karlsruhe (1990), p.108

[2]   H.O.Klages, H.Dobiasch, P.Doll, H.Krupp, M.Oexner, P.Plischke, B.Zeitnitz, F.P.Brady, J.C.Hiebert, Nucl. Instr. and Meth., 219, 269 (1984)

[3]   A.Ulrich, B.Busch, W.Krötz, G.Ribitzki, J.Wieser, Jahresbericht 1987, Beschleunigerlabor LMU und TU München, p.58

[4]   B. Forstbauer, Report KfK 3774B, Kernforschungszentrum Karlsruhe (1984)

*   II. Physikalisches Institut, Universität Göttingen, Germany

5.1.6. IMPROVEMENTS IN THE MANUFACTORING OF SUPER-CONDUCTING DETECTORS

S.HAHN, W.HEERINGA, H. SKACEL

Superconducting Al/Al$_2$O$_3$/Al tunnel junctions are powerful tools for high energy resolution spectroscopy of α-particles and low energy X-rays. The detector structures are evaporated on a sapphire or quartz substrate in a high vacuum evaporation chamber. The oxide layer is produced by thermal oxidation of the surface of the first aluminium layer. With these detectors an energy resolution of 3% was reached for the detection of 5.9 keV X-rays.

In order to further improve the energy resolution , a systematic investigation of the evaporation and oxidation parameters would be necessary. To raise the production rate of the tunnel junctions, the evaporation chamber was extended by a load lock system. It is shown in Fig. 1.
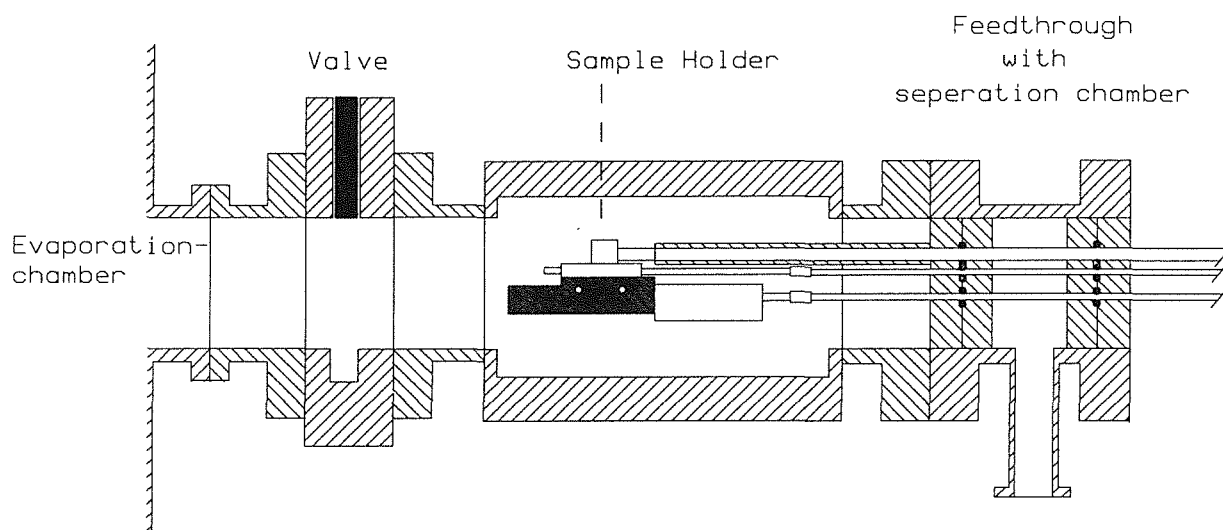
Fig. 1   Vacuum load lock

The substrate is fixed in the sample holder, on which a shutter mechanism is integrated. For the control of the shutter, for the fixing of the sample holder and for a thermal contact in the evaporation chamber, four steel rods are necessary. In order to stabilize and to seal these rods a rotary-pull feedthrough was developed which is shown in Fig. 2.

The rods are made of stainless steel which is covered with a 30 μm layer of chrome. They are moving in two cast sleeves of GZ-Cu Sn 7 Pb. The sealing is done by two viton O-rings for each rod. As a special feature a separation chamber is
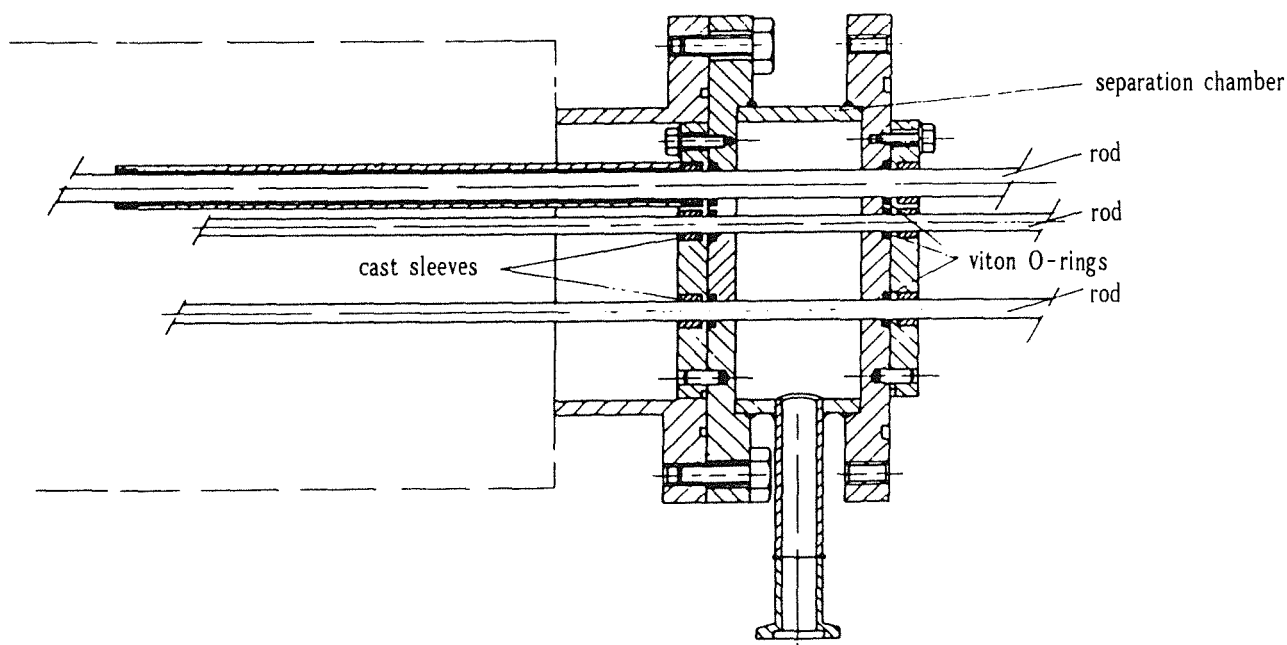
Fig. 1   Feedthrough

installed between the fixing points of the rods. The chamber is evacuated to 10^{-4}Pa so the inner O-rings have not to seal directly against atmospheric pressure.

With the vacuum lock, the time of manufactoring for a tunnel junction could be reduced from two to three days to a few hours. The mounting of the substrate in the sample holder and the adjustment of the shutter mechanism can be done using a microscope and takes only a few minutes.

The feedthrough seals to pressures below $5 \cdot 10^{-5}$ Pa with a leakage rate lower than 10^{-7} Pa, measured with a helium leak detector. Taking into account that the length of movement amounts to 70 cm, these results are very competitive compared to conventional high vacuum manipulators.

5.1.7.   BOLOMETERS AS DETECTORS FOR ALPHA - PARTICLES

R.BAYER, G.FOLTIN, W.HEERINGA, H.O.KLAGES, H.SKACEL

A bolometer is a microcalorimeter consisting of an absorber and a thermistor. The thermistor is a highly temperature-depending electrical resistor, which we made from a RuO_2-glass-mixture. In our set-up the absorber is a single-crystal of sapphire with the dimensions : $27 \times 7 \times 0.5$ mm^3 which serves to stop the incident particles. Stopping the particles causes a rise in the temperature of the bolometer

which will be measured by the change of the thermistor-resistance. The thermistor is melted directly onto the sapphire.

To raise the sensitivity for single-particle events we cooled the bolometer down to very low temperature. We used a ^{3}He-^{4}He-dilution cryostate and worked at temperatures below 50 mK. The bolometer within its mechanical set-up is shown in Fig. 1 and Fig. 2 .
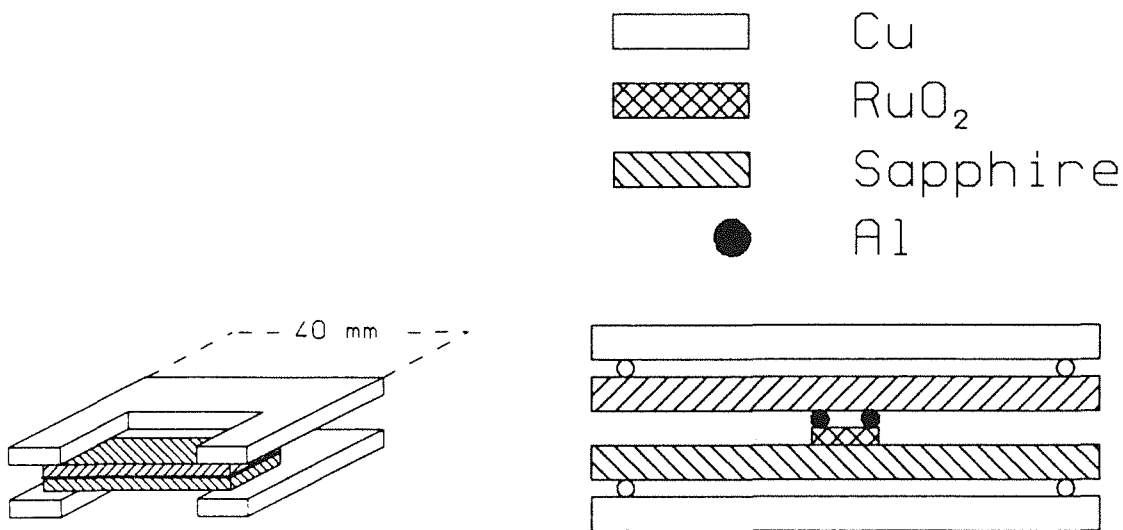
Fig. 1   Perspective view of the set-up   Fig. 2   Front view of the set-up
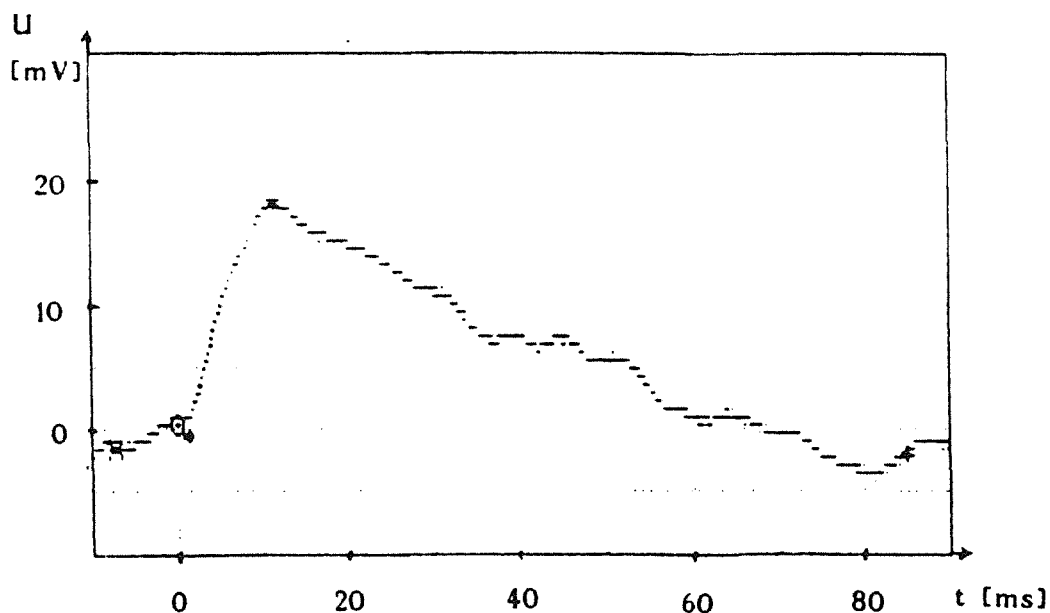
Fig. 3   Bolometer pulse

The wires between the sapphires and the copper-frames are of NbTi. The Al-wires are the electrical connections of the thermistor. We used a ^{210}Po-source which is emitting 4.5 MeV alpha-particles. The thermistor is biased with a

constant current source. An alpha-particle hitting the bolometer causes a temperature rise. Therefore the resistance of the thermistor decreases in the NTC-resistor used here and causes a voltage pulse. The heat-energy deposited in the bolometer will be conducted to the cold bath and so the temperature of the bolometer decreases to the original value it had before the particle hit it. A pulse, measured when an alpha-particle hit the bolometer , is shown in Fig. 3 . The risetime is so large because of the filtering time-constant of 10 ms. The decaytime is determined by the heat conductivity between the cold bath and the bolometer.

5.1.8.   CUSTOM - MADE STREAMER TUBES OUT OF CONDUCTIVE PLASTIC MATERIAL

K.DAUMILLER, P.DOLL, H.O.KLAGES

A large number of streamer tubes for many high energy physics and / or astrophysics experiments are mostly fabricated of extruded plastic profiles. Since the coating of the plastic cathode with the conductive graphite paint is one of the most difficult fabrication steps in the production process of conventional streamer tubes, we investigated the possibility of building streamer tube profiles using extruded conductive PVC as cathode material. For this purpose we employed 15×15 mm^2 plastic profiles from Akalit [1] a company that provided these profiles for the streamer tubes of the DELPHI detector at CERN [3].
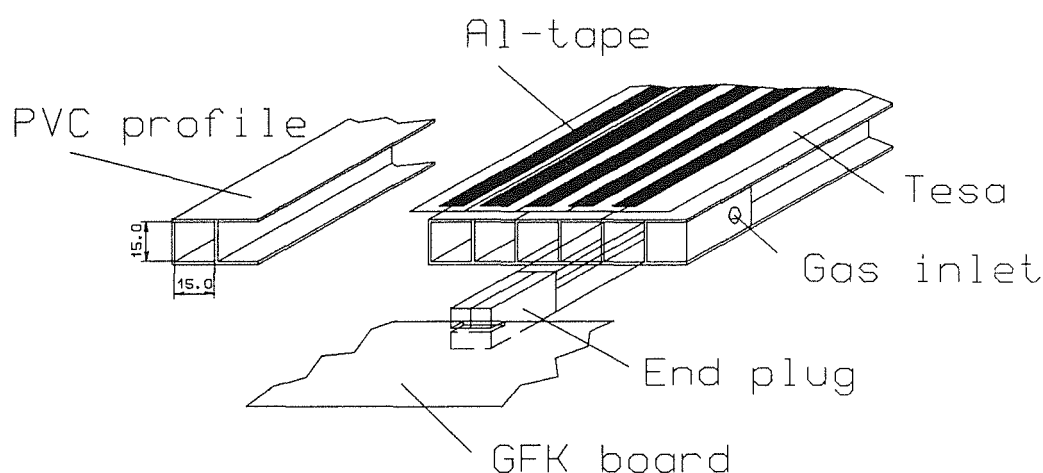
Fig. 1   Prototype construction out of conductive PVC

Fig 1 shows the construction of our prototype : 29 single profiles of 1100 mm length are mounted together gas tight on the upper and lower side by using a self adhesive plastic tape (Tesa 4104). This layer also provides the electric insulation between the cathode material and the influence strips that are placed on top of the detector, parallel to the 100 µm anode wires. These strips are made of 12 mm wide self adhesive aluminium-tape (Tesametal 4500), thus having a very good mechanical contact to the surface of the detector.The detector ends are closed gas-tight by PVC plugs and Tangit [4] glue. These plugs also support the Cu-clad epoxy boards holding the anode wires and the readout electronics. A frame of aluminum (not shown) gives mechanical stability for the whole construction.

Using an argon:isobutane mixture of 1:2 by volume the detector shows a countrate plateau from 4.6 to 5.2 kV. At an operating voltage of 5.0 kV the most frequent charge deposit on the anode wire is about 150 pC. Fig. 2 shows the spectra of the charge induced on the strip directly above the cell and its neighbours. The integrated number of events for the various charge distributions in Fig. 2 are identical. Rescaling has been done for the plots shown. The large pulse height of the influence signals (approximately 80 mV) allows us to process them without any amplification.
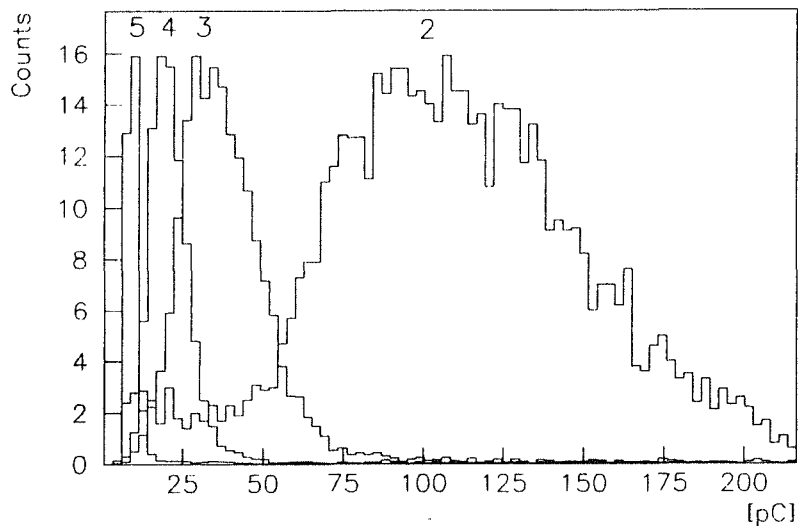
Fig. 2   Charge distribution on strip 2-5 for limited streamer discharges in cell 2

The anode wire signals, even larger, were also recorded in the experiment and provide the trigger for the individual cells. The influence charge on the strips was inverted by transformers and led to a LeCroy 2249 ADC. The crosstalk in the charge spectra between the direct strip and its neighbours is very small. This results in a small number of the strips being triggerd when a digital strip readout with discriminators is chosen. Considering the very rugged construction of this

prototype, the results obtained are very promising. Besides conductive PVC material we have also tested extruded Polypropylene and Polystyrol materials, kindly provided by the research department of the Röhm Company [2]. The operating characteristics of the tube produced out of Polypropylene look quite promising.

We conclude that the developement and mass production of streamer tubes, providing a comparatively high granularity for any large area detector is greatly facilitated by using advanced plastic techology.

[1]   Alkalit Kunststoff GmbH, A-2345 Brunn am Gebirge, Brunnenfeld-str. 45

[2]   Dr. H.Groß, Röhm GmbH, 6100 Darmstadt 1, private communication

[3]   Prof. W.Bartl, Institute for High Energy Physics, University Wien, private communication

[4]   Henkel KGaA, 4000 Düsseldorf 13, Henkelstr. 67

5.1.9.   ENERGY DETERMINATION OF HORIZONTAL COSMIC RAY MUONS WITH BURST COUNTERS

M.GETTERT, R.TREZECIAK, J.KNAPP, J.ENGLER

Introduction : A coarse energy determination of very high energy muons in the TeV range is desirable for muons in the core of extended air showers. Muons with an energy of more than a few TeV originate predominantly from the first interaction and give therefore valuable information about the physics in the corresponding primary processes.

To measure the energy of these muons the following detection principles could be used :
- transition radiation
- relativistic rise of ionization loss
- energy loss through radiative processes.

The first principle is a rather pretentious method, and not practicable for a large surface detector. For the KASCADE experiment, the latter two are under investigation. Detectors based on the last principle are often designated as burst counters.

Two detector modules of such burst counters have been built using 1 cm Pb slabs as bulk material for the radiator and liquid ionization chambers in between to detect the radiation. One unit is composed on 16 lead slabs. The radiation quanta are in the GeV range and initiate electromagnetic showers in the absorber plates. The construction principle for the ionization chambers is a swimming-pool system. The lead plates, which are used as anodes on ground potential, and the cathode electrode strips in between them are mounted in a container and plunged in the liquid. We use tetramethylsilane (TMS). The signals are collected on 6 vertical strips, which are on a potential of typically 3 keV. The strips are made of stainless steel and mounted in the middle of the 6 mm wide gaps. The signals are decoupled by ceramic blocking capacitors, and are fed to the preamplifier sitting directly on the top of the container cover.

Measurements : Low energy muons are well recognized and the corresponding track in the module can be reconstructed. It exhibits the typical Landau distribution with a most probable value of energy loss in TMS of 15 MeV per module, i.e. 1.80 MeV/gcm^{-2}. This figure coincides well with 1.78 MeV/gcm^{-2}, calculated with the Bethe-Bloch formula for 1 GeV muons, and demonstrates that the ionization chambers are calibrated correctly.

An example of radiating muons are shown in a Legoplot representation in Fig. 1 . The vertical scale gives the energy deposited in the corresponding channels of the modules. In a) a muon with one quantum and in b) with two quanta are shown.
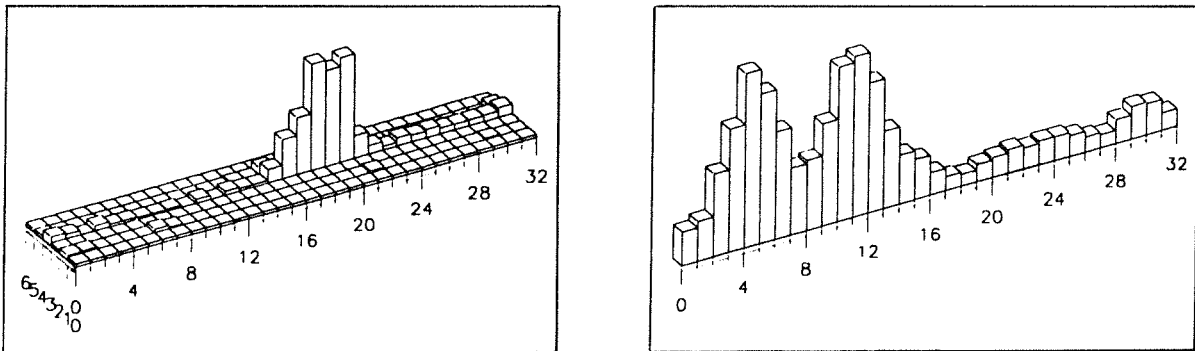
Fig. 1   Two examples of radiating muons.

In a first step of the analysis only the total amount of radiation energy is used and supplementary information, e.g. the number of quanta, is neglected. For this case, the acceptance of the trigger counters and the road conditions were calculated using the program code GEANT [1].

As a result the spectrum for primary muon energies is shown in Fig. 2, compared with measurements of Allkofer et al. [2] . One observes, that up to about
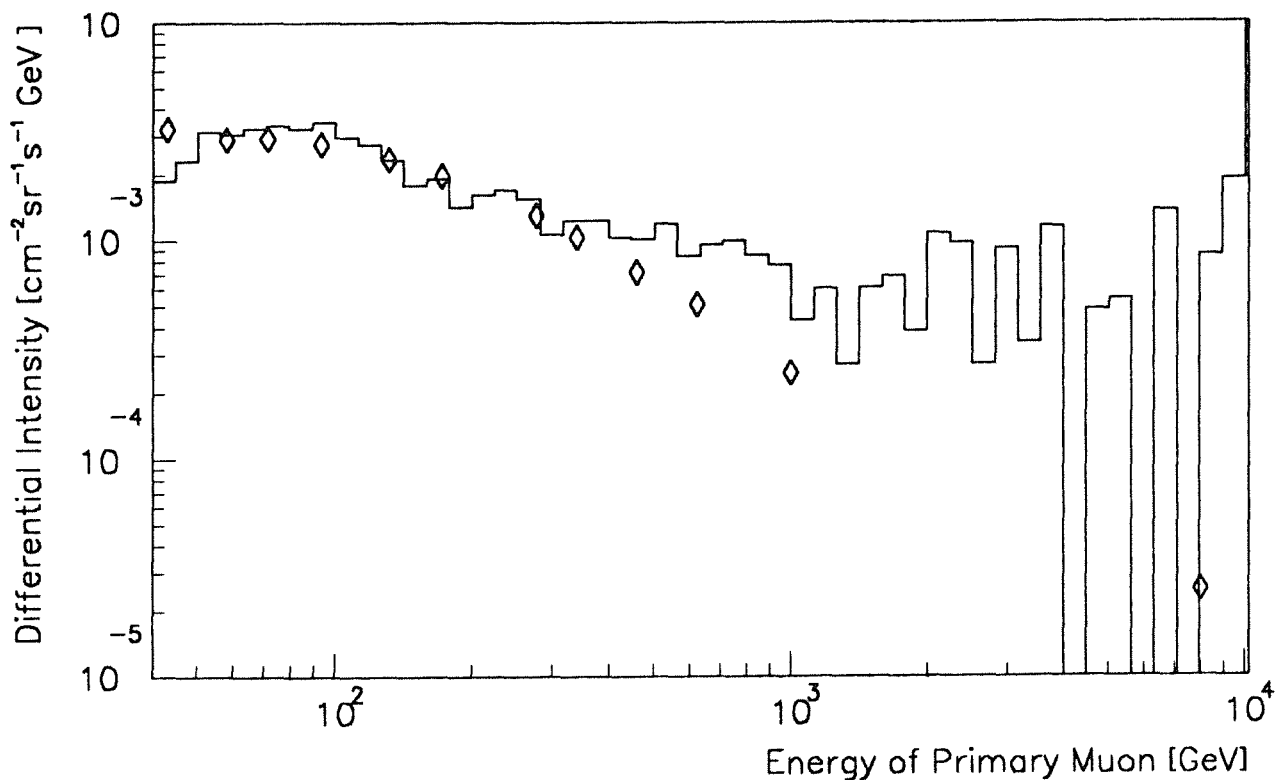
Fig. 2   Flux of horizontal muons at sea level at a zenith angle of 75°-90°.
          The rhombic signs represent data of ref. 2 .

1 TeV the data agree rather well with the flux of ref. 2. At higher energies in the TeV range, however, a too large flux of muons is obtained. The reason is obvious, and is owing to bremsstrahlung losses which are indistinguishable from direct pair production in conjunction with the steep muon energy spectrum. Low energy muons having lost a hard quantum of bremsstrahlung are recognized as a high energy muon. Inspite of the fact that this is a rare process, the large number of low energy muons spoils the spectrum at high energies.

In two directions an improvement of the measurements and the analysis are possible. Either more amount of radiating material can be used in order to improve the statistic or an additional variable should be measured. In the first case a more detailed analysis would be possible using also the number of emitted quanta as a constraint. As a second variable the ionization loss and its relativistic rise will give an additional information for low energy muons to reject events with bremsstrahlung.

A large ionization chamber without radiator and only measuring dE/dx is in preparation, and will be available in the near future.

[1]   R.Brun et al., GEANT user manual , CERN, DD/EE/84-1 (1987)
[2]   O.C.Allkofer and P,K,F:Grieder, Physik Daten, Vol.25-1 (1984)

5.2. INSTRUMENTATION

5.2.1. OPTICAL PROPERTIES OF LIQUID SCINTILLATORS

K.EITEL, H.GEMMEKE, R.MASCHUW, J.RAPP, F.K.SCHMIDT, J.WOLF

Optimization of large volume liquid scintillation counters like KARMEN requires precise knowledge of the absolute light output and the physical attenuation length of the scintillator and its components. For this purpose a two beam laser photometer was developed to measure the geometrically independent spectral attenuation length Λ of liquids defined by Beer's law of light attenuation (eq. 1).

$$I(x,\lambda) = I_0(\lambda) \cdot exp(-x/\Lambda(\lambda)) \qquad (1)$$

A scintillator chamber with a 100 cm^3 sample cell mounted on a "Valvo XP 3462" photomultiplier was used to determine the light output of scintillator cocktails in terms of photons per keV deposited energy. The sample size had to be kept small to minimize the effects of light attenuation.

The laser photometer in its two arms compares the loss of intensity in two cuvettes of different lengths. The ratio of these intensities used to calculate the attenuation length can be determined with a precision better than $3 \cdot 10^{-3}$. For cuvettes lengths of up to 1.5 m this methode enables the measurement of attenuation lengths of the order of 50 m with a precision of better than 10%.

The light source of the photometer is a pulsed tunable dye laser pumped by a nitrogen laser. It provides monochromatic light with adjustable wavelengths from 400 nm to 700 nm and bandwidth of 0.3 nm.

Using this photometer we investigated mineral oil based scintillators and their components (paraffins and aromates). Fig. 1 shows the spectra of attenuation of benzene and its methylated derivatives toluene, xylene and pseudocumene. These derivatives are widely used as solvents for scintillator cocktails.

Benzene and its derivatives differ in the number of CH- and CH_3- groups. The structure of the shown spectra is dominated by the absorption bands of these groups described by local mode theory of vibration [2]. Hence the dip at 635 nm corresponds to the 6th overtone on the CH_3 vibrational mode. The attenuation decreases with increasing number of this group and disappears in benzene. The
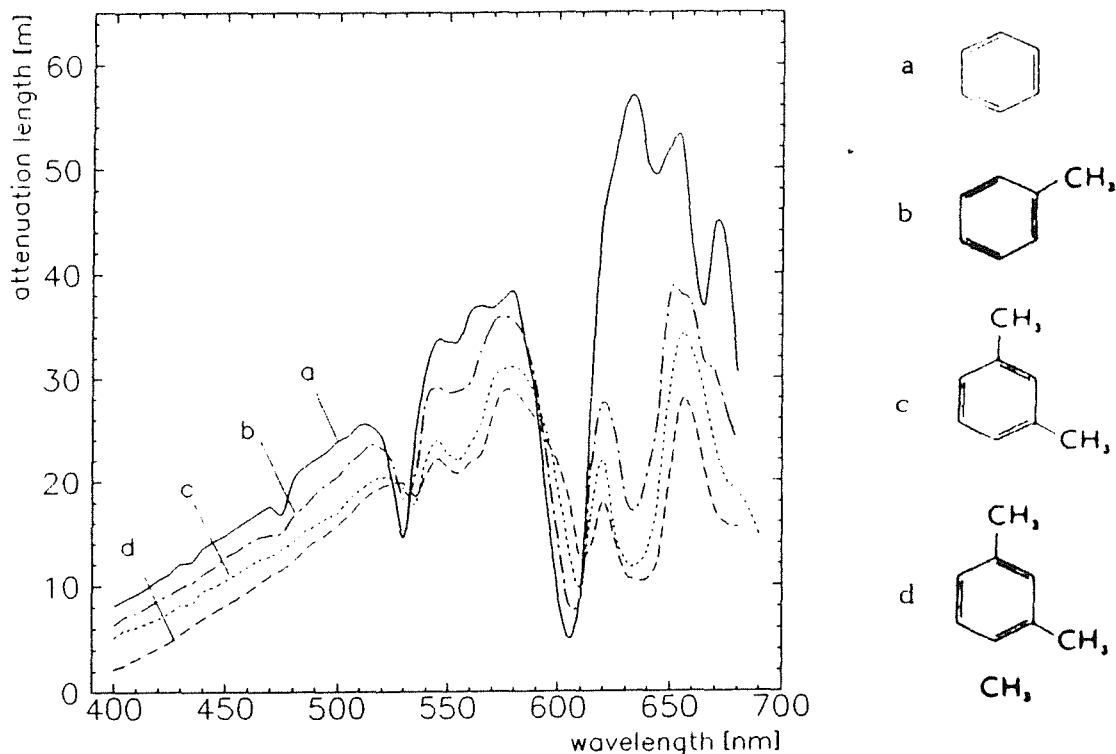
Fig. 1   Attenuation length of a) benzene, b) toluene, c) xylene,
          d) pseudocumene

dips at 607 nm, 532 nm and 475 nm are related to the 6th, 7th and 8th overtone of the local vibration of a CH-group [3] .

The attenuation spectra of mineral oils (paraffins) are shown in Fig. 2. The attenuation lengths of oils depend significantly on the purity of the samples, but also on the different charges of the same paraffin oil. The structure of the spectra in Fig. 2 can be explained in the same way as for the aromates using the vibrational local modes of CH_2- and CH_3- groups respectively [1] .

The scintillator applied in the KARMEN detector is a mixture of mineral oil, pseudocumene and PMP (1-phenyl-3-mesityl-2-pyrazoline). The attenuation spectra of two mixtures (75% paraffin of low viscosity and 25% pseudocumene; same with 2 g/l PMP added) and their components are plotted in Fig. 3 .The asterisks represent the calculated values of the attenuation length Λ for the mixture using equation (2) resulting from Lambert-Beer's law. The validity of this law is proved in the range from 400 nm to 700 nm by comparison of measured cocktails with calculated sums of pure constituents.

$$\frac{1}{\Lambda} = \sum_i \frac{c_i}{\Lambda_i} \quad ; \quad \sum_i c_i = 1 \tag{2}$$

c_i : concentration of the i-th component of the mixture.

Λ_i : attenuation length of the components
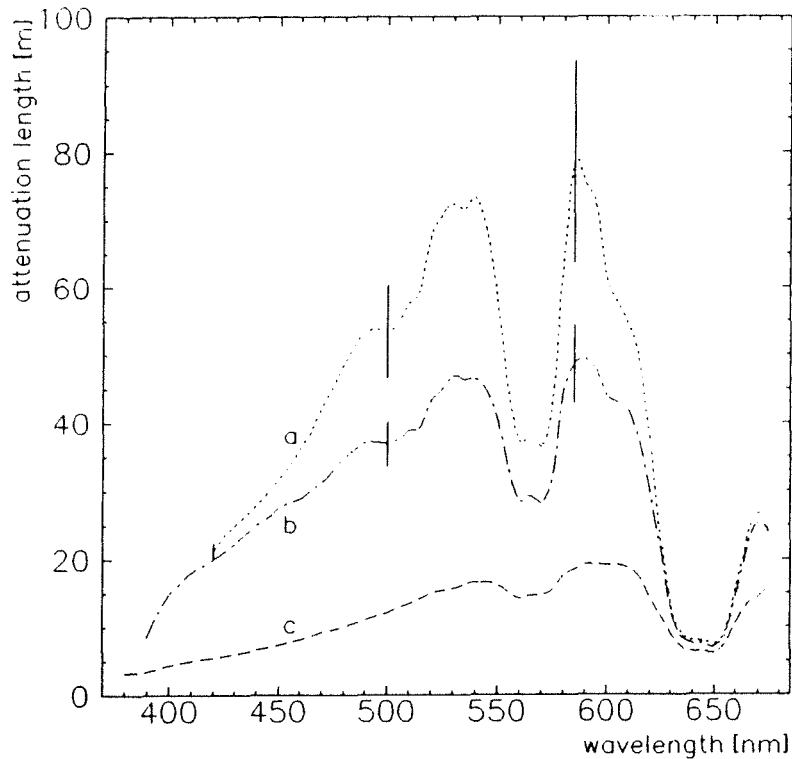
Fig. 2   Attenuation length of various paraffins. a) UVASOL, b) low viscosity oil, c) high viscosity oil.

The light output yields are measured with a photomultiplier tube (PMT) coupled to high-grade steel cuvette. Using the Compton edges of a ^{22}Na spectrum for energy calibration the light output (ADC-channels/keV) was measured depending on the variable height of the sample cuvette. The influence of attenuation was canceled by extrapolating the obtained data to the height of zero.

The light output in terms of photoelectrons/keV is deduced by using a LED (light emitting diode) calibration. The measured LED-resolution connects the amplitude of the LED with the number of photoelectrons detected in the PMT. The geometry of the cuvette, light collection and attenuation in the sample and spectral quantum efficiency of the PMT was considered by a light Monte-Carlo simulation to account for all device dependent contributions to the absolute light output.

The tested scintillators are bubbled with argon to exclude effects of oxygen quenching which reduces the light output considerably. Some of the results are listed in Tab. 1.

The obtained data of absolute light output combined with the spectral attenution length can now be used in Monte-Carlo simulations to optimize detector properties like energy, position and time resolution.
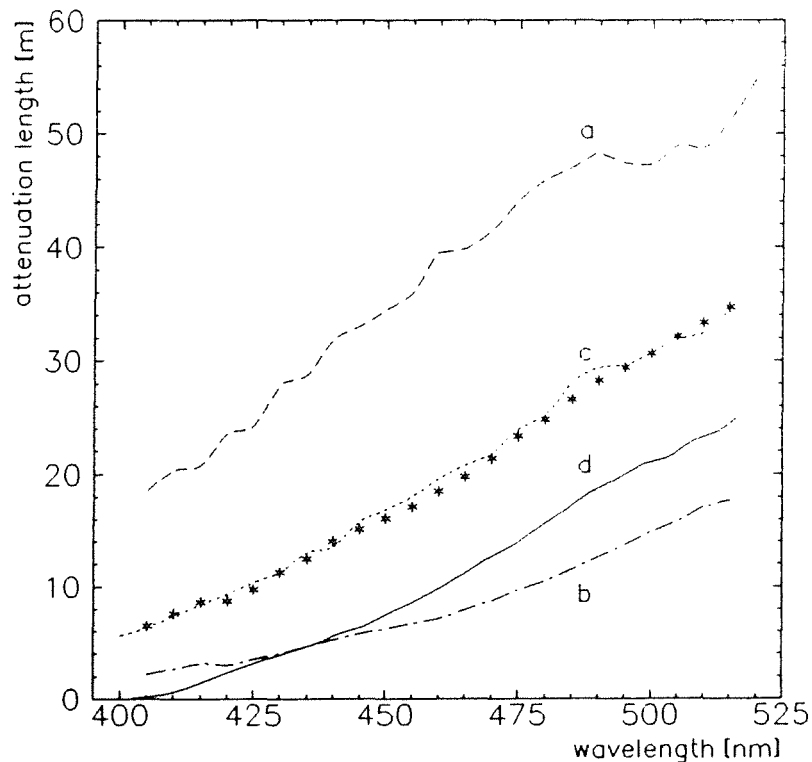
Fig. 3   a) paraffin of low viscosity, b) pseudocumene, c) 75% paraffin and 25% pseudocumene, d) solution c with 2g/l PMP, *) calculated Λ with eq. (2) .

scintillator	photons/keV	anthracene
KARMEN	6.8	46%
NE 235 H	8.1	56 %
NE 235 C	8.7	60 %

Tab. 1   Absolute light output and relative light output related to anthracene measured with ^{22}Na.

[1]   W.R.A.Greenlay et al.; "The discrete excitation of nonequivalent CH oscillators - a local mode analysis of the high energy overtone spectra of the alkanes"; J.Chem. Phys. 69(1), 1. Jul. 1978

[2]   B.R.Henry ; "Use of local modes in the description of highly vibrationally excited molecules"; Accounts of Chem. Research, Vol 10, 1977

[3]   C.K.N.Patel et al. ; "High overtones of C-H stretch in liquid benzene measured by laser optoacoustic spectroscopy"; J.Chem.Phys. 71(3), 1.Aug. 1979

5.2.2. DESIGN OF COUPLINGS FOR SPECIAL FIBER OPTIC CABLES

H.HUCKER

For the calibration of the photo multiplier tubes in the open we need 20 optical fibers 40 meters each. These cables have to be very resistant against all outdoor conditions. i.e. animal bites, water, kevla pulling protection etc. Light guide cables for these conditions were easily available but not the special rough connectors for them. They had to be designed by us.

Mechanical design of the light guide cable connector :

The light guide cable, which is in a brass protective cover, has a standard FSMA-connector. The gap between the brass cover and the light guide cable is filled with a special resin. It protects the cable against moisture and also makes it more resistant against tensile stress. The standard FSMA-connector, which is outside the brass cover, is protected against moisture and dirt by a cap.

Light guide cable connector
(for rough handling)
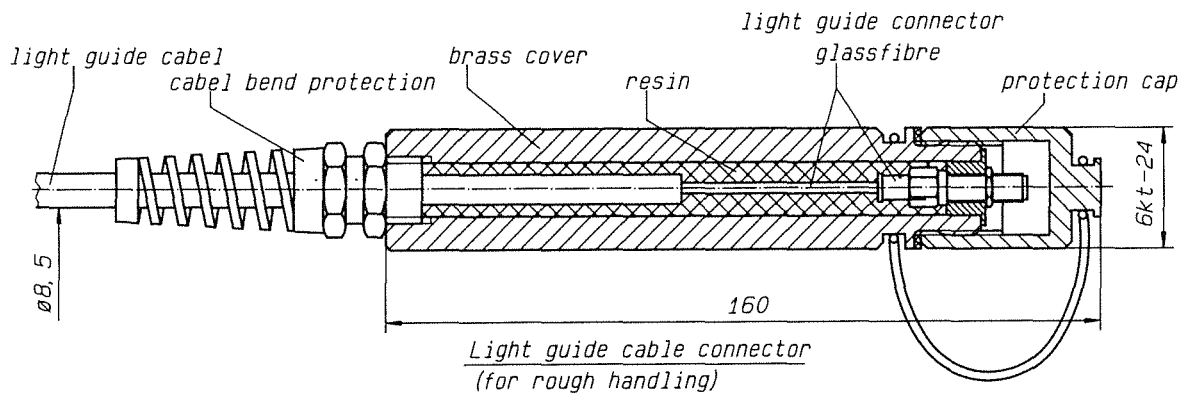
5.3. ACCELERATORS

5.3.1. OPERATION OF THE KARLSRUHE ISOCHRONOUS CYCLOTRON (KIZ)

F. SCHULZ, H. SCHWEICKERT

During the period of report the isochronous cyclotron KIZ was in full operation (Tables 1 and 2). The 5364 h of beam time for experiments in a year where a 6 week shut down period for servicing and improvements was needed, is a very good value. However, even with the almost round-the-clock operation we could not fulfill all the beam time requirements. This situation is expected to change in 1991 when the nuclear physics activities are planned to be drastically reduced. This tendency can be clearly seen in Table 2. For the first time in 25 years the machine was not mainly used for nuclear physics.

Cyclotron Operational	With Internal Ion Source		With external Ion Sources		Total	
For Experiments	4093 h	57.8 %	1276 h	18.0 %	5369 h	75.9 %
Beam Development, Testing new Components, Developments for Isotope Production	663 h	9.4 %	50 h	0.7 %	773 h	10.1 %
Total Time of Operation with the Beam on Targets	4756 h	67.2 %	1326 h	18.7 %	6082 h	86.0 %
Scheduled shut-down for Maintenance, Repair and Installation	378 h	5.3 %	35 h	0.5 %	413 h	5.8 %
Unscheduled Shut-down	455 h	6.4 %	125 h	1.8 %	581 h	8.2 %
Total Shift Time	5589 h	79.0 %	1486 h	21.0 %	7076 h	100.0 %

*Polarized Deuterons 351.5 h; $^6Li^{3+}$-Ions (156 MeV) 351.5 h

Tab. 1   Beam statistics of KIZ from January to December 1990

Pie chart segments:
- Machine Development 12 %
- Others 3 %
- Nuclear Reactions 26 %
- Engineering 10 %
- Solid State Physics 14 %
- Material Research 35 %
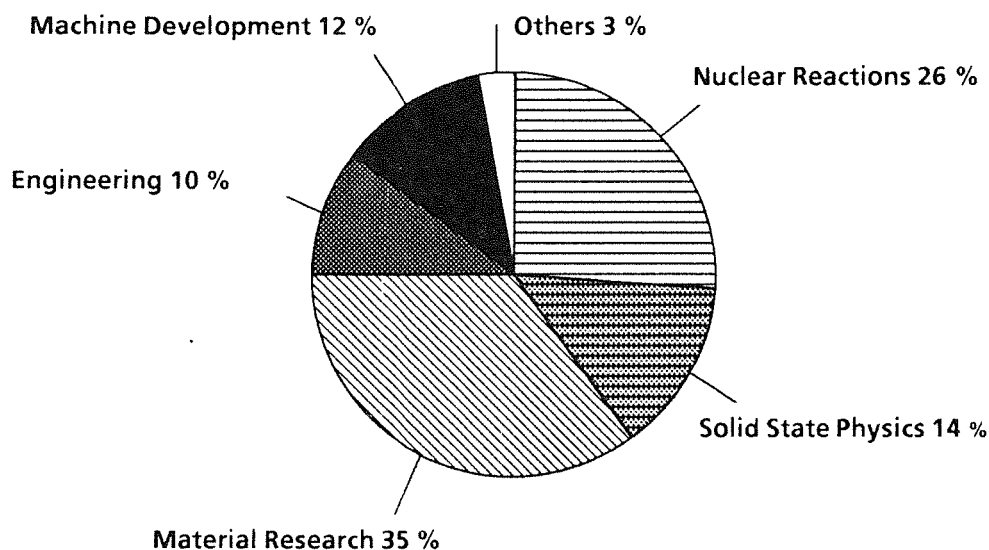
Internal Users

Institut für Kernphysik III	1089.25 h	20.31 %
Institut für Materialforsch. u. Festkörperphysik II	1084.00 h	20.21 %
Institut für Materialforsch. u. Festkörperphysik I	1013.92 h	18.90 %
Institut für Neutronenphys. u. Reaktortechnik	34.58 h	0.64 %
Institut für Radiochemie	11.33 h	0.21 %
	3233.08 h	60.27 %

External Users

Universität Erlangen	993.08 h	18.51 %
Technische Universität München	799.00 h	14.90 %
Universität Tübingen	237.50 h	4.43 %
Universität Münster	64.42 h	1.20 %
Universität	29.17 h	0.54 %
Universität Stuttgart	4.50 h	0.08 %
Universität Hamburg	3.17 h	0.06 %
Universität Heidelberg	3.08 h	0.06 %
Hahn-Meitner-Institut Berlin	0.83 h	0.02 %
Universität Bonn	0.75 h	0.01 %
Universität Frankfurt	5.25 h	0.10 %
Total Extern	2135.50 h	39.81 %
Total	5364.08 h	100.00 %

Tab. 2 Use and users of KIZ from January to December 1990

5.3.2. OPERATION OF THE COMPACT CYCLOTRON (KAZ)

J. MÖLLENBECK, H. SCHWEICKERT

During the period of report the cyclotron was operated successfully for isotope production and irradiation of machine parts, as well as for basic research. The 4000 h of beamtime was distributed equally among these activities. The machine
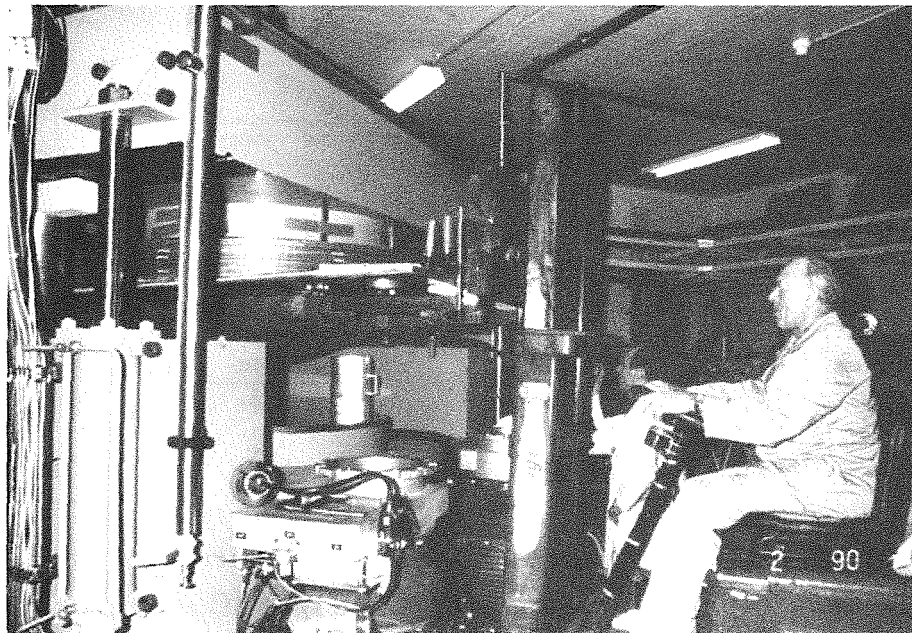
Fig. 1   In order to replace the main coil of the compact cylotron the machine had to be completely dismantled.

is only booked for about 60 % of the maximum available time. The reliability of the machine was again excellent.Because of a short-circuit in spring 1990 the main coil of the CP42H⁻ had to be exchanged. Fortunately we have had a spare coil and therefore the repair could be done in the very short time of only one weak. Fig. 1 gives you an impression of this activity.

5.3.3. TEST AND OPERATION OF THE CYCLOTRON POLARIZED ION SOURCE PLASMA WITH AN ECR-IONIZER

L. FRIEDRICH, E. HUTTEL, J. KALTENBAECK

In March 90 the last nuclear physics experiment with a polarized deuteron beam was carried out at the Karlsruhe cyclotron. For this last beam time with PASKA the conventional EB-ionizer was replaced by the ECR-ionizer shown in Fig. 1.
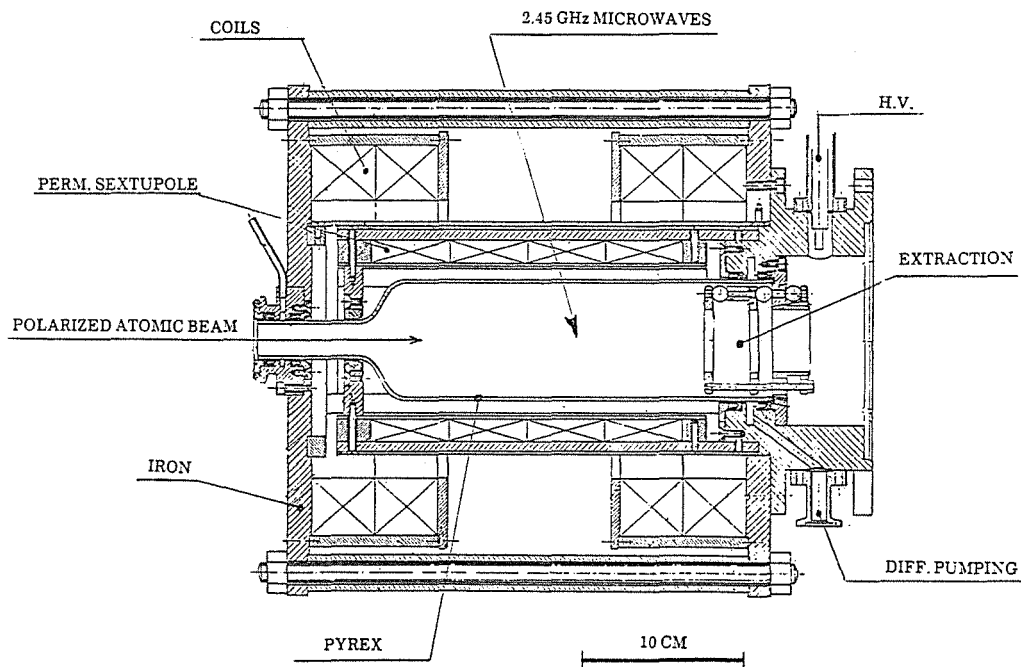
Fig. 1   Schematic of the ECR-ionizer

In a previous test phase one year ago a poor polarization of $P_3 = 0.32$ was achieved, measured from the assymmetry of the C(d,d)C elastic scattering. This has to be compared with a value of $P_3 = 0.55$ achieved with the conventional EB-Ionizer.

The polarization could be increased in two steps. An improved stabilization of the microwave power resulted in a polarization of $P_3 = 0.38$. The enlargement of the diameter of the extraction system from 40 to 50 mm resulted in $P_3 = 0.47$ which represents quite well the present state of the development. Obiously the large diameter enables a more efficient pumping of the D_2 molecular background, which is a source of unpolarized D^+ ions. This unpolarized background is much higher for an ECR ionizer than for a conventional EB Ionizer. The accelerated beam delivered by the EB ionizer is reduced to less than 1 % when the sextupoles are switched off, where as with an ECR ionizer 20 % of the beam have still been observed.

In order to stabilize the ECR discharge He was used as buffer gas. Thus only about 30 % of the total ionizer current had been D^+ ions. Because of this high background current the pure electrostatic beam transport into the cyclotron works unefficient due to space charge effects. A gain of intensity of the accelerated beam could be achieved by preselecting the deuteron beam using a (magnetic) solenoid lens following the ECR ionizer. From 165 µA D^+ focussed into the transport system 2.5 µA have been accelerated up to full energy. This has to be compared to 1-2 µA which was achieved with the EB ionizer.

In contrary to the EB ionizer the efficiency of an ECR ionizer increases with the intensity of the atomic beam (see Fig. 2) since the atomic beam itself and not a
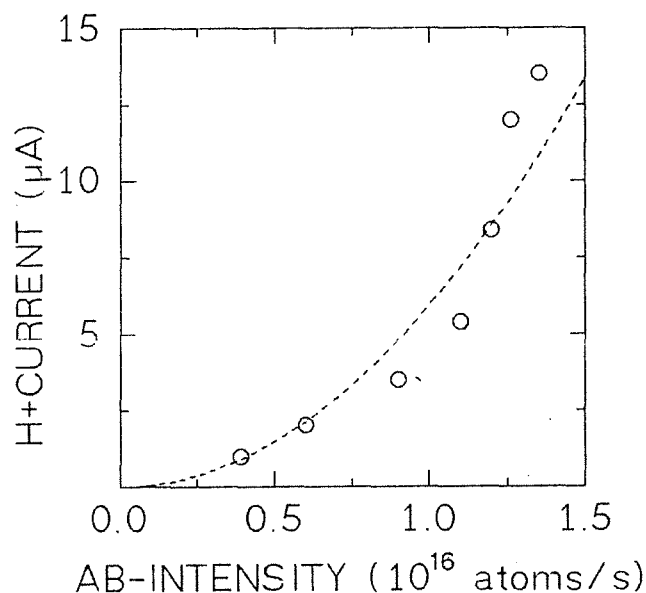
Fig. 2   The dependance of the H^+ current from the A.B.-intensity shows that efficiency of the ECR-ionizer increases with the A.B. intensity

filament delivers the major part of the electrons for the discharge. Therefore the benefit of an ECRionizer would be much larger if it will be combined with a well optimized 30 K atomic beam source and a vacuum configuration which minimizes the background.

5.3.4. DESIGN AND TEST OF A 30 K POLARIZED ATOMIC BEAM SOURCE

H.P.EHRET, L.FRIEDRICH, E.HUTTEL, J.KALTENBÄCK, L.WISS, P.ZIEGLER

At KfK a 30 K cold polarized atomic beam source has been developed under contract for a commercial manufacturer. *) The source is now delivered to the first customer.**)

The polarized atomic beam source is shown in Fig. 1. The horizontale design ensures most comfortable accessibility. Hydrogen molecules are dissociated by
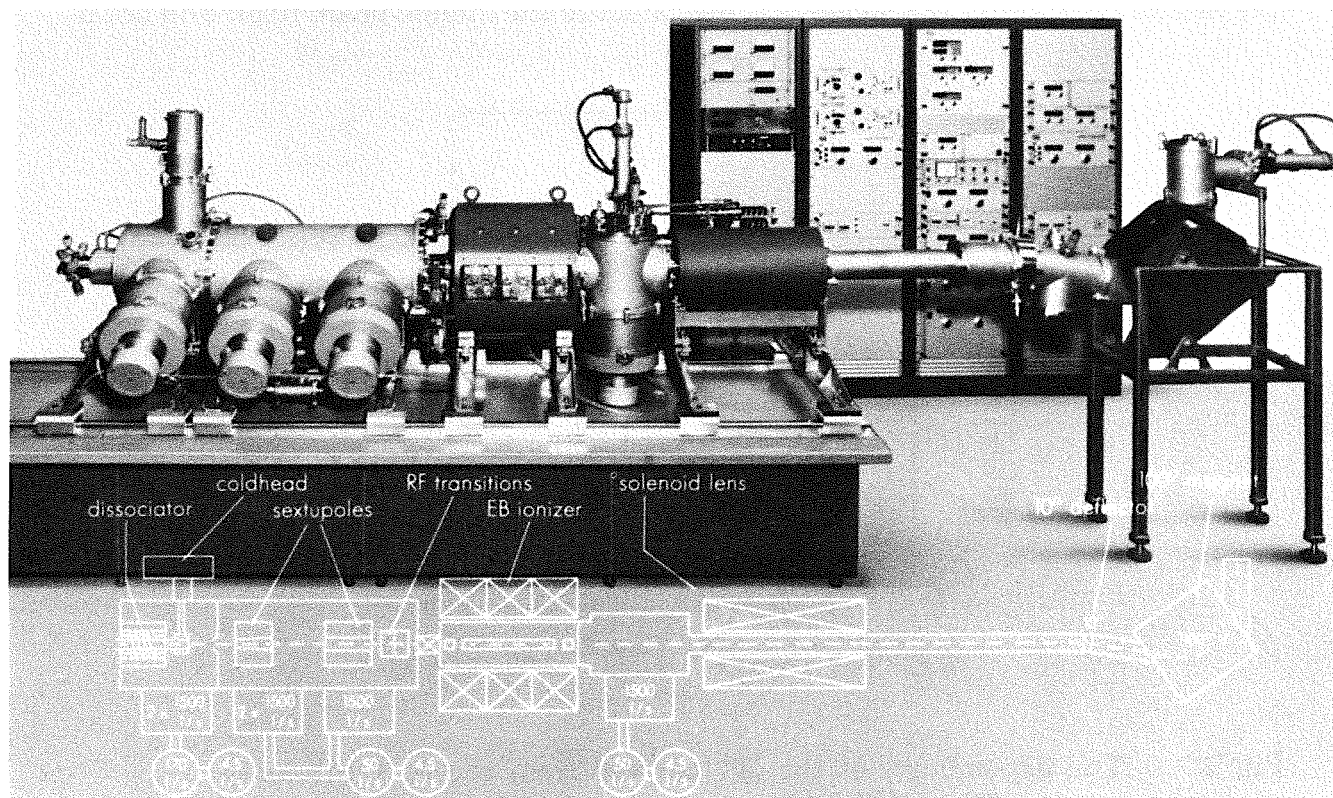
Fig. 1 Polarized atomic beam source designed at KfK and manufactured by NTG

means of an RF induced discharge. The atoms then pass through a nozzle which is cooled to 30 K by an He refrigerator. A suitable atomic beam is peeled out by a skimmer from the atomic flow leaving the nozzle. Two sextupoles are used for focusing and selecting the $m_j = 1/2$ components. The first sextupole is positioned 20 mm behind the skimmer orifice; it is tapered from 12.5 mm diameter at the entrance to 25 mm diameter at the exit. The second sextupole follows 300 mm after the first one and has a constant diameter of 28.5 mm. The pole tips of both sextupoles are made of cobalt iron up to a radius of 40 mm.

The electron polarization is transferred to the nucleus by means of RF transitions. The electron ionizer is of ANAC-CERN design. A solenoid lens, a -10° electrostatic deflector and a 100° magnet deliver a mass selected vertical beam with longitudinal polarization for injection into the cyclotron. While the electrostatic deflector leaves the direction of the spin uneffected, the 100° magnet rotates the proton spin by 86° and the deuteron spin by 279°. Thus the beam remains longitudinally polarized after the deflection.
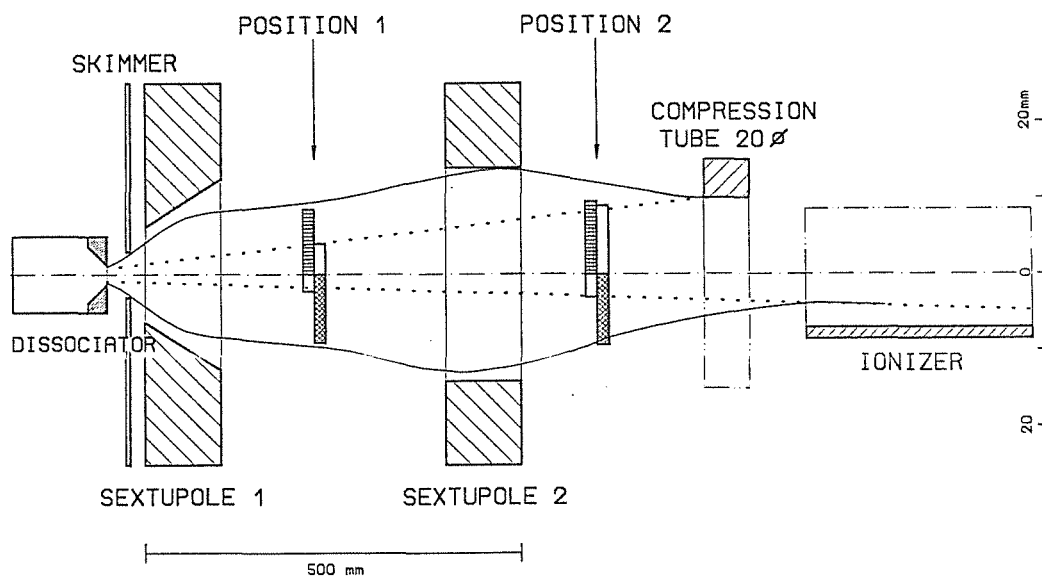
Fig. 2   Geometrical arrangement of the atomic beam profile measurements. There are shown two calculated beam envelopes, the upper for a beam which is accepted by the compression tube, the lower for a beam accepted by the ionizer. Corresponding measurements of the beam radii are given with sextupoles on (shadowed bars) and off (without shadowing).

In order to get some experimental information about the focusing properties of the sextupole magnets, profile measurements of the atomic beam were carried out

after the first and the second sextupole (Fig. 2). From these measurements it could be extracted that the effective ionization column of an EB ionizer is less than 8 mm, furthermore it turned out that the acceptance of the ionizer and not the sextupoles is a limit for the output of a 30 K atomic beam source.

The atomic flux measured at the entrance of the ionizer was about $2x10^{16}$ atoms/sec and typically 50 μA H^+ are obtained after the deflectionmagnet.

5.3.5. INVESTIGATION OF A 2.4 GHz ECR - PLASMA FOR ION ETCHING

M. EICHELBERGER, L. FRIEDRICH, E. HUTTEL, L. WISS

A large volume ECR-plasma source has been built up in cooperation with a commcerial company*) in order to investigate various magnetic field configurations whether they are usefull for plasma etching. The apparatus allows in a simple manner to test radial multipole configurations, longitudinal mirror fields induced by two coils, decreasing magnetic field of one coil and all the possible combinations. The plasma is excited by electron cyclotron resonance with 2.4 GHz. For a first orientation simple measurements of properties of a N_2 plasma were performed.

An experiment to measure the total ion flow to a disc having the diameter of a wafer with several small probes inserted in order to measure the homogenity of the plasma flow, failed. Because of the high energy of the electrons and their complex drift in the magnetic field it was impossible to perform correct measurements of the ion current.

Utilizable results were achieved with a double probe. Series of measurements with the various magnetic configurations showed that a field induced by one coil delivered the maximum ion current. The pressure was $2 \cdot 10^{-4}$ mb and the microwave power 200 W.

An interference method was developed to measure the thickness of the SiO_2 layer. This is derived from the intensity modulation of a Laser beam reflected by the SiO_2 coated wafer. The measurement of etching rates and their homogenity, which require the handling of somewhat toxic gases, are now in preparation.

5.3.6. THE COMPUTER CONTROL OF THE KARLSRUHE ISOCHRONOUS CYCLOTRON

J.BIALY,   H.HEINZMANN,   R.KAPPEL,   W.J.LINNEMANN,
J.W.PETERS, K.SCHLÖSSER, M.SCHMITT

The Dual Beam facility and the expansion of the Isotope Production at the Karlsruhe Compact Cyclotron (KAZ) made it necessary to extend and to modify the beamline computer control. The present beamline computer control of the KAZ is based on the NOVA 4 computer, which is not extendable in software and hardware. Additionally the Dual Beam facility requires simoultaneous operation of KIZ and KAZ.

Therefore the beamline controls need the same hardware and standards.In a first step the man-machine communication of the KIZ and KAZ- beamline control had to be standardized to simplify the operation of both beamline control systems by the operators.

The operation of both computer control systems can be achieved by using touchpanels, turnable incremental knobs and video terminals. All processes including block diagrams of the beamline sections, personal safety systems, beam profile measurements, beam diagnostics, analysis of status and interlock signals for trouble shooting as well as the status information of the lenses and their current values are monitored on several colour displays.

The basic idea of the new designed beamline computer control is to replace the vertical CAMAC highway branch by a so-called Control-LAN, which allows the linkup of a powerfull host- computer, distributed computers, micro-computers controlled process units and the Siemens PLC (Simatic), which communicate with one another by means of ETHERnet. Data transfer, task-to-task communication and program transfer between different computers are carried out by a single coaxial cable (Ethernet-LAN). This Control-LAN is decoupled from the main KfK- and the Cyclotron-LAN to prevent interferences, which might disturb the process control.

A micro-VAX II and a VAX-11/750 are used as host computers for software development and management. Both computers play a very important role as central data storage and back-up computers. They offer the possibility of storage and management of all stand-alone programs of the Starburst computers, which are running under the operating system RSX-11/S without any disk storage system. The programs are loaded via the Control-LAN. Each CAMAC-Crate is controlled by such a Starburst computer, which is based on the DEC J11 micro-
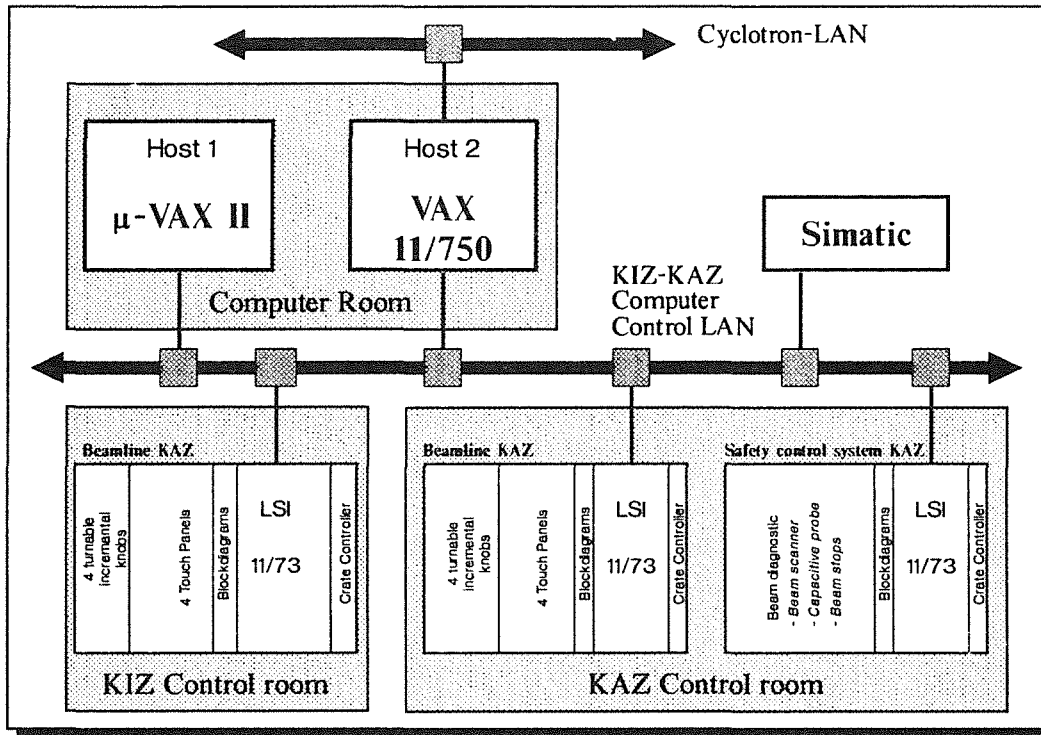
Fig. 1   The hardware of the KAZ beamline computer control.

processor and operates under real-time conditions. They are used for all process control tasks. The magnet power supplies are controlled via special Bruker microprocessors connected directly via terminal-servers to the Control-LAN. The Interlock system of the beamline components and the safety control system are carried out by the Simatic, which can be operated directly via the Control-LAN from each Starburst controlled operator's console.

The process software runs under the VMS and RSX-11/S multi-tasking operating system.The multi-tasking capability allows to create a modular-structured software, which simplifies maintenance and future upgrades of the software. The KIZ control system is already running successfully. This control system will be extended by the part of the KAZ control system at the end of the year 91 under the very hard conditions, which will not allow to switch off the KAZ for a longer time than one week over Christmas.

5.3.7.A   AN ECR SOURCE FOR Li^{3+} IONS [1]

R.ERNST, L.FRIEDRICH, E.HUTTEL, F.SCHULZ

A two-stage ECR ion source for Li^{3+} ions has been built for the Karlsruhe cyclotron. The $2\omega_{CE}$ mode is used in the first stage. In order to obtain the optimum Li vapor pressure the complete plasma chamber is heated to about 400°C. Microwaves of 7.5 GHz frequency and 100 W power are used. The source currently delivers 60 eµA Li^{3+} of which up to 5 eµA are accelerated to 156 MeV.

[1]   published in : Nucl. Instr. and Meth., **A287**, 337 (1990)

5.4.   APPLICATIONS

5.4.1.   NUCLEAR MEDICINE WITH SIMPLE DEVICES

J.BIALY, J.W.PETERS, M.SCHMITT

Throughout the last years the ENGYPAN system has been designed as a gamma measuring device, specially adapted to the requirements of mobile function diagnostic methods in nuclear medicine. In consists of a measuring interface capable of operating up to six single probe detectors simulaniously, which is coupled to a portable microcomputer. The development of ENGYPAN was continued. Mainly the operation of the CsJ-scintillation detectors has been improved. Additionally first tests to adapt CdTe semiconducter probes were carried out. Also further refinements on the general analyzing software were made to provide our clinical partners with tools for special application development.

The clinical tests of the CsJ detectors could be started. First results show good agreement of renal glant clearance values obtained with the ENGYPAN to those with common gamma camera techniques. But still some further efforts are necessary as well to improve reliability and sensitivity of the measuring probes as to better adapt the software to the clinicians' needs.

Additionally to the studies carried out in German hospitals, there will be also clinical studies in some North American hospitals. This is important to meet the dedicated requirements of American nuclear physicians.

Since the major development of the ENGYPAN system has been successfully finished, contacts to different firms have been established to take over routine production, marketing and service of the system on a commercial basis.

5.4.2.   PRODUCTION OF ISOTOPES FOR MEDICAL APPLICATIONS

K.H.ASSMUS, V.BECHTOLD, H.D.DENNERLEIN, H.DOHRMANN, S.DOSENBACH, E.ERBE, E.FOßHAG, K.GEHRLEIN, R.HÜFNER, N.KERNERT, J.KRAFT, W.MAIER, H.RIPP, U.SAHM, S.UHLE-MANN, J.WENDEL

At the Karlsruhe Compact Cyclotron several radioisotopes for medical applications are routinely produced. Pharmaceutical compagnies and research hospitals in Germany, France, Switzerland, Italy and England are the main customers. The status of the various products is as follows:

Ultra pure I-123 : During the last year the production was operating without unscheduled shut-downs. The chemistry was working perfectly and the quality could always meet our guaranteed specifications. The production of I-123 could be increased significantly. In June a back-up delivery for the Paul-Scherrer Institute (PSI) in Switzerland was performed.
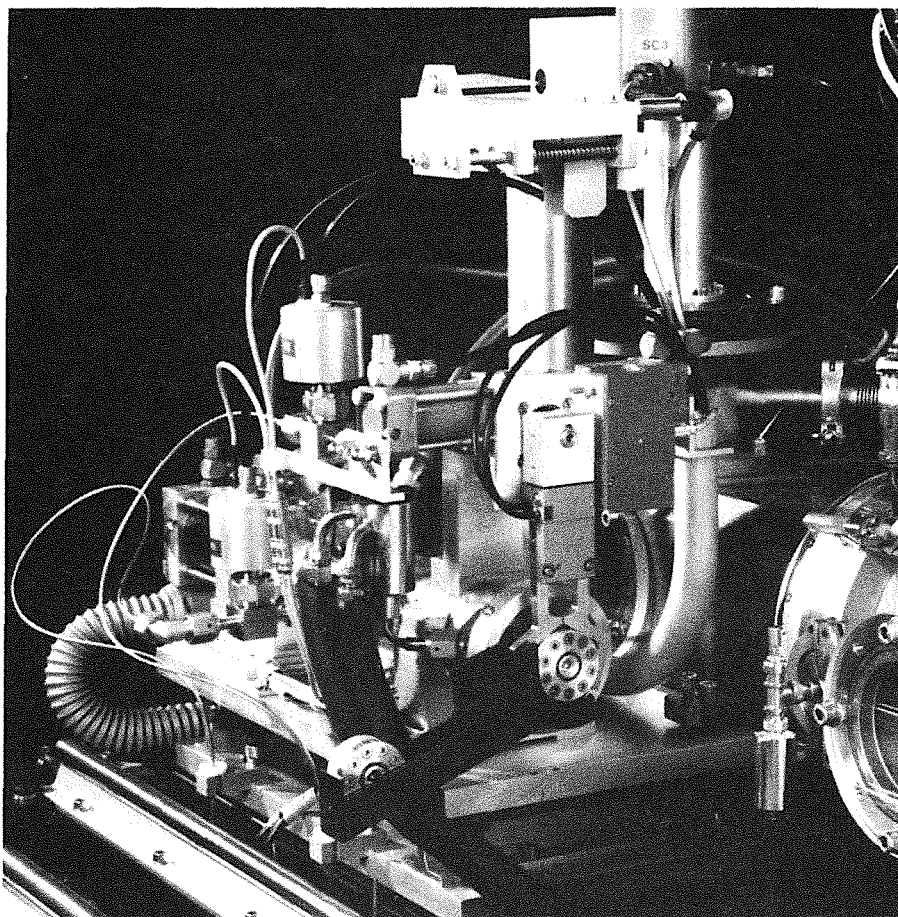
Fig. 1   The new gas target for I-123. The target chamber with a concial inner bore contributed to a 30 % increase of yield. In front of the target the window changing mechanism is shown, which can be remotely operated in case of target window failure, during routine production

Beginning of june a second iodine target was built-up and set successfully into operation. Fig. 1 shows the new gas target. Having now two identical targets this contributes to
- a larger production capacity
- a further increase in reliability of the iodine deliveries
- a reduction of radiation dose given to the operators

Negotiations are under way to settle a longterm contract with several pharmaceutical companies concerning the delivery of iodine-based pharmaceuticals. For this reason a new hot cell for a fully automized production process has been designed and will be constructed. First tests are scheduled for autum 1991.

Rb 81/Kr 81m generators : The number of generators being produced has been almost unchanged compared to last year. These generators are used for lung ventilation studies in hospitals. The new target station, which is almost identical to the KIPROS target for I-123, was successfully set into operation in October 1989. This resulted in an increase of productivity by a factor of 3.

Since the east german market is now open a new marketing effort has been started to introduce the KfK generators also to the hospitals in the eastern part of germany.

Ultra pure Rb-81 : Twice a week small amounts of the rubidium produced for the generators are delivered to the mass separator facility to produce ultra pure Rb-81 in a Rb-chloride solution for injection. This isotope is used for myocardial imaging and blood flow measurements in two research hospitals. The TT-supported project will be finished at the end of 1991.

New developments : The need for a centralized production of F-18 based radiopharmaceuticals is obious since a number of hospitals are getting or planning PET installations (Proton-Emission-Tomograph) without a cyclotron on side. They have asked KfK to deliver F-18 labelled products.

For the F-18 production an experimental target has been built and test irradiations are under way. The chemistry for labelling F-18 with Deoxyglucose is in a conceptial phase. It is planned to start a TT-project beginning of 1991 for the evaluation of a large scale production of F-18-Deoxyglucose (FDG). This FDG will be delivered as a radiopharmaceutical to hospitals around KfK to study mainly metabolism in the heart and the brain.

Because of a better availability of beam time at the KIZ Cyclotron in the future there are plans to use this machine also for the development of new radioisotopes and as a back-up for the routine isotope production.

5.4.3. RADIONUCLIDE TECHNIQUE FOR MECHANICAL ENGINEERING (RTM)

R.BLANKl, P.FEHSENFELD, B.GEGENHEIMER, H.IMMLER, P.HERRMANN, A.KLEINRAHM, R.KUBAT, H.ROTH, B.SCHÜSSLER

The activation service supplying thin layer activated machine components to industry and research institutes is following its postive tendency. The interest in the on-line wear and corrosion measurement technique, as developed at KfK, is worldwide increasing. A licence and know-how transfer agreement for application of the KfK activation and measurement technique in Japan has been stipulated with the renowned company Sumitomo Heavy Industries. The work fulfilling this contract has been started.

The National Institute For Petroleum And Energy Research of the USA has accepted the KfK technology for fundamental research in wear and lubrication. This new user is important for further propagation of the technology in the United States.

The developments of RTM have mainly concerned

A)   the irradiation equipment
      Construction and setting into operation of six advanced apparatuses for linear and spiral movement of the componentens in the cyclotron beam,installation of computer controlled angular adjusting and moving device.

B)   thin layer activation of ceramic materials.
      The damaging effects on ceramics from charged particle irradiation have been investigated in an extensive test program (limits of irradiation doses, recovering processes, influences of temperature and incident angle, etc.) for the most essential engineering ceramics Aluminium Oxide, Silicon Carbide, Silicon Nitride.

The results of the successfull investigations have been demonstrated in thin layer activation of ceramic engine parts as illustrated in the figures 1 and 2 below.
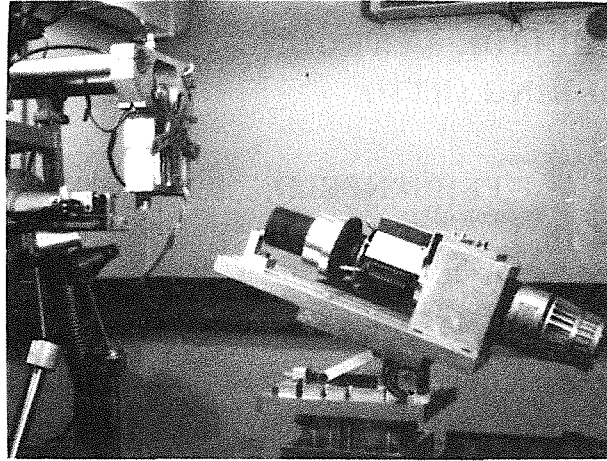
Fig. 1   The cylinder liner (center of the picture) of a ceramic combustion engine in irradiation position in front of the head of beam line (left on the picture) from the cyclotron. The ceramic liner (SiSiC) is adjusted on a rotary apparatus for homogeneous labelling of the inner cylinder wall. A collecting ring system, arranged below the liner fixture, enables temperature measurements of the rotated liner during irradiation.
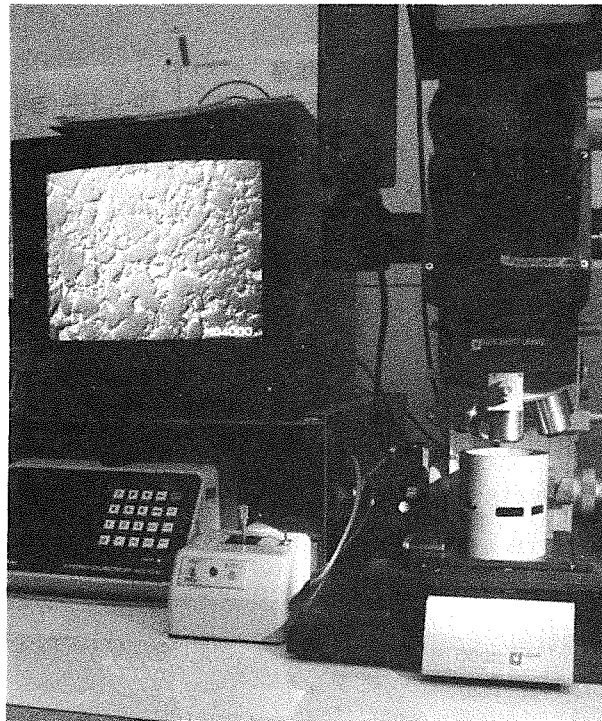
Fig. 2   The firgure is demonstrating the structure examination of the activated zone on the cylinder liner (right side of the fig.). The structure is illustrated on the screen (top, left).

5.4.4.   A COMPACT K-EDGE DENSITOMETER FOR URANIUM

P.MATUSSEK, I.MICHEL-PIPER, H.OTTMAR

A simplified version of a K-edge densitometer has been developed for use by safeguards inspectors to verify the uranium concentration in U-product solutions from a reprocessing plant. This compact densitometer meets the following design goals:

- To be easily adaptable to existing portable safeguards spectroscopy equipments;
- To keep the required additional hardware, including the radiation sources, at a minimum;
- To reduce the required sample sizes to small volumes;
- To provide simple and reliable operation for field applications;
- To ensure a measurement accuracy of better than 0.5% for counting times $\lesssim 10$ min.

These criteria have been met by realizing a simple measurement approach for K-edge densitometry proposed some time ago [1]. In this approach multi-energy transmission measurements are accomplished by means of a single isotopic source (^{57}Co), which in turn is used to generate additional radiations in the form of K X-rays from a uranium converter foil. In this way 5 different photon energies - 94.6 ($UK_{\alpha2}$), 98.4 ($UK_{\alpha1}$), 111.3($UK_{\beta1,3}$) and the ^{57}Co gamma rays at 122 and 136 keV - are available for transmission measurements below and above the K-absorbtion edge energy of uranium.

A small mechanical assembly containing the ^{57}Co source ($\sim 1\text{-}5 \cdot 10^8$ Bq), the uranium converter foil (~ 0.2 g/cm^2 of depleted uranium), the beam collimators, the cavity for the sample vial and some shielding for the detector has to be plugged onto the cap of standard Ge detector systems to perform the measurements. The analysis requires aliquots of about 2 ml. A dedicated software package running on standard PC-based portable spectroscopy systems provides automated spectrum analysis and evaluation of the uranium concentration.

The performance of the densitometer has been evaluated from measurements on uranium solutions covering a wide range of concentrations. Fig. 1 displays the instrument response for one pair of transmission energies (98.4/122.06 keV), which turns out to be strictly linear up to the highest concentrations occuring in practice. At the concentration levels typically existing in the U-product solutions (~ 300 to 500 g/l) the measurement precision and accuracy is about 0.2% for a counting time of 10 min.
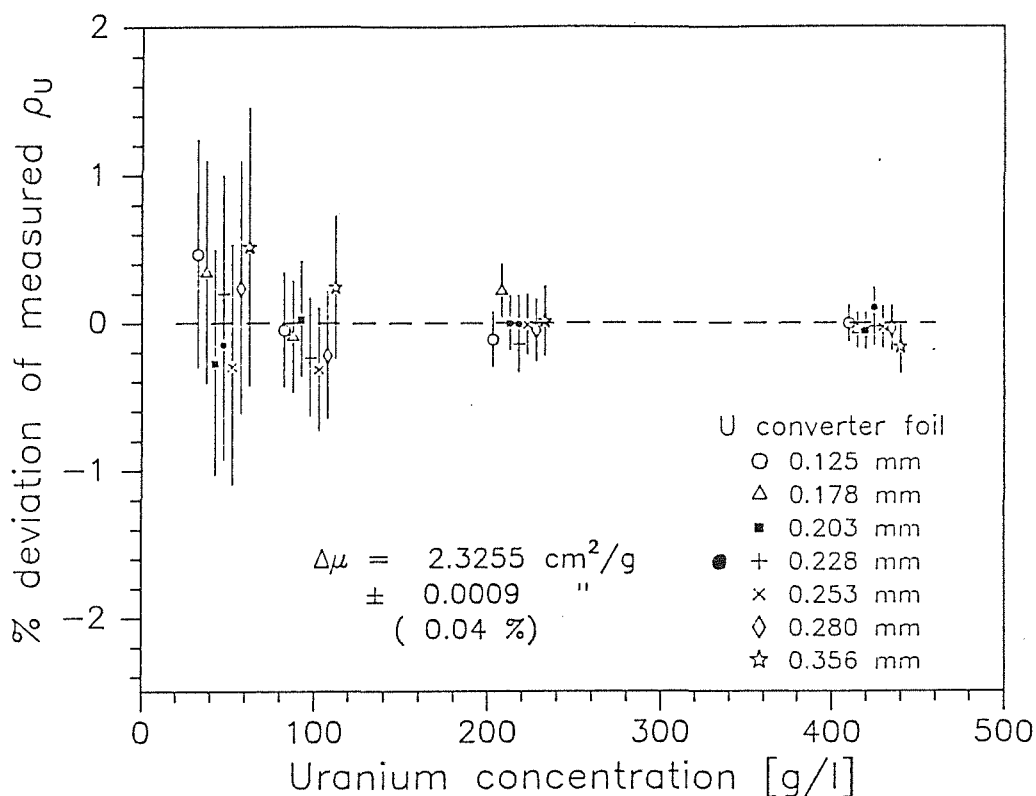
Fig. 1   Percent deviation between measured and declared U-concentration. Measurements performed with different U-converter foil thicknesses. Measurement errors refer to a counting time of 2000s.

[1]   H.Eberle, P.Matussek, H.Ottmar, I.Michel-Piper, M.R.Iyer, P.P.Chakraborty, Nucl. Safeguards Technology 1978, Vol II p. 29, Vienna (1979)

5.4.5.   ON - SITE ANALYSIS OF INPUT SOLUTIONS IN A REPROCESSING PLANT FOR INTERNATIONAL SAFEGUARDS : A PREMIÈRE

H.EBERLE, H.OTTMAR

The safeguarding of nuclear materials by international safeguards authorities (Euratom, IAEA) is based on an independent verification of the declared material balance in individual nuclear facilities. The inspections involve physical

verification measurements on a number of samples withdrawn from the plant. For reasons of timeliness and cost effectiveness, and because of increasing problems encountered in the transport of nuclear materials, the safeguards authorities are aiming at carrying out these measurements directly at the facility as far as possible.

In a reprocessing plant a key verification measurement involves the analysis of the highly radioactive input dissolver solution for its uranium and plutonium content. This difficult analytical determination, usually performed by means of the elaborate technique of Isotope Dilution Mass Spectrometry (IDMS) on samples shipped to remote specialized laboratories, can now be accomplished on site with an alternative measurement technique. The alternative approach of on-site measurements becomes feasible by utilizing a hybrid X-ray spectrometer developed at our laboratory. It combines the techniques of energy-dispersive K-edge densitometry and X-ray fluorescence analysis of K X-rays [1,2].
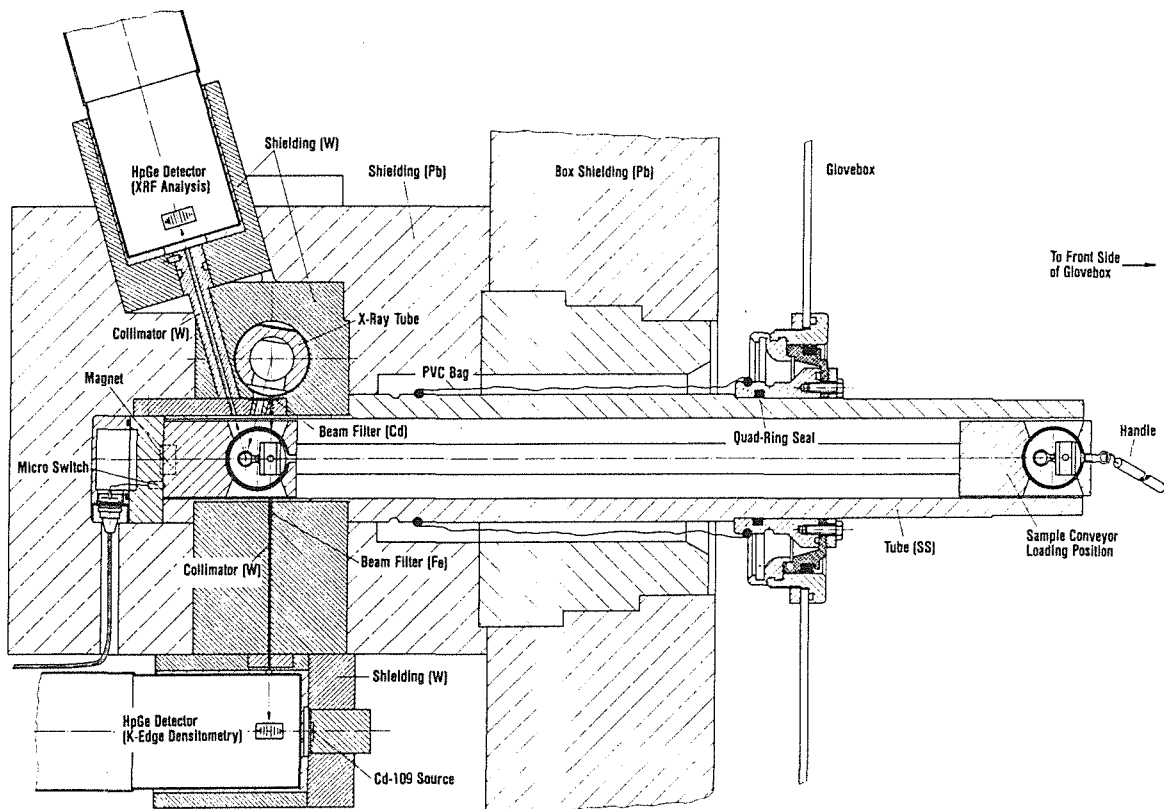
Fig. 1   Layout of the hybrid K-edge / K-XRF instrument installation at UP3

The on-site measurements on input solutions are now practiced for the first time by the Euratom Safeguards Directorate in the new reprocessing plant UP3 at La Hague, France. The layout of the instrument installation at UP3 is shown in

Fig. 1 . The instrument is attached to a shielded cell required for the handling of the highly radioactive dissolver solutions.

The execution of the verification measurements on the input solution proceeds in a fairly simple and straightforward manner, requiring only a few user interactions. A total sample volume of about 2 ml is transferred into 2 seperate vials for K-edge densitometry and XRF. When loaded into the spectrometer the samples are interrogated with suitably filtered X-ray beams from an X-ray tube operated at 150 kV/ 15 mA. The X-ray spectra from the simultaneous K-edge densitometry and XRF measurements are counted with 2 HpGe detectors for about 1 h and directly evaluated for the uranium and plutonium concentration.

The two elements usually occur in dissolver solutions at concentrations of about 200-250 g U/l and 1.5-2.5 g Pu/l. At these levels the measurement accuracy is estimated to 0.3% for uranium and to 0.7% for plutonium. The results obtained during the first months of instrument operation indicated fairly good agreement between predicted and actually achieved performance data.

[1]   H.Ottmar, H.Eberle, P.Matussek, I.Michel-Piper, KfK report 4012 (1986)

[2]   H.Ottmar, H.Eberle, L.Koch, Journal INMM Vol. XV 632 (1986)

5.4.6.   MEASUREMENT OF ACTINIDES IN LIQUID SAMPLES WITH A KED / XRF ANALYZER

H.EBERLE, H.OTTMAR

The KED/XRF analyzer developed for the International Atomic Energy Agency (IAEA) is designated for the measurement of actinides (mainly Th, U, Pu) in liquid samples. The analyzer incorporating the techniques of K-edge densitometry (KED) and K-XRF analysis is installed and operated in the Safeguards Analytical Laboratory of the IAEA in Seibersdorf, Austria [1].

Initial measurements conducted on uranium solutions for instrument calibration revealed an unexpectedly large nonlinearity of the instrument response for KED. The cause has been identified as a result of insufficient beam collimation between sample and detector, which allowed a significant fraction of the forward-peaked coherently scattered radiation reaching the detector. As a matter of fact it was found that the solid angle subtended by the collimator

between sample and detector must not significantly be larger than about 10^{-4} sr in order to maintain a linear calibration curve. The set-up was modified accordingly to comply with this requirement.
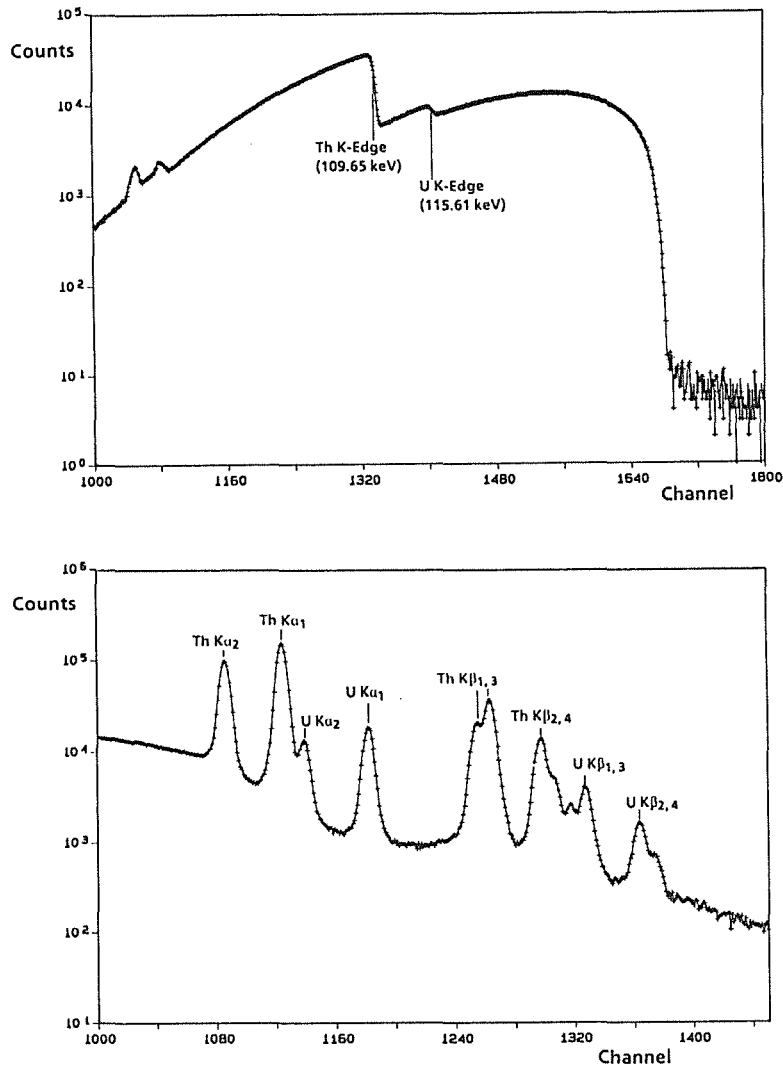
Fig. 1   KED spectrum (top) and K-XRF spectrum (bottom) from a Th / U-solution

The first application of the analyzer dealt with the measurement of Th in mixed Th/U samples. The top spectrum in Fig. 1 shows a typical KED spectrum for a Th/U solution. The transmission measurements with the tailored bremsstrahlung continuum from an X-ray tube operated at 140 kV are performed on high-precision cuvettes with a path length of 4 cm. The major element Th is typically measured with a precision of about 0.2% in a counting time of 1000 s. The precision of the KED measurement for the minor element U is about a factor of 10 lower for Th:U ratios of 10:1. The minor element is therefore better determined

from the simultaneous XRF measurement, where a parallel sample contained in a small PE vial is irradiated by a second X-ray beam. The bottom spectrum in Fig. 1 shows the relevant section of the XRF spectrum containing the K X-rays from Th and U . From this measurement the minor element U is also determined with a precision of about 0.4% at a Th:U weight ratio of 10.

[1]   H.Ottmar, H.Eberle, KfK Report 4660 148 (1990)

5.4.7.   ERROR COMPONENTS IN K - EDGE DENSITOMETRY (KED)

H. OTTMAR

The Working Group for Techniques and Standards for Non-Destructive Analysis (NDA) of the European Safeguards and Research Association (ESARDA) is currently establishing performance values for NDA techniques used to measure fissile materials. The respective measurement techniques are mainly based on active and passive neutron and gamma counting. They play an important role in the international safeguarding of nuclear materials, since the accuracy and reliability of those techniques determine to a large extent the effectivity and credibility of safeguards.

The Working Group does not intend to launch just single performance values but to establish more detailed error patterns for the individual NDA techniques in order to enable a better assessment of their overall performance in different applications. To the coordinated efforts of the group we have contributed input data on the technique of K-edge densitometry (KED), which has become an established analysis method for the determination of U and Pu concentrations in liquors. The basis of the method is absorption edge spectrometry at the K-absorption edge, which is effected by means of transmission measurements with a suitably tailored bremsstrahlung continuum from an X-ray tube.

Individual error components of KED are related with the counting process, the procedure for data evaluation, the composition and geometry of the sample, specific instrument properties such as stability and linearity, the calibration etc. Tab. 1 summarizes the major identified error components and their estimated magnitude. The given figures, which are partly based on practical experiences and partly calculated from relevant physical data, have been forwarded as a discussion basis for the establishment of performance data for KED.

Error Source	Type of Error*	Approximate Magnitude (%)	Comment
Counting precision	R	0.1-0.2	Single actinide sample > 100 g/l, 1000 s
		0.2-0.3	Major actinide (>100 g/l) in mixed sample, 1000 s
Cell length	R,S	0.01	For high-quality cuvette
		0.2-1.0	For standard plastic vial
Positioning of cell	R	<0.1	Depends on dimensional tolerances for vials and vial holder
Sample matrix	S	<0.3	Effects calculable for matrix elements differing by 2 or more units from atomic number of analyte
Uranium isotopic comp.	S	0.013	Per ^{235}U enrichment % deviation from true value
Plutonium isotopic comp.	S	<0.1	For medium to high burnup plutonium
Calibration constant	S	0.1	Depends on error of reference values and on the number and the counting precision of the calibration runs
Nonlinearity	S	<0.2	For counting rates <20 kcps at concentrations> 200 g/l
Instrument variability	S	<0.3	For long-term drifts to be monitored from control charts

Tab. 1   Survey of Error Components in KED.
         * R = Random; S = Systematic

5.4.8. RUBIDIUM ANALYSIS BY K-EDGE DENSITOMETRY

H.EBERLE, H.OTTMAR

The technique of K-edge densitometry was applied to verify the elemental content of Rb in a sample of Rb-carbonate. The analysis was carried out in support of the Van de Graaff group at our laboratory, where the Rb sample enriched in ^{87}Rb was used as target material for neutron capture cross-section measurements. The purpose of the present analysis was to assure that the Rb content of the sample calculated from the total weight of the compound and its nominal stoichiometry had not been invalidated by a possible take-up of moisture.

K-edge densitometry is preferably applied as a method for the determination of elemental concentrations in liquid samples. Therefore the Rb sample was dissolved in a defined volume (20 ml) of destilled water. An aliquot of about 2 ml was filled into a quartz cell of well-defined path length (1cm) for the energy-differential photon transmission measurement near the K-absorption edge of Rb at 15.20 keV. A highly collimated X-ray beam from an X-ray tube operated at 18 kV was utilized for the transmision measurement. Fig. 1 shows the energy
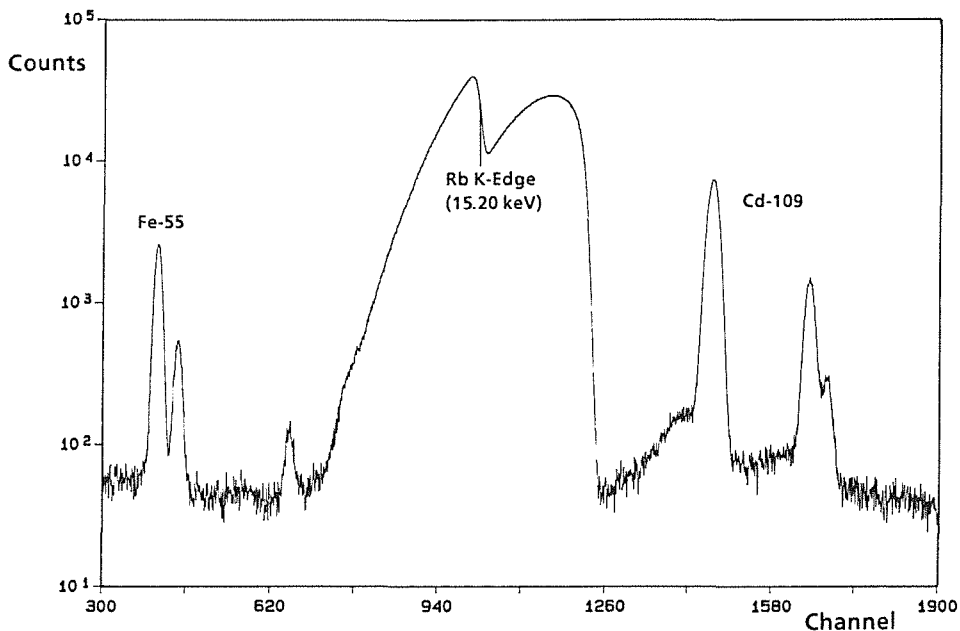
Fig. 1   Discontinuity of the photon transmission at the K-edge energy of Rb

distribution of the transmitted X-ray beam as recorded with a Si(Li) detector. The discontinuity of the photon transmission at the K-edge energy of Rb clearly shows up. The discrete photon energies in the spectrum originate from isotopic sources

(^{55}Fe,^{109}Cd). They were added as reference lines for the purpose of digital stabilization and energy calibration.

The concentration of Rb is simply determined from the change of the photon transmission across the absorption edge. This determination requires a single calibration factor which describes the change of the photon mass attenuation coefficient of the analyte at its K-edge energy. The calibration factor was derived from a comparison measurement on a reference sample with known Rb content. Different procedures determining the photon transmission both at energies slightly displaced from the K-edge and directly at the K-edge energy were applied for the evaluation of the K-edge jump from the measured spectra. The combination of the different results finally yielded a Rb concentration of 15.81 ± 0.044 mg Rb/ml. This value was very close to the expected nominal value of 15.86 mg Rb/ml.

5.4.9. DETERMINATION OF Th / U RATIOS IN SOLUTIONS - AN APPLICATION OF THE L - XRF SYSTEM WITH GRAPHITE PREFILTER

P.MATUSSEK, I.MICHEL-PIPER

The performance evaluation of the EDXRF system with graphite prefilter has been continued. This system is especially suited for the analysis of actinide solutions in the low concentration range. The lower limit of detection has been evaluated to 0.1 mg actinides per liter solution in 10 minutes counting time. The improvement as compared to conventional EDXRFA is achieved by using a cylindrical arrangement of graphite monocrystals between sample and detector that serves as a bandpass filter transmitting the L X-rays of the actinides of interest and suppressing the strong scattered excitation radiation. The goal of the present investigation was to study the potential of the system to determine the concentration ratio of elements in mixed actinides solutions. About 50 liquid samples with various Th/U ratios have been measured. The concentration of the actinides covered the range from 5 mg/l to 100 mg/l, the Th/U ratio varied between 100:1 and 1:100. Th/U mixtures have been used as test case for U/Pu mixtures because of the easier handling of the former materials. Further the possiblity has been studied to use Th as an internal standard for the absolute determination of U (and Pu) concentrations in solutions. Fig. 1 shows some typical L-XRF spectra obtained with the present system. The concentration of the major actinide
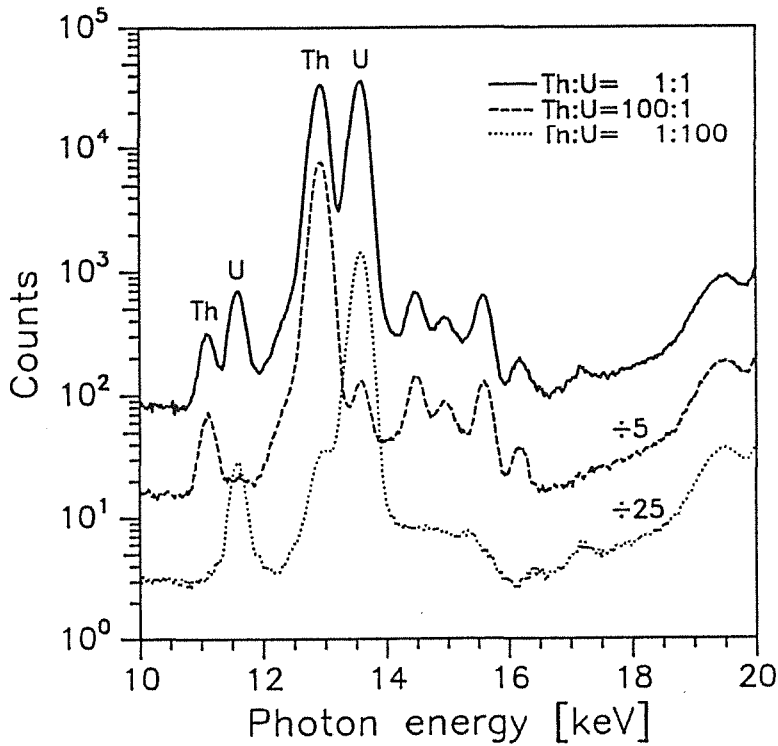
Fig. 1 Typical XRF spectra from three different Th/U solutions measured with wave-length-disper-sive prefilter (concentration of the major component 500 mg/l, counting time 2000s).

component was 500 mg/l for all three samples presented. The uncertainties of the Th/U assay originate from the counting statistics observed in both the Th and U fluorescence peak, respectively. For typical Th/U ratios from 20:1 to 200:1 the precision of the Th/U measurement is therefore mainly determined by the amplitude of the smaller peak, i.e. by the concentration of the minor element. The following values of the relative precision achievable for Th/U or U/Pu ratio assays have been deduced from the present measurements for counting times of 1 hour :

relative precision of Th / U assay	minor element concentration
<0.5%	>25 mg / l
1.5%	5 mg / l
8%	1 mg / l

Comparing these results to the precisions obtained from EDXRFA using K-X rays we found that L-XRFA with graphite prefilter extends the range of measurable actinide ratios towards lower concentrations by a factor of about 50. However, it should be noted that in contrast to K-XRFA the direct measuement of input solutions from the reprocessing is not posssible with energy-dispersive L-XRFA due to the strong interference of the K-XRF lines from the fission

products Sr and Rb with the L-XRF lines of the actinides of interest. These elements have to be removed prior to the EDXRF assay of input solutions.

5.4.10. A COMPARISON OF XRF METHODS FOR THE U, Pu ANALYSIS IN POWDER SAMPLES PREPARED BY THE FUSION TECHNIQUE

I. MICHEL-PIPER, H. OTTMAR

The quantitative determination of plutonium in oxide and mixed-oxide (MOX) powders normally requires wet chemistry. Alternative analysis methods, which are less time consuming and easier to handle, are presently investigated by Euratom and IAEA for the future instrumentation of their on-site laboratories in nuclear facilities.

X-ray fluorescence (XRF) analysis is currently considered as most promising method to simplify the analytical procedure, and to offer at the same time the desired measurement precision of $\leq$ 0.5 %. Of course, the application of XRF to the analysis of a solid material needs a special sample preparation, too. This may be accomplished by means of the fusion technique, where in a RF-field the oxide powder is fused together with a suitable flux material into homogeneous glass pellets. This kind of sample preparation will require a few minutes only.

Another aspect concerns the choice of the suitable XRF spectrometer, leaving the option between wave-length dispersive or energy-dispersive systems. In order to assess the typical measurement situation encountered in the analysis of the samples in question, some qualitative comparison measurements were carried out on glass pellets containing uranium between 1 - 2 weight % (60 - 120 mg). Specifically, the following 3 variants of X-ray spectrometry were compared :

— Energy-dispersive spectrometry of K-XRF lines;

— Energy-dispersive spectrometry of L-XRF lines with and without graphite prefiltering;

— Wave-length dispersive spectrometry of L-XRF lines with a crystal sequence spectrometer.

In all three cases X-ray tubes were used for the excitation of fluorescence lines. The characteristic spectral features obtained with the 3 types of XRF spectrometry from the measurements on the uranium containing glass pellets served as basis for an estimate of the expected measurement precision for

plutonium in case of mixed-oxide analysis. It turns out that for an assumed U/Pu ratio of 50 the desired precision of 0.5 % for the minor element plutonium can be reached in any mode within a counting time of 1000 s.

In relation to the analysis of MOX powders at larger U/Pu ratios some other observations and considerations also need to be taken into account for an overall assessment of the different modes of XRF spectrometry :

Spectral Features. The best signal-to-background ratio was observed for the energy-dispersive L-XRF method with graphite prefiltering. However, this mode suffers from the limited resolving power, providing a separation of the U and Pu Lα lines which corresponds to about 3 times of the energy resolution (FWHM). It has not yet been demonstrated if this resolution is sufficient to allow an accurate and unbiased peak area determination at larger U/Pu ratios. This problem does not exist with wave-length dispersive L-XRF and energy-dispersive K-XRF, where the respective U and Pu X-rays are sufficiently resolved.

Sample Quantity. Samples prepared for L-XRF must not contain more than about 50-100 mg of MOX powder (1-2 weight % of a typical glass pellet) in order to avoid strong self-shielding of the L X-rays. For the analysis of MOX powders this will leave some doubts about the representativity of sampling. A better situation will be given with K-XRF, where the maximum possible amount of MOX powder (about 10 weight % or 0.5 g) could be fused into the glass pellets without introducing a significant non-linearity into the instrument response.

Calibration. The problem of instrument calibration for quantitative analysis appears somewhat easier for L-XRF as long as glass pellets are produced with low U, Pu levels in a strongly absorbing matrix (e. g. Ba, La). This will assure a linear calibration curve, which could reliably be established by means of representative reference samples. Another situation exists for K-XRF, where the glass pellets - even at the highest possible content of MOX material - still remain fairly transparent for the K X-rays. This will make the measurement sensitive to geometrical variations of the pellets. In this case the best approach to accurate measurements may involve the use of a suitable internal standard (e. g. Pb).

Costs, Implementation. Some practical aspects such as costs and ease of adaptation to gloveboxes also represent factors which may determine the selection of an adequate XRF spectrometer. In general, energy-dispersive systems cost about half the price of a wave-length dispersive spectrometer, and they can easier be coupled to a glovebox environment. When balancing advantages and disadvantages of the various configurations, one might probably argue in favour of a system based on K-XRF spectrometry for the application in question.

5.4.11. AN INVESTIGATION OF THE ELEMENTAL COMPOSITION OF Ta SAMPLES BY EDXRFA

P.MATUSSEK

Two pure-metal Tantalum foils from different suppliers have been investigated for minor-element concentrations using energy - dispersive X - ray fluorescence analysis (EDXRFA). A X-ray tube with Rh anode and Rh beam filter has been used to generate the excitation radiation. The fluorescence radiation was observed by a high-resolution SiLi detector under 90° relative to the incoming beam. The total counting rate was limited to 10,000 cps in order to preserve the high energy resolution. Fig. 1 shows a sectional display of the fluorescence spectra for the two Ta foils. The counting time was about 2 hours for each sample. Besides the dominating L X-rays of Ta the K X-ray lines of Fe, Zr, Nb and Mo have been identified. The absolute element concentrations have not been determined due to the lack of suitable calibration standards. Instead of this the relative differences of the elemental concentrations for the two Ta samples have been evaluated. The
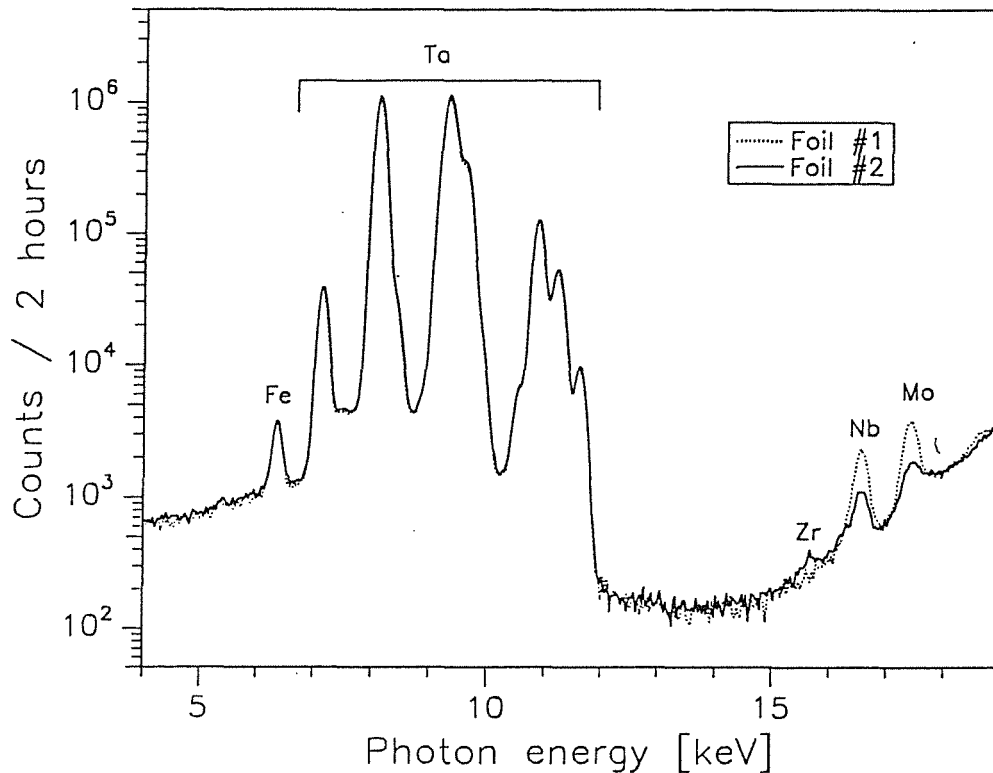
Fig. 1   XRF spectra of two different pure-metal Ta foils

results are given in Tab. 1 along with the declared concentration range of the minor elements.

Element	Rel. deviation of element concentration (# 1 -# 2) / #2	declared concentration range
Fe	(+ 3 ± 3) %	~ 30 ppm
Zr	(- 75 ± 25) %	~ 10 ppm
Mo	(+ 140 ± 5) %	100 - 500 ppm
Nb	(+ 250 ± 5) %	100 - 500 ppm

Tab. 1   Varation of element content in Ta - metal foils

The experiment demonstrates very well the potential and limitations of EDXRFA : This simple non-destructive analysis technique does in general not require any sample preparation, element concentrations down to some 10 ppm can be determined within counting times of about 1 hour, simultaneous multi-element analysis is possible. On the other hand, in certain energy regions the assay of minor elements is difficult or impossible : The measurement of elements with atomic numbers Z below Ti (e.g. C in Si) is rather cumbersome because it requires sophisticated equipment (windowless detector, evacuated counting chamber, polished sample surface e.t.c.). Further, the quantitative determination of minor elements in low concentrations is not possible if their fluorescence lines are hidden within the predominant L-series complex of the major constituent. In the present case of La foils the "black window" ranges from 7 keV to 12 keV corresponding to the K X-rays of the elements Ni to As (see Fig. 1). Minor elements with atomic numbers directly adjacent to the Z value of the major component can only be analyzed if their concentrations are greater than 1:1000. Wavelength-dispersive XRFA will probably give better results in these cases due to its superior energy resolution.

5.4.12.A GAMMA - SPECTROSCOPIC MEASUREMENTS OF THE ^{235}U ISOTOPE ABUNDANCE IN A UF$_6$ SAMPLE (PERFORMED IN THE FRAMEWORK OF THE REIMEP-86 INTERLABORATORY EXERCISE) [1]

P.MATUSSEK

This report describes the measurement of the ^{235}U/U isotope abundance in a certified UF$_6$ sample by means of gamma spectrometry. The work was performed in the framework of the REIMEP-86 interlaboratory exercise. The ^{235}U/U abundance value obtained from the measurements presented in this report was 3.5005±0.0031 % ^{235}U/U which compares very well to the certified value of 3.5001±0.0010 % ^{235}U/U. The report describes in detail the experimental set-up, the data evaluation and the error analysis. Some hints are given to improve the precision and to reduce the measurement time in future experiments of this type.

1)   published as : KfK Report 4784 (1990)

5.4.13.A ELEMENTAL COMPOSITION OF THE HUMAN ARTERIES [1]

E.ROKITA, T.CICHOCKI, D.HECK, L.JARCZYK, A.STRZAL-KOWSKI, M.SYCH

The studies were undertaken to expand the data base of elemental composition of human arterial wall. For the experiment, 4 types of human arteries (aorta, Willis circle, coronary and popliteal artery) were used. By proton-induced X-ray emission (PIXE) method the concentrations of P, S, Cl, K, Ca, Fe, Cu, Zn, Br, Rb, Sr and Pb were found. Differences appeared in elemental composition depending on artery type. Concentrations of elements involved in mineralization processes correlated with the age of patients, but did not correlate with advancement of atherosclerotic processes as seen in histological examination. One part of the material was measured by PIXE method in combination with proton microprobe (micro-PIXE) to reveal distributions of concentrations within the arterial wall. The micro-PIXE studies revealed higher concentrations of Zn and Br in tunica

media (TM) as compared with tunica adventitia (TA) as well as a lower content of all detected elements in atheroma than in the proper wall of the aorta.

5.4.14.A ELEMENTAL COMPOSITION OF INORGANIC DEPOSITS IN THE WALL OF HUMAN AORTA [1]

E.ROKITA,   T.CICHOCKI,   D.HECK,   L.JARCZYK,   J.KUNZ, A.STRZALKOWSKI,

Inorganic deposits in human aorta were examined using a proton microprobe in combination with the proton induced X-ray emission method and with the Rutherford backscattering technique. The material consisted of autopsy samples with or without atherosclerotic symptoms. The morphology of the investigated arteries was verified histologically. The in situ concentrations of N, O, P, S, Cl, K, Ca, Fe, Cu, Zn, Br, Sr and Pb were determined both within the inorganic deposits and in the surrounding organic matrix (crystal ghost). S concentration in the aortic wall decreases with the age of patients as a result of the fall in the proteoglycan content. The differences in Fe concentrations depend on the amount of blood present in the sample. Sr / Ca ratio was found to be similar to that detected in the other organs. Therefore the accumulation of Sr within the mineralized tissue results from chemical similarity of Sr and Ca. Pb was only accumulated within a part of investigated deposits. The incorporation of Pb ions in the crystal lattice is probably correlated with the accidental exposure to elevated Pb level. Cu atoms are present within atheroma in the form of blood-derived Cu-macromolecules adsorbed onto the deposit surface. A quantitative proof has been obtained that Zn is adsorbed on the surface of the deposits. The deposits can be divided into 2 groups on the basis of K concentration, probably an indication of intra-and extracellular sites of mineralization.

5.4.15.A ARTERY WALL CALCIFICATION : CORRELATION OF ATHEROSCLEROSIS WITH MINERALIZATION [1]

T.CICHOCKI, D.HECK, L.JARCZYK, E.ROKITA, A.STRZAL-KOWSKI, M.SYCH

Popliteal arteries from 14 individuals (17-85 years old) were investigated. The concentrations and localizations of P, S, Cl, K, Ca, Fe, Cu, Zn and Br were measured by means of PIXE and micro-PIXE methods. The presence of PO_4^{3-} and CO_3^{2-} groups was assessed using the IR technique. The amount of P and Ca increased with age approaching at places 9% and 20% and mineral deposits were detected in tunica media. At the same time an increase in the Ca/P ratio and in the crystallinity of deposits was observed. The samples from old individuals also contained more CO_3^{2-} groups. The concentrations and localization of Zn and Br showed artery wall layer-dependent changes. In some places of the artery wall, minerals were also found in young persons. They were not correlated with places of blood vessel branching.

6. LIST OF PUBLICATIONS

6.1 PUBLICATIONS AND REPORTS

BECHTOLD, V.; SCHWEICKERT, H.
Gastargetvorrichtung.
DE-OS 38 08 973 (5.10.1989)

BEER, H.
Capture cross section measurements of Xe and
Kr isotopes by fast cyclic activation.
In: Cierjacks, S. [Hrsg.]
Progress Report on Nuclear Data Research in
the Federal Republic of Germany for the
Period April 1, 1989 to March 31, 1990
NEANDC(E)-312 U Vol. 5(June 1990) S.1-2
INDC(Ger)-35/LN + Special

BIALY, J.; PETERS, J.W.; SCHMITT, M.
Vielfachmessvorrichtung zum Messen und
Darstellen des Aktivitätsverlaufs radio-
aktiver Quellen oder Substanzen.
DE-OS 38 36 732 (3.5.1990)

BRANCUS, I.M.; REBEL, H.; WENTZ, J.;
CORCALCIUC, V.
The extended sum-rule model view of light and
intermediate mass fragment emission in
nuclear reactions at intermediate energies.
KfK-4646 (November 89)
Physical Review C, 42(1990) S.2157

BRANCUS, I.M.; WENTZ, J.; HOHN, H.U.
LIMES - a computer program for analyses of
light and intermediate-mass fragment
emission in heavy ion reactions by an
extended sum-rule model.
KfK-4610B (Oktober 89)

CELLO-COLLABORATION
Measurement of the reaction $\gamma\gamma \rightarrow rho + rho^-$
with the CELLO-detector.
Physics Letters B, 218(1989) S.493-98

CICHOCKI, T.; HECK, D.; JARCZYK, L.;
ROKITA, E.; STRZALKOWSKI, A.; SYCH, M.
Artery wall calcification: correlation of
atherosclerosis with mineralization.
Pathologica, 81(1989) S.139-49

DOLL, P.
Neutron-proton scattering.
KfK-4706 (Februar 90)

DOLL, P.; FINK, G.; HAUPENTHAL, M.;
FINLAY, R.W.; HAUBER, S.; KLAGES, H.O.;
SCHIELER, H.; SMEND, F.; WICKE, G.D.
Pulse shape discrimination with a large NaI
crystal.
Nuclear Instruments and Methods A,
285(1989) S.464-68

DORN, A.; KÄLBER, W.; MEISEL, G.
Ein Dauerstrich-Farbstofflaser mit
hochstabiler Frequenz.
KfK-4709B (Mai 90)

DREXLIN, G.; EBERHARD, V.; GEMMEKE,
H.; GIORGINIS, G.; GRANDEGGER, W.;
GUMBSHEIMER, R.; HUCKER, H.;
HUSSON, L.; KLEINFELLER, J.;
MASCHUW, R.; PLISCHKE, P.; SPOHRER,
G.; SCHMIDT, F.K.; WOCHELE, J.;
WÖLFLE, S.; ZEITNITZ, B.; BODMAN, B.;
BURTAK, F.; FINCKH, E.; GLOMBIK, A.;
KRETSCHMER, W.; SCHILLING, F.;
VÖTISCH, D.; EDGINGTON, J.A.;
GORRINGE, T.; MALIK, A.; BOOTH, N.E.;
DODD, A.; PAYNE, A.G.D.
The high resolution neutrino calorimeter
KARMEN.
4th Pisa Meeting on Advanced Detectors,
LaBiodola, I, May 21-25, 1989
Nuclear Instruments and Methods A,
289(1990) S.490-95

DREXLIN, G.; GILS, H.J.; [HRSG.]
Annual report on nuclear physics activities
July 1, 1988 - June 30, 1989.
KfK-4660 (Mai 90)

ERNST, R.; FRIEDRICH, L.; HUTTEL, E.;
SCHULZ, F.
An ECR source for Li^{3+} ions.
Nuclear Instruments and Methods A,
287(1990) S.337-40

FRIEDRICH, L.; HUTTEL, E.;
SCHMELZBACH, P.
Vorrichtung zur Ionisation eines polarisierten
Atomstrahls.
DE-OS 38 29 338 (1.3.1990)

GILS, H.J.; HECK, D.; ÖHLSCHLÄGER, J.;
SCHATZ, G.; THOUW, T.J.; MERKEL, A.
A multi-transputer system for parallel Monte-
Carlo simulations of extensive air showers.
Computer Physics Communications, 56(1989)
S.105-13

GIORGINIS, G.
Drift-field uniformity in long drift devices.
Nuclear Instruments and Methods A,
294(1990) S.417-23

GSOTTSCHNEIDER, G.
Kinematisch vollständige Messung des Auf-
bruchs von ^{6}Li mit Hilfe des Magnetspektro-
graphen 'Little John'.
KfK-4803 (Dezember 90)

HEERINGA, W.; GUMBSHEIMER, R.
Kryostat fuer den Betrieb einer ^{3}He^{4}He-
Mischeinheit.
DE-OS 34 35 229 (3.4.1986)
DE-PS 34 35 229 (6.3.1989)

HEERINGA, W.; KLAGES, H.O.; WÖLFL, C.;
FINLAY, R.W.
Spin-spin cross sections of ^{27}Al and ^{93}Nb for
neutrons from 20 to 50 MeV.
Physical Review Letters, 63(1989) S.2456-59

HEIDE, N.; REBEL, H.; CORCALCIUC, V.;
SRIVASTAVA, D.K.
Evidence for diffractive dissociation of ^{6}Li and
obtainability of the off-shell T-matrix from
break-up experiments.
Revue Roumaine de Physique, 34(1989)
S.1187-93

HEIDE, N.; SRIVASTAVA, D.K.; REBEL, H.
Interference and off-shell effects of fragment
scattering in elastic break-up of light ions.
Physical Review Letters, 63(1989) S.601-09

HORZEL, J.
Aufbau eines Teststandes - einschliesslich
Triggersystem, Gasversorgungssystem und
Elektronik - zur Untersuchung von Vieldraht-
Proportionalkammern mit kosmischen
Myonen.
Diplomarbeit, Universität Karlsruhe 1990
KfK-4815 (Dezember 90)

JANY, P.
Teilchennachweis mit supraleitenden
Tunneldioden.
KfK-4771 (August 90)Dissertation,
Universität Karlsruhe 1990

KÄLBER, W.; RINK, J.; BEKK, K.; FAUBEL,
W.; GÖRING, S.; MEISEL, G.; REBEL, H.;
THOMPSON, R.C.
Nuclear radii of thorium isotopes form
laserspectroscopy of stored ions.
Zeitschrift für Physik A, 334(1989) S.103-08

KÄPPELER, F.; BAO, Z.Y.; REFFO, G.;
WANG, S.N.
The s-process branching at ^{185}W and^{186}Re.
In: Cierjacks, S. [Hrsg.]
Progress Report on Nuclear Data Research in
the Federal Republic of Germany for the
Period April 1, 1989 to March 31, 1990
NEANDC(E)-312 U Vol. 5(June 1990) S.4-6
INDC(Ger)-35/LN + Special

KÄPPELER, F.; GALLINO, R.; BUSSO, M.;
PICCHIO, G.; RAITERI, C.M.
s-process nucleosynthesis: classical approach
and asymptotic giant branch models for low
mass stars.
The Astrophysical Journal, 354(1990) S.630

KÄPPELER, F.; ZHAO, W.; BEER, H.;
RATZEL, U.
^{88}Sr and ^{89}Y: the s-process at magic neutron
number N = 50.
The Astrophysical Journal, 355(1990) S.348

KÄPPELER, F.; ZHAO, W.; BEER, H.;
RATZEL, U.
^{88}Sr and ^{89}Y: the s-process at magic neutron
number N = 50.
In: Cierjacks, S. [Hrsg.]
Progress Report on Nuclear Data Research in
the Federal Republic of Germany for the
Period April 1, 1989 to March 31, 1990
NEANDC(E)-312 U Vol. 5(June 1990) S.3
INDC(Ger)-35/LN + Special

KIENER, J.
Coulomb-Dissoziation von 156 MeV ^{6}Li-
Projektilen.
KfK-4691 (Februar 90)
Dissertation, Universität Tübingen 1990

KLAY, N.
Das Niveauschema von ^{176}Lu und dessen
Bedeutung in der s-Prozess Nukleosynthese.
KfK-4675 (Februar 90)
Dissertation, Universität Heidelberg 1990

MATUSSEK, P.
Gamma-spektroscopic measurements of the
$235U$ isotope abundance in a UF_6 sample (per-
formed in the framework of the REIMEP-86
interlaboratory exercise).
KfK-4784 (Oktober 90)

MEISEL, G.; KÄLBER, W.; RINK, J.
Verfahren zur Reduktion der spektralen
Breiten von Anregungsspektrallinien.
DE-OS 39 11 052 (11.10.1990)

MOOSBURGER, M.; ASCHENAUER, E.;
DENNERT, H.; EYRICH, W.; LEHMANN, A.;
RUDELOFF, R.; SCHLÖSSER, H.; WIRTH,
H.; GILS, H.J.; REBEL, H.; ZAGROMSKI, S.
($6Li$, $6He$) reaction and Gamow-Teller β-decay.
Physical Review C, 41(1990) S.2925-28

OCHS, A.; BUSCHER, H.P.; GEROK, W.;
HECK, D.; THOM, H.
Copper uptake in short time cultivated rat
hepatocytes and copper accumulation within
the rat liver during cholestasis studied by
proton induced X-ray emission (PIXE).
Braetter, P. [Hrsg.]
Trace Element Analytical Chemistry in
Medicine and Biology : Proc.of the 5th
Internat.Workshop, Neuherberg, April 15-18,
1988 Vol. 5
Berlin [u.a.] : de Gruyter 1988 S.498-503

REBEL, H.; BURKHARDT, S.
Investigations with the 156 MeV $6Li$ beam at
the Karlsruhe Isochronous Cyclotron.
Collected results.
Karlsruhe : KfK, 1990

ROKITA, E.; CICHOCKI, T.; HECK, D.;
JARCZYK, L.; STRZALKOWSKI, A.; SYCH,
M.
Elemental composition of the human arteries.
Trace Elements in Medicine, 6(1989) S.82-85

ROKITA, E.; CICHOCKI, T.; HECK, D.;
JARCZYK, L.; KUNZ, J.; STRZALKOWSKI,
A.
Elemental composition of inorganic deposits in
the wall of human aorta.
Trace Elements in Medicine, 6(1989) S.158-64

SCHROTH, H.J.; BIALY, J.; HANS, F.J.;
OBERHAUSEN, E.; PETERS, J.W.;
SCHMITT, M.; WARNKE, P.
Bestimmung des zerebralen Blutflusses
mittels des $81Rb$/supra(81m)Kr- Generator-
systems.
NuklearMedizin, 29(1990) S.7-12

SCHULTHEISS, C.; GEERK, J.; KAROW,
H.U.
Verfahren und Vorrichtung zur Erzeugung
epitaktisch und/oder hochexturiert gewach-
sener, fremdphasenarmer Filme von Hoch-
Tsub(c)-Oxidsupraleitern auf Substra-ten.
DE-PS 38 34 402 (3.1.1989)

SRIVASTAVA, D.K.; BASU, D.N.; REBEL,
H.; GILS, H.J.
Orbital dispersion and wavefunction mapping
in inclusive break-up experiments.
Zeitschrift für Physik A, 335(1990) S.417-20

SRIVASTAVA, D.K.; REBEL, H.; HEIDE, N.
A prior-form distorted-wave born approxima-
tion analysis of the elastic breakup of 156 MeV
$6Li$ projectiles.
KfK-4565 (Juni 89)
Nuclear Physics A, 506(1990) S.346-66

TOUKAN, K.A.; KÄPPELER, F.
The stellar neutron capture cross sections of
$94Zr$ and $96Zr$.
In: Cierjacks, S. [Hrsg.]
Progress Report on Nuclear Data Research in
the Federal Republic of Germany for the
Period April 1, 1988 to March 31, 1989
NEANDC(E)-302 U Vol. 5(June 1989) S.3
INDC(Ger)-34/LN + Special
The Astrophysical Journal, 348(1990) S.357

TOUKAN, K.A.; KÄPPELER, F.
The stellar neutron capture cross sections of
$94Zr$ and $96Zr$.
In: Cierjacks, S. [Hrsg.]
Progress Report on Nuclear Data Research in
the Federal Republic of Germany for the
Period April 1, 1989 to March 31, 1990
NEANDC(E)-312 U Vol. 5(June 1990) S.3
INDC(Ger)-35/LN + Special

WENTZ, J.
Emission leichter und mittelschwerer Teilchen
bei Kernreaktionen von 156 MeV $6Li$-Ionen an
supra(nat)Ag.
KfK-4725 (Mai 90)

WIESCHER, M.; STEININGER, R.;
KÄPPELER, F.
$7Li(n, \gamma)8Li$-trigger reaction to a primordial
r-process?
The Astrophysical Journal, 344(1989) S.464-70

WIRTH, H.; ASCHENAUER, E.; EYRICH, W.;
LEHMANN, A.; MOOSBURGER, M.;
SCHLÖSSER, H.; GILS, H.J.; REBEL, H.;
ZAGROMSKI, S.

Investigation of spin-isospin strength in
^{48}Ca$\rightarrow^{48}$Sc and ^{90}Zr$\rightarrow^{90}$Nb using the
(^{6}Li,^{6}He)reaction.
Physical Review C, 41(1990) S.2698-2701

WISSHAK, K.; GUBER, K.; KÄPPELER, F.;
KRISCH, J.; MÜLLER, H.; RUPP, G.; VOSS, F
The Karlsruhe 4n barium fluoride detector.
KfK-4652 (Dezember 89)
Proc.of the 7th Symp.on Radiation Measure-
ments and Applications,
Ann Arbor, Mich., May 21-24, 1990
Nuclear Instruments and Methods A, 292
(1990) S.595-618

WISSHAK, K.; GUBER, K.; KÄPPELER, F.;
RUPP, G.; MÜLLER, H.; VOSS, F.
First measurements with the Karlsruhe 4n
BaF$_2$ detector.
In: Cierjacks, S. [Hrsg.]
Progress Report on Nuclear Data Research in
the Federal Republic of Germany for the
Period April 1, 1988 to March 31, 1989
NEANDC(E)-302 U Vol. 5(June 1989) S.4
INDC(Ger)-34/LN + Special

WISSHAK, K.; VOSS, F.; KÄPPELER, F.;
REFFO, G.
A new approach for precise measurements of
keV neutron capture cross sections: the
examples of ^{93}Nb, ^{103}Rh, and ^{181}Ta.
KfK-4674 (April 90)

WISSHAK, K.; VOSS, F.; KÄPPELER, F.;
REFFO, G.
Measurements of keV neutron capture cross
sections with a 4n barium fluoride detector:
examples of ^{93}Nb, ^{103}Rh, and ^{181}Ta.
Physical Review C, 42(1990) S.1731-50

WISSHAK, K.; VOSS, F.; KÄPPELER, F.;
REFFO, G.
A new approach for presice measurements of
keV neutron capture cross sections: the
examples of niobium, rhodium and tantalum.
In: Cierjacks, S. [Hrsg.]
Progress Report on Nuclear Data Research in
the Federal Republic of Germany for the
Period April 1, 1989 to March 31, 1990
NEANDC(E)-312 U Vol. 5(June 1990) S.7-8
INDC(Ger)-35/LN + Special

6.2. CONFERENCE CONTRIBUTIONS

53.Physikertagung gemeinsam mit
derFrühjahrstagung DPG, Kern- und
Hochenergie-physik, Energietechnik -
PhysikalischeGrundlagen, Fachdidaktik der
Physik,Gravitation und Relativitätstheo-
rie,Strahlenwirkung und -schutz, Physiker in
der Automatisierungstechnik, Fortbildungs-
veranstaltung, Bonn, 13.-17.März 1989
Verhandlungen der Deutschen Physikalischen
Gesellschaft, R.6, Bd.24 (1989)

HEIDE, N.; CORCALCIUC, V.; GILS, H.J.;
KIENER, J.; REBEL, H.; WENTZ,
J.;ZAGROMSKI, S.; SRIVASTAVA, D.K.
Break-up of 156 MeV ^{6}Li at large asymptotic
relative momenta of the fragments and the
prior-DWBA.

DOLL, P.; FINK, G.; HAUBER, S.; KLAGES,
H.O.;KNÖPFLE, K.T.
Efficiency and line shapes of a large NaI
detector.

5th IAP Astrophysics Meeting on
Astrophysical Ages and Datations, Paris, F,
June 26-30, 1989

BEER, H.
The radiogenic ^{207}Pb component and the ^{235}U
clock.

ZHAO, W.; KÄPPELER, F.
An improved ^{175}Lu(n,γ)supra(176m)Lu cross
section: the cosmic clock supra(176g)Lu in
trouble.

Few Body XII : Contributed Papers from the
12th Internat.Conf.on Few Body Problems in
Physics, Vancouver, CDN, July 2-8, 1989
TRI-89-2 (July 89)

DOLL, P.; EBERHARD, V.; FINK, G.;
FINLAY, R.W.; FORD, T.D.; HEERINGA, W.;
KLAGES, H.O.; KRUPP, H.; WÖLFL, CHR.
New results for the n-p spin correlation
parameter Asub(yy) below 50 MeV.

DOLL, P.; FINK, G.; HAUBER, S.;
HEERINGA, W.; KLAGES, H.O.; SCHIELER,
H.; SMEND, F.; WICKE, G.
n + ^{3}He - radiative capture to ^{4}He.

DOLL, P.; FINK, G.; HAUBER, S.;
HAUPENTHAL, M.; KLAGES, H.O.;
SCHIELER, H.; SMEND, F.: WICKE, G.
Preliminary results on the H(n,γ) ^{2}H capture
experiment.

Internat.Nuclear Physics Conf., Sao Paulo, BR,
August 20-26, 1989

WIRTH, H.; ASCHENAUER, E.; EYRICH, W.;
LEHMANN, A.; MOOSBURGER, M.; GILS,
H.J.; REBEL, H.; ZAGROMSKI, S.
Systematic investigation of spin-isospin
strength using the (^{6}Li, ^{6}He) reaction.

Tagung 'Progress in Fisica', Oradea, R, 5.-
7.Oktober 1989

BRANCUS, I.M.; REBEL, H.; WENTZ, J.
The extended sum-rule model view of light and
intermediate mass fragment emission in
nuclear reactions at intermediate energies.

Internat.Conf.on Radioactive Nuclear Beams,
Berkeley, Calif., October 16-18, 1989

AGUER, P.; AZAIEZ, F.; BARHOUMI, S.;
BIMBOT, R.; BOGAERT, G.; CLAPIER, F.;
DISDIER, D.; FORTIER, S.; GILS, H.J.;
KIENER, J.; KIOUS, M.; KRAUS, L.;
LEFEBVRE, A.; LINCK, I.; REBEL, H.;
STEPHAN, C.; TASSAN-GOT, L.; THIBAUD,
J.P.; VILLARI, A.
Use of the GANIL radioactive beams for
astrophysical purposes.

13th Nuclear Physics Symp., Oaxtepec, MEX,
January 3-6, 1990

DOLL, P.
Neutron-proton scattering.

21st Internat.Cosmic Ray Conf., Adelaide,
AUS, January 6-19, 1990 Conf.Papers Vol. 10
(HE Sessions) S.275 Adelaide : University of
Adelaide, 1990

CAPDEVIELLE, J.N.; GABRIEL, P.; GILS,
H.J.; GRIEDER, P.; HECK, D.; HEIDE, N.;
KNAPP, J.; MAYER, H.J.; ÖHLSCHLÄGER,
J.; REBEL, H.; SCHATZ, G.; THOUW, T.
Air shower simulations for KASCADE.

DAUMILLER, K.; DOLL, P.; HECK, D.;
HEERINGA, W.; KLAGES, H.O.; KRIEG-
LEDER, W.; MAYER, H.J.; MÜLLER, H.;
SCHIELER, H.; SCHMALZ, G.; VÖLKER, G.
The detector array of the KASCADE project.

DOLL, P.; ENGLER, J.; GILS, H.J.; HECK, D.;
HEIDE, N.; KEIM, H.; KLAGES, H.O.;
KNAPP, J.; MAYER, H.J.; MÜLLER, H.;
ÖHLSCHLÄGER, J.; REBEL, H.; SCHATZ,
G.; SCHMALZ, G.; THOUW, T.; ZAGROMSKI,
S.; ZEITNITZ, B.
The KASCADE project.

ENGLER, J.; GABRIEL, P.; GILS, H.J.; KEIM,
H.; KNAPP, J.; REBEL, H.; ZAGROMSKI, S.
The central detector for the KASCADE project.

Expertentreffen Kernphysik, Schleching,
27.Februar - 7.März

MASCHUW, R.
Neutrinophysik.

Rossendorf-Meeting on Cyclotron Applications
in Medicine and Engineering, Dresden, DDR,
March 12-16, 1990

BECHTOLD, V.
Isotope production at the Karlsruhe compact
cyclotron.

BIALY, J.; PETERS, J.W.; SCHMITT, M.
'Engypan' - ein tragbares Messgerät fuer die
Funktionsdiagnostik in der Nuklearmedizin.

FEHSENFELD, P.; KLEINRAHM, A.
Radionuklidtechnik im Maschinenbau.

SCHWEICKERT, H.
Die Zyklotronanlagen des
Kernforschungszentrums Karlsruhe.

54.Physikertagung gemeinsam mit der
Frühjahrstagung DPG, Atomphysik,
Energietechnik - Physikalische Grundlagen,
Extraterrestrische Physik, Gravitation und
Relativitätstheorie, Kurzzeitphysik,
Massenspektrometrie, Physik und Medizin,
Plasmaphysik, Quantenoptik,
Strahlenwirkung und Strahlenschutz,
Fortbildungsveran- staltung, Muenchen, 12.-
16.März 1990 Verhandlungen der Deutschen
Physikalischen Gesellschaft, R.6, Bd.25 (1990)

KÄLBER, W.; MEISEL, G.; RINK, J.;
THOMPSON, R.C.
Zeitaufgeloeste Laserspektroskopie an Ionen
in einer Hochfrequenz-Falle.

KOWALEWSKA, D.; BEKK, K.; GÖRING, S.;
HANSER, A.; KAELBER, W.; MEISEL, G.;
REBEL, H.
Laser-Spektroskopie an einem Polonium-
Atomstrahl.

Frühjahrstagung DPG, Teilchenphysik,
Hamburg, 21.-24.März, 1990 Verhandlungen
der Deutschen Physikalischen Gesellschaft,
R.6, Bd.25 (1990)

BOLZ, J.; ENGLER, J.; KEIM, H.; KNAPP, J.
Untersuchungen von TMS-
Ionisationskammern für das KASCADE-
Kalorimeter.

ENGLER, J.; GETTERT, M.; KEIM, H.;
KNAPP, J.
Messungen mit einem TMS-Kalorimeter mit
Uran, Blei und Eisen als Absorber.

ENGLER, J.; VATER, G.
Mischungen von Flüssigkeiten für schnelle
Ionisationskammern.

DOLL, P.; ENGLER, J.; GILS, H.J.; HECK, D.;
HEIDE, N.; KEIM, H.; KLAGES, H.O.;
KNAPP, J.; MAYER, H.J.; MÜLLER, H.;
ÖHLSCHLÄGER, J.; REBEL, H.; SCHATZ,
G.; SCHMALZ, G.; THOUW, T.; ZAGROMSKI,
S.; ZEITNITZ, B.
The Karlsruhe cosmic ray project KASCADE.

KNAPP, J.
Simulation des Zentralkalorimeters von
KASCADE.

MAYER, H.J.; KLAGES, H.O.
Monte Carlo simulation for the KASCADE air shower array.

KARMEN-COLLABORATION;
KLEINFELLER, J.
Eigenschaften, des KARMEN Neutrino Kalorimeters.

Spring Meeting of Nuclear Physics Sections of Belgische Natuurkundige Vereniging, Societe Belge de Physique, Institut National de Physique Nucleaire et de Physique des Particules, Oesterreichische Physikalische Gesellschaft, Schweizerische Physikalische Gesellschaft, Nederlandse Natuurkundige Vereniging, Deutsche Physikalische Gesellschaft, Institut de Recherche Fondamentale, the Institute of Physics, Dansk Fysisk Selskab, Strasbourg, F, March 26-30, 1990 Verhandlungen der Deutschen Physikalischen Gesellschaft, R.6, Bd.25 (1990)

ASCHENAUER, E.; DENNERT, H.; EYRICH, W.; LEHMANN, A.; MOOSBURGER, M.; SCHLÖSSER, H.; WIRTH, H.; GILS, H.J.; REBEL, H.; ZAGROMSKI, S.
(^{6}Li,^{6}He)-measurements as an alternative calibration for solar-neutrino-detectors.

BAYER, R.; FINKBEINER, F.; FOLTIN, G.; HAHN, A.; HEERINGA, W.; JANY, P.; KLAGES, H.O.; SKACEL, H.; STROBELT, T.
Cryogenic particle detection.

BEER, H.
Capture cross section measurements of Xe and Kr isotopes by fast cyclic activation.

BOODMANN, B.; BURTAK, F.; FINCKH, E.; GLOMBIK, A.; HANIKA, T.; KRETSCHMER, W.; MEYER, R.; SCHILLING, F.; MASCHUW,R
First experiences with the KARMEN anticounter in its final setup.

DAUMILLER, K.; DOLL, P.; GILS, H.J.; KLAGES, H.O.; KRIEGLEDER, W.; MAYER, H.J.; MÜLLER, H.; SCHIELER, H.; SCHMALZ, G.; VÖLKER, G.; WETZEL, Y.
The detector array of the KASCADE project.

DAUMILLER, K.; DOLL, P.
Cosmic muon detection with limited streamer tubes.

DOLL, P.; ENGLER, J.; GILS, H.J.; HECK, D.; HEIDE, N.; KEIM, H.; KLAGES, H.O.; KNAPP, J.; MAYER, H.J.; MÜLLER, H.; ÖHLSCHLÄGER, J.; REBEL, H.; SCHATZ, G.; SCHMALZ, G.; THOUW, T.; ZAGROMSKI, S.; ZEITNITZ, B.
The Karlsruhe cosmic ray project KASCADE.

EITEL, K.; RAPP, J.; WOLF, J.; GEMMEKE, H.; MASCHUW, R.
Optical properties of liquid scintillators.

ENGLER, J.; GABRIEL, P.; GILS, H.J.; HEIDE, N.; KEIM, H.; KNAPP, J.; REBEL, H.; ZAGROMSKI, S.
The central detector of KASCADE.

KARMEN-COLLABORATION;
GRANDEGGER, W.
Experimental results and MC-calculations for cosmic muon induced reactions in the KARMEN neutrino detector.

GSOTTSCHNEIDER, G.; KIENER, J.; ZAGROMSKI, S.; GILS, H.J.; HEIDE, N.; REBEL, H.; WENTZ, J.
Particle-particle correlation measurements at extremely small relative angles.

KÄPPELER, F.; BAO, Z.Y.; JAAG, S.; REFFO, G.; WANG, S.N.
The s-process branching at ^{185}W and ^{186}Re.

KOWALEWSKA, D.; BEKK, K.; HANSER, A.; MEISEL, G.; REBEL, H.
Laser spectroscopy of polonium isotopes.

MOOSBURGER, M.; ASCHENAUER, E.; DENNERT, H.; EYRICH, W.; LEHMANN, A.; SCHOLZ, N.; WIRTH, H.; GILS, H.J.; REBEL, H.; ZAGROMSKI, S.
Study of excitation and decay of Gamow-Teller strength by use of the (^{6}Li,^{6}He p).

PARLOG, M.; POPESCU, D.; WENTZ, J.; ZAGROMSKI, S.; BRANCUS, I.M.; CORCALCIUC, V.; GILS, H.J.; REBEL, H.
Intermediate-mass fragment emission in light ion induced nuclear reactions at 26 MeV/amu.

VOSS, F.; BEER, H.
Remarks on the limits of accuracy of Maxwellian averaged neutron capture cross sections.

WIRTH, H.; ASCHENAUER, E.; DENNERT,
H.; EYRICH, W.; LEHMANN, A.;
MOOSBURGER, M.; SCHLÖSSER, H.; GILS,
H.J.; REBEL, H.; ZAGROMSKI, S.
Systematic investigation of Gamow-Teller
strength in light and medium heavy nuclei
using the (^{6}Li,^{6}He) reaction.

KARMEN-COLLABORATION; WÖLFLE, S.
Calibration and monitoring of the KARMEN
neutrino detector.

Symp.on Nuclear Astrophysics during the
199th National Meeting of the American
Chemical Society, Boston, Mass., April 22-27,
1990

KÄPPELER, F.
Progress in s-process nucleosynthesis.

European Physical Society Nuclear Study
Conf., Heraklion, GR, May 20-25, 1990
Vortr.: ILL, Grenoble, F, 7.November 1990

MASCHUW, R.
KARMEN, neutrinophysics between 5 and 50
MeV.

Proc.of the 7th Symp.on Radiation
Measurements and Applications, Ann Arbor,
Mich., May 21-24, 1990

WISSHAK, K.; GUBER, K.; KÄPPELER, F.;
KRISCH, J.; MÜLLER, H.; RUPP, G.; VOSS,F.
The Karlsruhe 4n barium fluoride detector.
KfK-4652 (Dezember 89)

Internat.School on Nuclear Physics: Nuclear
Reactions, Kiev, SU, May 28 - June 8, 1990

PARLOG, M.; POPESCU, D.; WENTZ, J.;
ZAGROMSKI, S.; BRANCUS, I.M.;
CORCALCIUC, V.; GILS, H.J.; REBEL, H.
Intermediate-mass fragment emission in light
ion induced nuclear reactions at 26 MeV/amu

REBEL, H.; SRIVASTAVA, D.K.
Mechanisms of Li-projectile break-up.

Internat.Symp.on Nuclear Astrophysics:
Nuclei in the Cosmos, Baden, A, June 18-22,
1990

GALLINO, R.; BUSSO, M.; KÄPPELER, F.;
PICCHIO, G.; RAITERI, C.M.
Propagation of neutron capture cross section
uncertainties on the s-process nucleosynthesis
in massive and in low mass stars.

JAAG, S.; KÄPPELER, F.
The stellar cross section of ^{209}Bi: implications
for the s-process.

KÄPPELER, F.; ZHAO, W.; BEER, H.;
RATZEL, U.
The s-process at magic neutron number N =
50.

KÄPPELER, F.
The s-process: branchings and chronometers.

NEMETH, ZS.; KÄPPELER, F.
supra (180m) Ta at stellar temperatures.

SCHATZ, G.
Nuclei in cosmic rays.

WISSHAK, K.; VOSS, F.; KÄPPELER, F.;
REFFO, G.
Neutron capture cross section measurements
with the Karlsruhe 4n BaF$_2$ detector: the
examples of ^{93}Nb, ^{103}Rh, and ^{181}Ta.

8th Internat.Symp.on Radiopharmaceutical
Chemistry, Princeton, N.J., June 24-29, 1990

QUAIM, S.M.; TARKANYI, F.; STÖCKLIN,
G.; SAJJAD, M.; LAMBRECHT, R.M.;
SCHWEICKERT, H.
Excitation functions of (p,2n) and (p,pn)
reactions on highly enriched ^{123}Xe with special
reference to the production of ^{123}I.

TARKANYI, F.; QAIM, S.M.; STÖCKLIN,
G.;SAJJAD, M.; LAMBRECHT, R.M.;
SCHWEICKERT, H.
Excitation functions of (p,2n) and (p,pn)
reactions and differential and integral yields of
^{123}I in proton induced nuclear reactions on
highly enriched ^{124}Xe.

6th Internat.Symp.on Very High Energy
Cosmic Ray Interactions, Tarbes, F, July 8-17,
1990

CAPDEVIELLE, J.N.; GABRIEL, P.; GILS, H.J.; GRIEDER, P.; HECK, D.; HEIDE, N.; KNAPP, J.; MAYER, H.J.; ÖHLSCHLÄGER, J.; REBEL, H.; SCHATZ, G.; THOUW, T.
E.A.S. simulations for the KASCADE project.

7th Internat.Conf.on Polarization Phenomena in Nuclear Physics, Paris, F, July 9-13, 1990

FRIEDRICH, L.; HUTTEL, E.
Design and test of a 30 K polarized atomic beam source.

12th European Cosmic Ray Symp., Nottingham, GB, July 15-21, 1990

DOLL, P.; ENGLER, J.; GABRIEL, P.; GETTERT, M.; GILS, H.J.; HANSER, A.; HECK, D.; HEIDE, N.; KEIM, H.; KLAGES, H.O.; KNAPP, J.; KRIEGLEDER, W.; MATHES, H.J.; MAYER, H.J.; MÜLLER, H.; ÖHLSCHLÄGER, J.; REBEL, H.; SCHATZ, G.; SCHIELER, H.; SCHMALZ, G.; THOUW, T.; VOELKER, G.; ZAGROMSKI, S.; ZEITNITZ, B.
The Karlsruhe cosmic ray project KASCADE.

31st Herstmonceux Conf., Elements and the Cosmos, Cambridge, GB, July 16-20, 1990

BEER, H.
Capture cross sections, s-process analysis and the key branchings at ^{85}Kr and ^{95}Zr.

World Hydrogen Energy Conf., Honolulu, Hawaii, July 22-27, 1990

ZEITNITZ, B.; HEERINGA, W.; KLAGES, H.O.; MARX, G.; PLIRTH, W.; SCHÜTZE, M.; KREYSA, G.
Experimental study of possible cold fusion in titanium and palladium electrodes.

KAON workshop, Vancouver, CDN, July 23-28, 1990

GEMMEKE, H.
Status of KARMEN and first results.

Internat.Summer School of Nuclear Physics, Predeal, R, August 28 - September 8, 1990

REBEL, H.
New interest in cosmic rays. Aspects of the KASCADE project.

Congress of the European Association of Nuclear Medicine, Strasbourg, F, August 28 - September 2, 1989

BIALY, J.; FEINENDEGEN, L.E.; PETERS, W.J.; SCHMITT, M.; SUATMADJI, A.; SZABO, Z.; VOSBERG, H.; WIRRWAR, A.
Investigation of the pharmacokinetics of supra(99M)Tc-mercaptoacetyltriglycine (MAG$_3$) with a portable gamma detector.

Internat.Summer School 'Recent Advances in Experimental Nuclear Physics', Poiana Brasov, R, August 30 - September 9, 1988

BRANCUS, I.M.; REBEL, H.
Extended sum-rule model for light and intermediate mass-fragment emission in heavy ion reactions.

Workshop on Physics with Heavy Ions Stored in Electromagnetic Traps, GSI, Darmstadt, September 4, 1990

MEISEL, G.; RINK, J.; KÄLBER, W.
Time resolved spectroscopy of ions in a Paul trap.

Transputer-Anwendertreffen (TAT '90), Aachen, 16.-18.September 1990

BEKK, K.; GILS, H.J.; KEIM, H.; KLAGES, H.O.; SCHIELER, H.; LEICH, H.; MEYER, U.; WAGNER, P.
Echtzeit-Signalverarbeitung mit Transputern inn dem astrophysikalischen Experiment KASCADE.

Workshop über Mittelenergie, Hambach, 28.September 1990

ZEITNITZ, B.
Status und erste Ergebnisse des Neutrinoexperiments KARMEN.

Internat.School on Neutron Physics, Alushta,
SU, October 8-18, 1990

BEER, H.
Neutron capture and s-process nucleo-
synthesis.

Internat.Symp.on Capture Gamma Ray
Spectroscopy, Asilomar, Calif., October 14-19,
1990

KLAY, N.; KÄPPELER, F.; BEER, H.;
SCHATZ, G.
^{176}Lu - an s-process thermometer.

NEMETH, ZS.; KÄPPELER, F.; REFFO, G.
The supra(180m)Ta($\gamma\gamma'$) ^{180}Ta cross section at
1.33 and 4.0 MeV and its astrophysical
consequences.

6th Internat.Symp.on Very High Energy
Cosmic Ray Interactions, Tarbes, F, July 8-17,
1990 Workshop on Galactic Particle
Accelerators, Ringberg, November 12-16, 1990

SCHATZ, G.
The KASCADE extensive air shower project.

6.3. SEMINAR TALKS

REBEL, H.
Coulomb dissociation as an alternative to
radiative capture.
ISOLDE-Seminar on Nuclear Astrophysics,
CERN, Geneve, CH, 19.-20.Juni 1989

KLAGES, H.O.
n-p scattering and n-^{3}He reaction studies with
the POLKA polarized white neutron beam.
Vortr.: Los Alamos National Laboratory, Los
Alamos, N.M., 12.Juli 1989

KLAGES, H.O.
KASCADE - studies of UHE cosmic ray
showers.
Vortr.: University of California, Davis, Calif.,
14.Juli 1989

ZEITNITZ, B.
Neutrinophysics at ISIS: first results from
KARMEN.
Vortr.: University of California, Davis, Calif.,
14.Juli 1989

KLAGES, H.O.
KASCADE, an experiment to study the origin
and composition of UHE cosmic rays.
Vortr.: Universite Catholique de Louvain, B,
2.November 1989

KIENER, J.
Coulomb-dissociation of 156 MeV ^{6}Li-projec-
tiles.
Vortr.: Centre de Spectrometrie nucleaire et de
Spectrometrie de Masse, Orsay, F, 7.November
1989

KLAGES, H.O.
Experimente zur Spinabhängigkeit der
Nukleon-Nukleon Wechselwirkung.
Vortr.: Universität Heidelberg, 24.November
1989

KÄPPELER, F.
^{176}Lu at stellar temperatures.
Vortr.: Instituto di Fisica Generale, Universita
di Torino, I, 29.November 1989

KLAGES, H.O
KASCADE - ein neues Höhenstrahlungs-
Experiment in Karlsruhe.
Vortr.: Universität Erlangen, 5.Dezember
1989

DOLL, P.
The Karlsruhe cosmic ray air shower
experiment.
Vortr.: University of Mexico, Mexico City,
8.Januar 1990

DOLL, P.
Neutron-Proton Streuung.
Vortr.: Physikalisches Kolloquium,
Universität Göttingen, 19.Januar 1990

GILS, H.J.
Das Karlsruher Luftschauer-Experiment
KASCADE.
Vortr.: Physikalisches Institut, Universität
Tübingen, 9.Februar 1990

SCHATZ, G.
Das KASCADE-Höhenstrahlexperiment.
Vortr.: Workshop, Ahrenshoop, 17.-20.April
1990

CAPDEVIELLE, J.N.; GABRIEL, P.; GILS,
H.J.; GRIEDER, P.K.F.; HECK, D.; HEIDE, N.
KNAPP, J.; MAYER, H.J.; ÖHLSCHLÄGER,
J.; REBEL, H.; SCHATZ, G.; THOUW, T.J.
Luftschauer Simulation für KASCADE.
Vortr.: Inst.f.Hochenergiephysik der
Akademie der Wissenschaften der DDR,
Zeuthen, DDR, 10.Mai 1990

SCHATZ, G.
Das KASCADE-Höhenstrahl-Experiment.
Vortr.: Physikalisches Kolloquium,
Universität Siegen, 23.November 1989
Vortr.: Universität Bern, CH, 11.Mai 1990

MASCHUW, R.
KARMEN, Neutrinophysik bei niedrigen
Energien.
Vortr.: Universität Giessen, 14.Mai 1990

MASCHUW, R.
KARMEN, Neutrinophysik an
Mittelenergiebeschleunigern.
Vortr.: Universität Bonn, 17.Mai 1990

KLAGES, H.O.
The extensive air shower project KASCADE.
Vortr.: Zentralinstitut der Akademie der
Wissenschaften, Budapest, H, 13.Juni 1990

KÄPPELER, F.
Astrophysik mit dem Karlsruher 4π BaF$_2$
Detektor.
Vortr.: Universität Wien, A, 15.Juni 1990

SCHATZ, G.
The KASCADE extensive air shower
experiment.
Vortr.: Universitaet Moskau, SU, 15.Juni 1990

KÄPPELER, F.
Neutron capture reactions: clues to stellar
helium burning.
Vortr.: Euratom Geel, B, 17.Juli 1990

KÄPPELER, F.
The role of cross sections for deciphering the s-
process.
Vortr.: University of Notre Dame, Notre
Dame, Ind., 21.September 1990
Vortr.: Astronomy Colloquium, University of
Illinois, Urbana, Ill., 25.September 1990

MEISEL, G.; RINK, J.; KÄLBER, W.
Ions in a Paul trap: how to make them seem to
stand still.
Vortr.: Politechnika Poznanska, Poznan, PL,
9.Oktober 1990

BEER, H.
Empirical aspects of neutron capture and s-
process nucleosynthesis.
Vortr.: Istituto de Fisica Generale, Universita
di Torino, I, 7.November 1990

GILS, H.J.
Kosmische Strahlung bei höchsten Energien.-
Das Karlsruher Forschungsprojekt KASCADE
Vortr.: Akad.Verb. PALATO SINAPIA,
Universität Karlsruhe, 7.November 1990

MASCHUW, R.
KARMEN, neutrinophysics between 5 and
50 MeV.
Vortr.: ILL, Grenoble, F, 7.November 1990

SCHWEICKERT, H.
Isotope production at the Karlsruhe Compact
Cyclotron.
Vortr.: M.D.Anderson Hospital, Houston, Tex.,
12.November 1990

KÄPPELER, F.
Elementsynthese im stellaren
Heliumbrennen.
Vortr.: Physikalisches Kolloquium,
Universität Tübingen, 14.November 1990

REBEL, H.
Die wissenschaftliche Motivation des
KASCADE-Experimentes.
Vortr.: Zentralinstitut fuer Kernforschung
Rossendorf, Dresden, 13.Dezember 1990

GILS, H.J.
Detektorsysteme und Datenverarbeitung im
KASCADE-Experiment.
Vortr.: Zentralinstitut fuer Kernforschung
Rossendorf, Dresden, 14.Dezember 1990

7. PERSONNEL

Head of the Institute, sec. **IK I** :

Prof. Dr. B. Zeitnitz

Scientific and Technical staff :

Argast, J.

Bauer, F.[1]

Bayer, R.[1]

Bolz, J.[1]

Csabo, Th.

Daumiller, K.[1]

Deutsch, G., Mrs.

Dittmann, R.

Doll, P., Dr.

Drexlin, G., Dr.

Eberhard, V., Dipl.-Phys.[2]

Eitel, K.[1]

Engler, J., Dr.

Foltin, G.[1]

Gabriel, P., Dipl.-Phys.[2]

Gemmeke, H., Dr.

Gettert, M., Dipl.-Phys.[2]

Giorginis, G., Dr.

Glasstetter, R.[1]

Grandegger, W., Dipl.-Phys.[2]

Grundel, G., Mrs.

Gumbsheimer, R., Dipl.-Ing.

Hahn, A.[1]

Haunschild, D.[1]

Heeringa, W., Dr.

Heneka, B., Mrs.

Hucker, H.

Hüther, H., Dipl.-Ing.

Husson, L., Ing.

Jany, P., Dr.

Keim, H., Ing.

Kern, H.

Klages, H.O., Dr.

Kleifges, M., Dipl.-Phys.[2]

Kleinfeller, J., Dr.

Knapp, J., Dr.

Kriegleder, W., Dipl.-Phys.[2]

Kröner, F.

Maschuw, R., Dr.

Mayer, H.-J., Dr.

Mielke, H.H., Dipl.-Phys.[2]

Mondry, G., Dipl.-Phys.[2]

Moucka, D., Mrs.[1]

Paulus, W.

Plischke, P., Dr.

Plitt, K., Mrs.

[1] Student
[2] Graduate student

Rapp, J.[1]

Schieler, H., Dipl.-Phys.[2]

Schmalz, G., Dipl.-Ing.

Schmidt, F.K., Dr.

Simonis, H.-J., Dr.

Skacel, H.

Spohrer, G.

Treceziak, R.[1]

Stark, B.

Vater, G., Mrs.[1]

Völker, G., Dipl.-Phys.[2]

Wetzel, Y., Mrs.[1]

Wochele, J., Dr.

Wölfle, S., Mrs., Dipl.-Phys.[2]

Wolf, J., Dipl.-Phys.[2]

Ziegler, P.

Guest Scientists:

Brady, P., Prof. Dr.

Wegner, P. Dr..

Head of the Institute, sec. **IK III** :

Prof. Dr. G. Schatz

Scientific and technical staff:

Antoni, I., Mrs.	Heide, N., Dr.
Beer, H., Dr.	Horzel, J.[1]
Bekk, K., Dr.	Jaag, S.[1]
Burkhardt, S., Mrs.	Kälber, W., Dr.
Bollmann, E., Dipl.-Phys.	Käppeler, F., Dr.
Boschert, H.[1]	Kaltenbeck, J.
Dorn, A.[1]	Kiener, J., Dipl.-Phys.
Eberle, H., Ing.	Klay, N., Dipl-Phys.
Emmler, J., Mrs.[1]	Kölmel, U.[1]
Engster, J.	Kowalewska, D., Mrs., Dipl.-Phys.[2]
Feurer, B.	Mathes, H. , Dipl.-Phys.[2]
Garcia-Orijuela, C.[1]	Matussek, P., Dipl.-Phys.
Gerstenhöfer, Th., Dipl.-Phys.[2]	Meisel, G., Priv.-Doz., Dr.
Gils, H.J., Priv.-Doz., Dr.	Michel-Piper, I. Mrs., Dipl.-Ing.
Grill, A.[1]	Mielke, H.[1]
Gsottschneider, G.[1]	Müller, H.
Guber, K., Dipl.-Phys.[2]	Müller, K.[1]
Göring, S., Dipl.-Phys.	Neuberger, D.[1]
Hanser, A., Dr.	Öhlschläger, J., Dipl.-Math.
Heck, D., Dr.	Ottmar, H., Dr.

[1] Student
[2] Graduate student

Rämer, Chr., Mrs., Dipl.-Ing.

Ratzel, U.[2]

Rebel, H., Prof. Dr.

Riegel, M.

Rink, J., Dipl-Phys.[2]

Rupp, G.

Schanz, W.[1]

Schatz, H.[1]

Schmidt, K.A., Dipl.-Phys.

Schruft, R.[1]

Schulze, B., Mrs.[1]

Steininger, R.[2]

Supper, R.[1]

Thouw, T., Dr.

Tepe, M.[1]

Voß, F., Dr.

Weber, N.

Wentz, J.[1]

Wisshak, K., Dr.

Zagromski, S., Dipl-Ing.

Zirker, A., Mrs.

[1] Student
[2] Graduate student

Guest Scientists:

Brâncuş, I.M., Mrs., Dr.

Capdevielle, J.N., Prof. Dr.

Corcalciuc, V., Dr.

Duma, M. , Dipl.-Math.

Gorski, B., Mrs., Dr.

Khristiansen, G.B., Prof. Dr.

Koehler, P. , Dr.

Miller, W. , Ing.

Nemeth, Z., Dr.

Pârlog, M., Dr.

Popescu, D., Dr.

Trautvetter, H.-P., Prof. Dr.

Wdowczyk, J., Prof. Dr.

Wiescher, M., Prof. Dr.

Wilig, T. , Dr.

Zabierowski, J., Dr.

Xia, Y., Dr.

Zhao, W., Mrs., Dipl.-Phys.

1 Student
2 Graduate student

Head of the

Cyclotron Laboratory :

Dr. H. Schweickert

Scientific and technical staff :

Acharya, H., Mrs.	Heinzmann, H., Dipl.-Inf.
Assmus, K.H.	Herrmann, P.
Bauer, G.	Hüfner, R., Dr.
Bechtold, V., Dr.	Huttel, E., Dr.
Bialy, J., Dipl.-Phys.	Immler, H., Dipl.-Ing.
Biber, J.	Kappel, W.-R., Ing.
Blank, R.	Kauther, P.
Dennerlein, H.D.	Kernert, N., Dipl.-Phys.
Dohrmann, H., Ing.	Kessel, M.
Dosenbach, S.,Mrs.	Kirste, E., Mrs.
Dressen, R.	Kleinrahm, J., Dr.
Ehret, H.-P.	Klinger, G.
Erbe, D.	Konrad, J.
Erdel, E.	Kraft, J.
Fehsenfeld, P., Dr.	Kraus, H.
Fischböck, T.	Krieg, U.
Foßhag, E., Dr.	Kubat, R., Dipl.-Ing.
Franz, J.	Lang, R.
Friedrich, L., Dr.	Maier, W.
Gehrlein, K.	Mangold, D.
Gegenheimer, B.	Martin, A.
Günther, O.	Mayl, R.
Heger, V.	Möck, W.
Heidenreich, K.	Möllenbeck, J., Ing.

[1] Student
[2] Graduate student   - 203 -

Peters, J.W., Dipl.-Phys.

Ripp, H.

Roth, H., Ing.

Schimpf, P.

Schlösser, K., Dr.

Schmitt, M.

Schönstein, E.

Schüssler, B.

Schütz, R.

Schulz, F., Ing.

Seidel, H.

Seitz, J.

Seufert, H.

Stöbener, E., Ing.

Süpfle, M.

Uchatius, R., Mrs.

Uhlemann, S., Mrs.

Wendel, J.[2]

Wiss, L.

Guest Scientists :

Linnemann,. W., Dr.

[1] Student
[2] Graduate student   - 204 -